Peroxisomal Components Function to Regulate Lipolysis at the Lipid Droplet Surface

by

Matthew N Anderson-Baron

A thesis submitted in partial fulfillment of the requirements for the degree of

Doctor of Philosophy

Department of Cell Biology
University of Alberta

Abstract

Organelles serve to compartmentalize biochemical functions within the eukaryotic cell. However, to collectively maintain cellular homeostasis, organelles must communicate in some way in order to coordinate these functions. Two such organelles, the peroxisome and the lipid droplet, are both involved in the metabolism of cellular lipids. Therefore, it is likely that they communicate in order to coordinate their metabolic activity.

Peroxisomes are small, ubiquitous organelles that produce and decompose hydrogen peroxide and metabolize particular species of lipid. Lipid droplets serve as the main storage reservoir for excess fatty acids and cholesterol within the cell. Studies have revealed intimate physical connections between peroxisomes and lipid droplets; however, little is known about the mechanisms that regulate their communication. This thesis outlines the characterization of genes involved in peroxisome biogenesis in *Drosophila* and previously undocumented functions of peroxisomal components Pex13 and Pex14 at the lipid droplet surface.

The subcellular localization of predicted peroxisome proteins was examined in *Drosophila melanogaster*. PEX genes encoding proteins called peroxins control the biogenesis and maintenance of the peroxisome population. The majority of the peroxins localized to peroxisomes in S2 cells, a cell line derived from *Drosophila* embryos. In addition, proteins expressing a canonical peroxisomal targeting signal, -SKL, at their C-terminus are likewise localized to peroxisomes in S2 cells. A comprehensive analysis of the various peroxisomal protein targeting pathways revealed that overall peroxisome biogenesis and function are well conserved in *Drosophila*, validating the use as a model

system to further investigate peroxisome activities, such as peroxisome-lipid droplet interactions.

S2 cells cultured in the presence of oleate exhibit changes in peroxisome phenotype and upregulation of *Pex14*. Furthermore, knockdown of *Pex14* in both S2 cells and *Drosophila* larvae resulted in increased lipolysis and decreased triglyceride stores. Analysis of the subcellular localization of the various confirmed peroxins revealed that Pex3, Pex13, and Pex14 localized to the lipid droplet surface in S2 cells and normal rat kidney cells when cultures were supplemented with excess oleate. In addition, increased levels of Pex14 at the lipid droplet surface affected the localization of Hormone-sensitive lipase. Further, expression of the *Drosophila* homologue of CGI-58 was reduced in cells treated with dsRNA targeting *Pex14*. In contrast, the localization of Pex14 to the lipid droplet surface was perturbed by the overexpression of *Lipid storage droplet-1*.

Collectively, a subset of the peroxisome biogenesis proteins are diverted to the lipid droplet surface during periods of elevated lipid droplet metabolism, where they modulate the localization and expression of other proteins at the lipid droplet. It is proposed that peroxisomal components influence the metabolism of lipid droplets by gating the mobilization of free fatty acids from triglyceride stores.

Preface

Portions of Chapter 1 of this thesis have been published as:

Anderson-Baron, M. and Simmonds, A.J. (2018). Peroxisome Protein Prediction in *Drosophila melanogaster*. In Proteomics of Peroxisomes – Identifying Novel Functions and Regulatory Networks, Subcellular Biochemistry, Volume 89, del Río L., Schrader M., ed. (Singapore: Springer).

This paper represents a collaboration of both authors. I performed the systematic review of research articles, manuscript production, and editing. Andrew J. Simmonds performed manuscript production and editing.

Chapter 2 and portions of Chapter 5 of this thesis has been published as:

Baron, M.N., Klinger, C.M, Rachubinski, R.A., and Simmonds, A.J. (2016). A Systematic Cell-Based Analysis of Localization of Predicted *Drosophila* Peroxisomal Proteins. Traffic *17*, 536 – 553.

This paper presents a collaboration of all authors. I performed all the data collection and replication, analysis, manuscript production and editing. In addition, I provided portions of the experimental design. Chris M. Klinger performed the bioinformatic analysis. Richard A. Rachubinski performed manuscript editing and intellectual contributions. Andrew J. Simmonds performed data analysis, experimental design, manuscript editing, and provided intellectual contributions. Andrew J. Simmonds was the supervisory and

corresponding author for this publication. Chapter 2 contains data published in this manuscript. Chapter 5 contains materials and methods published in this manuscript.

No portions of Chapter 3 have been published.

Dedication

I dedicate this thesis to the memory of my dog, Coco, who was a tremendous source of emotional support for the majority of my academic career. He was such a big part of our lives, but unfortunately, he didn't get to stay for the end of this journey. Rest in peace, Coco. You will always be my best little buddy.

Acknowledgements

First and foremost, I would like to express my sincerest gratitude to my supervisor and mentor, Dr. Andrew Simmonds, for the guidance and support over the course of my graduate career. Working in Dr. Simmonds' laboratory provided an environment that nurtured my growth as a scientist and researcher. He allowed me to pursue projects that were of interest to me, despite those projects being outside his area of expertise. The ability to explore these topics kept me engaged in the work I was doing and my love of science grew. Dr. Simmonds was also incredibly generous. He provided unwavering intellectual and emotional support over the years, and for that, I am forever grateful.

To my supervisory committee, Dr. Richard Rachubinski and Dr. Edan Foley, your continual intellectual support is greatly appreciated. Many fruitful experiments were the result of our meetings. To the "unofficial" member of my supervisory committee, Dr. Sarah Hughes, your assistance and support did not go unnoticed. I sincerely appreciate all the help over the years.

To the members of the Simmonds Lab, past and present, I am thankful for the camaraderie and intellectual support. In particular, I would like to thank Julie Haskins, whose experience and technical prowess were an invaluable asset to my research project.

I would like to acknowledge the funding sources that made this research possible: Alberta Innovates Health Solutions; the Canadian Institute of Health Research via the Banting & Best CGS-M award; and the University of Alberta via the Walter H. Johns Graduate Fellowship, the FOMD Doctoral Recruitment Scholarship, the Queen Elizabeth II Scholarship, and the FOMD 75th Anniversary Award.

To all the members of the Cell Biology staff and professors: I have received so much help from so many different people over the last five years and I am grateful to all of you. To my fellow graduate students: I am so thankful for the camaraderie and support. I have made many friends in my time as a graduate student. Thank you for making this experience such an enjoyable one.

To my Mom, Dad, Sam, and Jenna: you have provided me with everything I could ever ask for. Your love and support have always allowed me to pursue whatever path I chose and for that, I am grateful.

Finally, I could not have done this without my wife, Jalene, who has been a source of unwavering support and encouragement since day one. You have always inspired me to work harder and to be a better person. You were always there to console me during the struggles and to celebrate with me during the victories. Thank you for always being my biggest fan.

Table of Contents

List of Tables

List of Figures

List of Abbreviations

ABCD1	ATP-binding cassette subfamily D, member 1
ACAA1	β-ketoacyl-CoA thioalase
ACSF3	Acyl-CoA synthetase family member 3
Acsl	Acyl-CoA synthetase
ACSL3	Acyl-CoA synthetase long-chain family member 3
ACSL4	Acyl-CoA synthetase long-chain family member 4
AGPS	Alkylglycerone phosphate synthase
AGXT	Alanine-glyoxylate aminotransferase
AMACR	α-methylacyl-CoA racemase
ATGL	Adipose triglyceride lipase
ATP2CD1	ATPase type 2C member 1
Bmm	Brummer
BSA	Bovine Serum Albumin
CCS	Copper chaperone for superoxide dismutase
CCT1	CTP:phosphocholine cytidylyltransferase 1
CFP	Cyan fluorescent protein
CG	Celera Genomics
CGI-58	Comparative gene identification 58
CROT	Carnitine O-octanoyltransferase
DG	Diacylglycerol
DAO	D-amino acid oxidase
DDO	D-aspartate oxidase
DBP	D-bifunctional protein
DGAT	Diacylglycerol acyltransferase
DHSB	Developmental Studies Hybridoma Bank
DHSR4	Dehydrogenase/reductase SDR family member 4
DMEM	Dulbecco's modified eagle's medium
DPiM	*Drosophila* protein interaction map
Drp1	Dynamin related protein 1
dsRNA	Double stranded RNA
eLD	Expanding lipid droplet

ER	Endoplasmic reticulum
FAR1/2	Fatty acyl-CoA reductase 1/2
FBS	Fetal Bovine serum
FFA	Free fatty acid
Fis1	Mitochondrial fission 1 protein
FIT2	Fat storage-inducing transmembrane protein 2
FSG	Fish skin gelatin
G0S2	G0/G1 switch gene 2
GA	Glutaraldehyde
GFP	Green fluorescent protein
GNPAT	Glyceronephosphate O-acyltransferase
GOT1	Glutamate oxaloacetate transaminase
HACL1	2-hydroxyacyl-CoA lyase 1
HAO 1/2	Hydroxyacid oxidase 1/2
HMGCL	3-hydroxy-3-methylglutaryl-CoA lyase
HMGCR	3-hydroxy-3-methylglutaryl-CoA reductase
HSL	Hormone-sensitive lipase
IDE	Insulin degrading enzyme
IF	Immunofluorescence
iLD	Initial lipid droplet
iTEM	Immuno-transmission electron microscopy
LAL	Lysosomal acid lipase
LBP	Enoyl CoA hydratase
LD	Lipid droplet
LKAP	Limkain-b1
LSD1	Lipid storage droplet 1
LSD2	Lipid storage droplet 2
MADAG	Monoalk(en)yl diacylglycerol
MARCM	Mosaic analysis with a repressible cell marker
MDH1	Malate dehydrogenase 1
MDV	Mitochondrial derived vesicle
MGAT	Monoacylglycerol acyltransferase

MGL	Monoglyceride lipase
MP17	Mpv17-like protein
mPTS	Membrane peroxisomal targeting signal
MSEA	Metabolite set enrichment analysis
MUL1	Mitochondrial ubiquitin ligase activator of NFKB
NLS	Nuclear localization signal
NRK	Normal rat kidney
NUDT7	Peroxisomal coenzyme A diphosphatase
PBD	Peroxisome biogenesis disorder
PKA	Protein-kinase A
PLIN	Perilipin
PMP	Peroxisomal membrane protein
PMP34	Peroxisomal membrane protein 34
PMP70	Peroxisomal membrane protein 70
PMVK	Phosphomevalonate kinase
PPAR	Peroxisome proliferator-activated receptor
PPV	Pre-peroxisomal vesicle
PRDX1	Peroxidredoxin 1
PTS1	Peroxisomal targeting signal 1
PTS2	Peroxisomal targeting signal 2
PXA1	Peroxisomal ABC-transporter
RFP	Red fluorescent protein
RpL30	Ribosomal Protein L30
ROS	Reactive oxygen species
Rtnl1	Reticulon-like 1
S2	Schneider 2
SKL	Serine lysine leucine
SLC22A5	Solute carrier family 22 member 5
SLC25A17	Solute carrier family 25 member 17
SLC27A2	Solute carrier family 27 member 2
SOD1	Superoxide dismutase 1
SPCx	Non-specific lipid transfer protein

SPoCK	Secretory Pathway Calcium ATPase
STED	Stimulated emission depletion
TEM	Transmission electron microscopy
TG	Triglyceride
TMEM135	Transmembrane protein 135
TOR	Target of rapamycin
UA	Uranyl acetate
UAS	Upstream activating sequence
VLCFA	Very long chain fatty acid
w^{1118}	*white*^{1118}
XDH	Xanthine dehydrogenase

Chapter 1: Introduction

Portions of this chapter have been published as:

Anderson-Baron, M. and Simmonds, A.J. (2018). Peroxisome Protein Prediction in *Drosophila melanogaster*. In Proteomics of Peroxisomes – Identifying Novel Functions and Regulatory Networks, Subcellular Biochemistry, Volume 89, del Río L., Schrader M., ed. (Singapore: Springer).

1.1. Peroxisomes

Peroxisomes are small, membrane-bounded organelles that are found in virtually all eukaryotic species. Peroxisomes range in size from 0.1 – 1.0 μm in diameter, and their biogenesis and function are highly conserved from yeast to humans (reviewed in Smith and Aitchison, 2013). Johannes Rhodin first described peroxisomes in 1954 (Rhodin, 1954) and Christian De Duve later provided a biochemical definition for the peroxisome (De Duve and Baudhuin, 1966). Peroxisomes were originally biochemically defined as organelles containing a hydrogen peroxide producing oxidase and catalase for the production and decomposition of hydrogen peroxide (De Duve and Baudhuin, 1966). Within mature peroxisomes is a dense matrix containing a number of different enzymes, which carry out a variety of metabolic functions within the cell. Correspondingly, numerous metabolic pathways localize within the peroxisome, most notably the β-oxidation of specific lipid species and the production and decomposition of hydrogen peroxide (Hryb and Hogg, 1979; Kramar et al., 1978; Lazarow, 1978). Peroxisomes are highly dynamic, responding rapidly to changes in the cellular environment. These responses are observed by changes in peroxisome size, shape, and abundance within the cell (reviewed in Smith and Aitchison, 2013). Peroxisome biogenesis occurs either *de novo* from the endoplasmic reticulum (ER) or via fission from existing mature peroxisomes. Matrix proteins are post-translationally targeted to the peroxisome via the Peroxisome Targeting Signal 1 (PTS1) pathway, whereby the presence of a serine-lysine-leucine (SKL) tripeptide at the C-terminus signals the delivery of the cargo to the peroxisome (Gould et al., 1989). The less characterized Peroxisome Targeting Signal 2 (PTS2) pathway is mediated by the recognition a nine amino acid sequence near the N-

terminus of cargo (Swinkels et al., 1991) by the soluble cargo receptor Pex7 (Marzioch et al., 1994; Zhang and Lazarow, 1995).

Since their initial discovery, ongoing research has revealed new functions and highlighted the importance of peroxisomes in cellular homeostasis and the metabolism by various tissues. Peroxisome biogenesis is controlled by the PEX genes, which encode the peroxins. Thirty-four different peroxins have been described, and mutations in their PEX genes result in deficient peroxisome formation and/or function (reviewed in Smith and Aitchison, 2013). Defects in peroxisome biogenesis or function in humans lead to a class of genetic disorders termed the Peroxisome Biogenesis Disorders (PBDs) (reviewed in Steinberg et al., 2006). PBDs manifest as complex sequelae, which include cognitive dysfunction, learning impairments, craniofacial abnormalities, liver and kidney dysfunction, progressive hearing loss, and retinopathy (reviewed in Steinberg et al., 2006). The severity of PBDs highlights the importance of peroxisome maintenance and function in tissue homeostasis and human health.

1.1.1. The PTS1 import pathway

Most matrix proteins are targeted to the peroxisome via the PTS1 pathway, which is highly conserved across species, with slight variations in the PTS1 signal. A SKL tripeptide at the C-terminus of cargo proteins is recognized by Pex5p, the soluble cargo receptor for the PTS1 pathway in yeast (Van der Leij et al., 1993), which traffics the cargo to the peroxisomal membrane (Gould et al., 1989; Purdue and Lazarow, 1996). PEX5, along with its cargo, dock at the peroxisomal membrane by interacting with PEX14, a transmembrane peroxisomal protein (Albertini et al., 1997). This interaction

occurs via a conserved di-aromatic penta-peptide motif found at the N-terminus of PEX5 (Neuhaus et al., 2014). Proteins are transported across the peroxisome membrane in their fully folded state, in contrast to other organelles where polypeptides are unfolded during the translocation process (Walton et al., 1995). The mechanism of translocation is not well described; however, models exist that support a transient-pore system, which is dynamically formed by the import constituents themselves. In this model, the topology of PEX5 changes during import, switching from a cytosolic state to a membrane-bound state and inserting into the peroxisome membrane to form a pore along with PEX13 and PEX14 (Albertini et al., 1997; Elgersma et al., 1996a). This is supported by evidence that PEX5 forms homo-oligomers, and the membrane-bound state exists in higher molecular weight complexes (Reguenga et al., 2001). This is also supported by functional evidence that the peroxisome pore is remarkably dynamic as it can accommodate gold particles up to 9 nm in size (Walton et al., 1995). Once the receptor-cargo complex has translocated across the membrane, PEX5 dissociates from the cargo (Ma et al., 2013). Similar to the translocation process, the mechanism by which cargo is released is not entirely clear. However, it has been shown in yeast that Pex8p is involved through an interaction with Pex5p (Ma et al., 2013). Once the cargo has been released, PEX5 can then be recycled back to the cytoplasm for another round of import. This occurs via the action of the peroxisomal RING-finger complex composed of PEX2, PEX10, and PEX12. These transmembrane proteins reside in the peroxisome membrane where they function as a ubiquitin ligase complex during peroxisome protein import (Magraoui et al., 2012; Platta et al., 2009). PEX2 facilitates the polyubiquitination of PEX5 (Platta et al., 2009). PEX12 facilitates the monoubiquitination of PEX5 (Platta et al., 2009). These ubiquitination events determine whether PEX5 gets recycled (monoubiquitination) or degraded by the

Figure 1.1

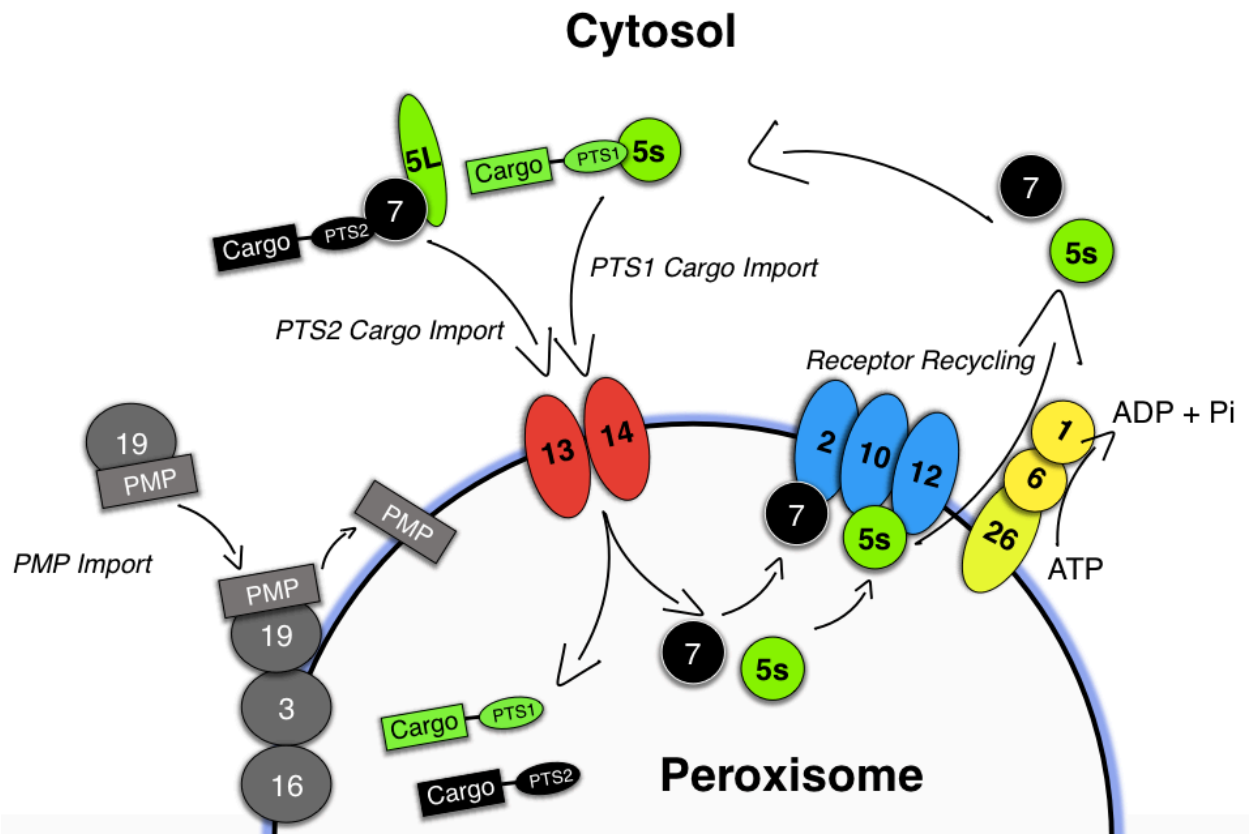
Cytosol
5L
Cargo
PTS1
5s
7
Cargo
PTS2
PTS1 Cargo Import
PTS2 Cargo Import
Receptor Recycling
7
5s
ADP + Pi
19
PMP
13
14
2
10
12
1
6
26
7
5s
ATP
PMP Import
PMP
PMP
19
3
16
7
5s
Cargo
PTS1
Cargo
PTS2
Peroxisome

Figure 1.1. Protein targeting to mammalian peroxisomes. PEX5s (short isoform) recognizes the PTS1 on the C-terminus of cargo and targets the complex to the peroxisome membrane where it interacts with PEX13 and PEX14. The complex translocates across the peroxisome membrane and the cargo is released. PEX5s is ubiquitinated by a complex composed of PEX2, PEX10, and PEX12. PEX5s is exported back to the cytosol by a complex composed of PEX6 and PEX1, which hydrolyzes ATP during this process. This complex is tethered to the membrane by PEX26 in mammals. PEX7 recognizes the PTS2-containing cargo, along with a co-receptor. The co-receptor in mammals is the long isoform of PEX5 (PEX5L). This complex is imported and PEX7 is recycled via similar mechanisms to PEX5 and the PTS1 pathway. PEX19 recognizes peroxisomal membrane proteins in the cytosol and targets them to the peroxisome. PEX19 interacts with PEX3 and PEX16 at the membrane and the cargo is inserted into the membrane.

proteasome (polyubiquitination) (Magraoui et al., 2012; Platta et al., 2009). The majority of the import process is ATP-independent, with the exception of the recycling of PEX5. In order for PEX5 to re-enter the cytosol, ATP hydrolysis occurs by the action of a AAA-ATPase complex composed of PEX1 and PEX6 (Miyata and Fujiki, 2005), which is anchored to the membrane by PEX26 (Matsumoto et al., 2003). The canonical mammalian PTS1 import pathway is outlined in Figure 1.1.

1.1.2 The PTS2 import pathway

The peroxisome PTS2 pathway is relatively less characterized than the PTS1 pathway. While present in yeast and mammalian species, both PEX7 and proteins with a canonical PTS2 are absent in *Caenorhabditis elegans* (Motley et al., 2000). Few proteins employ the PTS2 pathway for delivery to the peroxisome in yeast and mammalian species, however, upwards of one-third of all peroxisomal proteins in plants utilize this pathway for delivery (reviewed in Lazarow, 2006). The PTS2 signal is a 9-amino acid stretch found near the N-terminus of cargo (Swinkels et al., 1991). Despite the fact that the PTS1 pathway is more common, many key peroxisomal enzymes utilize the PTS2 pathway for peroxisomal targeting in different species. In mammals, thiolase (Osumi et al., 1991; Swinkels et al., 1991), mevalonate kinase (Wanders and Romeijn, 1998), alkylglycerone phosphate synthase (AGPS) (de Vet et al., 1998), and phytanoyl-CoA hydroxylase (Jansen et al., 1997) are targeted to the peroxisome via the PTS2 pathway. PEX7 recognizes the PTS2-containing cargo in the cytosol (Marzioch et al., 1994; Zhang and Lazarow, 1995) and, along with its co-receptor, targets the cargo to the peroxisome. In mammals, the co-receptor is the long isoform of PEX5 (Otera et al., 2000). Two

different co-receptors exist in yeast: Pex18p and Pex21p. This interaction between Pex7p and its co-receptors is essential for PTS2 import (Purdue et al., 1998). This complex docks at the peroxisome membrane by also interacting with PEX14, and translocating across the pore and into the matrix. PEX7 recycling and degradation occur via a similar mechanism that is used by PEX5, although their regulation is independent of each other (Hagstrom et al., 2014). The canonical PTS2 pathway is outlined in Figure 1.1.

1.1.3 The peroxisomal membrane protein targeting pathway

The delivery of peroxisomal membrane proteins (PMPs) to peroxisomes involves PEX3, PEX16, and PEX19 (Götte et al., 1998; Höhfeld et al., 1991; Honsho et al., 1998). Some recent models suggest that a subset of PMPs are targeted to the ER prior to peroxisome localization. In these models, it is proposed that these PMPs may perform ER-specific functions, including involvement in peroxisome biogenesis (Mayerhofer, 2016). Fujiki et al. first demonstrated that PMPs are translated on free polysomes in the cytosol and are post-translationally targeted to the peroxisome membrane (Fujiki et al., 1984). PEX19 is the cytosolic cargo receptor for the PMP pathway, which recognizes the PMP signal, termed the mPTS (Sacksteder et al., 2000). PMPs may contain one or several mPTSs, which consist of a cluster of positively charged amino acid resides flanked by transmembrane segments (Rottensteiner et al., 2004). This interaction is strongly conserved. It has been shown that when PEX19 is mislocalized to the nucleus by the addition of a nuclear localization signal (NLS), PMPs that contain an mPTS are likewise localized to the nucleus (Sacksteder et al., 2000). PEX19 also functions as a chaperone by preventing PMP aggregation and degradation (Jones et al., 2004; Sacksteder et al., 2000).

After PEX19 binds its cargo, it docks at the peroxisomal membrane through an interaction with PEX3 (Fang et al., 2004), forming a trimeric complex (Pinto et al., 2006). Following this docking step, the PMP is then inserted into the peroxisomal membrane. It is unclear how this process occurs; however, it has been noted that PEX3 contains a strongly hydrophobic region at its C-terminus, which may be responsible for disrupting the membrane bilayer and allowing insertion of the PMP (Pinto et al., 2009). PEX16 has likewise been shown to be involved in the docking of PEX19 and its cargo at the peroxisomal membrane (Matsuzaki and Fujiki, 2008); however, this function is not conserved across species as its been shown that most yeasts do not possess a PEX16 homologue (Kiel et al., 2006). The PMP import pathway is shown in Figure 1.1.

1.1.4. Peroxisome de novo biogenesis

De novo biogenesis of peroxisomes occurs at the ER, whereby pre-peroxisomal vesicles (PPVs) bud off of the ER membrane, and later fuse to form a mature peroxisome (Titorenko et al., 2000). There are two biochemically distinct subclasses of PPVs that are associated with different subsets of peroxins. One class of PPVs contains PEX2, PEX10, and PEX12, which together form the RING-finger complex. The other class contains PEX13 and PEX14, which form the docking complex (van der Zand et al., 2012). Each PPV is not functional on its own, but rather becomes import competent following fusion. Once fusion has occurred, import of peroxisomal matrix proteins can take place and the peroxisome becomes functional (Figure 1.2) (van der Zand et al., 2012). This distinction amongst the PPV population is likely to ensure the proper stoichiometric ratios of PEX proteins in the nascent peroxisome. More recently, it has been shown that

mitochondrially derived vesicles, particularly in PEX3-deficient cells, are targeted to peroxisomes and contribute to peroxisome formation and function (Sugiura et al., 2017). The process of *de novo* peroxisome biogenesis at the ER is dependent on PEX3, PEX16, and PEX19 (Götte et al., 1998; Höhfeld et al., 1991; Honsho et al., 1998). Yeast cells lacking either Pex3p or Pex19p are able to form PPVs; however, these vesicles are degraded by autophagy before they are able to mature (Knoops et al., 2014). Once PEX3, PEX16, and PEX19 are localized to the ER, ER-resident proteins are utilized for the generation of membrane structures that form budding vesicles and the subsequent recruitment of other PMPs (Agrawal et al., 2016). Studies in yeast have also highlighted important roles for Pex30p and Pex31p in the formation of ER subdomains that form the budding structures of PPVs (Joshi et al., 2016; Mast et al., 2016). *De novo* peroxisome biogenesis is outlined in Figure 1.2.

1.1.5. Peroxisome division

Increases in peroxisome numbers are primarily controlled through the growth and division of existing mature peroxisomes (Lazarow and Fujiki, 1985; Motley and Hettema, 2007). When the metabolic demand of a cell increases, the peroxisome population rapidly responds through the growth and division of existing. During cell division, peroxisomes also undergo fission, and approximately half of the population is transported along microtubules to be inherited by the daughter cell (Hoepfner et al., 2001). Division of peroxisomes involves the growth of the membrane and the formation of tubular membrane extensions that constrict and undergo scission to form new daughter

Figure 1.2

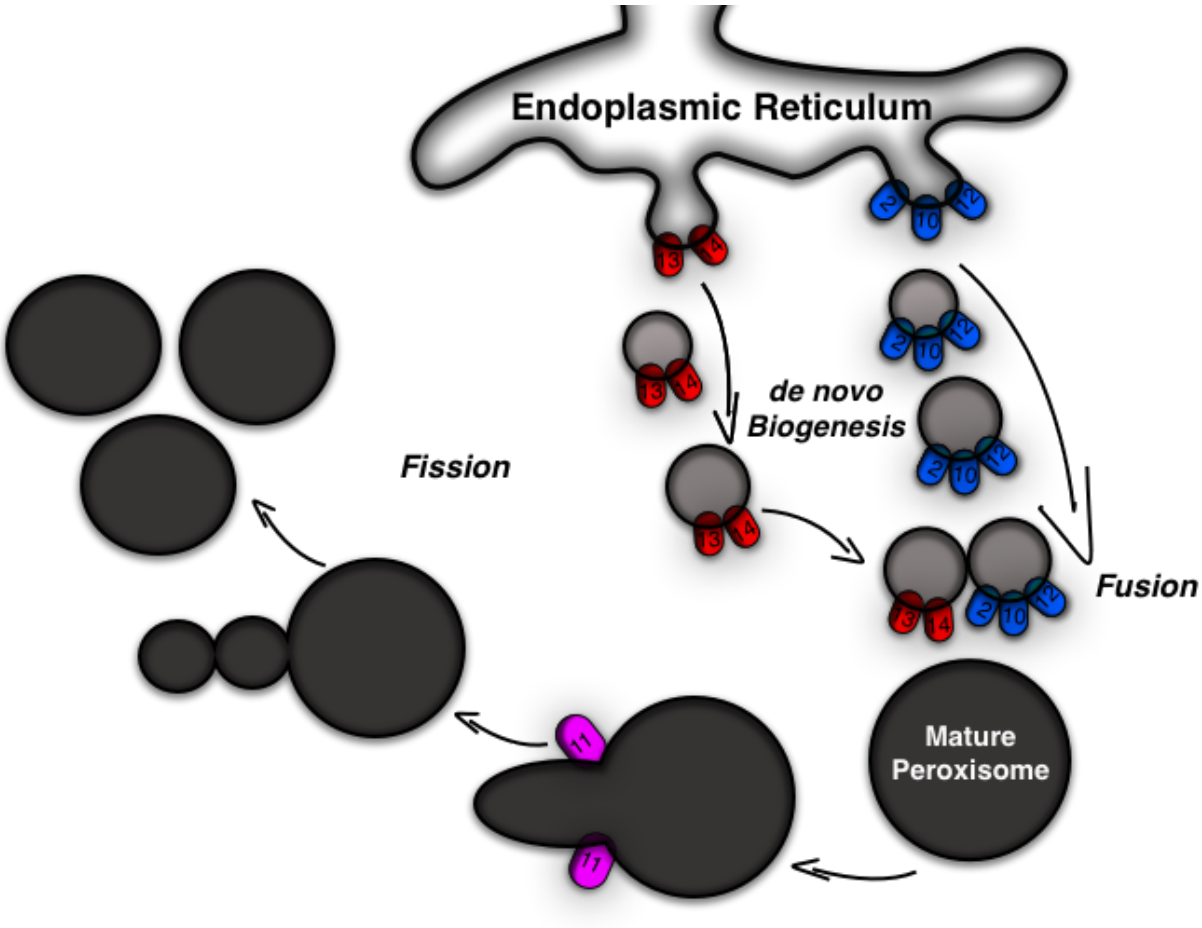
Endoplasmic Reticulum
de novo
Biogenesis
Fission
Fusion
Mature
Peroxisome

Figure 1.2. Peroxisome biogenesis and division. Peroxisome biogenesis occurs *de novo* at the ER, whereby biochemically distinct populations of PPVs budding from the ER. One population contains the docking complex composed of PEX13 and PEX14 (shown in red) and the other contains the RING-finger complex composed of PEX2, PEX10, and PEX12 (shown in blue). PPVs fuse to become import competent, which mature to functional peroxisomes. Peroxisome proliferation can also occur via fission of mature peroxisomes. PEX11 promotes elongation of the peroxisome membrane, which ultimately undergoes scission to form daughter organelles.

peroxisomes. PEX11 plays a prominent role in peroxisome fission (Marshall et al., 1995). It is involved in the elongation of the peroxisome membrane prior to fission. This process is facilitated by its amphipathic helices found at the N-terminus that interact with membrane lipids and promote membrane deformation (Delille et al., 2010; Opaliński et al., 2011). In addition, PEX11β functions as a GTPase activator of Dynamin related protein 1 (Drp1) during fission (Williams et al., 2015). Together, this machinery carries out the elongation and subsequent scission of the peroxisome membrane. Peroxisome division is outlined in Figure 1.2.

1.1.6. Pexophagy

Pexophagy is the selective degradation of peroxisomes by autophagy and it is important for maintaining cellular homeostasis (reviewed in Cho et al., 2018). Selective autophagy is induced by the ubiquitination of organelle membrane proteins (reviewed in Cho et al., 2018), which has been observed with the induction of pexophagy (Kim et al., 2008). Kim et al. showed that the exogenous expression of PMP34 fused with a ubiquitin moiety on the cytoplasmic tail enhanced pexophagy in COS-7 cells (Kim et al., 2008). The ubiquitin modification is bound by the protein p62, which serves as an autophagy signalling hub and targets substrates to autophagosomes (Bjørkøy et al., 2005; Komatsu et al., 2007). Other adaptors are also involved, such as NBR1, which has been shown to promote pexophagy when overexpressed (Deosaran et al., 2013).

Other peroxins also contribute to the regulation of pexophagy. Sargent et al. showed that PEX2 is upregulated during starvation and overexpression of PEX2 during amino acid starvation lead to the degradation of peroxisomes (Sargent et al., 2016). In

addition, the AAA ATPase complex, composed PEX1, PEX6, and PEX26 in mammals, has been shown to prevent pexophagy. Loss of the AAA-ATPase complex caused an accumulation of ubiquitinated PEX5 on the peroxisome membrane, which lead to the degradation of peroxisomes by pexophagy (Law et al., 2017).

1.2. The Drosophila melanogaster model organism

The fruit fly, *Drosophila melanogaster*, was one of the first laboratory animals used for biological research. The first laboratory *Drosophila* strains were isolated by Thomas Hunt Morgan at Columbia University in the early 1900s (reviewed in Bilder and Irvine, 2017; reviewed in Kaufman, 2017; reviewed in Wangler et al., 2015). Flies have been used since to uncover fundamental biological processes and as a model for human disease. Some of the attributes that make *Drosophila* a valuable multicellular laboratory model include a short lifespan, amenability to forward genetic studies, a large number of progeny, a sequenced and annotated genome, and easy and inexpensive maintenance (reviewed in Bilder and Irvine, 2017; reviewed in Kaufman, 2017; reviewed in Wangler et al., 2015). Fertilized female *Drosophila* deposit eggs externally, which hatch into wandering larvae after 24 hours. When raised at 25°C, the larval stage proceeds through three instars, separated by molts, over four days. During the larval stage, the precursors of the adult tissues are present as small sacs of cells known as imaginal discs. During the subsequent five-day pupal stage, most larval tissues are degraded and the adult forms from the imaginal discs. Adults are sexually mature within 24 hours (reviewed in Bilder

and Irvine, 2017; reviewed in Kaufman, 2017; reviewd in Wangler et al., 2015). Fly researchers have developed many unique genetic tools such as 'balancers', multiple inverted chromosomes that prevent homologous crossing over during meiosis, fostering simple maintenance of deleterious mutant alleles (reviewed in Casso et al., 1999). Another tool used often in fly studies is mosaic analysis with a repressible cell marker (MARCM), which allows the labelling of cells that share a single progenitor (Wu and Luo, 2006). Transgenic tools such as the GAL4-UAS system enabled precise tissue-specific analyses in the context of whole animals (Brand and Perrimon, 1993; Rodríguez et al., 2012). The GAL4/UAS system has become particularly useful in UAS-mediated RNAi amplicon expression of a large collection of transgenes targeting almost any *Drosophila* gene of interest (reviewed in Dietzl et al., 2007; reviewed in Rodríguez et al., 2012). Despite the fact that *Drosophila* has been a laboratory workhorse, until recently there has been little published research of their peroxisome biology. However, in the past decade, several studies have shown that the key processes of peroxisome biogenesis and function are conserved in *Drosophila* and that flies are an excellent platform to discover new roles for peroxisomes. *Drosophila* researchers have access to an extensive collection of cultured cells from multiple stage and tissue origins. The most commonly used are Schneider 2 (S2) cells, a primary cell line derived from dissociated *Drosophila* embryos (Schneider, 1972). Notably, S2 cells are highly amenable to genetic manipulation by dsRNA treatment. When added to cultures of S2 cells, dsRNA amplicons of almost any size (generally 200-500 base pairs,) are taken up and processed by the endogenous RNAi enzymes to induce robust gene silencing (Kao and Megraw, 2004). This makes them effective for unbiased identification of factors involved in processes including

peroxisome biogenesis, movement, fission and function (reviewed in Wynant et al., 2014).

1.3. Peroxisomes in Drosophila melanogaster

1.3.1. Early studies of peroxisomes in Drosophila melanogaster

The first studies related to *Drosophila* peroxisome protein activity were published in the 1980s. These focused on two enzymes: xanthine dehydrogenase (XDH) (*CG7642*) and D-amino acid oxidase (DAO) (*CG12338*) and their roles in specific tissues (Beard and Holtzman, 1987; Reaume et al., 1991; St Jules et al., 1989; 1990; 1991). The *rosy* gene encodes *Drosophila* XDH. The name *rosy* stems from the observation that mutation resulted in a brownish-red eye color phenotype (Reaume et al., 1991). In 1987, Beard and Holtzmann analyzed the $rosy^{506}$ null mutation (Beard and Holtzman, 1987). They found that XDH co-fractionated with other predicted peroxisome enzymes, and while peroxisomes were observed in the gut of homozygous $rosy^{506}$ flies, they lacked XDH activity (Beard and Holtzman, 1987). Reaume et al. analyzed the tissue-specific expression of *rosy* by in-situ hybridization and found high levels of expression in the gut and the malpighian tubules (Reaume et al., 1991), considered the insect analogue of the mammalian kidney (Gautam et al., 2017). The highest levels of XDH activity were detected in the apical region of the eye, and the protein was detected at the interface between the retina and the lamina using an XDH-specific antibody (Reaume et al., 1991). Similar assays of *Drosophila* DAO activity identified membrane-bounded structures in

the fat body and gut epithelium of both larva and adult *Drosophila* (St Jules et al., 1989; 1991). These structures were round, sometimes dumbbell-shaped, and 0.5 – 1.0 μm in diameter, which was considered consistent with peroxisome morphology (St Jules et al., 1989; 1991). In 1990, St. Jules et al., used enzymatic assays to identify populations of puncta that were reactive to DAO antibodies in cells of the fat body and the eye, which were considered presumptive peroxisomes (St Jules et al., 1990).

The first version of an assembled and annotated sequence of the *Drosophila* euchromatic genome released in the early 2000s facilitated the first computational prediction of *Drosophila* peroxisome protein homologues (Adams et al., 2000). Note that *Drosophila* genes without a known name or function were given a CG (Celara Genomics) identification number (Adams et al., 2000). In 2004, Oba et al., characterized the predicted product of the *CG6178* gene and found similarities to luciferase (Oba et al., 2004), a known peroxisome targeted enzyme in fireflies (Gould et al., 1988). The protein encoded by *CG6178* was found to possess long-chain fatty acyl-CoA synthase activity, consistent with the canonical functions of a peroxisomal enzyme (Oba et al., 2004). In addition, the predicted CG6178 protein had a serine-lysine-leucine (SKL) C-terminal motif (Oba et al., 2004), the canonical PTS1 (Gould et al., 1989).

As multiple genome sequences became available, a comparative evolutionary analysis of the predicted subcellular localization of proteins in several metazoan species identified 544 unique proteins that could potentially localize to peroxisomes in *Drosophila* (Hazkani-Covo et al., 2004). Comparison of *Drosophila melanogaster*, *Saccharomyces cerevisiae,* and *Homo sapiens* genomes identified the homologue of Ca^{2+}/Mg^{2+} ATPase (SPCA), named *Secretory Pathway Calcium ATPase* (*SPoCK*) (*CG32451*) in *Drosophila* (Southall et al., 2006). Notably, *SPoCK* encodes three protein

isoforms, only one of which localized to peroxisomes (Southall et al., 2006). Peroxisome localization of the C-isoform of SPoCK was confirmed by colocalization with a catalase antibody in peroxisome fractions prepared from S2 cells (Southall et al., 2006). Similar to other previously characterized *Drosophila* peroxisome enzymes, the C-isoform of SPoCK was found to be highly expressed in malpighian tubules. Given the function of SPoCK, it was hypothesized that peroxisomes may have an important role in calcium signalling in malpighian tubules (Southall et al., 2006).

1.3.2. Identification of Drosophila peroxisome biogenesis protein homologues

Peroxisome studies were aided by development of an S2 cell line that stably expresses GFP fused to the canonical PTS1 signal at its C-terminus (GFP-SKL), serving as a peroxisome marker compatible with live cell imaging (Kural et al., 2005). In 2011, Mast et al. performed dsRNA knockdown of the expression of each of the *Drosophila* genes homologous to *S. cerevisiae* and *H. sapiens* PEX genes (Mast et al., 2011). Knockdown of *Pex1, Pex5*, *Pex13*, and *Pex16* abolished the punctate GFP-positive signal, indicating that proteins encoded by these genes were involved in PTS1-mediated import (Mast et al., 2011). Similarly, dsRNA knockdown of *Pex2*, *Pex3*, *Pex6*, *Pex12*, and *Pex14* produced a cytosolic GFP signal with few peroxisomes remaining, also confirming that these genes likely encoded peroxins (Mast et al., 2011). Lastly, knockdown of *Pex11* and *Pex19* resulted in fewer and larger GFP-positive peroxisomes, whereas knockdown of *Pex20* and *Pex23* resulted in smaller and more numerous peroxisomes, which is consistent with the function of these peroxins in *S. cerevisiae* and *H. sapiens* (Mast et al., 2011).

In 2012, Faust et al. made a more encompassing prediction of the *Drosophila* peroxisome proteome (Faust et al., 2012). Potential *Drosophila* peroxisome proteins were predicted by sequence similarity to known vertebrate homologs (Faust et al., 2012). Known peroxisome proteins from *H. sapiens* were used to BLAST the *Drosophila* proteome, and PTS1-locating software was used to identify any other predicted fly proteins that possessed the canonical PTS1 or some variation. This analysis identified 82 potential peroxisomal proteins, including the PEX gene homologs identified by Mast et al. (Faust et al., 2012; Mast et al., 2011). They also noted the *Drosophila* genome encoded three isoforms of *Pex11* and two splice isoforms of *Pex5*, which may correspond to the long and short isoforms of PEX5 found in mammalian systems, although this has not yet been confirmed experimentally (Faust et al., 2012).

1.3.3. Functional characterization of Drosophila peroxins

In 2012, Fakieh et al. characterized intracellular sorting of Pex3 in *Drosophila* S2R+ cells (Fakieh et al., 2013), an adhesive variant of S2 cells (Yanagawa et al., 1998). When the yeast Pex3p protein was expressed in S2R+ cells, the protein colocalized with the peroxisome marker mRFP-PTS1, indicating a conservation of Pex3 transport in *Drosophila* (Fakieh et al., 2013). Localization of yeast Pex3p to the peroxisome required either RSR or RHRGK motifs at the N-terminus of the protein, as the double mutant appeared to be trapped in the ER (Fakieh et al., 2013). In addition, when the N-terminus of the *Drosophila* Pex3 was used to replace the N-terminus of the yeast Pex3p, the resulting chimera was found to properly localize to peroxisomes in wild-type yeast cells,

confirming that the sorting of Pex3 from the ER to the peroxisome is evolutionarily conserved (Fakieh et al., 2013).

The putative peroxisomal acyl-CoA oxidase, encoded by *CG17544*, was found to colocalize with peroxisomes (Faust et al., 2012). Enoyl-CoA hydratase (LBP) encoded by *CG4389* has several splice isoforms. Some LBP isoforms localized to peroxisomes, while others localized to other subcellular structures (Faust et al., 2012). Only the B-isoform appeared to overlap with peroxisomes (Faust et al., 2012). In addition, superoxide dismutase 1 (SOD1), encoded by *CG11793,* has –AKV at its C-terminus, a variation of PTS1, which localizes to both peroxisomes and the cytosol (Faust et al., 2012). When the AKV was mutated to AKL, SOD1 localization shifted to completely peroxisomal (Faust et al., 2012). When the last three residues were deleted (ΔAKV), the fusion protein was completely cytosolic (Faust et al., 2012). This suggests that in *Drosophila*, the non-canonical AKV signal interacts weakly with the Pex5 soluble cargo receptor for PTS1-mediated import.

1.3.4. Conservation of Drosophila peroxisome membrane protein trafficking

While there has been considerable effort spent on *Drosophila* PEX homologues, less is known about the other peroxisome proteins, including those localized to the peroxisome membrane. Faust et al. generated an S2 line expressing a PMP34-cerulean fusion protein (Faust et al., 2012). PMP34 formed donut-shaped structures that coalesce around the periphery of SKL positive puncta in S2 cells (Faust et al., 2012). Cyan fluorescent protein (CFP)-tagged Peroxisome Membrane Protein 70 (PMP70) has also been shown to mark the presumptive peroxisome membrane (Nakayama et al., 2011).

1.3.5. The apparent lack of PTS2-mediated trafficking and the role of Drosophila Pex7

Drosophila do not seem to use a canonical PTS2 import pathway for peroxisome matrix protein targeting. A homologue of PEX7, the soluble cargo receptor for PTS2-containing cargo, was identified by the predictions made by Mast et al. (Mast et al., 2011) and Faust et al. (Faust et al., 2012). AGPS (*CG10253*) catalyzes the exchange of fatty acids for long-chain fatty alcohols in the peroxisome (Malheiro et al., 2015). AGPS utilizes the N-terminal PTS2 pathway in humans. Mutations in human *PEX7* result in AGPS mislocalization and manifests as rhizomelic chondrodysplasia punctata (reviewed in Aubourg and Wanders, 2013). The predicted homologous *Drosophila* enzyme, also named AGPS, was found to have a canonical PTS1 sequence at its C-terminus (Faust et al., 2012). When C-terminal fusions of mCherry to AGPS were constructed to expose a potential PTS2 and mask the PTS1 and expressed in S2 cells, these were found to mislocalize to the cytosol (Faust et al., 2012). However, when mCherry was fused to the N-terminus to expose the canonical PTS1, it strongly overlapped with tagged PMP34, which suggested AGPS utilizes the PTS1 import pathway in *Drosophila* (Faust et al., 2012). In addition, the N-terminus (residues 1-72) of human AGPS (hAGPS) fused to mCherry localizes to peroxisomes in COS-7 cells, mammalian fibroblast-like cells derived from monkey kidney tissue (Jensen et al., 1964), but not in S2 cells (Faust et al., 2012). Faust et al. concluded that, although a PEX7 homologue is conserved in *Drosophila*, their peroxisomes rely solely on the PTS1 import pathway for the transport of cargo into the matrix.

However, *Pex7* dsRNA knockdown does have effects on peroxisome size and number and other peroxisome related activities (Di Cara et al., 2017). Mast et al. reported no effect on the peroxisome population when S2 cells were treated with *Pex7* dsRNA (Mast et al., 2011); however, these differences in what was observed may have been due to dsRNA incubation times. This suggests that despite the absence of a canonical PTS2 trafficking motif, Pex7 has a role in peroxisome activity. The large *Drosophila* community has supported several large-scale efforts to systematically examine the role of each gene in the genome. For example, the MODEncode consortium has performed basic tissue-expression characterization of most *Drosophila* genes (Roy et al., 2010). The expression of *Pex7* was noteworthy in that it was highly expressed in CNS-derived cell lineages (Roy et al., 2010). Similar support for a role for *Pex7* in *Drosophila* comes from unbiased forward-genetic screens. A whole-genome RNAi screen for *Drosophila* mutants that enhance the phenotype associated with fly homologues of genes that are linked to human intellectual disability (Inlow and Restifo, 2004) identified *Pex7*. More recently, Di Cara et al., showed that despite the lack of a canonical PTS2 pathway in *Drosophila*, the *Drosophila* Pex7 can rescue the targeting of the PTS2-containing human thiolase to peroxisomes in *PEX7* mutant human fibroblasts (Di Cara et al., 2018).

1.3.6. Proteins regulating peroxisome dynamics in Drosophila S2 cells

The availability of S2 cells stably expressing the GFP-SKL peroxisome reporter has facilitated several live-cell studies of peroxisome dynamics (Kim et al., 2007; Kulić et al., 2008; Kural et al., 2005). The first systematic RNAi screens in S2 cells expressing GFP-SKL found that peroxisomes require kinesin and cytoplasmic dynein for movement,

as RNAi knockdown of genes encoding either protein abolishes the bidirectional movement of peroxisomes along microtubules (Kim et al., 2007). The overexpression of dominant-negative inhibitors to dynein-dependent processes were found to significantly inhibit peroxisome movement (Kim et al., 2007). Furthermore, it was found that kinesin and dynein are not antagonistic in peroxisome movement, but rather oligomers of each protein cooperatively coordinate peroxisome movement along microtubules *in vivo* (Kural et al., 2005). Kulic et al. monitored peroxisome movement in GFP-SKL S2 cells and found that populations moved in unison over long time frames and showed correlations with microtubule tip positions (Kulic et al., 2008). Two different peroxisome populations were observed: i) relatively stationary peroxisomes that move <100 nm over a 5-second window whose trajectories do not follow microtubule lengths and ii) rapidly moving peroxisomes whose trajectories were parallel to microtubule processes (Kulic et al., 2008). In addition, motor-dependent longitudinal microtubule oscillations affect peroxisome movement throughout the cell (Kulic et al., 2008). Thus, it was concluded that peroxisome mobility is a result of both movement along microtubule tracks and movement of the microtubule tracks themselves (Kulic et al., 2008).

1.3.7. Large-scale protein-interaction screens

The availability of a sequenced genome incorporating validated transcript sequencing has fostered several large-scale mass spectrometry protein interaction studies in flies. This includes the *Drosophila* Protein interaction Map (DPiM) project, based on mass spectrometry of the proteins co-affinity purified from 3,488 different tagged bait proteins expressed in S2R+ cells. DPiM interactions were further scored statistically to

define a high-quality interaction map (Guruharsha et al., 2011). DPiM identified known interactions like Pex5 and Pex14 (Guruharsha et al., 2011). This study also showed high-confidence interactions between Pex5/Pex14 and ribosomal protein S15Ab, β-tubulin at 85D and histone H3.3B (Guruharsha et al., 2011). The significance of these interactions is not currently known. In addition, extensive interaction networks for glutamate oxaloacetate transaminase (GOT1) (*CG8430*) were identified by DPiM, identifying its interaction with SOD1, copper chaperone for superoxide dismutase (CCS) (*CG17753*), as well as ribosomal proteins such as Rps21 (Guruharsha et al., 2011). In a separate study, O'Sullivan et al. reported an interaction between acyl-CoA synthetase long-chain (Acsl), a peroxisomal enzyme, and reticulon-like 1 (Rtnl1) (*CG33113*), a structural protein found in the ER and other organelles such as the lipid droplets (O'Sullivan et al., 2012). This suggests that *Drosophila* peroxisomes may interact with proteins normally found in other organelles like the ER or lipid droplets.

1.3.8. Drosophila as a model for human peroxisome biogenesis disorders

In 2010, Chen et al. reported that peroxisomes are important for spermatocyte development in the testes of *Drosophila* (Chen et al., 2010). Homozygous mutant *Pex2* males showed a growth defect and were sterile (Chen et al., 2010). During normal spermiogenesis, immature spermatids move away from the testis wall and differentiate into mature spermatocytes (Lin et al., 2000). The immature spermatids of the *Pex2* mutants were indistinguishable from the wild-type; however, very few mature spermatoctyes were detected (Chen et al., 2010). The same phenotype was observed in *Pex10* and *Pex12* mutants (Chen et al., 2010), which is consistent with the observation

that Pex2, Pex10, and Pex12 function in a complex during peroxisome biogenesis (Platta et al., 2009). Spermatocytes in the mutants were found to be defective during differentiation with failed cytokinesis during meiotic division. The mutant testes were found to express low levels of nuclear cyclin A, which suggests that the spermatocytes do not reach the G2/M transition during meiosis (Santel et al., 1997). In addition, low levels of *don juan*, a spermatocyte arrest gene (Santel et al., 1997), were detected (Chen et al., 2010). This suggests that peroxisome deficiencies lead to cell cycle arrest in spermatocytes of *Drosophila.* It is possible that a disruption to the energy metabolism due to peroxisome deficiency within the spermatocytes leads to cell cycle arrest. Membrane protein import appears normal in the PEX mutants; however, matrix protein import is dysfunctional as GFP-SKL does not form punctate structures (Chen et al., 2010). Consistent with what is observed in PBD patients, *Pex10* and *Pex12* mutant *Drosophila* had elevated levels of very-long chain fatty acids (VLCFAs), which were increased when flies were raised on a high-fat diet and become even more elevated with age (Chen et al., 2010).

In 2011, Nakayama et al. reported that some pathophysiological effects associated with Zellweger's Syndrome, the most common form of PBD, were mirrored in *Drosophila* with homozygous loss of function *Pex3* or *Pex16* mutations (Nakayama et al., 2011). *Pex3* mutants were homozygous larval lethal, but *Pex16* mutants survived to adulthood (Nakayama et al., 2011; Xia and Wishart, 2011). In order to analyze the peroxisome population in fly tissues, GFP-SKL and CFP- PMP70 were expressed to mark the peroxisome matrix and membrane, respectively (Nakayama et al., 2011). Both signals were absent in the *Pex3* mutant (Nakayama et al., 2011). Both signals were present in the malpighian tubules of the *Pex16* homozygous mutant; however, the

peroxisome number appeared greatly reduced (Nakayama et al., 2011). *Pex16* mutants recapitulated many symptoms of Zellweger's syndrome: growth defects (despite normal feeding rates), reduced lifespans, elevated VLCFA, and locomotor defects (Nakayama et al., 2011). In addition, they also displayed the *rosy* eye color phenotype (Nakayama et al., 2011). Structural defects were also observed in the dendritic trees of the optic lobe (Nakayama et al., 2011). These defects began at the pupal stage, did not worsen after 10 days, and could be rescued by the overexpression of Pex16 in the fat body or specific neurons (Nakayama et al., 2011). In addition, similar to the findings of Chen et al., *Pex16* mutants exhibited arrested spermatocyte development and the absence of mature sperm resulting in male sterility (Nakayama et al., 2011).

Mast et al. analysed the developmental phenotypes associated with a homozygous *Pex1* mutant and found considerable similarities to symptoms of Zellweger's patients with a corresponding null *Pex1* mutation (Mast et al., 2011). Mutant *Pex1* larvae were significantly smaller than their wild-type counterparts and did not survive past second instar (Mast et al., 2011). They also displayed locomotor defects, but showed no defects in their musculature when analyzed by immunofluorescence using muscle-specific antibodies (Mast et al., 2011). When the nervous system was analyzed using neuron-specific antibodies, significant abnormalities were observed in the number of cells and organization of both the peripheral nervous system and the central nervous system, which is likely responsible for the locomotor defects observed (Mast et al., 2011). In addition, the structure of the malpighian tubules appeared abnormal in the *Pex1* mutants (Mast et al., 2011).

In 2017, Wangler et al. isolated *Pex2* and *Pex16* mutants via P-element insertion and found both exhibited similar phenotypes to previously described PEX mutants

(Wangler et al., 2017). Homozygous *Pex2* and *Pex16* mutants had elevated VLCFA, cells with cytoplasmic GFP-SKL in multiple tissues, shortened lifespans, and locomotor defects (Wangler et al., 2017). The authors performed a Metabolite Set Enrichment Analysis (MSEA) (analogous to Gene Set Enrichment Analysis) in which sets of metabolites are explored for enriched alterations (Xia and Wishart, 2011). MSEA revealed an increase in phospholipid precursors, and a corresponding decrease in phospholipid degradation products (Wangler et al., 2017). This suggested a defect in synthesis and a reduction in the breakdown of membrane lipids. MSEA also consistently showed altered carbohydrate metabolism, specifically in the pentose phosphate pathway, starch and sucrose metabolism, and glycolysis (Wangler et al., 2017). When the mutant flies were raised on a low-sugar diet, their lifespan was significantly decreased (Wangler et al., 2017). While wild-type flies showed decreased activity when fed low-sugar food, *Pex2* and *Pex16* mutants showed increased activity (Wangler et al., 2017). Activity was measured as the number of times a particular fly crossed a light beam within a minute. This was proposed to be an elevated foraging response as result of decreased carbohydrate levels. Overall, this suggests that metabolic activity in the peroxisome is intimately linked to carbohydrate metabolism in *Drosophila.*

Mast et al. was the first to use flies to examine the underlying transcriptional response to peroxisome deficiency (Mast et al., 2011). A comparative genome-wide transcriptome analysis between wild-type and homozygous *Pex1* mutant larvae revealed 551 genes that were 3-fold differentially expressed in the *Pex1* mutants (Mast et al., 2011). A gene ontology analysis of these proteins revealed an overrepresentation of genes involved in neural development (Mast et al., 2011), consistent with the observed defects of both the PNS and the CNS. In addition, there were defects associated with other

pathways, such as the antibacterial response, purine base metabolic processes, VLCFA metabolism, developmental hormone response, and eye pigmentation (Mast et al., 2011). Purines were first found in pea leaf peroxisomes, where it was discovered that peroxisomes could catabolize xanthine to uric acid and allantoin (Corpas et al., 1997). In addition, some steroid hormones, such as β-endorphin and β-lipotropin, are localized to peroxisomes in certain human tissues (Weinhofer et al., 2013), which suggests that peroxisomes are involved in hormone metabolism. One other response was genes involved in regulation of alternative RNA splicing, suggesting that this may play a role in peroxisome regulation (Mast et al., 2011). This demonstrates the efficacy of the fly model in probing systemic genetic responses to peroxisome deficiencies.

Changes in peroxisome phenotype have been observed in *Drosophila* mutants of non-peroxisomal genes, shedding new light on the physiological connections between peroxisomes and other organelles. In 2016, Chao, et al. analyzed the effect of perturbing *Dynamin related protein 1* (*Drp1*) (*CG3210*), the homologue of human dynamin-1-like protein (DNM1L), in wandering third instar larvae (Chao et al., 2016). DNM1L is a mitochondrial GTPase protein involved in mediating mitochondrial fission (Chang and Blackstone, 2007). Mutations in DNM1L cause infantile encephalopathy, which is typically characterized as a mitochondrial disease (Uziel et al., 2011). Although overexpression of *Drp1* had no effect, two different point mutations in *Drp1* had a significant effect on the peroxisome population in L3 larvae (Chao et al., 2016). Point mutations in similar regions in DNM1L, A395D and G350R have been previously characterized as disease causing in humans (Chao et al., 2016). Both mutations caused an increase in peroxisome size and altered cellular distribution (Chao et al., 2016). The increase in peroxisome size showed a concomitant decrease in peroxisome number per

cell, which suggests mutant *Drp1* causes a defect in peroxisome fission (Chao et al., 2016).

Acyl-CoA synthetase long-chain family member 4 (ACSL4) is an enzyme involved in lipid metabolism that has two variants: a short-form that is ubiquitously expressed and a long-form that is expressed primarily in the brain (Mercade et al., 2005). Mutations in human ACSL4 are associated with non-syndromic intellectual disability in humans (Longo et al., 2003). In 2016, Huang et al. analyzed the effects of a mutation of the single *Drosophila* gene encoding acyl-CoA synthetase long-chain (Acsl). They found that Acsl localizes to the ER, mitochondria, and peroxisomes in neuronal cells, but localizes primarily to peroxisomes in non-neuronal cells of the *Drosophila* brain (Huang et al., 2016). In addition, the brain lobes of *Acsl* mutants were significantly smaller than wild-type brain lobes, which could be rescued by the overexpression of human ACSL4 (Huang et al., 2016). Homozygous *Acsl* mutants showed disrupted neural synaptic activity, possibly due to a change in the lipid composition of the brains, which suggests that *Acsl* plays a role in regulating these activities, consistent with peroxisome function (Huang et al., 2016).

1.3.9. Identification of novel peroxisome functions using Drosophila

A recent publication by Di Cara et al. revealed novel peroxisome functions by demonstrating that they are involved in the immune response in *Drosophila* (Di Cara et al., 2017). RNAi-mediated targeting of *Pex5* or *Pex7* in S2 cells reduced phagocytosis of bacteria, shown by immunofluorescence, flow cytometry, and transmission electron microscopy (Di Cara et al., 2017). Peroxisome-deficient cells do not exhibit the

membrane protrusions found in wild-type cells when bacteria are being engulfed, which suggests defects in the cytoskeleton (Di Cara et al., 2017). These defects extended to cell motility, as *Pex5* and *Pex7* knockdown cells were unable to repopulate an area in liquid culture as efficiently as their wild-type counterparts (Di Cara et al., 2017). *Pex5* and *Pex7* knockdown cells also show lysosomal defects, as observed lysosomes were larger and fewer, with a mislocalization of Lamp1 (Di Cara et al., 2017), a late endosomal or lysosome marker (Rohrer et al., 1996). In wild-type cells, it was observed that peroxisomes coalesce around the site of phagocytosis when bacteria are being engulfed, which suggests that they play a role in this process (Di Cara et al., 2017). It has been shown that reactive oxygen species (ROS) are involved in signaling for the immune response to bacterial infection (Underhill and Ozinsky, 2002). Pioneering studies in plant cells found the presence of SOD in peroxisomes and they were discovered as sites of superoxide radical production (del Río, 2011; del Río et al., 2006). Wild-type cells showed a 10-fold increase in hydrogen peroxide levels in response to bacterial infection, whereas the hydrogen peroxide response was significantly attenuated in *Pex5* and *Pex7* knockdown cells (2.5-fold) (Di Cara et al., 2017). In addition, steady-state hydrogen peroxide levels in uninfected *Pex5* and *Pex7* knockdown cells were significantly higher than in wild-type cells, which suggests a dysregulation of hydrogen peroxide metabolism (Di Cara et al., 2017). Overexpression of catalase partially rescued the phagocytic defect in *Pex7* knockdown cells but not *Pex5* knockdown cells (Di Cara et al., 2017). In adult flies, knockdown of both *Pex5* and *Pex7* resulted in a lower survival rate in response to infection of both gram-negative and gram-positive bacteria (Di Cara et al., 2017). Anti-microbial peptides (AMP) are produced and secreted when the IMD pathway is activated (Myllymäki et al., 2014). AMP production was not observed in either *Pex5* or *Pex7*

knockdown cells (Di Cara et al., 2017). Together, this identified a new role for peroxisomes in immune cells, activating the immune response to bacterial infection (Di Cara et al., 2017).

1.4. Lipid droplets

Once thought to be simple lipid storage organelles, emerging evidence since their discovery has revealed lipid droplets (LDs) as diverse organelles that carry out an array of cellular and metabolic functions (reviewed in Fujimoto and Parton, 2011). They are highly conserved across all eukaryotic species, but are referred to as oil bodies in plant species (reviewed in Thiam and Beller, 2017). LDs are derived from the ER and consist of a single phospholipid leaflet that surrounds a core consisting of mainly cholesterol esters and neutral lipids in the form of triglyceride (TG) (reviewed in Fujimoto and Parton, 2011). There is some variation amongst the species of lipid found within the LD core depending on the species and cell type (reviewed in Thiam and Beller, 2017). The surface of the LD is also decorated with a host of LD-resident proteins that facilitate many of the metabolic functions that occur at the LD (reviewed in Fujimoto and Parton, 2011). LDs range considerably in size depending on the cell type and the availability of excess lipids. Their primary function is controlling the storage and mobilization of neutral lipids within the cell. These stores serve to provide lipid intermediates and a source of energy through the oxidation of their fatty acyl chains (reviewed in Fujimoto and Parton, 2011).

1.4.1. Lipid droplet biogenesis

In eukaryotes, LD biogenesis occurs at the ER where neutral lipids accumulate to form emulsion droplets that bud off of the ER to form nascent LDs (reviewed in Walther et al., 2017). The precise mechanism of the budding process remains a subject of investigation. The majority of neutral lipid synthesis in eukaryotes occurs at the ER, catalyzed by a host of ER-resident enzymes. The main pathway for TG synthesis, called the Kennedy pathway, uses glycerolphosphate and fatty acyl-CoA to make diglyceride (DG) (Weiss and Kennedy, 1956). The alternate monoacylglycerol pathway occurs in select cell types, whereby monoacylglycerol generated during TG hydrolysis is recycled by re-esterification catalyzed by monoacylglycerol acyltransferase (MGAT) enzymes (Coleman and Haynes, 1985; Yen and Farese, 2003). In either pathway, the final step uses DG to form TG, which is catalyzed by the diacylglycerol acyltransferase (DGAT) enzymes, DGAT1 and DGAT2 (Cases et al., 1998; Lardizabal et al., 2001), two enzymes that are central to TG synthesis. DGAT1 resides at the ER where it catalyzes the esterification of fatty acyl-CoA and DG to generate TG (Cases et al., 1998), although its substrate specificity is not limited to DG (Yen et al., 2005). In addition, DGAT1 helps protect the cell against lipotoxicity caused by excess fatty acids within the cell (Villanueva et al., 2009). In contrast, DGAT2 is found at both the ER and the LD surface where it catalyzes the formation of TG from fatty acid substrates derived from lipogenesis (Villanueva et al., 2009; Wilfling et al., 2013). Cholesterol esters are also

synthesized in the ER during LD biogenesis, catalyzed by acyl-CoA cholesterol acyltransferase in mammals (Oelkers et al., 1998).

As TG is synthesized in the ER, its accumulation begins to form a lens within the phospholipid leaflet (reviewed in Walther et al., 2017). It is unclear how sites of lens formation in the ER are determined, but it is suggested that the curvature of the ER membrane contributes to this. Lens formation occurs at ER tubules where local membrane curvature contributes to the disruption of the phospholipid leaflet (reviewed in Walther et al., 2017). Proteins, such as members of the reticulon family, may also be involved in determining these domains for lens formation in the ER (Hu et al., 2009; Voeltz et al., 2006). It has been shown the depletion of ER proteins that affect ER shape, such as atlastin, leads to aberrations in LD morphology (Klemm et al., 2013). In addition, Fat storage-inducing transmembrane protein 2 (FIT2) binds to lipids such as DG and TG, and may play a role in partitioning neutral lipids during LD formation at the ER (Gross et al., 2011).

Once a sufficient amount of TG has accumulated within the ER leaflet, the nascent LD begins to bud into the cytosol (reviewed in Walther et al., 2017). While some cells form intralumenal LDs, it is unclear what directs the growing bud into the cytosol rather than towards the interior of the lumen for the formation of cytosolic LDs. It has been suggested tension asymmetry across membrane monolayers influences the directionality of the growing bud (Chorlay and Thiam, 2018). As the budding LD continues to grow and the angle between the droplet and the ER membrane increases, scission occurs to release the nascent LD (Thiam and Forêt, 2016). The mechanism of scission is unclear, although it is likely that specific proteins facilitate this process. Not all LDs completely separate from the ER. While most LDs undergo scission from the ER

in mammalian cells (Wilfling et al., 2013), in yeast cells, a substantial proportion of LDs remain in contact with the ER (Jacquier et al., 2011).

Nascent LDs that bud off the ER are called initial LDs (iLDs) and are generally 400 – 800 nm in diameter (Wilfling et al., 2013). A proportion of iLDs are converted to expanding LDs (eLDs), which are characterized by local TG synthesis. As synthesis is carried out and TG is increasingly deposited within the core of the LD, the diameter of the LD consequently increases (reviewed in Walther et al., 2017). Excess fatty acids are taken up by the cell, facilitated by proteins on the cell membrane, such as CD36 (Su and Abumrad, 2009). These fatty acids are then esterified to a glycerol backbone to form TG that is stored in the core of the LD. This localized TG synthesis is catalyzed by a specific isoform of DGAT (DGAT2) and GPAT (GPAT4) (Kuerschner et al., 2008), which appear to relocalize from the ER via ER-LD contract sites.

1.4.2. Protein localization to lipid droplets

The single layer membrane of LDs has a variety of proteins associated with the surface, depending on the cell and tissue type. Targeting of proteins to the LD surface is unique in that, because of its phospholipid monolayer, it does not support the conventional transport of membrane proteins via the ER. This unique biophysical property means that it is energetically unfavorable for transmembrane proteins to reside at the LD surface (reviewed in Kory et al., 2016). Two classes of LD proteins have been described (reviewed in Kory et al., 2016). Class I proteins, such as GPAT4 (Wilfling et al., 2013), are dually localized to the ER and the LD. In the absence of LDs, they are found at the ER. Typically, they are transported with LDs during iLD formation;

however, they can be transported to eLDs from ER-LD contact sites (reviewed in Kory et al., 2016). The transport of proteins via ER bridges to eLDs is dependent on Arf1/COP-1 machinery, which promotes the formation of nanodroplets from the surface in order to reduce phospholipid content (Wilfling et al., 2014). This mechanism is thought to increase the surface tension, allowing an ER-bridge to form. Class I proteins access the LD surface via ER bridges with a hydrophobic hairpin domain that is anchored in the membrane. This domain does not completely span the membrane, allowing its transition from the ER membrane to the LD surface (Wilfling et al., 2014). Mutations in the hydrophobic domain result in LD mislocalization (Abell et al., 2002).

Class II proteins are translated in the cytosol and target the LD surface via hydrophobic regions. Most bind to the LD surface via multiple amphipathic helices and have distinct targeting sequences to the LD (reviewed in Kory et al., 2016). CTP:phosphocholine cytidylyltransferase 1 (CCT1) contains an amphipathic helix that is both necessary and sufficient to target it to the LD surface in *Drosophila* (Krahmer et al., 2011), although, this may be a *Drosophila* specific localization, as CCT1 has not been observed at the LD in mammalian cells (Aitchison et al., 2015). Recent models suggest that the amphipathic helices of class II proteins are unfolded in solution and only refold once they bind to the LD surface, at which point the helices becomes embedded in the membrane with their hydrophilic residues facing the cytosol (reviewed in Seelig, 2004).

Some families of proteins that are localized to the LD surface are affected by protein crowding (Kory et al., 2015). Molecular crowding plays a prominent role in determining the protein composition of LDs, particularly during certain metabolic functions, such as lipolysis. By this mechanism, proteins compete for binding sites on the LD surface (Kory et al., 2015). In addition, it has been shown that some LD proteins,

such as the family of Perilipins (PLINs), compete with other each other or other proteins at the LD surface, which affects protein targeting (Wolins et al., 2006). This competition in turn affects the metabolic activity of the LD.

1.4.3. Lipases

TG molecules contain three fatty acyl chains, which during lipolysis, are hydrolyzed by distinct lipase molecules. Adipose triglyceride lipase (ATGL) catalyzes the first step of lipolysis to generate DG and a free fatty acid (FFA) (Zimmermann et al., 2004). ATGL has a strong specificity for TG molecules with little activity against DG or monoglyceride (MG). However, it has been observed to have some phospholipase activity (Notari et al., 2006). Hormone-sensitive lipase (HSL) can hydrolyze multiple substrates, but during lipolysis, it is the rate-limiting enzyme for the hydrolysis of DG to MG and FFA (Haemmerle et al., 2002). Lastly, monoglyceride lipase (MGL) cleaves the last remaining fatty acyl chain from MG, releasing the glycerol back bone as a by-product (Karlsson et al., 1997). While both ATGL and HSL are highly expressed in adipose tissue, MGL has a fairly ubiquitous expression across tissues (reviewed in Lass et al., 2011). ATGL, HSL, and MGL are the main lipases active during lipolysis; however, other lipases function to catabolise TG. Carboxyl ester lipase is a non-specific lipase that has broad specificity for TG, DG, MG, cholesterol esters, phospholipids, and ceramide (Hui and Howles, 2002; Rudd and Brockman, 1984). Adiponutrin, also known as PNPLA3, also exhibits TG hydrolase activity and has important implications in non-alcoholic fatty liver disease (Winberg et al., 2014). Lysosomal acid lipase (LAL) localizes to lysosomes and late endosomes for the hydrolysis of cholesterol esters and TG

present in low-density lipoproteins and chylomicrons that are taken up by the cell (reviewed in Quiroga and Lehner, 2018; Sauro et al., 1985). Hepatic lipase is synthesized in hepatocytes and secreted into the circulation where it hydrolyzes TG and phospholipids in high-density and intermediate-density lipoproteins (reviewed in Quiroga and Lehner, 2018). *Drosophila* specific lipases are described in section 1.5.3, and outlined in Figure 1.3 (page 44).

1.4.4. Perilipins

The PLINs are the major LD-associated family of proteins. PLINs serve as the major regulators of lipid storage and mobilization in the LD. They lack a putative transmembrane domain, and it remains unclear how they interact with the LD surface, although, a recent study showed the presence of 11-mer repeats that formed amphipathic helices that were necessary for binding PLINs to micelles and LDs (Rowe et al., 2016). There are five known PLIN family members, with PLIN1 and PLIN2 being the most conserved across species (reviewed in Itabe et al., 2017; Kimmel et al., 2010).

PLIN1 was initially discovered as a heavily phosphorylated protein in white adipose tissue (Blanchette-Mackie et al., 1995). It is primarily expressed in adipocytes and resides on the LD surface (Blanchette-Mackie et al., 1995). Under basal conditions it is bound to Comparative gene identification 58 (CGI-58) (Yamaguchi et al., 2004), which is an activator of ATGL. When lipolysis is initiated, a signalling cascade causes the phosphorylation of PLIN1, which releases CGI-58 (Yamaguchi et al., 2007) and recruits HSL to the LD surface (Wang et al., 2009).

PLIN2 was originally named “adipose differentiation-related protein” because of its observed induction during early adipocyte differentiation (Jiang and Serrero, 1992). However, it was later discovered that PLIN2 is ubiquitously expressed across multiple cell and tissue types (reviewed in Itabe et al., 2017). Early studies showed that overexpression of PLIN2 in COS-7 cells and fibroblasts results in LD accumulation (Gao and Serrero, 1999; Imamura et al., 2002). PLIN2 is also upregulated in cells that are supplemented with fatty acids, which in turn are stored as TG (reviewed in Itabe et al., 2017). This suggested that PLIN2 promotes LD formation and serves to protect TG stores from lipolysis at the LD. Like some peroxisome proteins, its expression is also regulated by peroxisome proliferator-activated receptor α (PPARα) signaling in various cell types (Dalen et al., 2006). PLIN2 protein levels contribute to the maintenance of TG stores within LDs, as degradation of PLIN2 by the proteasome leads to depletion of TG levels via lipolysis (Kaushik and Cuervo, 2015).

1.4.5. Regulation of lipolysis

Lipolysis is the process by which neutral lipids stored within LDs are hydrolyzed to release free fatty acids. A signaling cascade causes the hydrolytic cleavage of the fatty acyl chains of TG molecules, and the resulting free fatty acids can then be oxidized in other organelles, such as mitochondria or peroxisomes (reviewed in Lass et al., 2011). These FFAs can also be re-esterified to glycerol to produce TG for storage. The balance of fatty acid re-esterification and oxidation is affected by the cellular concentration of FFAs (Langin, 2006).

In adipose cells, lipolysis is initiated by hormonal β-adrenergic stimulation resulting in a signaling cascade that activates cAMP-dependent protein kinase A (PKA). PKA phosphorylates PLIN1 at the LD surface, which causes the dissociation of CGI-58 from PLIN1 (Granneman et al., 2007; Zimmermann et al., 2004). CGI-58, also called α/β hydrolase domain containing protein 5, is a highly conserved activator of ATGL. Under basal conditions, it is bound to PLIN1 at the LD surface and is released upon lipolytic stimulation. CGI-58 can then interact with ATGL on the LD surface and activate its lipase activity (Lass et al., 2006). Maximal stimulation occurs at equimolar concentrations between ATGL and CGI-58 (Lass et al., 2006). It is unclear what the mechanism of activation is; however, direct protein-protein interaction between the two proteins is required (Lass et al., 2006). However, protein-protein interaction is not sufficient: CGI-58 must also be bound to the LD surface to activate ATGL (Gruber et al., 2010). CGI-58 contains an unstructured region found at its N-terminus that is responsible for LD-localization and ATGL activation (Gruber et al., 2010). ATGL is also phosphorylated at two sites, however, it remains unclear how this phosphorylation affects its activity. The known phosphorylation sites do not seem to affect LD localization or TG hydrolysis (Duncan et al., 2010). It has also been shown in HeLa cells that the delivery of ATGL to the LD surface depends on vesicular transport machinery and its protein components, like Arf1 and protein coatamers COPI and COPII. In their absence, ATGL remained localized at the ER (Soni et al., 2009).

ATGL is negatively regulated by G0/G1 switch gene 2 (G0S2), a highly conserved and ubiquitously expressed protein that was originally identified as a cell-cycle regulator (reviewed in Heckmann et al., 2013). G0S2 is highly expressed in adipocytes, and its overexpression causes massive lipid accumulation (Yang et al., 2010). In addition,

its expression is inhibited by lipolytic stimulators, such as TNFα (Yang et al., 2010). G0S2 directly interacts with the N-terminus of ATGL, although this interaction is not competitive with CGI-58 (Yang et al., 2010). The enzymatic function of ATGL is also inhibited by PLIN2, which coats the surface of the LD and serves to block ATGL from accessing TG molecules within the core of the LD (Granneman et al., 2007).

HSL is primarily regulated by phosphorylation. β-adrenergic stimulated PKA phosphorylates HSL, which increases its enzymatic activity and allows it to interact with PLIN1 at the LD surface. HSL has five sites which can by phosphorylated by other kinases besides PKA (reviewed in Lass et al., 2011). MGL is present at relatively high levels across most tissue; however, the mechanism of regulation is unclear (reviewed in Lass et al., 2011).

1.5. Lipid droplets in *Drosophila melanogaster*

1.5.1. Lipid metabolism in Drosophila melanogaster

Fly development is characterized by large changes in lipid storage and mobilization. During oogenesis, large amounts of LDs are synthesized by the mother and eventually deposited into the developing egg to supply energy and membrane substrate for the developing embryo. Impairments in this process lead to developmental arrest or death of the embryo (Grönke et al., 2005). The stages of larval development are mainly dedicated to feeding and accumulating mass, whereby large amounts of lipid are stored in

the fat body, the *Drosophila* equivalent of adipose tissue. For example, the fat content of the larvae dramatically increases during development, followed by a 3-fold reduction during pupariation (Church and Robertson, 1966). Stored lipids are required to provide the energy needed to support the dramatic tissue remodeling that occurs during *Drosophila* development. The fat body contains numerous LDs of varying size, which represent an important caloric source during the development of the animal. LDs within the fat body can be as large as tens of micrometres in diameter (reviewed in Kühnlein, 2012). Other larval tissues, such as the malpighian tubules, the gut, and imaginal discs, also contain a number of smaller LDs. During pupal metamorphosis, larval tissues are disintegrated and replaced by adult tissues. During this process, LDs are collected in the adult fat body. From this stage forward, the adult fat body contains the majority of the LDs in the body (DiAngelo and Birnbaum, 2009).

1.5.2. Lipid biosynthesis in Drosophila melanogaster

TG biosynthetic pathways are well conserved in *Drosophila*. The *Drosophila* genome encodes a single homologue of the mammalian mitochondrial GPAT1 and GPAT2 (*CG5508*) which catalyzes the initial steps of TG biosynthesis. *CG5508* is highly expressed throughout *Drosophila* development and is particularly enriched in the adult fat body (Gelbart and Emmert, 2011). Overexpression of *CG5508* in the salivary glands causes massive LD accumulation (Tian et al., 2011). The *Drosophila* genome also has homologs of mammalian ER-localized GPAT3 and GPAT4, encoded by *CG3209* and *CG15450,* respectively. *CG3209* is expressed ubiquitously while *CG15450* is testis-specific. However, both genes remain functionally uncharacterized (Chintapalli et al.,

2007). *CG3812* and *fu12* encode the *Drosophila* homologs of the mammalian AGPAT1 and AGPAT2, which catalyze the second step of TG biosynthesis. Both genes are also not functionally characterized; however, *fu12* in highly expressed in the fat body (Chintapalli et al., 2007). While in mammals, the third step of TG biosynthesis is catalyzed by three different lipins, *Drosophila* has a single homologue, *CG8709.* This gene is also functionally uncharacterized; however, it does contain characteristic lipin domains (Valente et al., 2010). In addition, *CG8709* has been shown to be critical for adipose tissue development and to control the size and morphology of LDs in *Drosophila* larvae (Ugrankar et al., 2011). Moreover, *CG8709* is highly expressed in tissues that contain substantial LDs, such as the fat body, malpighian tubules, and the gut (Ugrankar et al., 2011).

The final step of TG biosynthesis in *Drosophila* is catalyzed by *midway (mdy),* which encodes the homologue of DGAT1 in *Drosophila.* Recombinant *mdy* has been shown to possess DGAT1 activity (Buszczak et al., 2002). The *mdy* gene is highly expressed in the adult fat body, but also shows broad expression across all tissues (Gelbart and Emmert, 2011). In addition, *mdy* hypomorphic mutants are female sterile due to deficient lipid loading in the developing oocyte (Buszczak et al., 2002), and adult flies with impaired *mdy* activity are lean (Beller et al., 2010). Overexpression of *mdy* in larval salivary glands causes massive LD accumulation (Tian et al., 2011). In mammals, DGAT2 is found at the LD surface for localized TG synthesis in eLDs. While a putative DGAT2 homologue has yet to be identified in *Drosophila*, its genome encodes three DGAT family members that have yet to be functionally characterized: *CG1941, CG1942,* and *CG1946* (reviewed in Kühnlein, 2011). All three genes are expressed in the gut and fat body (Gelbart and Emmert, 2011). While more primitive insect species have only one

DGAT, this is likely not the case for *Drosophila* as DGAT2 is essential for localized TG synthesis in the formation of larger LDs, which are found in many fly tissues. It is possible that one of the uncharacterized DGAT family members encodes the putative DGAT2.

1.5.3. Lipases in Drosophila melanogaster

The proteins required for lipid mobilization are well conserved in *Drosophila*. The *Drosophila* ATGL homologue, *Brummer* (*Bmm*), plays a central role in both basal and stimulated lipolysis (Grönke et al., 2005; 2007). *Bmm* has a paralog, Doppelgänger von brummer (Grönke et al., 2005). Like ATGL, Bmm associates with the LD surface and controls TG mobilization (Grönke et al., 2005). Overexpression of *Bmm* protects flies from lipid accumulation caused by a high-fat diet (Birse et al., 2010) and conversely, results in large LD accumulations when knocked down in cells (Guo et al., 2008). *Bmm* expression is induced by starvation (Grönke et al., 2005), and its expression is repressed by *target of rapamycin* (*TOR*), which acts as a nutrient sensor (Luong et al., 2006). *Drosophila* Hsl is encoded by *CG11055.* Hsl was found to be a part of the embryonic LD proteome (Cermelli et al., 2006), and it accumulates on the surface of LDs in starved larval fat body cells (Bi et al., 2012). Interestingly, epitope-tagged Hsl does not localize to the surface of LDs under starvation conditions in *Lsd1* mutants (Bi et al., 2012), which suggests that Lsd1 is required for targeting Hsl to the LD surface. Currently, a putative Mgl has not yet been identified in *Drosophila.* The regulation of lipolysis in *Drosophila* is outlined in Figure 1.3.

Figure 1.3

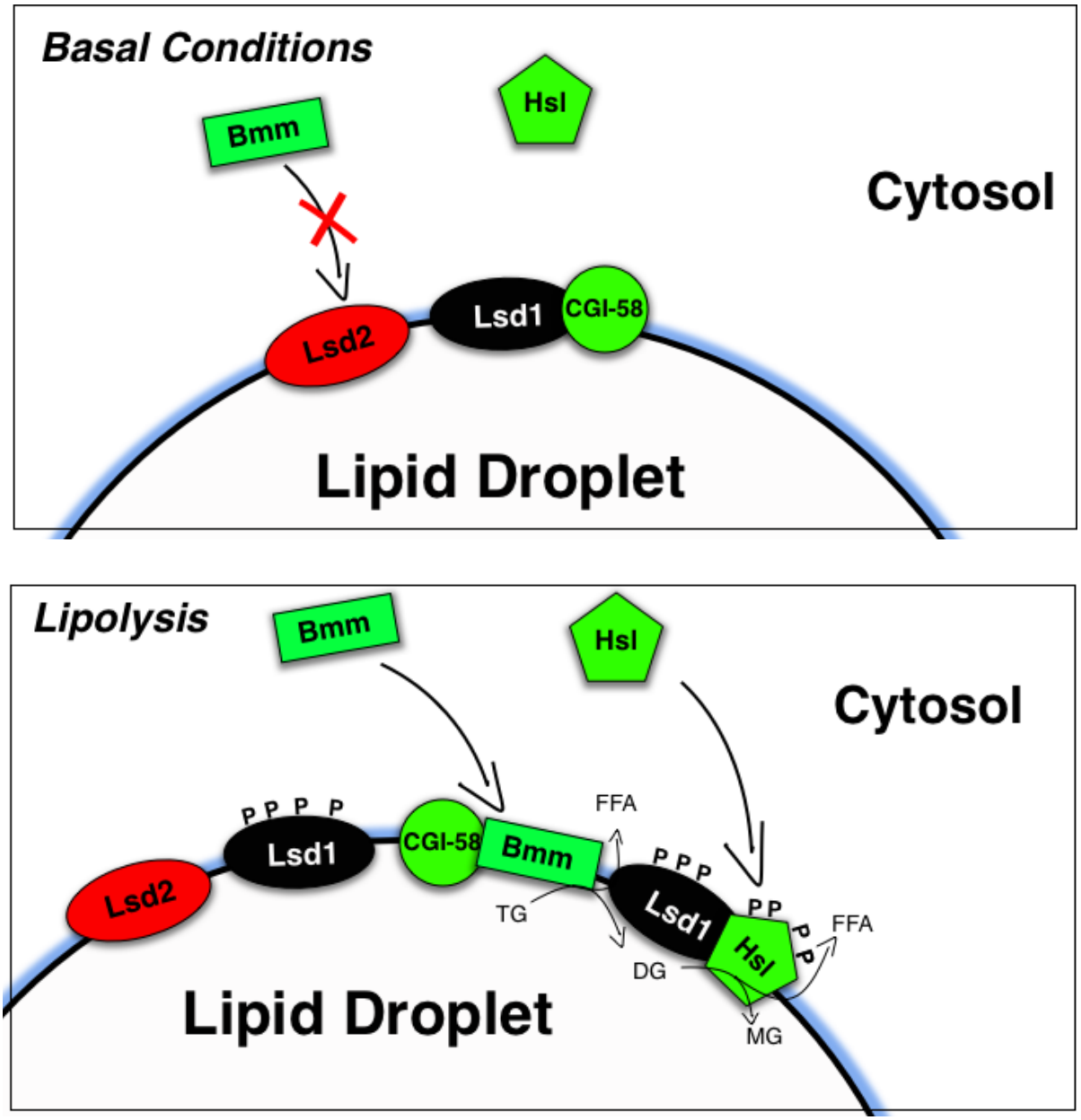
Basal Conditions
Bmm
Hsl
Cytosol
Lsd2
Lsd1
CGI-58
Lipid Droplet
Lipolysis
Bmm
Hsl
Cytosol
P P P P
Lsd1
CGI-58
Bmm
FFA
Lsd2
TG
P P P
Lsd1
P P
Hsl
P P
FFA
DG
MG
Lipid Droplet

Figure 1.3. Regulation of lipolysis in *Drosophila melanogaster*. Under basal conditions, Lsd2 blocks cytosolic lipases from the LD surface. In addition, Lsd1 is bound to CGI-58 at the LD surface. During lipolysis, a signalling cascade causes the phosphorylation of Lsd1, which releases CGI-58, which recruits Bmm to the LD surfaces and catalyzes the hydrolysis of TG to DG, releasing an FFA. Hsl is also phosphorylated and recruited to the LD surface by phosphorylated Lsd1. Hsl catalyzes the hydrolysis of DG to MG, releasing another FFA.

1.5.4. Perilipins in Drosophila melanogaster

There are two members of the PLIN family in *Drosophila*: *PLIN1* and *PLIN2*, which are also called *Lsd1* and *Lsd2*, respectively (reviewed in Kühnlein, 2012). Both have been shown to modulate lipid storage in *Drosophila.* Studies have revealed that Lsd1 is the target of PKA phosphorylation (Arrese et al., 2008), and the phosphorylated form of Lsd1 plays an essential role in promoting lipolysis (Beller et al., 2010). Moreover, Bi et al. showed that Lsd1 is essential for Hsl to target the LD surface (Bi et al., 2012), consistent with the mammalian function of PLIN1. Lsd2 protects TG stores in the LD from Hsl and Bmm in the cytosol (Bi et al., 2012). *Lsd2* mutant flies are lean, whereas overexpression of *Lsd2* results in massive LD accumulation (Teixeira et al., 2003). The regulation of lipolysis in *Drosophila* is outlined in Figure 1.3.

1.5.5. Lipid metabolism in macrophages and S2 cells

S2 cells are thought to be derived from a macrophage-like lineage (Schneider, 1972). Cell of a macrophage lineage must be able to handle rapid spikes of lipids acquired via phagocytosis of dead cells. Dysfunctional lipid metabolism in mammalian macrophages leads to various pathologies, such as pulmonary alveolar proteinosis (reviewed in Remmerie and Scott, 2018), which is characterized by an accumulation of lipoprotein compounds derived from surfactant (Shah et al., 2000). Lipids are taken up by macrophages via plasma membrane receptors, such as CD36, and degraded in the lysosome via LAL (reviewed in Remmerie and Scott, 2018). This generates FFA, which is usually oxidized in the mitochondria. In addition, macrophages can take up acetylated LDL particles by endocytosis and pinocytosis (Jones et al., 2000), which, if not

eliminated properly, results in the formation of foam cells (reviewed in Remmerie and Scott, 2018). Free cholesterol that is generated at the lysosome via LAL is effluxed at the plasma membrane or it is used to form cholesterol fatty acid esters at the ER, which are stored in the LD and make up the "foam" of the foam cell (Maxfield and Tabas, 2005). Foam cells are either degraded through the de-esterification and subsequent secretion of cholesterol esters, or localized foam cell formation leads to the formation of plaques (Yu et al., 2013).

Mammalian macrophages display unique tissue-specific epigenetic features, which result in specialized transcriptional profiles (Lavin et al., 2014; Scott et al., 2016). These unique profiles suggest that macrophages in mammals have tissue-specific functions. Although all macrophage lineages take up and process lipids, lipid metabolism is considered "accessory" as not all lineages are particularly active in this function. For example, lung alveolar macrophages and liver Kupffer cells are transcriptionally enriched with lipid metabolic genes (Gautier et al., 2012; Scott et al., 2016). The ability of alveolar macrophages to process lipids that are taken up through the phagocytosis of dead cells is critical to proper lung function. This is highlighted by the pathologies that result from defective or absent lipid metabolism in these macrophages (Kitamura et al., 1999; Suzuki et al., 2008). Kupffer cells in mice show an upregulation of lipid metabolism and bile acid signalling genes in response to dietary fat and cholesterol, whereas macrophages derived from bone-marrow do not (McGettigan et al., 2017). PPARγ is highly expressed in both alveolar macrophages and Kupffer cells and has been suggested to control the inflammatory potential of these cells (Gautier et al., 2012; Scott et al., 2016). Fatty acids can act as PPAR agonists and activate PPAR, which induces a transcriptional response in

macrophages (reviewed in Grygiel-Górniak, 2014). This leads to the upregulation of lipid metabolic genes in macrophages.

Certain types of mammalian macrophages are highly inflammatory and microbicidal, characteristics that are linked to elevated production of ROS (reviewed in Remmerie and Scott, 2018). ROS are a by-product of lipid oxidation and the burst of reactive oxygen species has been shown to be necessary for engulfment of bacteria during infection in S2 cells and *Drosophila* hemocytes (Di Cara et al., 2017). In addition, it has been shown that supplementing mammalian macrophages with saturated fatty acids provokes an immune response and inflammation attenuates oxidative metabolism (Namgaladze and Brüne, 2016).

S2 cells have been extensively used for studies of LD biology (Beller et al., 2006; Guo et al., 2008; Kory et al., 2015; Krahmer et al., 2011; Sui et al., 2018; Wang et al., 2016; Wilfling et al., 2013, 2014). Under standard culture conditions, S2 cells contain few LDs, but rapidly form LDs that are detectable by light microscope when the culture media is supplemented with fatty acids. For example, S2 cells are cultured with 1 mM oleate, they form many small LDs that are easily visible after 24 hours (Guo et al., 2008). This is standard for LD studies in S2 cells.

S2 cells have been used in RNAi screens for LD phenotypes (Beller et al., 2010; Guo et al., 2008). S2 cells are highly amenable to RNA interference using dsRNA, with targeted genes showing an average of 80-90% knockdown (Ulvila et al., 2006). In addition, dsRNAs amplicons used in *Drosophila* are hundreds of base pairs long and are processed to smaller siRNAs once inside the cell. Compared to the 21-23 base pair dsRNA amplicons used in mammalian systems, this reduces off-target effects (Ulvila et al., 2006).

Guo et al. utilized S2 dsRNA screening to identify novel regulators of LDs by scoring changes in LD size, number, distribution, and morphology after knockdown of a particular gene by dsRNA. With their analysis, 227 genes were identified that affect LD biology, many of which were previously unidentified (Guo et al., 2008). This means that approximately 1.5% of the *Drosophila* genome is involved in LD formation and regulation. These were sorted into five classes based on distinct LD phenotypes that were visually scored. Many of the genes found to affect LDs were involved in phospholipid biosynthesis and vesicular transport (Guo et al., 2008), which present previously unidentified regulators of LD biology.

1.6. Known connections between peroxisomes and lipid droplets

Given that both peroxisomes and LDs are critical organelles for lipid metabolism, it is thought that these organelles likely coordinate their metabolic functions. Recent lines of evidence have revealed intimate physical connections between peroxisomes and LDs. Binns et al. found that yeast cells cultured in the presence of oleate have peroxisomes that are in direct contact with the surface of LDs (Binns et al., 2006). Moreover, these peroxisomes have extensions, termed "pexopodia", that protrude into the core of the LD. A proteomic analysis of these cells found peroxisomal β-oxidation enzymes within the LD fraction (Binns et al., 2006). It is thought that as particular species of fatty acids are produced during TG hydrolysis, they are directed into adjacent peroxisomes for oxidation. Similar observations have been made in COS-7 and HepG2 cells expressing

GFP-PTS1, whereby peroxisomes were found in close association with LDs (Schrader, 2001). Immunogold staining using an anti-catalase antibody in 3T3-L1 adipocytes and mouse epididymal white adipose tissue revealed dumbbell-shaped peroxisomes near the periphery of LDs (Blanchette-Mackie et al., 1995). Lastly, protein-protein interactions have been observed between peroxisomal proteins and LD resident proteins using a bi-molecular fluorescence complementation assay. In this study, multiple PEX proteins were found to interact with LD proteins Erg6 and Pet10 in yeast cells (Pu et al., 2011).

Other physiological links between peroxisomes and LDs in whole animals have been established. Martens et al. generated *Pex5* knockout mice with dysfunctional peroxisomes in the adipose tissue and the central and peripheral nervous system (Martens et al., 2012). These mice exhibited dysfunctional adipose tissue as a result of decreased lipolysis and increased fat mass. Reduced levels of adrenaline and noradrenaline in circulation were also detected (Martens et al., 2012). This likely contributed to decreased lipolytic levels as beta-adrenergic signalling stimulates lipolysis.

Bülow et al. generated *Drosophila Pex19* mutants, which recapitulated many of the hallmarks of PBDs, including elevated VLCFAs, neurodegeneration, and decreased survival rates (Bülow et al., 2018). In addition, *Pex19* mutants showed elevated levels of lipolysis and decreased lipid stores in the fat body. This was likely a consequence of elevated *Lipase3*, which showed a 250-fold increase in expression relative to the wild-type control (Bülow et al., 2018). Lastly, mitochondrial defects were also observed in the *Pex19* mutant, which was attributed to aberrant levels of fatty acid oxidation in the mitochondria (Bülow et al., 2018).

1.7. Hypothesis and rationale

While there is correlative evidence that peroxisomes and LDs interact to coordinate lipid metabolism, little is known about the mechanisms of these interactions. Given the importance of these two organelles in cellular lipid metabolism, deciphering how they communicate will have significant impacts on how diseases like lipodystrophies and PBDs are understood.

This thesis presents experiments testing my hypothesis that components of the peroxisome regulate lipid metabolism at the LD in *Drosophila*. In addition, I hypothesize that peroxisome biogenesis and enzyme trafficking is conserved between *Drosophila* and other organisms.

I found that the majority of the peroxins, PMPs, and enzyme homologues in *Drosophila* localized to peroxisomes in S2 cells. Knockdown of several peroxins confirmed a functional conservation. I also found that Pex13 and Pex14 are targeted to the surface of LDs during times of increased LD metabolism. Knockdown of *Pex14* results in smaller, more numerous LDs and increased lipolytic activity in S2 cells. These phenotypes were also observed in *Drosophila* larvae when *Pex14* was knocked down in the fat body. In addition, overexpression of *Pex14* disrupts the targeting of Hsl to the LD surface during lipolysis and conversely, overexpression of *Lsd1* blocks the targeting of Pex14 to the LD surface during lipolysis. Lastly, knockdown of *Pex14* results in differential expression and localization of CGI-58 in lipolytic S2 cells. Altogether, I propose a model whereby Pex13/Pex14-containing vesicles are targeted directly to LDs

during periods of increased lipid metabolism and serve to regulate the flux of lipids stored in LDs.

Chapter 2: A systematic cell-based analysis of localization of predicted *Drosophila* peroxisomal proteins

This chapter has been published as: **Baron, M.N., Klinger, C.M, Rachubinski, R.A., and Simmonds, A.J.** (2016). A Systematic Cell-Based Analysis of Localization of Predicted *Drosophila* Peroxisomal Proteins. Traffic *17*, 536 – 553.

2.1. Abstract

A previous sequence-based comparison of the predicted proteome of *Drosophila melanogaster* to human proteins identified 82 potential homologues of proteins involved in peroxisomal biogenesis, homeostasis or metabolism. However, the subcellular localization of these proteins relative to the peroxisome was not determined. Accordingly, I systematically tested the localization and selected functions of epitope-tagged proteins in *Drosophila* Schneider 2 cells to determine the subcellular localization of the 82 potential *Drosophila* peroxisomal protein homologues. Excluding the PEX proteins, 34 proteins localized primarily to the peroxisome, eight showed dual localization to the peroxisome and other structures, and 26 localized exclusively to organelles other than the peroxisome. In addition, the effect of overexpression of each of the 82 genes on the peroxisome phenotype was analyzed. This work establishes a basic understanding of peroxisome protein localization in *Drosophila*. This work will facilitate the use of *Drosophila* as a genetically tractable, multicellular model system for studying key aspects of peroxisome biology and how they function in cellular lipid metabolism.

2.2. Background

Much of our current knowledge of the functions of peroxisomes and how they are assembled has come from studies of yeast and mammalian cell culture. However, there is a need for alternative laboratory models for PBDs, particularly genetically tractable multicellular models. Specific peroxin deficiencies have been examined in a variety of organisms, including nematode, fruit fly, zebrafish and mouse (reviewed in Van Veldhoven and Baes, 2013). Overall, the peroxisome assembly pathway is relatively well conserved from yeast to human. However, there are differences in peroxisome formation and function between these species (reviewed in Van Veldhoven and Baes, 2013). For example, in yeast and human, a minority of matrix proteins relies on the PTS2 pathway for import into the peroxisome (reviewed in Smith and Aitchison, 2013). PEX7/Pex7p recognizes PTS2 cargo in the cytosol and delivers it to the peroxisomal matrix after docking at the peroxisomal membrane (Marzioch et al., 1994; Zhang and Lazarow, 1995). An exception is *Caenorhabditis elegans* (a nematode), which lacks both a PEX7 homologue and proteins with a canonical PTS2 signal. In *C. elegans*, homologues of PTS2-containing proteins in other species instead contain a PTS1 (Motley et al., 2000). PTS1 is recognized in the cytosol by the soluble cargo receptor, PEX5, which in a manner akin to that of PEX7, delivers its cargo to the peroxisomal matrix following docking at the peroxisomal membrane (Van der Leij et al., 1993; Purdue and Lazarow, 1996). No *bona fide* PTS2-containing cargo protein has been identified in *Drosophila* (Faust et al., 2012), even though a presumptive *Pex7* gene is present in the genome. Differences in targeting pathways for homologous peroxisomal proteins in different

organisms highlight the need for improved understanding of peroxisome biology in different organisms.

Drosophila melanogaster is a readily tractable organism to model many human disorders (reviewed in Pandey and Nichols, 2011), including the PBDs (Mast et al., 2011). However, while previous studies (Faust et al., 2012; 2014; Mast et al., 2011) have established specific homologues of PEX and other peroxisomal enzyme genes, in general, the overall functional conservation of these pathways in *Drosophila* has not been tested. Previous *in silico* comparison of the human and *Drosophila* genome sequences identified a group of 82 potential *Drosophila* homologues of human peroxisome-associated genes from a query encompassing 112 human peroxisomal protein sequences (Faust et al., 2012). However, only a few of the potential peroxisomal proteins identified by this computer-based analysis were functionally tested for peroxisomal localization or function. Therefore, I performed a comprehensive screen in S2 cells aimed at evaluating the subcellular localization of the proteins encoded by all these genes. Using a combination of live-imaging via protein fusions to red fluorescent protein (RFP) or, where appropriate, to a small FLAG epitope, I evaluated the specific localization of each candidate peroxisomal protein. The localization of each was examined *vis-à-vis* peroxisomes labeled with GFP tagged at its C-terminus with the canonical PTS1, Ser – Lys – Leu (GFP-SKL). This evaluation included a basic functional analysis of the consequences of overexpression, and in some cases knock down, of these genes by measuring changes in peroxisome volume and number. The data showed that most of the proteins predicted to be involved in peroxisome biogenesis or function in *Drosophila* localize to the peroxisome, while a few proteins localize to the peroxisome and another

subcellular compartment. In addition, the PTS1 and membrane protein import pathways seem relatively well conserved in *Drosophila,* while the PTS2 import pathway does not.

2.3. Results

2.3.1. The majority of Drosophila Pex proteins localize to peroxisomes in S2 cells

I first characterized the cellular localization of the predicted *Drosophila* homologues of the known peroxins. Previous functional assays for Pex function using dsRNA-based knock down have been shown to alter peroxisome protein targeting in *Drosophila* S2 cells stably expressing the fluorescent reporter, GFP-PTS1 (Mast et al., 2011). In S2 cells, the GFP-PTS1 reporter (Wiemer et al., 1997) marks the majority of endogenous peroxisomes. This was confirmed by immunofluorescence detection of peroxisomes with an anti-SKL antibody, as a positive control (Figure 2.1). In addition, at this time there were no antibodies available to any *Drosophila* peroxisome proteins that could be used as an alternative peroxisome marker. It is possible that overexpression of some of the proteins examined could affect GFP-PTS1 import; however, without a suitable alternative, GFP-PTS1 was the most appropriate peroxisome marker available. As a negative control, RFP-Gawky (Gw) was transfected into GFP-SKL S2 cells. Gw localizes to cytoplasmic mRNA processing bodies (Schneider et al., 2006), which appear as punctate cytoplasmic structures that do not overlap with the peroxisome marker (Figure 2.1).

To analyze the subcellular localization of each predicted *Drosophila* Pex protein, I expressed the open reading frame for each candidate gene as a fusion to a sequence

Figure 2.1

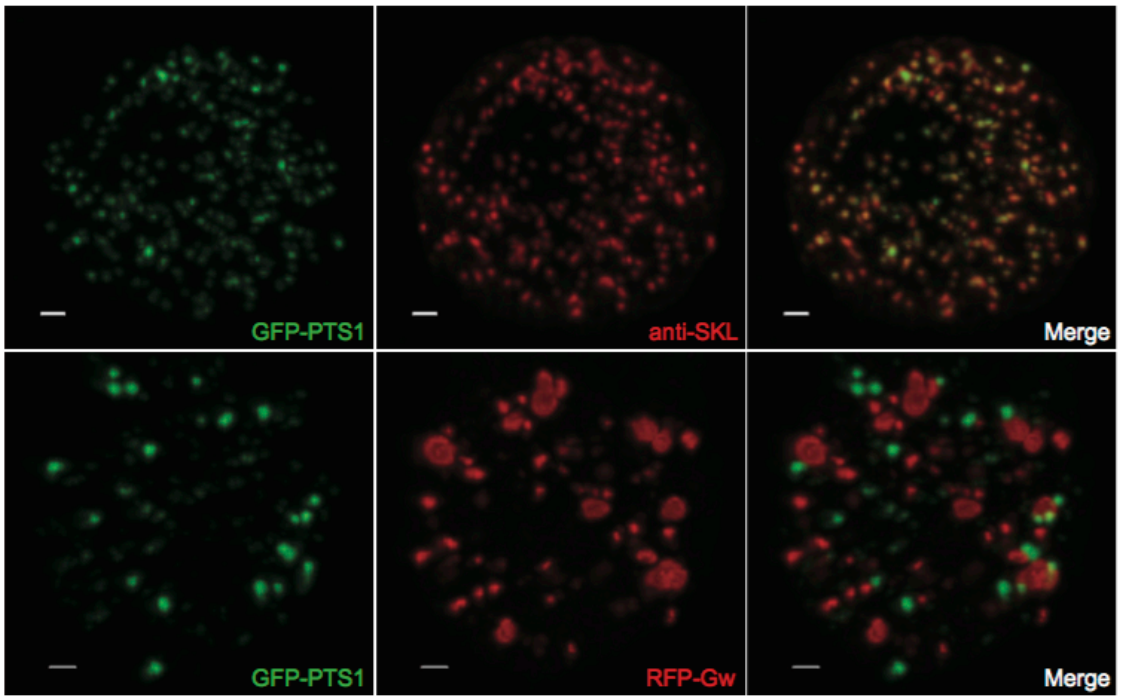

Figure 2.1. Extent of colocalization between the signals for GFP-PTS1 and anti-SKL (positive control) or RFP-Gw (negative control). Top panels show S2 cells stably expressing GFP-PTS1 (panels at left). Cells were fixed in 4% paraformaldehyde and probed with an anti-SKL antibody and a red fluorescent secondary antibody (top middle panel). Overlap between the GFP-PTS1 and anti-SKL signals is indicated by yellow in the merge (top right panel). Bottom panels show S2 cells stably expressing GFP-PTS1, shown in green (bottom left panel), and transfected with plasmid encoding the Gw protein fused to mRFP, which localizes to punctate structures in the cytosol (bottom middle panel). The merged image (bottom right panel) shows limited overlap between the GFP and mRFP signals. Each image is a maximum projection of a three-dimensional volume encompassing the entire cell. The scale bar represents 1 μm.

encoding RFP at the N- or C-terminus of the protein. Appending RFP to proteins can sometimes cause aberrant protein aggregation or mislocalization in the cell due to steric hindrance (Huang et al., 2014) or compromised protein folding (Huang et al., 2014; Wang et al., 2010) resulting from the relatively large size of RFP, RFP-tagged proteins that did not colocalize with GFP-PTS1-labeled peroxisomes were re-tested as N- and C-terminal fusions to a 3xFLAG epitope [roughly 2.8 kDa (Miceli et al., 1994)].

The degree of colocalization between the signal for a tagged candidate protein and GFP-PTS1-labeled peroxisomes was measured using Pearson's coefficient and expressed as a percentage (Figure 2.2.A). The Pearson's correlation coefficient (PCC) measures the pixel-to-pixel covariance between two signals (Dunn et al., 2011). A value of +1.0 indicates perfect correlation, whereas a value of -1.0 indicates a perfectly negative correlation, and a value of 0 denotes no relationship between the two signals. Because the PCC uses the mean intensity of a signal, it is unaffected by differences in the signal intensity of each pixel and therefore, the signal offset (Dunn et al., 2011). For all measured Pearson's calculations, each cell was measured individually and extracellular space was eliminated from the measurements, as pixels lacking either signal can inflate the PCC value (Dunn et al., 2011).

While other methods of measuring colocalization exist, such as Mander's overlap coefficient (MOC) (Manders et al., 1993), the PCC was chosen as the appropriate measure of colocalization between predicted peroxisomal proteins and the peroxisome marker. Several experimentally observed deficiencies have been observed with MOC (Adler and Parmryd, 2010; Dunn et al., 2011). One concern is that the MOC is highly sensitive to background signal. This can be cumbersome to remove as background "noise" can be variable within an image and may require background levels to be

determined locally (Dunn et al., 2011). In particular, because many of the proteins being examined do not have an experimentally determined subcellular localization, the signal from proteins that localize to the cytosol may be considered background and could cause spurious MOC measurements. In addition, the MOC is sensitive to offset, which, if not set correctly, can have significant effects on MOC measurements (Adler and Parmryd, 2010). It was found that the PCC reports a 0 value when no relationship is observed between two signals, while a 0 value for the MOC is only reported when the two signals are completely exclusive from one another (Adler and Parmryd, 2010). This can cause false positives. In fact, it was found that when pixels from two signals were randomly shuffled, an MOC of 0.6 could still be produced, whereas this reduced the PCC to a 0 value, indicating no relationship (Adler and Parmryd, 2010).

GFP-PTS1 labeled essentially all peroxisomes, as colocalization between the anti-SKL signal and the GFP-PTS1 reporter was 84.2%. As a negative control, S2 cells stably expressing GFP-PTS1 were transfected with RFP-Gawky, a component of cytoplasmic mRNA processing bodies (Schneider et al., 2006). The degree of colocalization between GFP-PTS1 and RFP-Gawky was 4.8%. This value provided a basal background level resulting from two signals that should not colocalize and appear completely distinct from one another. The average percent colocalization of tagged candidate Pex proteins with GFP-PTS1 is shown in Figure 2.2A and summarized in Table 2.1. Predicted *Drosophila* homologues to the peroxisomal biogenesis factors Pex1, Pex2, Pex10, Pex11A/C, Pex11C, Pex12, Pex13, Pex14 and Pex16, which have been shown in other organisms to be localized to peroxisomes, also showed strong colocalization with the peroxisomal GFP-PTS1 signal (Figure 2.2A). The tag used and the terminus of the protein to which it was appended is shown in Table 2.1. 3xFLAG-Pex6 formed punctate structures that

strongly colocalized with the peroxisomal GFP-PTS1 signal; however, it also showed a cytosolic signal, resulting in a decreased Pearson's coefficient (56%) (Figure 2.2A). It is possible that the observed cytosolic signal is an artefact of overexpression. Unexpectedly, 3xFLAG-Pex3 exhibited less than 30% colocalization with GFP-PTS1 (Figure 2.2A) and preferentially localized to reticular-like structures consistent in appearance to the ER. This localization was observed for Pex3 tagged at both the N- and the C-terminus. The localization pattern observed may be an artifact of Pex3 overexpression. This increased expression may cause impaired transport of the epitope-tagged Pex3 out of the ER to the peroxisome membrane. The relative increased levels of Pex3 at the ER may represent a *bona fide Drosophila*-specific steady state for Pex3, or an artifact of *Pex3* overexpression.

Tagged Pex5 showed both a punctate signal that partially overlapped with GFP-PTS1 and a generalized cytosolic signal (Figure 2.3). This bipartite localization for Pex5 is consistent with its known role as a soluble receptor for PTS1-containing cargo that shuttles between the cytosol and the peroxisome (Dodt and Gould, 1996; reviewed in Lanyon-Hogg et al., 2010;).

Tagged chimeras of Pex7 and Pex19 showed punctate structures that colocalized with peroxisomes as well as a diffuse signal in the cytosol (Figures 2.5). Pex7p in yeast has been shown to function as a shuttling receptor for PTS2-containing proteins between the cytosol and the peroxisome (Marzioch et al., 1994; Zhang and Lazarow, 1995). The localization of *Drosophila* Pex7 to both the cytosol and peroxisomes in S2 cells is consistent with its proposed function. However, previous studies were unable to find evidence for a functional PTS2 import pathway in *Drosophila* (Faust et al., 2012). This raises the interesting question of whether the purported Pex7 homologue of *Drosophila*

Figure 2.2

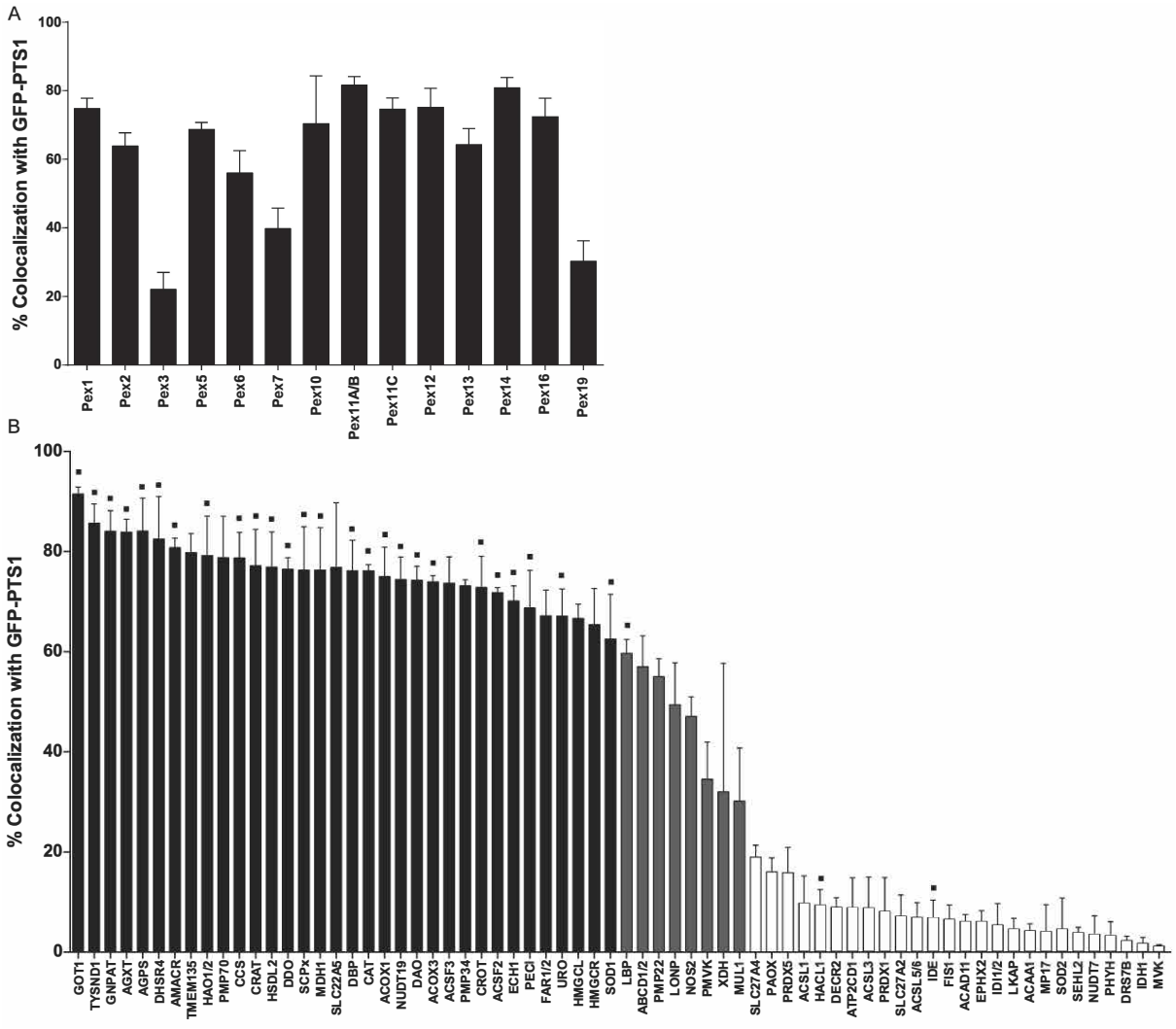
A
% Colocalization with GFP-PTS1
100
80
60
40
20
0
Pex1
Pex2
Pex3
Pex5
Pex6
Pex7
Pex10
Pex11A/B
Pex11C
Pex12
Pex13
Pex14
Pex16
Pex19
B
% Colocalization with GFP-PTS1
100
80
60
40
20
0
GOT1
TYSND1
GNPAT
AGXT
AGPS
DHSR4
AMACR
TMEM135
HAO1/2
PMP70
CCS
CRAT
HSDL2
DDO
SCPx
MDH1
SLC22A5
DBP
CAT
ACOX1
NUDT19
DAO
ACOX3
ACSF3
PMP34
CROT
ACSF2
ECH1
PEC1
FAR1/2
URO
HMGCL
HMGCR
SOD1
LBP
ABCD1/2
PMP22
LONP
NOS2
PMVK
XDH
MUL1
SLC27A4
PAOX
PRDX5
ACSL1
HACL1
DECR2
ATP2CD1
ACSL3
PRDX1
SLC27A2
ACSL5/6
IDE
FIS1
ACAD11
EPHX2
IDI1/2
LKAP
ACAA1
MP17
SOD2
SEHL2
NUDT7
PHYH
DRS7B
IDH1
MVK

Figure 2.2. Percent colocalization between tagged candidate *Drosophila* peroxisomal proteins and the peroxisomal marker GFP-PTS1 in *Drosophila* S2 cells. (A) Percent colocalization for predicted *Drosophila* Pex proteins. (B) Percent colocalization for predicted *Drosophila* peroxisomal proteins other than Pex proteins. Percent colocalization was calculated using Pearson's coefficient. Black bars, >60% colocalization; gray bars, 30–60% colocalization; white bars, <30% colocalization. Plasmids encoding candidate peroxisomal proteins fused to mRFP or the 3xFLAG epitope were transfected into S2 cells stably expressing GFP-PTS1, which labels peroxisomes. Values report the percent colocalization between the signals from a tagged candidate protein and GFP-PTS1 and represent the average of three independent measurements from three biological replicates (n = 3), for a total of nine total cells measured. Error bars represent the standard deviation. A filled square denotes a protein with a canonical PTS1 at its C-terminus.

actually functions in a currently undefined PTS2 import pathway or functions in a role unrelated to peroxisome biogenesis. Mammalian PEX19 functions as a shuttling receptor that recognizes peroxisomal membrane protein cargo in the cytosol and then docks to PEX3 to deliver its cargo either directly to the peroxisomal membrane or to the peroxisomal membrane via the ER (Fang et al., 2004; Sacksteder et al., 2000). A role for Pex19 in peroxisome biogenesis in *Drosophila* has been previously reported (Pandey and Nichols, 2011). The localization of Pex19 to both peroxisomes and the cytosol in S2 cells is consistent with a similar function for Pex19 in trafficking peroxisomal membrane proteins in *Drosophila*. mRFP- or 3xFLAG-tagged versions of the other predicted *Drosophila* Pex proteins largely localized to mature peroxisomes marked by the GFP-PTS1 reporter, similar to the peroxisomal localization of these proteins in yeast or human cells.

2.3.2. The majority of predicted peroxisomal proteins in Drosophila localize to peroxisomes in S2 cells

I investigated the subcellular localization of an additional 68 *Drosophila* proteins predicted to be peroxisomal (Faust et al., 2012). These proteins were identified from the Universal Protein Knowledgebase (uniprot.com) by querying the *Drosophila* proteome using the BLAST algorithm and, in addition, using PTS1-identifying algorithms such as PeroxiP (Emanuelsson et al., 2003), PProwler and PTS1 Prowler (Hawkins et al., 2007). In order to validate the original classification of these proteins as being peroxisomal in *Drosophila* (Faust et al., 2012), all putative *Drosophila* peroxisomal proteins were subjected to reciprocal BLASTp (Altschul et al., 1997) analysis against the 'refseq'

Homo sapiens proteome at NCBI (taxid:9606). BLAST settings were left at their default values. In cases where no corresponding human protein could be identified, the entirety of the non-redundant (NR) database was queried. This analysis allowed for reciprocal confirmation of the putative peroxisomal nature of the proteins identified in the original screen (Faust et al., 2012). Although the peroxisomal nature of most of the proteins was confirmed, 10 proteins had reciprocal best hits not consistent with the original classification (Faust et al., 2012). Two of these proteins were potentially homologous to other proteins (ACAA1 and FBpp0079472; DRS7B and FBpp0084910), while the remaining proteins did not have obvious homologues in *Drosophila*. These results are summarized in Table 2.3 (page 96).

Varying degrees of colocalization were found for the *Drosophila* proteins predicted to be peroxisome-localized that were not part of the peroxin genes (Figure 2.2B). The tag used and the terminus of the protein to which it was appended is shown in Table 2.2. The distribution of the percentage of colocalization between these proteins and peroxisomes fell broadly into three categories based on the overall trend in the data: >60%, 30 – 60% and <30%. This trend was supported by subsequent functional annotation of the proteins in each group. The percentage of colocalization of each candidate protein with the peroxisome marker is given in Table 2.2. Candidate proteins that fell into the >60% category showed strong colocalization with the GFP-PTS1 signal, indicative of peroxisomal localization. Candidate proteins that fell into the <30% category showed a localization distinct from the peroxisome marker, including the cytosol. Candidate proteins that fell in the 30 – 60% category exhibited punctate structures that overlapped with the GFP-PTS1 signal and simultaneously had an alternative localization, suggesting that this class of proteins localizes to both the

peroxisome as well as other cellular compartments.

2.3.2.1. Tagged candidate peroxisomal proteins exhibiting >60% colocalization with GFP-PTS1

Of the additional 68 candidate peroxisomal proteins in *Drosophila*, 34 tagged chimeras of these proteins showed >60% colocalization with GFP-PTS1, indicative of a preferential localization to peroxisomes (Figures 2.2B and 2.3). Most proteins in this group possess a canonical PTS1, −SKL (Gould et al.,1988), or a variation thereof at their C-terminus. These proteins require an N-terminal tag because a C-terminal tag would block the PTS1 and therefore disrupt peroxisomal localization. Proteins that strongly localized to the peroxisome with an N-terminal tag showed disrupted localization when tagged at their C-terminus. This screen revealed several proteins with non-canonical PTS1 signals that showed strong peroxisomal localization when tagged at the N-terminus, including malate dehydrogenase 1 (MDH1) (Figure 2.3), aspartate aminotransferase (GOT1), glyceronephosphate *O*-acyltransferase (GNPAT), alanine-glyoxylate aminotransferase (AGXT), copper chaperone for SOD (CCS) and dehydrogenase/reductase SDR family member 4 (DHSR4) (Figure 2.3), which have the non-canonical PTS1 sequences SNL, NKL, AKL, SKI, QKL and ARL, respectively. Several candidate proteins without an evident PTS1, such as acyl-CoA synthetase family member 3 (ACSF3) (Figure 2.3) and 3-hydroxy-3-methylglutaryl-CoA lyase (HMGCL), colocalized strongly with GFP-PTS1 when tagged at their N-terminus. ACSF3 is involved in fatty acid biosynthesis. It has a VSK at its C-terminus and localizes to the mitochondria in other species; however, it is reported to show substrate preference for lignoceric acid, a 24-carbon VLCFA (Watkins et al., 2007), which could explain the

observed peroxisomal localization in *Drosophila* S2 cells. HMGCL is a key enzyme in ketogenesis and catalyzes the terminal step in leucine catabolism. It has an RVK at its C-terminus and is reported to localize to both the mitochondria (Holmes et al., 1995) and peroxisomes (Ashmarina et al., 1994) in mammalian cells. The observed exclusive peroxisomal localization of HMGCL may be *Drosophila* specific. It remains to be determined whether proteins like ACSF3 and HMGCL possess atypical functional PTS1-type signals, gain access to the peroxisome by piggybacking on other proteins, or localize to peroxisomes by an alternative pathway (Islinger et al., 2009; Wu et al., 2000). Piggybacking occurs when oligomers are imported into an organelle as a complex, yet only one of the subunits has a targeting signal (Thoms, 2015), a phenomena that has been previously observed in peroxisomes (McNew and Goodman, 1994; Yang et al., 2001).

Peroxisomal membrane proteins that strongly colocalized with GFP-PTS1 when tagged at their N-terminus include the homologues of transmembrane protein 135 (TMEM135) (Figure 2.3), PMP70, solute carrier family 22 member 5 (SLC22A5), solute carrier family 25 member 17 (SLC25A17), fatty acyl-CoA reductase 1/2 (FAR1/2), and 3-hydroxy-3-methylglutaryl-CoA reductase (HMGCR). Peroxisomal membrane proteins are targeted to the peroxisome via a pathway that is independent of that for matrix protein targeting and involves the shuttling receptor Pex19 and relies on a distinct peroxisomal membrane targeting signal, the mPTS (Rottensteiner et al., 2004; Sacksteder et al., 2000). Previous work from our group suggests that the peroxisomal membrane protein trafficking machinery found in other organisms is functionally conserved in *Drosophila* (Mast et al., 2011).

Figure 2.3

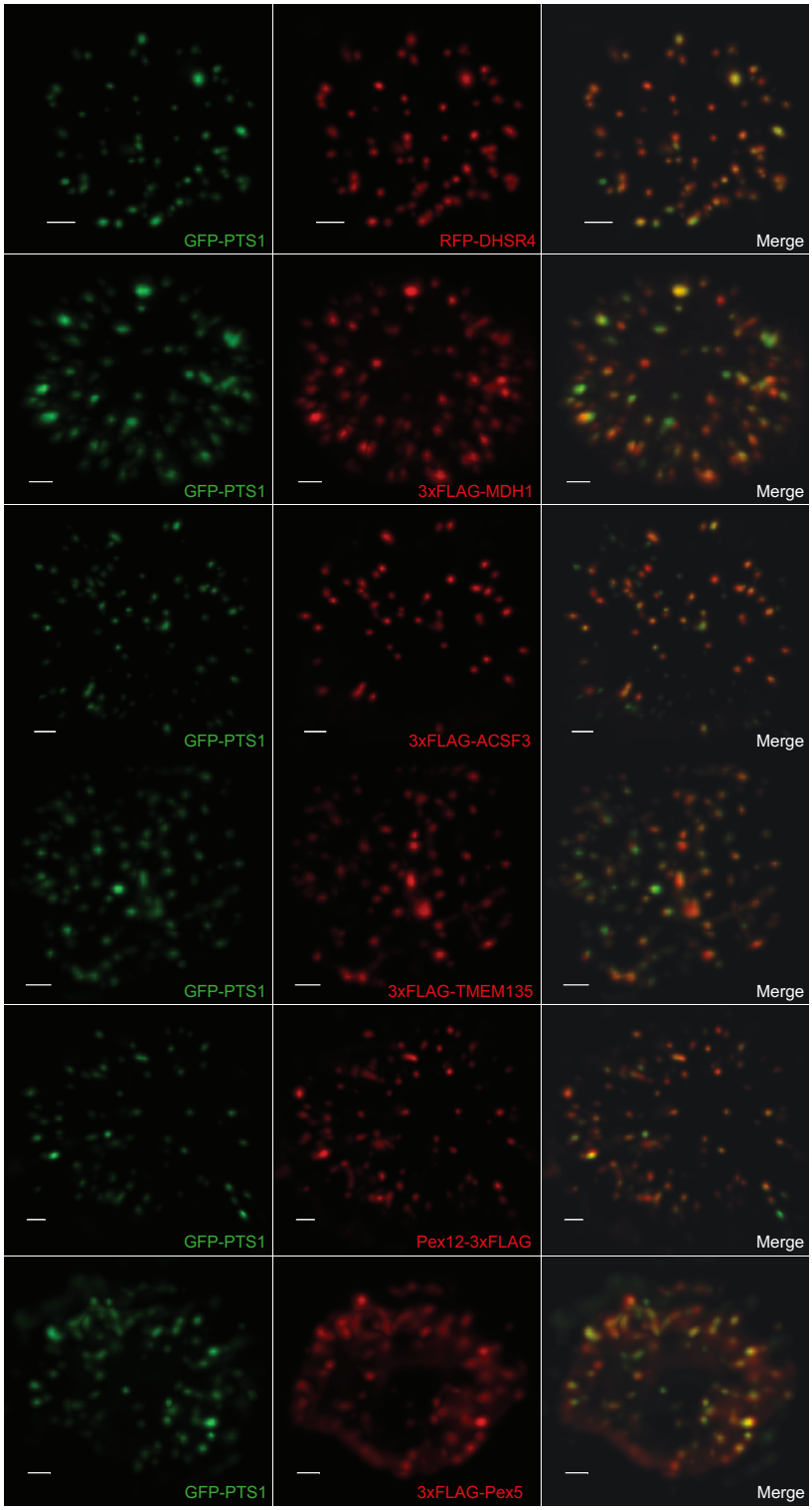
GFP-PTS1
RFP-DHSR4
Merge
GFP-PTS1
3xFLAG-MDH1
Merge
GFP-PTS1
3xFLAG-ACSF3
Merge
GFP-PTS1
3xFLAG-TMEM135
Merge
GFP-PTS1
Pex12-3xFLAG
Merge
GFP-PTS1
3xFLAG-Pex5
Merge

Figure 2.3: Candidate *Drosophila* peroxisomal proteins exhibiting >60% colocalization with peroxisomes in S2 cells. Chimeras of candidate peroxisomal proteins fused to either mRFP or a 3×FLAG epitope were expressed in S2 cells stably expressing GFP-PTS1 to label peroxisomes. Representative examples of chimeras exhibiting >60% colocalization with peroxisomes are shown. The GFP-PTS1 signal is shown in the left panels in green. mRFP- and 3xFLAG-tagged chimeric proteins are shown in the middle panels in red. Panels at the extreme right show the merged images, with colocalization indicated by a yellow signal. Each image is a maximum projection of a three-dimensional volume encompassing the entire cell. The scale bar represents 1 μm. Each cell is a representative image from three independent biological replicates (n = 3).

2.3.2.2. Tagged candidate peroxisomal proteins exhibiting <30% colocalization with GFP-PTS1

Twenty-six tagged chimeras of the 68 candidate peroxisomal proteins exhibited less than 30% colocalization with the GFP-PTS1 signal defining peroxisomes (Figure 2.2B). No protein in this group exhibited a pattern characteristic of peroxisomal localization. Notably, some proteins did form punctate structures, but these punctate structures did not coincide with the structures labeled by GFP-PTS1, suggesting that they localize to another organelle or aggregate. Based on their morphology and distribution, it is likely that such proteins localize to lysosomes, mitochondria, or lipid droplets. The homologue of Calcium-transporting ATPase type 2C member 1 (ATP2CD1) is an example of a protein in this group that localized to punctate structures distinct from peroxisomes (Figure 2.4).

Two proteins in this group, the homologues of 2-hydroxyacyl-CoA lyase 1 (HACL1) and insulin degrading enzyme (IDE) have a canonical PTS1 at their C-terminus. However, N-terminally tagged versions of these proteins did not colocalize with GFP-PTS1. FLAG-HACL1 localized to punctate structures distinct from those labeled by GFP-PTS1, whereas FLAG-IDE localized to the cytosol and plasma membrane (Figure 2.4). HACL1 is a thiamine pyrophosphate binding protein involved in fatty acid α-oxidation and its subcellular localization in *Drosophila* has not been previously reported (Faust et al., 2012; Gong et al., 2004). IDE is a metalloprotease that has been reported to localize to the cytosol and plasma membrane in *Drosophila* (Galagovsky et al., 2014), which is consistent with the localization observed for both 3xFLAG-IDE and mRFP-IDE in S2 cells. Although HACL1 and IDE contain a canonical

PTS1, their localization to non-peroxisomal structures could be due to their C-termini being cleaved by post-translational peptide processing, which could remove their PTS1. Alternatively, folding of their C-termini into their interiors could mask the PTS1 from its import receptor.

Some of the candidate *Drosophila* peroxisomal proteins examined have been previously reported to localize to cellular compartments other than peroxisomes. The homologue of Mitochondrial fission 1 protein (Fis1) tagged with the 3xFLAG epitope localized to punctate structures not labeled by GFP-PTS1 (Figure 2.4). This is consistent with reports that Fis1 localizes to mitochondria, where it functions in membrane fission (Jakobs et al., 2003; Koch et al., 2005; Stojanovski et al., 2004). In addition, 3xFLAG fusion to the homologue of peroxiredoxin 1 (PRDX1) showed a diffuse cytosolic signal (Figure 2.4) in agreement with reports of PRDX1 localizing to the cytosol (Radyuk et al., 2001). Overall, 27 predicted peroxisomal proteins did not appreciably localize to the peroxisome in S2 cells.

2.3.2.3. Tagged candidate peroxisomal proteins exhibiting 30–60% colocalization with GFP-PTS1

Of the 68 candidate *Drosophila* peroxisomal proteins, eight tagged chimeras showed 30 – 60% colocalization with peroxisomes marked by GFP-PTS1 (Figure 2.2B). Two phenotypic subgroups could be recognized within this group based on the subcellular distribution patterns of the tagged proteins. In one subgroup, fusion proteins localized to punctate structures that colocalized with GFP-PTS1-labeled peroxisomes, as

Figure 2.4

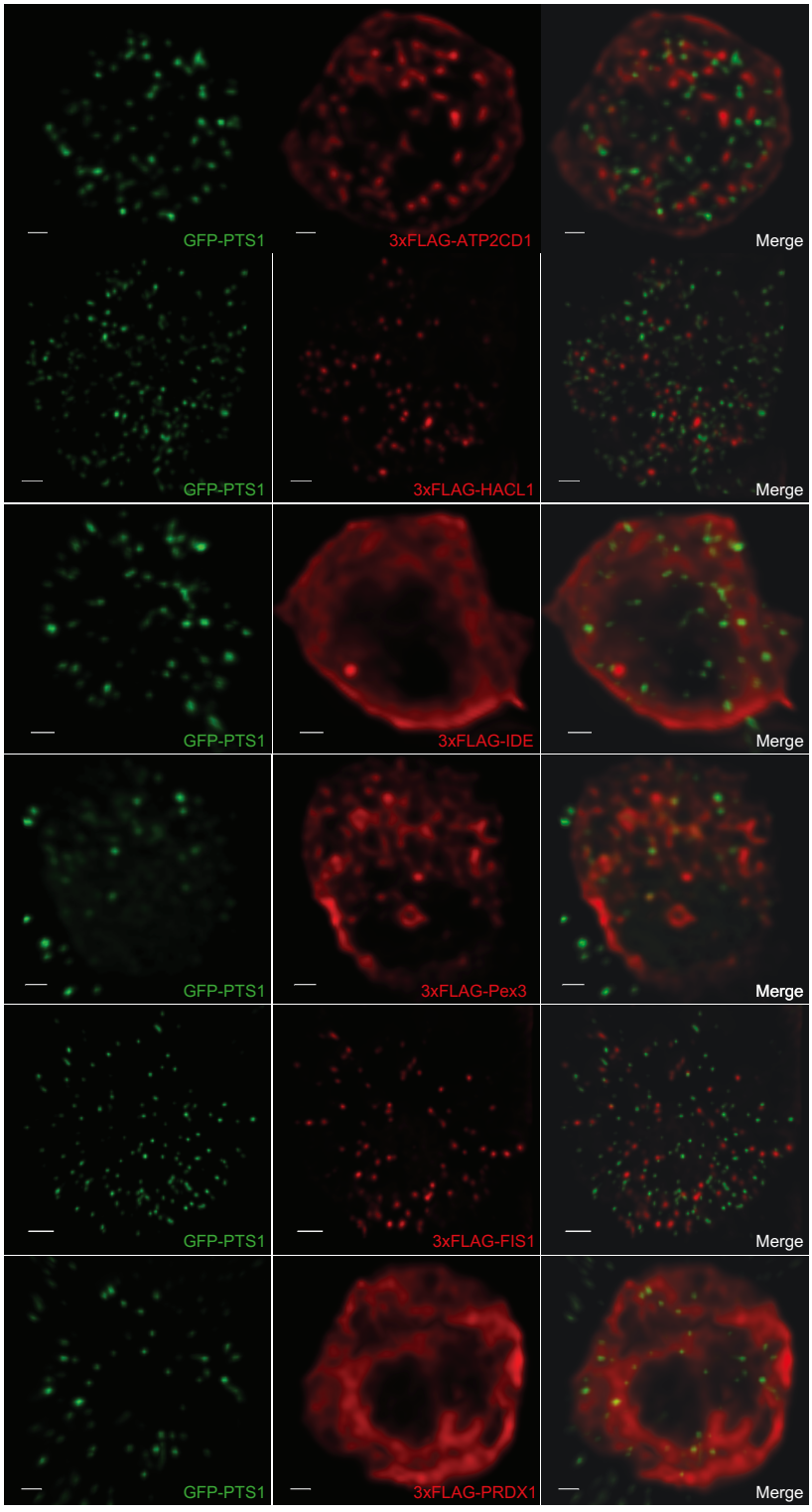
GFP-PTS1
3xFLAG-ATP2CD1
Merge
GFP-PTS1
3xFLAG-HACL1
Merge
GFP-PTS1
3xFLAG-IDE
Merge
GFP-PTS1
3xFLAG-Pex3
Merge
GFP-PTS1
3xFLAG-FIS1
Merge
GFP-PTS1
3xFLAG-PRDX1
Merge

Figure 2.4: Candidate *Drosophila* peroxisomal proteins exhibiting <30% colocalization with peroxisomes in S2 cells. Chimeras of candidate peroxisomal proteins fused to a 3×FLAG epitope were expressed in S2 cells stably expressing GFP-PTS1 to label peroxisomes. Representative examples of chimeras exhibiting <30% colocalization with peroxisomes are shown. The GFP-PTS1 signal is shown in the left panels, shown in green. The 3xFLAG-tagged chimeras are shown in the middle panels, shown in red. Panels at the extreme right show the merged images, with colocalization indicated by yellow signal. Each image is a maximum projection of a three-dimensional volume encompassing the entire cell. The scale bar represents 1 μm. Each cell is a representative image from three independent biological replicates (n = 3).

well as to other punctate structures that were distinct from peroxisomes. In a second subgroup, fusion proteins showed a diffuse cytosolic signal in addition to punctate structures that overlapped with GFP-PTS1-labeled peroxisomes (Figure 2.5A). Differences in the extent of colocalization of a fusion candidate peroxisomal protein with GFP-PTS1 were noted for the two groups. Proteins like the homologues of L-bifunctional protein (LBP) and ATP-binding cassette, subfamily D, member 1 (ABCD1) showed a high degree of colocalization with GFP-PTS1, nearly 60%, while XDH exhibited a lower degree of colocalization with GFP-PTS1, nearly 30% (Figure 2.2B and Figure 2.5A). These observations are consistent with all candidate peroxisomal proteins in the 30–60% colocalization group being localized to both peroxisomes and another cellular compartment and are suggestive of a dynamic exchange of these proteins between peroxisomes and other regions of the cell.

Of the eight proteins in this group, only the homologue of LBP has a canonical PTS1. 3xFLAG-LBP formed punctate structures (Figure 2.5A) that showed 59.6% colocalization with GFP-PTS1 (Figure 2.2B). LBP is an enoyl-CoA hydratase involved in fatty acid oxidation, and previous reports have documented the localization of LBP to multiple compartments, including lipid droplets (Beller et al., 2006; Cermelli et al., 2006), mitochondria (Tan et al., 2009), microtubule-associated complex (Hughes et al., 2008), and peroxisomes (Faust et al., 2012). The homologue of PMP22 fused to 3xFLAG formed punctate structures (Figure 2.5A) that partially overlapped with GFP-PTS1-labeled peroxisomes (55% colocalization) (Figure 2.2B). PMP22 is a peroxisomal integral membrane protein that is 22 kDa in size and has been predicted to localize to both peroxisomes (Faust et al., 2012) and the inner mitochondrial membrane (GOA Curators et al., 2007). These findings confirm that both soluble proteins, such as LBP,

Figure 2.5A

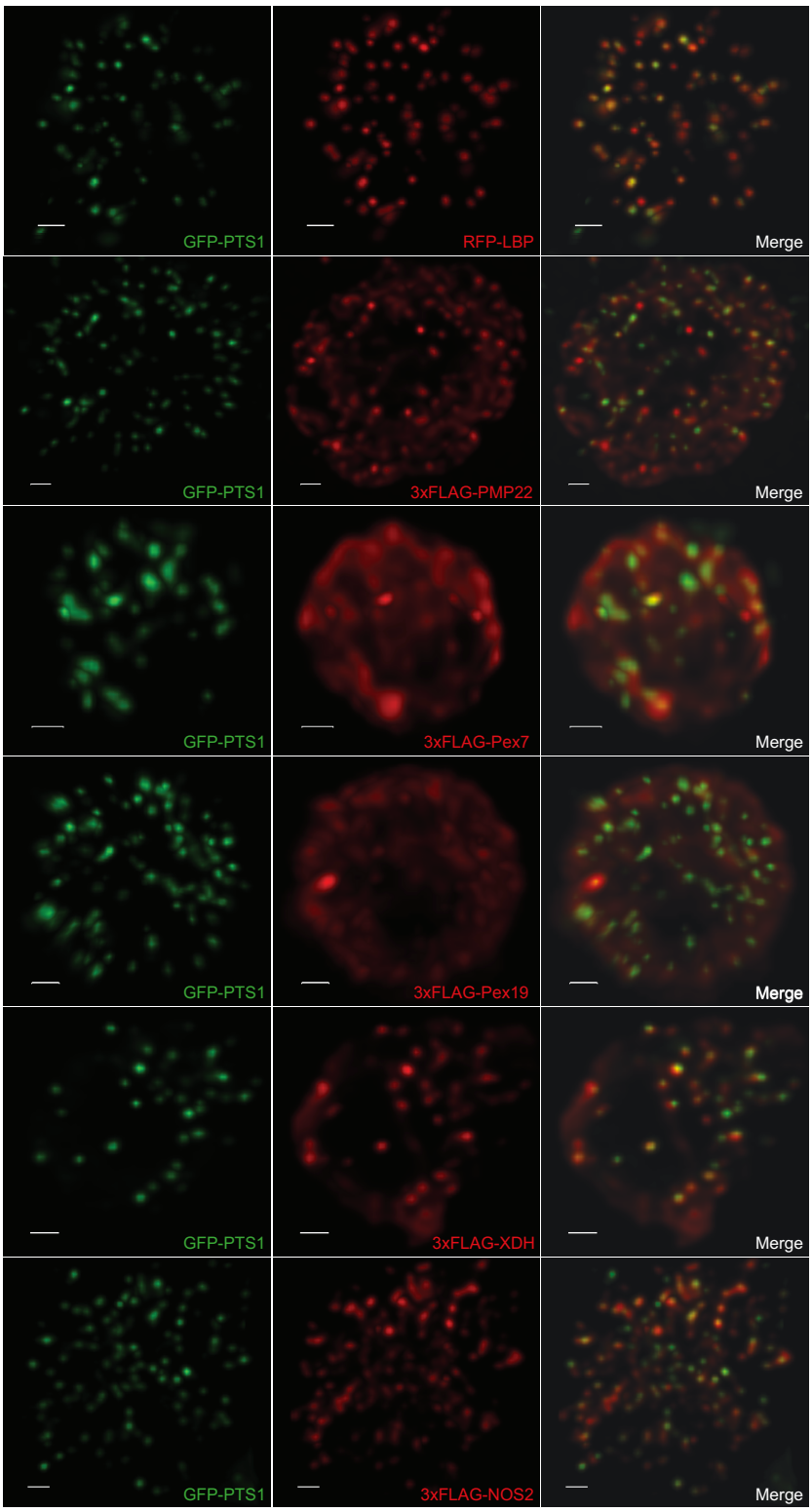
GFP-PTS1
RFP-LBP
Merge
GFP-PTS1
3xFLAG-PMP22
Merge
GFP-PTS1
3xFLAG-Pex7
Merge
GFP-PTS1
3xFLAG-Pex19
Merge
GFP-PTS1
3xFLAG-XDH
Merge
GFP-PTS1
3xFLAG-NOS2
Merge

Figure 2.5B

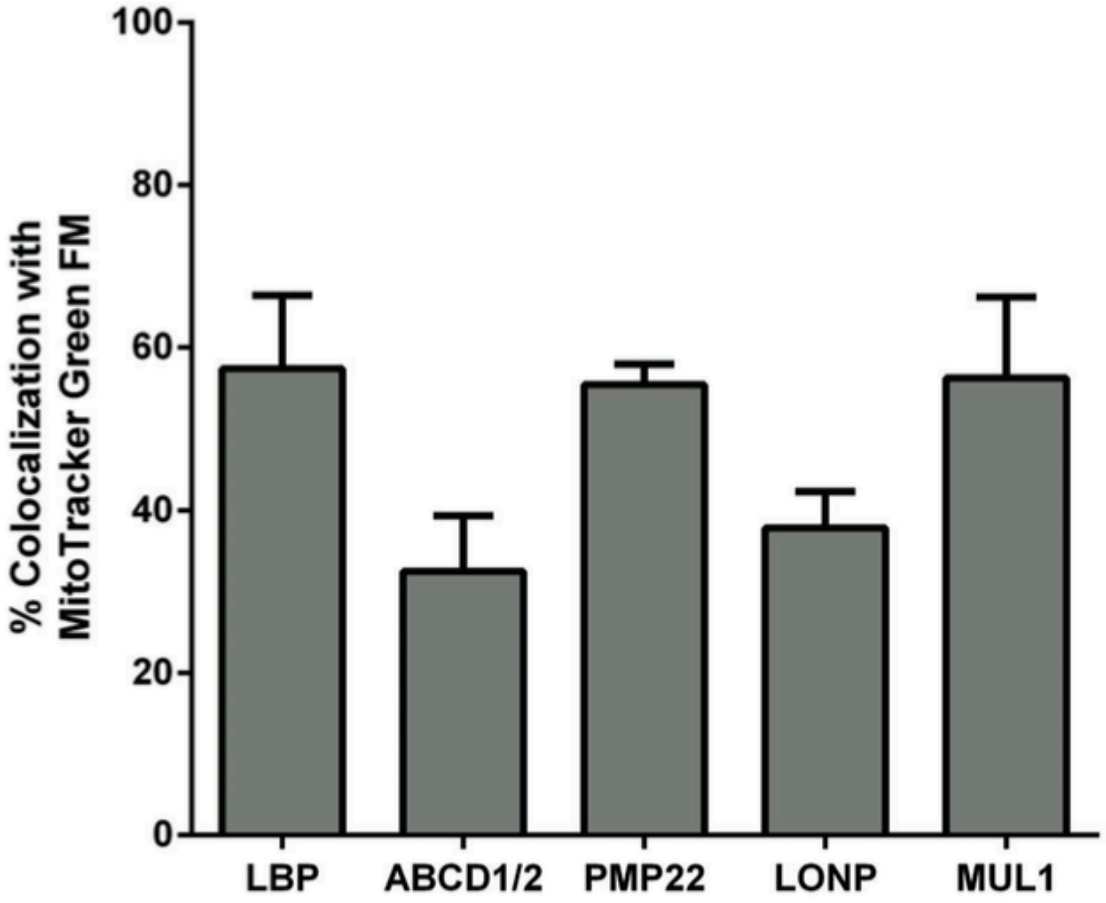
% Colocalization with MitoTracker Green FM
100
80
60
40
20
0
LBP
ABCD1/2
PMP22
LONP
MUL1

Figure 2.5: Candidate *Drosophila* peroxisomal proteins exhibiting 30-60% colocalization with peroxisomes in S2 cells. Chimeras of candidate peroxisomal proteins fused to either mRFP or a 3×FLAG epitope were expressed in S2 cells stably expressing GFP-PTS1 to label peroxisomes. (A) Representative examples of chimeras exhibiting 30–60% colocalization with peroxisomes are shown. The GFP-PTS1 signal is in the left panels, shown in green. RFP- and FLAG-tagged proteins are in the middle panels, shown in red. Panels at the extreme right show the merged images, with colocalization indicated by a yellow signal. Each image is a maximum projection of a three-dimensional volume encompassing the entire cell. The scale bar represents 1 μm. Each cell is a representative image from 3 independent biological replicates (n = 3). (B) Select chimeras were transfected into S2 cells that were subsequently stained with MitoTracker Green FM. The percent colocalization of the signals from a fusion protein and MitoTracker was determined by Pearson's coefficient, and the values represent the average of three individual cells from three biological replicates, for a total of nine cells measured. Error bars represent the standard deviation. A filled square denotes a protein with a canonical PTS1 at its C-terminus.

and membrane proteins, such as PMP22, can be targeted to both peroxisomes and other cellular compartments. 3xFLAG-XDH and the homologue of nitric oxide synthase 2A (NOS2) fused to 3xFLAG showed approximately 32% and 47% colocalization with GFP-PTS1, respectively (Figures 2.2B and 2.5A). Neither XDH nor NOS2 contains a canonical PTS1. XDH is involved in a variety of metabolic functions (Gelbart et al., 1974; Kim et al., 2001) and has been reported to localize to the microtubule-associated complex in *Drosophila* (Hughes et al., 2008), suggesting that XDH may be found in the cytosol, although, a peroxisomal localization for XDH has also been reported (Faust et al., 2012). These observations are consistent with a dual localization of 3xFLAG-XDH to both the cytosol and peroxisomes in S2 cells (Figure 2.5A). NOS2 is a flavodoxin with nitric oxide synthase activity and has been predicted to localize to both the cytosol (Gaudet et al., 2011) and the peroxisome (Faust et al., 2012). These results are also consistent with this dual localization for NOS2 (Figure 2.5A).

A select number of fusion proteins from the 30–60% category that have been previously predicted to localize to mitochondria were additionally analyzed for colocalization with mitochondria. Of the fusion proteins analyzed, five colocalized with the mitochondrial marker, MitoTracker Green FM, to an appreciable degree (Figure 2.5B). Fusion proteins mRFP-LBP, 3xFLAG-PMP22, and 3xFLAG-MUL1 showed greater than 50% colocalization with the mitochondrial marker, whereas 3xFLAG-ABCD1 and 3xFLAG-LONP showed 32.5% and 37.8% colocalization, respectively. The degree of colocalization between these fusion proteins and both peroxisomal and mitochondrial markers suggests that they localize to both peroxisomes and mitochondria in *Drosophila* S2 cells. Taken together these results show that a number of *Drosophila* proteins localize to mature peroxisomes and are likely also trafficked to additional

cellular compartments, such as mitochondria, where they may perform alternative functions.

2.3.3. Overexpression of genes coding for candidate peroxisomal proteins differentially affect peroxisome volume and number in S2 cells

Overexpression of genes encoding peroxins or peroxisomal proteins often leads to changes in the volume and number of peroxisomes in cells (Chang et al., 1999; reviewed in Subramani, 1998). It is likely that many of the genes analyzed were being expressed at higher than endogenous levels, and therefore effects on peroxisomal volume (Figure 2.6A; Table 2.4) and number (Figure 2.6B; Table 2.5) were investigated in S2 cells. Individual GFP-PTS1-labeled peroxisomes in untransfected S2 cells were roughly 0.173 μm^3 in volume (Figure 2.6A). Overexpression of some candidate genes resulted in larger peroxisomes (Figure 2.6A). Significant increases in peroxisome volume were observed for overexpression of the homologues of phosphomevalonate kinase (PMVK), mitochondrial ubiquitin ligase activator of NFKB (MUL1), Pex11C, carnitine O-octanoyltransferase (CROT) and α-methylacyl-CoA racemase (AMACR), AGPS, GNPAT, HMGCR, DAO, D-aspartate oxidase (DDO), HMGCL, Limkain-b1 (LKAP), Peroxisomal coenzyme A diphosphatase (NUDT7), Acyl-CoA synthetase long-chain family member 3 (ACSL3), SLC22A5, Pex1, and Pex19 (Figure 2.6A). Many of these are predicted to be peroxisomal matrix proteins, and increased amounts of matrix proteins have been shown to result in enlarged peroxisomes (Smith et al., 2000, 2002). The tagged homologue of MUL1 showed moderate colocalization of ~30% with the peroxisome marker (Figure 2.2B), and MUL1 has been predicted to regulate mitochondrial fission

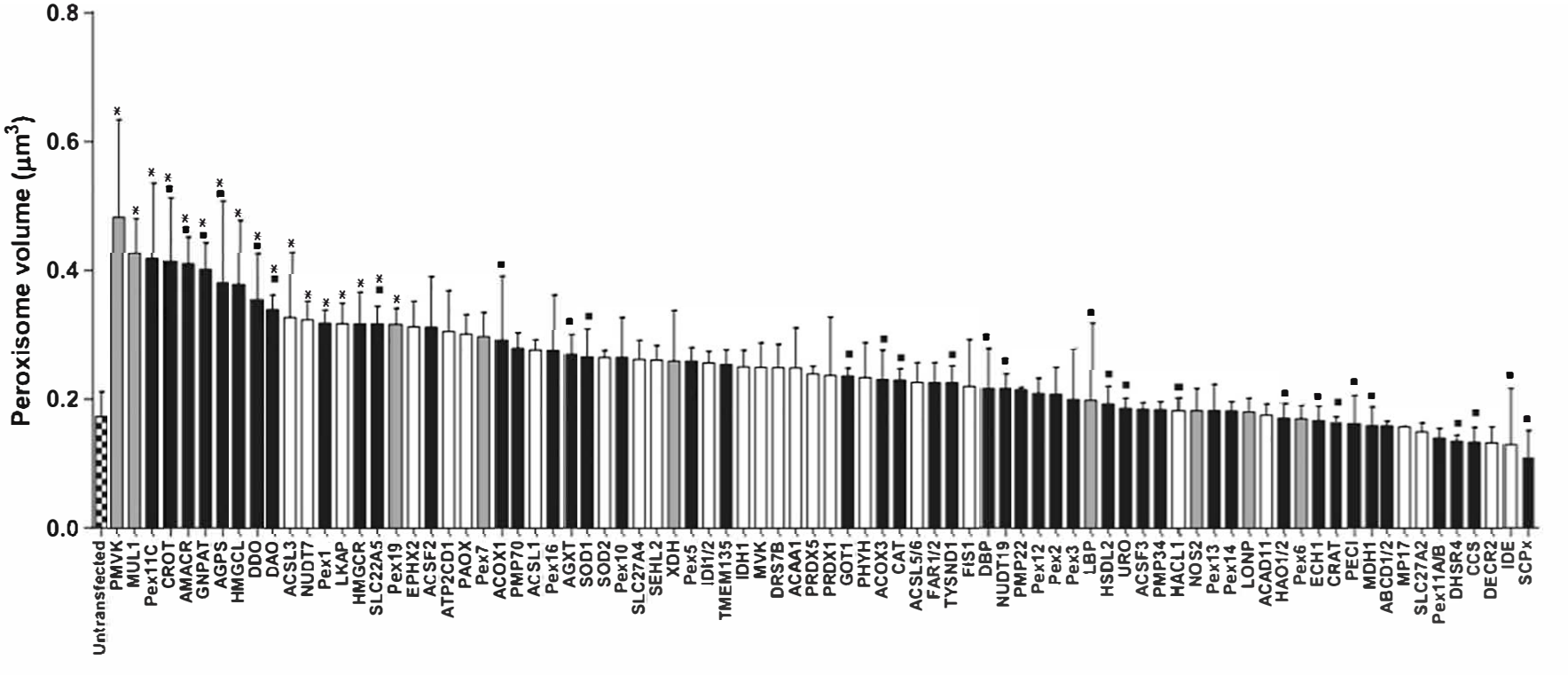
Peroxisome volume (μm3)
0.8
0.6
0.4
0.2
0.0
Untransfected
PMVK
MUL1
Pex11C
CROT
AMACR
GNPAT
AGPS
HMGCL
DDO
DAO
ACSL3
NUDT7
Pex1
LKAP
HMGCR
SLC22A5
Pex19
EPHX2
ACSF2
ATP2CD1
PAOX
Pex7
ACOX1
PMP70
ACSL1
Pex16
AGXT
SOD1
SOD2
Pex10
SLC27A4
SEHL2
XDH
Pex5
IDI1/2
TMEM135
IDH1
MVK
DRS7B
ACAA1
PRDX5
PRDX1
GOT1
PHYH
ACOX3
CAT
ACSL5/6
FAR1/2
TYSND1
FIS1
DBP
NUDT19
PMP22
Pex12
Pex2
Pex3
LBP
HSDL2
URO
ACSF3
PMP34
HACL1
NOS2
Pex13
Pex14
LONP
ACAD11
HAO1/2
Pex6
ECH1
CRAT
PECI
MDH1
ABCD1/2
MP17
SLC27A2
Pex11A/B
DHSR4
CCS
DECR2
IDE
SCPx

Figure 2.6A

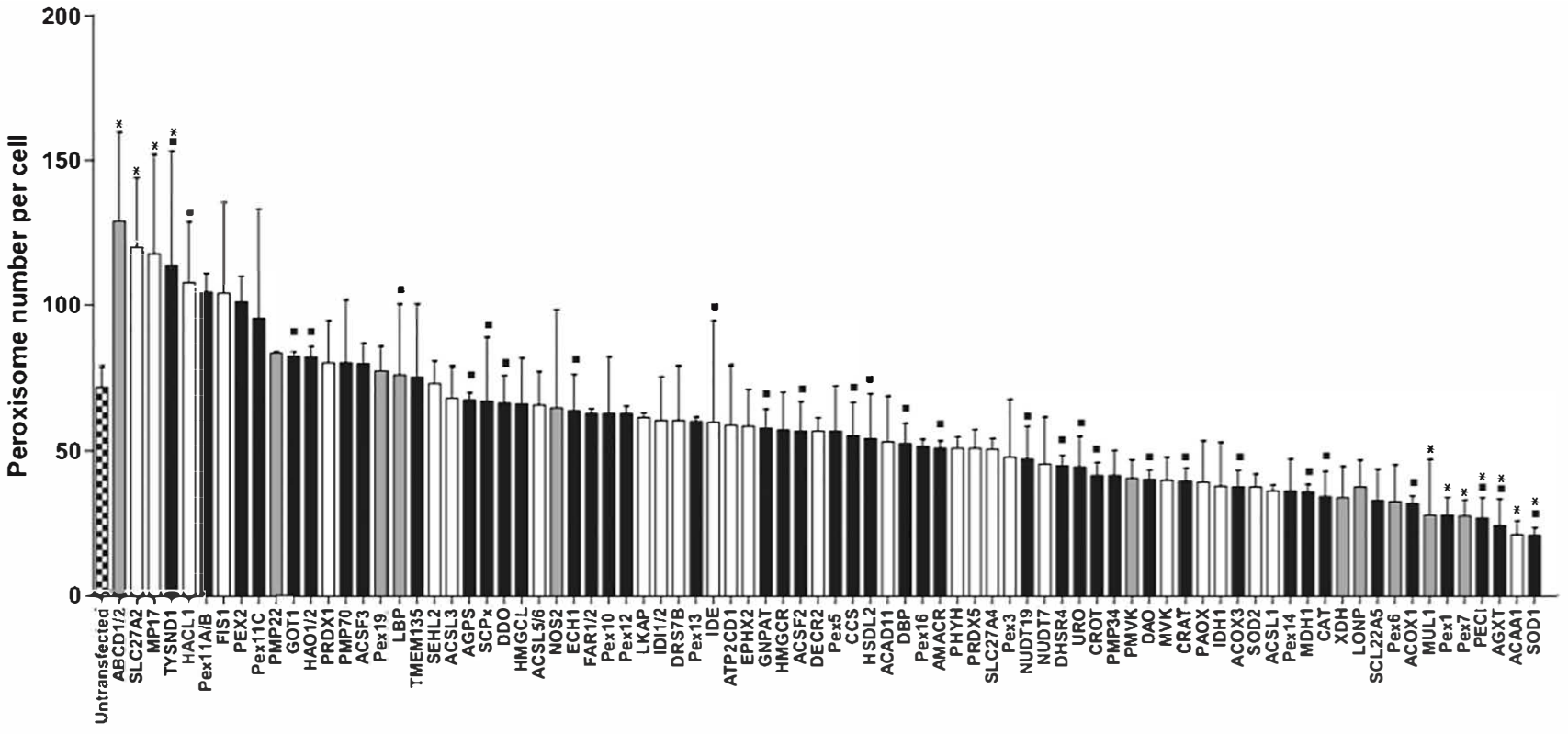
Peroxisome number per cell
200
150
100
50
0
Untransfected
ABCD1/2
SLC27A2
MP17
TYSND1
HACL1
Pex11A/B
FIS1
PEX2
Pex11C
PMP22
GOT1
HAO1/2
PRDX1
PMP70
ACSF3
Pex19
LBP
TMEM135
SEHL2
ACSL3
AGPS
SCPx
DDO
HMGCL
ACSL5/6
NOS2
ECH1
FAR1/2
Pex10
Pex12
LKAP
IDI1/2
DRS7B
Pex13
IDE
ATP2CD1
EPHX2
GNPAT
HMGCR
ACSF2
DECR2
Pex5
CCS
HSDL2
ACAD11
DBP
Pex16
AMACR
PHYH
PRDX5
SLC27A4
Pex3
NUDT19
NUDT7
DHSR4
URO
CROT
PMP34
PMVK
DAO
MVK
CRAT
PAOX
IDH1
ACOX3
SOD2
ACSL1
Pex14
MDH1
CAT
XDH
LONP
SCL22A5
Pex6
ACOX1
MUL1
Pex1
Pex7
PECI
AGXT
ACAA1
SOD1

Figure 2.6B

Figure 2.6: Effect of overexpression of genes for candidate *Drosophila* peroxisomal proteins on peroxisome volume and number in S2 cells. Genes encoding candidate *Drosophila* peroxisomal proteins were expressed under control of the actin promoter. Plasmids were transfected into S2 cells stably expressing GFP-PTS1 to label peroxisomes. Black bars, >60% colocalization; gray bars, 30–60% colocalization; white bars, <30% colocalization. Peroxisome volume (A) and number (B) were determined. Peroxisome volume is reported in μm^3. Values report the average of three individual measurements from three independent biological replicates (n = 3) for a total of nine individual cells measured. Error bars represent the standard deviation. A filled square denotes a protein with a canonical PTS1 at its C-terminus. An asterisk denotes genes whose overexpression had a statistically significant effect on peroxisome volume (A) or number (B) relative to untransfected controls, determined using an upaired Student's *t*-test. *, $p < 0.05$.

(Yun et al., 2014), suggesting that MUL1's effect on peroxisome volume is likely indirect. In addition, the overexpression of several peroxins such as Pex1, Pex11C, and Pex19 led to increases in peroxisomal volume (0.318, 0.297, and 0.316 μm^3, respectively). Pex11C, like Pex11A/B, is a positive regulator of peroxisomal fission in yeast, and overexpression of the *PEX11* gene in yeast leads to smaller peroxisomes (Marshall et al., 1995). Therefore, it was somewhat surprising that overexpression of Pex11C led to enlarged peroxisomes (Figure 2.6A), which suggests that it may perform a function unrelated to peroxisome fission in *Drosophila.* The overexpression of the predicted peroxisomal proteins did not cause a significant decrease in peroxisome volume.

Untransfected S2 cells grown in serum-free medium typically contain between 60 and 80 peroxisomes per cell (Figure 2.6B). Overexpression of most genes encoding candidate *Drosophila* peroxisomal proteins had little effect on the number of peroxisomes. However, overexpression of some genes, including those coding for superoxide dismutase 1 (SOD1), β-ketoacyl-CoA thiolase (ACAA1), MUL1, 3,2-trans-enoyl-CoA isomerase (PECI), AGXT, Pex1, and Pex7 did result in a significant decrease in the number of peroxisomes per cell. How the overexpression of these genes leads to a smaller number of peroxisomes in a cell is unclear at present; however, given that mature peroxisomes do not fuse (Motley and Hettema, 2007), overexpression is likely interfering with the *de novo* peroxisome biogenesis pathway or with the peroxisome fission pathway, resulting in a decrease in the overall peroxisome number per cell.

Overexpression of four genes led to a significant increase in peroxisome number in S2 cells (Figure 2.6B). Two of the four genes encoded proteins that localized strongly to GFP-PTS1-labeled peroxisomes (Figure 2.2B), which were the homologues of

ABCD1/2 and the peroxisomal leader peptide-processing protease TYSND1. TYSND1 is a matrix protein with no known direct role in peroxisome fission. The overproduction of TYSND1 might increase the protein content of peroxisomes, which could signal to the cell to increase the number of peroxisomes. Human homologues of these proteins could represent potential therapeutic targets for upregulating peroxisome numbers in cells of PBD patients as a means of at least partially alleviating their peroxisomal metabolic deficiencies. ABCD1/2 is an ABC transporter that transports fatty acids and/or fatty acyl-CoAs into the peroxisome (Guimarães et al., 2005). The observed effect on peroxisome number when ABCD1/2 is overexpressed could be a result of increased fatty acid uptake into peroxisomes, which might induce peroxisome fission.

Two other genes, when overexpressed, led to increased numbers of peroxisomes in cells encoded proteins that showed <30% colocalization with GFP-PTS1-labeled peroxisomes. The homologues of Solute carrier family 27, member 2 (SLC27A2) and Mpv17-like protein (MP17) did not localize to peroxisomes (Figure 2.2) and caused an increase in peroxisome number when overexpressed (Figure 2.6B). Because both of these proteins did not localize to peroxisomes in S2 cells, it is likely that this is an indirect effect on the peroxisome population.

The total peroxisome capacity of a cell overproducing a candidate *Drosophila* peroxisomal protein, as measured by the total peroxisomal volume of the cell, varies from the wild-type condition to various degrees depending on the protein being overexpressed (Table 2.5). This suggests that control of overall peroxisome population within a cell is controlled and modulated by a number of factors, pathways, and events.

2.3.4. Drosophila Pex5 directs the peroxisomal import of PTS1-containing cargo

In yeast cells, matrix proteins targeted to peroxisomes via the PTS1 pathway rely on the receptor Pex5p for their import (Van der Leij et al., 1993). D-Bifunctional protein (DBP) is an enzyme with oxidoreductase activity that is involved in the β-oxidation of very-long chain fatty acids (Mehtälä et al., 2013). The homologue of DBP contains the PTS1 signal, -AKL, and mRFP-DBP strongly colocalized (76.2%) with peroxisomes in S2 cells (Figures 2.3 and 2.7). Knock down of *Pex5* by dsRNA treatment caused a reduction in the number of mRFP-DBP-labeled punctate structures and a redistribution of mRFP-DBP signal to the cytosol (Figure 2.7), consistent with a role for *Drosophila* Pex5 in targeting PTS1-containing proteins to the peroxisome.

2.3.5. Pex19 functions in membrane protein recruitment to the peroxisome

3xFLAG-ABCD1 is a membrane protein that preferentially (57%) localizes to peroxisomes (Figure 2.5). Transport of ABCD1 to peroxisomes is independent of the PTS1 targeting pathway, as knock down of *Pex5* by dsRNA treatment did not affect the localization of 3xFLAG-ABCD1 to punctate structures, but resulted in mislocalization of GFP-PTS1 to the cytosol (Figure 2.7). Conversely, knock down of *Pex19* by dsRNA treatment did not affect the localization of GFP-PTS1 to punctate structures, but resulted in the mislocalization of 3xFLAG-ABCD1 and its accumulation in the cytosol (Figure 2.7). This result is consistent with a role for *Drosophila* Pex19 in trafficking membrane proteins to the peroxisome (Sacksteder et al., 2000).

2.3.6. Drosophila expresses a protein homologous to Pex7 but it does not appear to function in PTS2-mediated import

Corresponding to previous reports (Faust et al., 2012), I was unable to confirm any potential peroxisomal protein containing a PTS2 signal. When human proteins with a confirmed PTS2 signal were transgenically expressed in S2 cells, no transport to peroxisomes was observed (Faust et al., 2012). One possible explanation for the lack of apparent PTS2 pathway in *Drosophila* is that homologues to PTS2-containing proteins have evolved to use the PTS1 pathway for their import into peroxisomes. This scenario has been observed in *C. elegans* (Motley et al., 2000). However, given that a Pex7 homologue appears to be expressed in *Drosophila*, and that this protein showed appreciable concentration in peroxisomes (Figure 2.5), the question arises as to whether this protein has a role in PTS1-mediated transport. This does not appear to be the case as knock down of *Pex7* by dsRNA treatment did not affect the localization of RFP-DBP, while knock down of *Pex5* caused its mislocalization to the cytosol (Figure 2.7).

There does appear to be a non-conventional pathway trafficking cargo to peroxisomes in *Drosophila* that does not rely on the PTS1 or the PTS2 system. The homologue of FAR1/2 contains neither a putative PTS1 nor PTS2, yet it strongly (67.2%) localized to peroxisomes in S2 cells when tagged with a 3xFLAG epitope at its N-terminus (Figure 2.7). It is possible that FAR1/2 possesses a non-conventional PTS1 that has not been previously described; however, appending the 3xFLAG epitope to the C-terminus did not disrupt its localization. In addition, the knockdown of *Pex5* and the putative *Pex7* did not disrupt the localization of 3xFLAG-FAR1/2 to punctate structures; however, it is difficult to conclude that these punctate structures are peroxisomes as the GFP-PTS1 signal is disrupted in *Pex5* dsRNA treated cells. This result suggests that

Figure 2.7

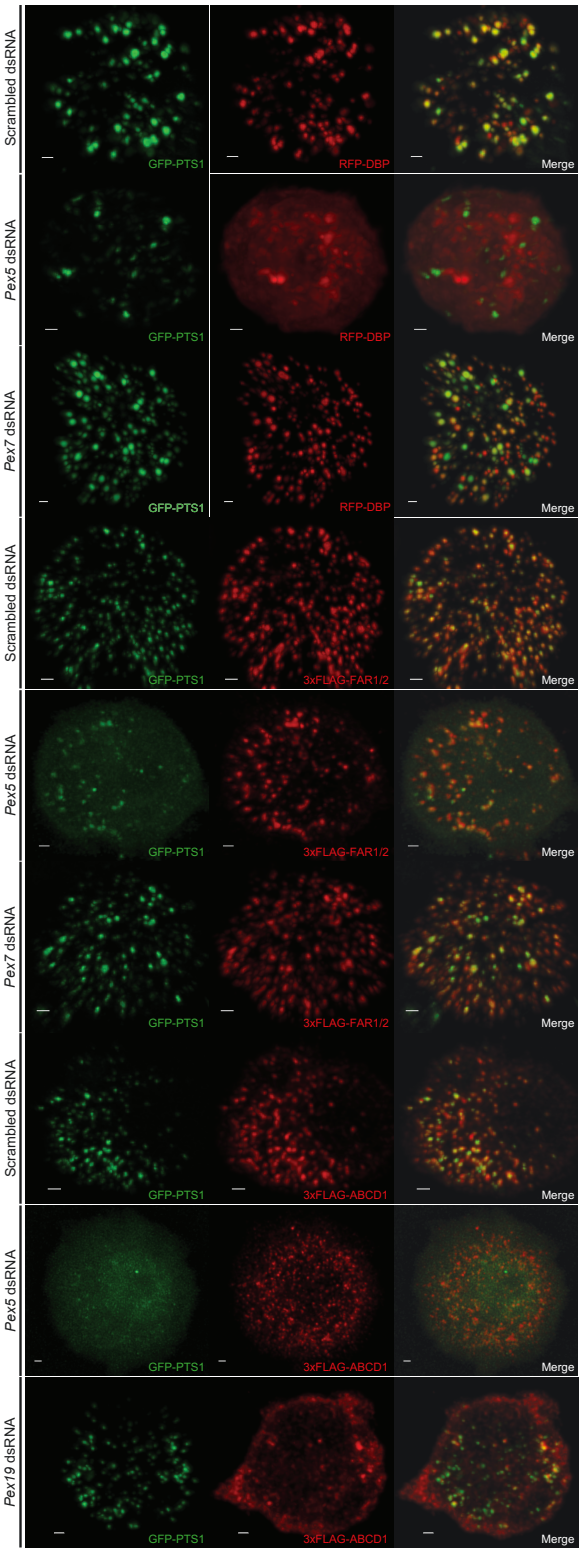
Scrambled dsRNA
GFP-PTS1
RFP-DBP
Merge
Pex5 dsRNA
GFP-PTS1
RFP-DBP
Merge
Pex7 dsRNA
GFP-PTS1
RFP-DBP
Merge
Scrambled dsRNA
GFP-PTS1
3xFLAG-FAR1/2
Merge
Pex5 dsRNA
GFP-PTS1
3xFLAG-FAR1/2
Merge
Pex7 dsRNA
GFP-PTS1
3xFLAG-FAR1/2
Merge
Scrambled dsRNA
GFP-PTS1
3xFLAG-ABCD1
Merge
Pex5 dsRNA
GFP-PTS1
3xFLAG-ABCD1
Merge
Pex19 dsRNA
GFP-PTS1
3xFLAG-ABCD1
Merge

Figure 2.7. Localization of proteins to peroxisomes is dependent on Pex5 and Pex19, but not Pex7. Chimeras of the homologues of peroxisomal proteins DBP, FAR1/2 and ABCD1 fused to mRFP or a 3×FLAG epitope were expressed in S2 cells stably expressing GFP-PTS1 to label peroxisomes. Transfected cells were treated with dsRNA targeting *Pex5, Pex7* or *Pex19* transcripts, as labelled. Control cells were treated with scrambled dsRNA for comparison. Representative images show the localization of each fusion protein under each dsRNA treatment. The GFP-PTS1 signal is shown in green in the left panels. RFP- and FLAG-tagged chimeric proteins are shown in red in the middle panels. Panels on the extreme right show the merged images of the green and red signals, with colocalization indicated by the yellow signal. Each image is a maximum projection of a three-dimensional volume encompassing the entire cell. The scale bar represents 1 μm. Each is a representative image from three independent biological replicates (n = 3).

FAR1/2 is targeted to peroxisomes independently of a PTS1 or PTS2 import pathway; however, further experimentation will be required to validate these observations (Figure 2.7).

2.4. Summary and conclusions

A systematic screen in *Drosophila* S2 cells was performed to determine the subcellular localization of proteins previously predicted to have a role in peroxisome function or biogenesis in *Drosophila* based on homology to human proteins with known peroxisomal functions (Faust et al., 2012). I evaluated 14 predicted *Drosophila* Pex proteins and 68 predicted *Drosophila* peroxisomal proteins. Of these 68 proteins, 34 proteins were found to localize preferentially to peroxisomes, while eight proteins localized to both the peroxisome and other punctate structures that most likely represent other organelles. Twenty-six proteins did not localize to the peroxisome, which suggests that certain human peroxisomal proteins are absent or targeted elsewhere in *Drosophila*. In addition, it may be possible that the correct homologues were not identified in the initial bioinformatic screen. A re-analysis of the original screen (Faust et al., 2012) identified 10 reciprocal best hits for homologues of human peroxisomal proteins that were not identified in the original screen. Of those original 10 genes, seven genes encoded proteins that showed less than 30% localization to peroxisomes in this analysis. This result would suggest that these seven original putative *Drosophila* homologues of human peroxisomal proteins were incorrectly identified in the original screen (Faust et al., 2012). In addition, this analysis also identified genes for candidate peroxisomal proteins that have an effect on peroxisome size and number when overexpressed in S2

cells. How overexpression of these genes reduces or increases a cell's peroxisome population is a topic for future investigation. Overall, these results strongly support the notion that peroxisome function and the mechanisms of peroxisome biogenesis are largely conserved between *Drosophila* and human. Thus, *Drosophila* can be a valuable multicellular organism with which to study peroxisome-LD interactions.

One notable difference between *Drosophila* and human is the apparent absence of a PTS2 import pathway mediated by the PTS2 receptor, Pex7, in *Drosophila*. Although a protein homologous to human Pex7 is found in *Drosophila*, and notwithstanding its appreciable localization to the peroxisome in S2 cells, this putative *Drosophila* Pex7 homologue appeared not to function in any aspect of protein targeting to peroxisomes. Further studies are needed to define the physiological role of this Pex7 homologue in *Drosophila*.

Table 2.1. Percent colocalization between tagged candidate *Drosophila* Pex proteins and GFP-PTS1 in S2 Cells. Colocalization between tagged candidate *Drosophila* Pex proteins and the peroxisomal marker GFP-PTS1 in *Drosophila* S2 cells measured as a percentage. Plasmids encoding candidate Pex proteins fused to mRFP or the 3xFLAG epitope were transfected into S2 cells stably expressing GFP-PTS1, which labels peroxisomes. The column on the extreme left gives the unique FlyBase gene ID (CG number) for each gene. The second column gives the human homologue. The third column gives the percent identity between the corresponding *Drosophila* and human proteins. The fourth column gives the C-terminal three amino acids of the *Drosophila* protein. The fifth column gives the tag used to measure colocalization and its appended location on the protein. The column on the extreme right gives the percent colocalization between the signal from tagged candidate Pex proteins and GFP-PTS1 and represents the average of three individual measurements from three biological replicates for a total of nine cells measured.

FlyBase CG Number	Human Gene	% Identity	C-term	Tag/Location	% Colocalization w/ GFP-PTS1
CG6760-PA	*PEX1*	27	TLA	FLAG/N-term	74.80 ± 3.03
CG7081-PA	*PEX2*	26	QSV	FLAG/N-term	63.87 ± 3.85
CG6859-PA	*PEX3*	33	SSA	FLAG/N-term	22.03 ± 4.95
CG14815-PB	*PEX5*	38	FKD	FLAG/N-term	68.73 ± 2.02
CG11919-PA	*PEX6*	26	YSV	FLAG/N-term	56.00 ± 6.52
CG6486-PA	*PEX7*	42	LVV	FLAG/N-term	39.73 ± 6.01
CG7864-PA	*PEX10*	30	NYA	FLAG/N-term	70.37 ± 13.98
CG8315-PA	*PEX11A/B*	33	TPA	FLAG/N-term	81.63 ± 2.47
CG13827-PA	*PEX11C*	28	LNK	FLAG/N-term	74.63 ± 3.23
CG3639-PA	*PEX12*	28	YET	FLAG/C-term	75.17 ± 5.52
CG4663-PA	*PEX13*	29	GFA	FLAG/N-term	64.27 ± 4.67
CG4289-PA	*PEX14*	26	EIM	FLAG/N-term	80.83 ± 3.01
CG3947-PA	*PEX16*	37	WST	FLAG/N-term	72.40 ± 5.40
CG5325-PA	*PEX19*	27	PTM	FLAG/N-term	30.27 ± 5.95

Table 2.2. Percent colocalization between tagged candidate *Drosophila* peroxisomal proteins and GFP-PTS1 in S2 Cells. Colocalization between tagged candidate *Drosophila* peroxisomal proteins and the peroxisomal marker GFP-PTS1 in *Drosophila* S2 cells measured as a percentage. Plasmids encoding candidate peroxisomal proteins fused to mRFP or the 3xFLAG epitope were transfected into S2 cells stably expressing GFP-PTS1, which labels peroxisomes. The column on the extreme left gives the unique FlyBase gene ID (CG number) for each. The second column gives the human homologue. The third column gives the percent identity between the corresponding *Drosophila* and human proteins. The fourth column gives the C-terminal three amino acids of the *Drosophila* protein. The fifth column gives the tag used to measure colocalization and its appended location on the protein. The column at extreme right gives the percent colocalization between the signal from tagged candidate proteins and GFP-PTS1 and represents the average of three individual measurements from three biological replicates for a total of nine cells measured. Black highlighted sequences, >60% colocalization of tagged *Drosophila* protein with GFP-PTS1; gray highlighted sequences, 30–60% colocalization of tagged *Drosophila* protein with GFP-PTS1; unhighlighted sequences, <30% colocalization of tagged *Drosophila* protein with GFP-PTS1.

CG Number	Human Gene (PTS1*)	% Identity	C-term	Tag/Location	% Colocalization w/ GFP-PTS1
CG8430-PA	*GOT1**	55	NKL	RFP/N-term	91.5 ± 1.40
CG3589-PA	*TYSND1**	20	SKL	RFP/N-term	85.7 ± 3.80
CG4625-PA	*GNPAT**	25	AKL	RFP/N-term	84.07 ± 4.13
CG3926-PA	*AGXT/SPAT**	44	SKI	RFP/N-term	83.9 ± 2.56
CG10253-PA	*AGPS**	50	AKL	RFP/N-term	83.8 ± 7.10
CG10672-PA	*DHSR4/PECR**	50	ARL	RFP/N-term	82.50 ± 8.50
CG9319-PA	*AMACR**	49	AKL	RFP/N-term	80.77 ± 1.95
CG11737-PA	*TMEM135*	30	FAS	FLAG/N-term	79.80 ± 3.82
CG18003-PA	*HAO1/2**	47	AKL	RFP/N-term	79.20 ± 7.89
CG12703-PA	*PMP70*	56	FGS	FLAG/C-term	78.80 ±8.29
CG17753-PA	*CCS**	42	QKL	RFP/N-term	78.70 ± 5.15
CG1041-PA	*CRAT**	34	SKL	RFP/N-term	77.17 ± 7.25
CG5590-PA	*HSDL2**	57	SKL	FLAG/N-term	76.93 ± 6.98

CG12236-PA	*DDO**	32	SKL	FLAG/N-term	76.50 ± 2.30
CG17597-PA	*SCPx**	63	AKL	RFP/N-term	76.30 ± 8.66
CG5362-PA	*MDH1**	66	SNL	FLAG/N-term	76.30 ± 8.50
CG6331-PA	*SLC22A5*	33	KSG	FLAG/C-term	76.23 ±13.8
CG3415-PA	*DBP**	53	AKL	RFP/N-term	76.20 ± 6.07
CG6871-PA	*CAT**	65	SKF	RFP/N-term	76.20 ± 1.21
CG5009-PA	*ACOX1**	43	AHL	RFP/N-term	75.03 ± 5.87
CG10194-PA	*NUDT19**	31	TKL	FLAG/N-term	74.43 ± 4.46
CG12338-PA	*DAO**	33	SKL	RFP/N-term	74.26 ± 2.82
CG9527-PA	*ACOX3**	42	AKL	RFP/N-term	73.97 ± 1.24
CG18155-PB	*ACSF3*	26	VSK	FLAG/N-term	73.70 ± 5.24
CG32250-PA	*PMP34*	46	KRN	FLAG/C-term	73.17 ± 1.21
CG12428-PA	*CROT**	30	SKL	RFP/N-term	72.87 ± 6.19
CG12512-PA	*ACSF2**	36	ARL	FLAG/N-term	71.87 ± 9.13
CG9577-PA	*ECH1**	45	AKL	RFP/N-term	70.13 ± 3.04
CG13890-PA	*PEC1**	35	AKL	RFP/N-term	68.77 ± 7.48
CG5065-PA	*FAR1/2*	38	PFL	FLAG/N-term	67.17 ± 5.16
CG7171-PA	*URO**	44	SHL	FLAG/N-term	67.10 ± 5.44
CG10399-PA	*HMGCL*	56	RVK	FLAG/N-term	66.63 ± 2.87
CG10367-PA	*HMGCR*	45	TIS	FLAG/N-term	65.43 ± 7.18
CG11793-PA	*SOD1**	61	AKV	FLAG/N-term	62.53 ± 8.95
CG4389-PB	*LBP**	27	SKL	RFP/N-term	59.67 ± 2.75
CG2316-PA	*ABCD1/2*	46	FLS	FLAG/N-term	57.00 ± 6.16
CG11077-PA	*PMP22*	26	LNS	FLAG/N-term	55.03 ± 3.61
CG8798-PC	*LONP*	32	PYS	FLAG/C-term	49.40 ± 8.41
CG6713-PA	*NOS2*	44	SQP	FLAG/N-term	47.10 ± 3.90
CG10268-PA	*PMVK*	38	QYR	FLAG/C-term	34.53 ± 7.44
CG7642-PA	*XDH*	51	IVP	FLAG/N-term	32.07 ± 25.64
CG1134-PA	*MUL1*	29	FIA	FLAG/N-term	30.20 ± 10.57
CG7400-PA	*SLC27A4*	45	IRF	FLAG/N-term	18.97 ± 2.94
CG8032-PA	*PAOX*	28	ALD	FLAG/C-term	16.03 ± 2.81
CG7217-PA	*PRDX5*	56	GKK	FLAG/N-term	15.87 ± 5.08
CG3961-PA	*ACSL1*	46	HLD	FLAG/N-term	9.77 ± 5.48
CG11208-PA	*HACL1**	53	SKL	FLAG/N-term	9.40 ± 3.12
CG3699-PA	*DECR2*	29	TPR	FLAG/C-term	8.97 ± 1.89
CG32451-PA	*ATP2CD1*	63	DFV	FLAG/N-term	8.87 ± 5.98
CG8732-PH	*ACSL3*	46	YAS	FLAG/N-term	8.83 ± 6.19
CG1633-PA	*PRDX1*	69	TTS	FLAG/N-term	8.13 ± 6.81
CG30194-PD	*SLC27A2*	36	DFV	FLAG/N-term	7.17 ± 4.28

CG3961-PC	*ACSL5/6*	48	HLD	FLAG/C-term	6.97 ± 2.93
CG17510-PE	*FIS1*	47	ARK	FLAG/N-term	6.57 ± 2.89
CG4860-PA	*ACAD11*	24	GKE	FLAG/N-term	6.17 ± 1.36
CG1882-PA	*EPHX2*	11	KPK	FLAG/C-term	6.13 ± 2.16
CG5517-PA	*IDE**	45	SKL	FLAG/N-term	5.73 ± 2.55
CG5919-PA	*IDI1/2*	48	QRF	FLAG/N-term	5.43 ± 4.29
CG17018-PA	*LKAP*	16	KIA	FLAG/N-term	4.60 ± 2.17
CG9149-PA	*ACAA1*	38	RLS	FLAG/N-term	4.27 ± 1.42
CG12355-PB	*MP17*	28	SET	FLAG/C-term	4.10 ± 5.37
CG8905-PA	*SOD2*	58	LGC	FLAG/N-term	3.93 ± 6.81
CG3943-PA	*SERHL*	32	KEA	FLAG/N-term	3.90 ± 1.04
CG11095-PA	*NUDT7*	15	MRT	FLAG/N-term	3.50 ± 3.77
CG14688-PB	*PHYH*	13	RKA	FLAG/N-term	3.30 ± 2.81
CG31548-PA	*DRS7B*	41	CPR	FLAG/N-term	2.30 ± 0.90
CG7176-PA	*IDH1*	71	AAK	FLAG/N-term	1.77 ± 1.20
CG33671-PA	*MVK*	30	LDD	FLAG/N-term	0.50 ± 0.87

Table 2.3. Summary of reciprocal BLASTp analysis of predicted *Drosophila* peroxisomal proteins. Summary of reciprocal BLASTp analysis of predicted *Drosophila* peroxisomal proteins. Putative *Drosophila melanogaster* peroxisomal proteins identified in the original screen were subject to reciprocal BLASTp analysis against the 'refseq' *Homo sapiens* proteome at NCBI (taxid:9606). Results showing the *Drosophila* FlyBase ID used for each query and the corresponding BLAST hit and E-value for each are presented. Sequences shadowed in red highlight 10 reciprocal best hits for homologues of human peroxisomal proteins not identified in the original screen.

Name	Top BLAST	E-value	Next Best	E-value	Better hit?
CG9149-PA	NP_005882.2	1.67E-161	NP_006102.2	1.35E-109	FBpp0079472
CG4860-PA	NP_000008.1	6.57E-166	NP_001600.1	7.81E-97	NO
CG5009-PA	NP_004026.2	0	NP_003491.1	2.95E-129	
CG9527-PA	NP_003492.2	0	NP_009223.2	1.97E-85	
CG12512-PA	NP_079425.3	7.81E-146	NP_872423.3	6.15E-37	
CG18155-PB	NP_777577.2	1.7E-73	NP_005613.2	6.88E-11	
CG3961-PA	NP_976313.1	0	NP_001192179.1	0.00E+00	
CG8732-PH	NP_004448.2	0	NP_075266.1	0.00E+00	
CG3961-PC	NP_976313.1	0	NP_001192179.1	0.00E+00	
CG1041-PA	NP_001244292.1	5.44E-140	NP_001136405.1	4.72E-100	
CG12428-PA	NP_066974.2	8.14E-114	NP_001244292.1	1.36E-75	
CG3415-PA	NP_000405.1	0	NP_055049.1	6.72E-22	
CG3699-PA	NP_116172.2	1.09E-35	NP_057370.1	7.62E-34	NO
CG10672-PA	NP_066284.2	2.67E-87	NP_005785.1	1.00E-78	
CG9577-PA	NP_001389.2	6.57E-92	XP_006710803.1	4.13E-19	
CG4389-PB	NP_000173.2	0	NP_001957.2	1.30E-85	
CG13890-PA	NP_006108.2	4.1E-49	NP_001137442.1	2.24E-29	
CG17597-PA	NP_002970.2	0	NP_001290182.1	3.71E-09	
CG9319-PA	NP_055139.4	1.48E-123	XP_011513828.1	2.56E-35	

CG11208-PA	NP_036392.2	0	NP_006835.2	1.25E-54	
CG7176-PA	NP_005887.2	0	-	-	
CG10672-PA	NP_066284.2	2.67E-87	NP_005785.1	1.00E-78	NO
CG14688-PB	NP_001094346.1	4.5E-81	NP_001032626.1	0.01	NO
CG10253-PA	NP_003650.1	0	NP_919417.1	6.08E-24	
CG4625-PA	XP_005273370.1	1.55E-82	NP_065969.3	5.08E-26	
CG5065-PA	NP_115604.1	6.51E-148	NP_060569.3	1.09E-136	
CG6871-PA	NP_001743.1	0	-	-	
CG17753-PA	NP_005116.1	6.47E-78	NP_000445.1	7.06E-35	
CG1882-PA	NP_071343.2	1.03E-114	NP_057090.2	8.95E-102	
CG6713-PA	NP_000611.1	0	NP_000932.3	1.45E-65	
CG1633-PA	NP_005800.3	6.65E-98	NP_002565.1	5.58E-97	
CG7217-PA	NP_036226.1	3.45E-62	-	-	
CG11793-PA	NP_000445.1	2.94E-59	NP_005116.1	6.93E-34	
CG8905-PA	NP_000627.2	7.00E-93	NP_001185689.1	3.6	
CG10367-PA	NP_000850.1	0	-	-	
CG5919-PA	NP_001304885.1	1.65E-67	NP_150286.1	4.13E-53	
CG33671-PA	NP_000422.1	5.40E-41	-	-	
CG10268-PA	NP_006547.1	3.25E-43	-	-	
CG5517-PB	NP_004960.2	0	NP_001229290.1	2.35E-157	
CG8798-PC	NP_001263409.1	0	NP_001287877.1	1.81E-145	
CG3943-PA	XP_011528386.1	1.24E-42	XP_005265391.1	3.11E-04	
CG3589-PA	-		-	-	
CG3926-PA	NP_000021.1	3.79E-119	NP_066977.1	5.7	
CG12338-PA	NP_003640.2	1.34E-63	NP_001908.3	1.04E-45	
CG11236-PA	NP_003640.2	2.72E-52	NP_001908.3	8.54E-42	
CG8430-PA	NP_002070.1	2.48E-168	NP_002071.2	1.05E-133	
CG31548-PA	NP_066284.2	1.89E-31	NP_057330.2	4.68E-29	

CG18003-PA	NP_060015.1	5.46E-124	NP_057611.1	4.05E-111
CG10399-PA	NP_000182.2	1.23E-138	NP_001035865.1	6.45E-135
CG5590-PA	NP_115679.2	4.89E-161	NP_000405.1	1.45E-15
CG17018-PA	XP_011521062.1	2.76E-92	-	-
CG5362-PA	NP_005908.1	3.21E-159	-	-
CG1134-PA	NP_078820.2	3.46E-47	NP_001158.2	3.87E-06
CG10194-PA	NP_001099040.1	1.83E-54	XP_011513889.1	3.2
CG11095-PA	NP_001230679.1	5.31E-28	NP_001099133.1	1.51E-11
CG8032-PA	NP_787033.1	1.77E-80	XP_006710537.1	2.07E-26
CG7171-PA	-	-	-	-
CG7642-PA	XP_011531397.1	0	-	-
CG2316-PA	NP_005155.1	0	NP_000024.2	0
CG12703-PA	NP_002849.1	0	NP_005155.1	7.51E-150
CG32451-PA	NP_001186113.1	0	NP_055676.3	0
CG17510-PE	NP_057152.2	6.25E-40	-	-
CG12355-PB	NP_001121895.1	3.68E-29	NP_002428.1	8.42E-13
CG11077-PA	NP_002428.1	4.42E-26	NP_116072.2	6.11E-10
CG6331-PA	NP_003051.1	1.83E-107	NP_004247.2	2.42E-107
CG32250-PA	NP_006349.1	2.13E-88	NP_110407.2	3.24E-32
CG30194-PD	NP_940982.1	0	NP_005085.2	0
CG7400-PA	NP_005085.2	0	NP_940982.1	0
CG11737-PA	NP_075069.3	2.59E-66	XP_006723513.1	7.5
CG6760	XP_005250490.1	3.90E-100	NP_996671.1	1.84E-65
CG7081-PA	NP_000309.1	3.24E-37	NP_002608.1	3.45E-05
CG6859-PA	NP_003621.1	1.24E-59	NP_001295.2	6.5
CG14815-PB	NP_001124496.1	1.89E-119	NP_001243685.1	2.05E-87
CG11919-PA	NP_001303242.1	7.72E-108	NP_009057.1	1.81E-71
CG6486-PA	NP_000279.1	2.51E-82	NP_001128728.1	6.85E-21

CG7864-PA	NP_002608.1	2.03E-44	NP_008844.1	5.57E-10
CG8315-PA	NP_003837.1	1.74E-35	NP_003838.1	9.78E-33
CG13827-PA	NP_542393.1	1.84E-32	-	-
CG3639-PA	NP_000277.1	8.68E-27	NP_002608.1	0.004
CG4663-PA	XP_009440785.1	2.47E-46	NP_001034794.1	3.3
CG4289-PA	NP_004556.1	6.40E-24	-	-
CG3947-PA	NP_004804.1	3.88E-58	-	-
CG5325-PA	NP_002848.1	4.55E-27	-	-

Table 2.4. Effect of overexpression of genes encoding candidate *Drosophila* peroxisome proteins on peroxisome volume in S2 cells. Effect of overexpression of genes encoding candidate *Drosophila* peroxisomal proteins on peroxisome volume in *Drosophila* S2 cells. Plasmids encoding candidate peroxisomal proteins fused to mRFP or the 3xFLAG epitope were transfected into S2 cells stably expressing GFP-PTS1, which labels peroxisomes. Rows that are black represent proteins that showed greater than 60% colocalization with GFP-PTS1. Rows that are gray represent proteins that showed 30-60% colocalization with GFP-PTS1. Rows that are white represent proteins that showed less than 30% colocalization with GFP-PTS1. The column on the left gives the FlyBase CG number. The middle column gives the human homologue. The right column gives the average volume of peroxisomes in μm^3 in transfected cells and represents the average of three individual measurements from three biological replicates for a total of nine cells measured.

FlyBase CG Number	Human Gene (PTS1*)	Peroxisome Volume (μm^3)
	Untransfected	0.173 ± 0.038
CG10268-PA	*PMVK*	0.482 ± 0.151
CG1134-PA	*MUL1*	0.426 ± 0.055
CG13827-PA	*PEX11C*	0.417 ± 0.118
CG12428-PA	*CROT**	0.414 ±0.098
CG9319-PA	*AMACR**	0.410 ±0.041
CG4625-PA	*GNPAT**	0.401 ± 0.042
CG10253-PA	*AGPS**	0.380 ± 0.127
CG10399-PA	*HMGCL*	0.377 ± 0.100
CG12236-PA	*DDO**	0.354 ± 0.072
CG12338-PA	*DAO**	0.339 ±0.022
CG8732-PH	*ACSL3*	0.327 ± 0.101
CG11095-PA	*NUDT7*	0.323 ± 0.027
CG6760-PA	*PEX1*	0.318 ± 0.020
CG17018-PA	*LKAP*	0.317 ± 0.032
CG10367-PA	*HMGCR*	0.316 ± 0.049
CG6331-PA	*SLC22A5*	0.316 ±0.027
CG5325-PA	*PEX19*	0.316 ± 0.025
CG1882-PA	*EPHX2*	0.312 ± 0.040
CG12512-PA	*ACSF2**	0.311 ±0.078
CG32451-PA	*ATP2CD1*	0.305 ± 0.063
CG8032-PA	*PAOX*	0.301 ± 0.030

CG6486-PA	*PEX7*	0.297 ± 0.038
CG5009-PA	*ACOX1**	0.291 ± 0.100
CG12703-PA	*PMP70*	0.278 ± 0.024
CG3961-PA	*ACSL1*	0.276 ± 0.016
CG3947-PA	*PEX16*	0.275 ± 0.086
CG3926-PA	*AGXT**	0.269 ± 0.030
CG11793-PA	*SOD1**	0.266 ± 0.044
CG8905-PA	*SOD2*	0.265 ± 0.011
CG7864-PA	*PEX10*	0.265 ± 0.062
CG7400-PA	*SLC27A4*	0.262 ± 0.029
CG3943-PA	*SERHL*	0.261 ± 0.023
CG7642-PA	*XDH*	0.259 ± 0.078
CG14815-PB	*PEX5*	0.259 ± 0.021
CG5919-PA	*IDI1/2*	0.256 ± 0.018
CG8798-PC	*LONP*	0.255 ± 0.021
CG11737-PA	*TMEM135*	0.254 ± 0.023
CG7176-PA	*IDH1*	0.250 ± 0.026
CG33671-PA	*MVK*	0.250 ± 0.380
CG31548-PA	*DRS7B*	0.249 ± 0.036
CG9149-PA	*ACAA1*	0.249 ± 0.062
CG7217-PA	*PRDX5*	0.240 ± 0.012
CG1633-PA	*PRDX1*	0.237 ± 0.091
CG8430-PA	*GOT1**	0.236 ± 0.012
CG14688-PB	*PHYH*	0.234 ± 0.054
CG9527-PA	*ACOX3**	0.231 ± 0.046
CG6871-PA	*CAT**	0.230 ± 0.017
CG3961-PC	*ACSL5/6*	0.226 ± 0.031
CG5065-PA	*FAR1/2*	0.226 ± 0.031
CG3589-PA	*TYSND1**	0.226 ± 0.026
CG17510-PE	*FIS1*	0.220 ± 0.073
CG3415-PA	*DBP**	0.217 ± 0.062
CG10194-PA	*NUDT19**	0.216 ± 0.023
CG11077-PA	*PMP22*	0.214 ± 0.004
CG3639-PA	*PEX12*	0.208 ± 0.024
CG7081-PA	*PEX2*	0.207 ± 0.042
CG6859-PA	*PEX3*	0.199 ± 0.078
CG4389-PB	*LBP**	0.198 ± 0.121
CG5590-PA	*HSDL2**	0.192 ± 0.027
CG7171-PA	*URO**	0.186 ± 0.016
CG18155-PB	*ACSF3*	0.184 ± 0.010
CG32250-PA	*PMP34*	0.184 ± 0.013
CG11208-PA	*HACL1**	0.182 ± 0.019
CG6713-PA	*NOS2*	0.182 ± 0.034

CG4663-PA	*PEX13*	0.182 ± 0.041
CG4289-PA	*PEX14*	0.182 ± 0.014
CG4860-PA	*ACAD11*	0.175 ± 0.017
CG18003-PA	*HAO1/2**	0.170 ± 0.024
CG11919-PA	*PEX6*	0.169 ± 0.021
CG9577-PA	*ECH1**	0.167 ± 0.023
CG1041-PA	*CRAT**	0.164 ± 0.009
CG13890-PA	*PEC1**	0.162 ± 0.044
CG5362-PA	*MDH1**	0.158 ± 0.030
CG2316-PA	*ABCD1/2*	0.158 ± 0.007
CG12355-PB	*MP17*	0.156 ± 0.001
CG30194-PD	*SLC27A2*	0.149 ± 0.014
CG8315-PA	*PEX11A/B*	0.139 ± 0.015
CG10672-PA	*DHSR4/PECR**	0.134 ± 0.009
CG17753-PA	*CCS**	0.133 ± 0.023
CG3699-PA	*DECR2*	0.132 ± 0.025
CG5517-PA	*IDE**	0.129 ± 0.086
CG17597-PA	*SCPx**	0.109 ± 0.042

Table 2.5. Effect of overexpression of genes encoding candidate *Drosophila* peroxisome proteins on peroxisome number in S2 cells. Effect of overexpression of genes encoding candidate *Drosophila* peroxisomal proteins on peroxisome number in *Drosophila* S2 cells. Plasmids encoding candidate peroxisomal proteins fused to mRFP or the 3xFLAG epitope were transfected into S2 cells stably expressing GFP-PTS1, which labels peroxisomes. Rows that are black represent proteins that showed greater than 60% colocalization with GFP-PTS1. Rows that are gray represent proteins that showed 30-60% colocalization with GFP-PTS1. Rows that are white represent proteins that showed less than 30% colocalization with GFP-PTS1. The column on the left gives the FlyBase CG number. The middle column gives the human homologue. The right column gives the average number of peroxisomes in transfected cells and represents the average of three individual measurements from three biological replicates for a total of nine cells measured.

FlyBase CG Number	Human Gene (PTS1*)	Peroxisomes/Cell
	Untransfected	72.00 ± 7.00
CG2316-PA	*ABCD1/2*	129 ± 30.79
CG30194-PD	*SLC27A2*	120.33 ± 23.69
CG12355-PB	*MP17*	117.67 ± 34.36
CG3589-PA	*TYSND1**	113.67 ± 39.55
CG11208-PA	*HACL1**	107.67 ± 21.13
CG8315-PA	*PEX11A/B*	104.33 ± 6.51
CG17510-PE	*FIS1*	104.00 ± 31.58
CG7081-PA	*PEX2*	101.00 ± 8.89
CG13827-PA	*PEX11C*	95.33 ± 37.86
CG11077-PA	*PMP22*	83.33 ± 0.58
CG8430-PA	*GOT1**	82.33 ± 1.53
CG18003-PA	*HAO1/2**	82.00 ± 3.61
CG1633-PA	*PRDX1*	80.00 ± 14.53
CG12703-PA	*PMP70*	80.00 ± 21.79
CG18155-PB	*ACSF3*	79.67 ± 7.02
CG5325-PA	*PEX19*	77.67 ± 8.08
CG4389-PB	*LBP**	76.33 ± 24.01
CG11737-PA	*TMEM135*	75.67 ± 24.68
CG3943-PA	*SERHL*	73.33 ± 7.37
CG8732-PH	*ACSL3*	68.33 ± 10.69
CG10253-PA	*AGPS**	67.67 ± 2.52

CG17597-PA	*SCPx**	67.33 ± 21.52
CG12236-PA	*DDO**	66.67 ± 9.50
CG10399-PA	*HMGCL*	66.33 ± 15.31
CG3961-PC	*ACSL5/6*	66.00 ± 11.53
CG6713-PA	*NOS2*	65.00 ± 33.41
CG9577-PA	*ECH1**	64.00 ± 12.49
CG5065-PA	*FAR1/2*	63.00 ± 1.73
CG7864-PA	*PEX10*	63.00 ± 19.08
CG3639-PA	*PEX12*	63.00 ± 2.65
CG17018-PA	*LKAP*	61.67 ± 1.53
CG5919-PA	*IDI1/2*	60.67 ± 15.04
CG31548-PA	*DRS7B*	60.67 ± 18.56
CG4663-PA	*PEX13*	60.33 ± 1.53
CG5517-PA	*IDE**	60.00 ± 34.51
CG32451-PA	*ATP2CD1*	59.00 ± 20.42
CG1882-PA	*EPHX2*	58.67 ± 12.74
CG4625-PA	*GNPAT**	58.00 ± 6.56
CG10367-PA	*HMGCR*	57.33 ± 13.05
CG12512-PA	*ACSF2**	57.00 ± 10.15
CG3699-PA	*DECR2*	57.00 ± 4.58
CG14815-PB	*PEX5*	57.00 ± 15.59
CG17753-PA	*CCS**	55.33 ± 11.59
CG5590-PA	*HSDL2**	54.33 ± 15.57
CG4860-PA	*ACAD11*	53.33 ± 15.70
CG3415-PA	*DBP**	52.67 ± 7.02
CG3947-PA	*PEX16*	51.67 ± 2.52
CG9319-PA	*AMACR**	51.00 ± 2.65
CG14688-PB	*PHYH*	51.00 ± 4.00
CG7217-PA	*PRDX5*	51.00 ± 6.56
CG7400-PA	*SLC27A4*	50.67 ± 3.79
CG6859-PA	*PEX3*	48.00 ± 19.97
CG10194-PA	*NUDT19**	47.33 ± 11.24
CG11095-PA	*NUDT7*	45.67 ± 16.20
CG10672-PA	*DHSR4/PECR**	45.00 ± 3.61
CG7171-PA	*URO**	44.67 ± 10.50
CG12428-PA	*CROT**	41.67 ± 4.51
CG32250-PA	*PMP34*	41.67 ± 8.62
CG10268-PA	*PMVK*	40.67 ± 6.43
CG12338-PA	*DAO**	40.33 ± 3.21
CG33671-PA	*MVK*	40.00± 8.00
CG1041-PA	*CRAT**	39.67 ± 4.51
CG8032-PA	*PAOX*	39.33 ± 14.29

CG7176-PA	*IDH1*	38.00 ± 15.13
CG9527-PA	*ACOX3**	37.67 ± 5.77
CG8905-PA	*SOD2*	37.67 ± 4.51
CG3961-PA	*ACSL1*	36.33 ± 2.08
CG4289-PA	*PEX14*	36.33 ± 10.97
CG5362-PA	*MDH1**	36.00 ± 2.65
CG6871-PA	*CAT**	34.33 ± 8.74
CG7642-PA	*XDH*	34.00 ± 10.82
CG8798-PC	*LONP*	33.67 ± 7.64
CG6331-PA	*SLC22A5*	33.00 ± 10.82
CG11919-PA	*PEX6*	32.67 ± 12.70
CG5009-PA	*ACOX1**	32.00 ± 2.65
CG1134-PA	*MUL1*	28.00 ± 19.30
CG6760-PA	*PEX1*	28.00 ± 6.08
CG6486-PA	*PEX7*	27.67 ± 5.51
CG13890-PA	*PEC1**	27.00 ± 7.00
CG3926-PA	*AGXT**	24.33 ± 9.24
CG9149-PA	*ACAA1*	21.33 ± 4.62
CG11793-PA	*SOD1**	21.00 ± 2.65

Table 2.6. Effect of overexpression of genes encoding candidate *Drosophila* peroxisomal proteins on total peroxisome volume per S2 cell. Effect of overexpression of genes encoding candidate *Drosophila* peroxisomal proteins on total peroxisome volume per S2 cell. Plasmids encoding candidate peroxisomal proteins fused to mRFP or the 3xFLAG epitope were transfected into S2 cells stably expressing GFP-PTS1, which labels peroxisomes. Rows that are black represent proteins that showed greater than 60% colocalization with GFP-PTS1. Rows that are gray represent proteins that showed 30-60% colocalization with GFP-PTS1. Rows that are white represent proteins that showed less than 30% colocalization with GFP-PTS1. The column on the left gives the FlyBase CG number. The middle column gives the human homologue. The right column gives the total peroxisome volume in μm^3 per cell calculated by multiplying the average number of peroxisomes per cell by the average volume of each individual peroxisome. The data represents the average of three individual measurements from three biological replicates for a total of nine cells measured.

FlyBase CG Number	Human Gene (PTS1*)	Total Peroxisome Volume (μm^3)
	Untransfected	12.46
CG13827-PA	*PEX11C*	39.75
CG10253-PA	*AGPS**	25.71
CG3589-PA	*TYSND1**	25.69
CG10399-PA	*HMGCL*	25.01
CG5325-PA	*PEX19*	24.54
CG12236-PA	*DDO**	23.60
CG4625-PA	*GNPAT**	23.26
CG17510-PE	*FIS1*	22.88
CG8732-PH	*ACSL3*	22.34
CG12703-PA	*PMP70*	22.24
CG9319-PA	*AMACR**	20.91
CG7081-PA	*PEX2*	20.91
CG2316-PA	*ABCD1/2*	20.38
CG10268-PA	*PMVK*	19.60
CG11208-PA	*HACL1**	19.60
CG17018-PA	*LKAP*	19.55
CG8430-PA	*GOT1**	19.43
CG11737-PA	*TMEM135*	19.22
CG3943-PA	*SERHL*	19.14

CG1633-PA	*PRDX1*	18.96
CG12355-PB	*MP17*	18.36
CG1882-PA	*EPHX2*	18.31
CG10367-PA	*HMGCR*	18.12
CG32451-PA	*ATP2CD1*	18.00
CG30194-PD	*SLC27A2*	17.93
CG11077-PA	*PMP22*	17.83
CG12512-PA	*ACSF2**	17.73
CG12428-PA	*CROT**	17.25
CG7864-PA	*PEX10*	16.70
CG5919-PA	*IDI1/2*	15.53
CG4389-PB	*LBP**	15.11
CG31548-PA	*DRS7B*	15.11
CG3961-PC	*ACSL5/6*	14.92
CG14815-PB	*PEX5*	14.76
CG11095-PA	*NUDT7*	14.75
CG18155-PB	*ACSF3*	14.66
CG8315-PA	*PEX11A/B*	14.50
CG5065-PA	*FAR1/2*	14.24
CG3947-PA	*PEX16*	14.21
CG18003-PA	*HAO1/2**	13.94
CG12338-PA	*DAO**	13.67
CG7400-PA	*SLC27A4*	13.28
CG3639-PA	*PEX12*	13.10
CG7217-PA	*PRDX5*	12.24
CG14688-PB	*PHYH*	11.93
CG1134-PA	*MUL1*	11.93
CG8032-PA	*PAOX*	11.84
CG6713-PA	*NOS2*	11.83
CG3415-PA	*DBP**	11.43
CG4663-PA	*PEX13*	10.98
CG9577-PA	*ECH1**	10.69
CG5590-PA	*HSDL2**	10.43
CG6331-PA	*SLC22A5*	10.43
CG10194-PA	*NUDT19**	10.22
CG3961-PA	*ACSL1*	10.03
CG33671-PA	*MVK*	10.00
CG8905-PA	*SOD2*	9.98
CG6859-PA	*PEX3*	9.55
CG7176-PA	*IDH1*	9.50
CG4860-PA	*ACAD11*	9.33
CG5009-PA	*ACOX1**	9.31

CG6760-PA	*PEX1*	8.90
CG7642-PA	*XDH*	8.81
CG9527-PA	*ACOX3**	8.70
CG8798-PC	*LONP*	8.59
CG7171-PA	*URO**	8.31
CG6486-PA	*PEX7*	8.22
CG6871-PA	*CAT**	7.90
CG5517-PA	*IDE**	7.74
CG32250-PA	*PMP34*	7.67
CG3699-PA	*DECR2*	7.52
CG17753-PA	*CCS**	7.36
CG17597-PA	*SCPx**	7.34
CG4289-PA	*PEX14*	6.61
CG3926-PA	*AGXT**	6.54
CG1041-PA	*CRAT**	6.51
CG10672-PA	*DHSR4/PECR**	6.03
CG5362-PA	*MDH1**	5.69
CG11793-PA	*SOD1**	5.59
CG11919-PA	*PEX6*	5.52
CG9149-PA	*ACAA1*	5.31
CG13890-PA	*PEC1**	4.37

Chapter 3: Pex13 and Pex14 function at the lipid droplet surface to regulate lipolysis

3.1. Abstract

Previous studies have shown that peroxisomes and lipid droplets physically interact in cells under certain conditions, particularly when the culture medium is supplemented with excess lipid (Binns et al., 2006; Schrader, 2001). Despite growing evidence of physical interaction, little is still known about what mechanism facilitates this interaction or what function peroxisomes perform at lipid droplets. This chapter outlines my analysis of peroxisome and lipid droplet interactions in *Drosophila melanogaster*. S2 cells cultured in the presence of oleate showed an upregulation of *Pex14* expression. Further, knockdown of *Pex14* in S2 cells showed increased lipolytic activity. This phenotype was recapitulated in whole animals when *Pex14* expression was knocked down in the fat body of *Drosophila* larvae. In addition, when the subcellular localization of each Pex protein was analyzed in S2 cells under conditions of increased lipid droplet metabolism, it was found that Pex3, Pex13, and Pex14 all localize to the surface of the LD. This phenotype was conserved in mammalian cells. The localization of Pex14 to the lipid droplet surface was not observed when the perilipin, *Lsd1* was simultaneously overexpressed in S2 cells. Conversely, the simultaneous overexpression of *Pex14* and the lipase, *Hsl*, resulted in the mislocalization of Hsl to the cytosol. Lastly, knockdown of *Pex14* in S2 cells results in differential expression levels of *CGI-58*, a major regulator of lipolysis. In summary, it appears that Pex13 and Pex14 are targeted to the LD surface during periods of increased lipid metabolism, where they function to regulate lipid mobilization.

3.2. Background

Organelles compartmentalize biochemical functions within the eukaryotic cell. Physical partitioning of particular biochemical processes into discrete compartments enhances the efficiency of the biochemical reactions involved. However, to maintain cellular homeostasis, these organelles must communicate in some way in order to jointly coordinate these processes. Two such organelles, the peroxisome and the LD, are both involved in the metabolism of cellular lipids. Because of their involvement in similar metabolic processes, the metabolic pathways that occur at each respective organelle overlap through common metabolites or intermediates. Therefore, it is critical for peroxisomes and LDs to communicate in order to cooperatively regulate lipid metabolism.

Studies have revealed that LDs interact with a number of other organelles (reviewed in Gao and Goodman, 2015). Proteomic studies have shown specific organelle proteins, such as ER luminal chaperones and mitochondrial oxidative enzymes, within LDs (Pu et al., 2011; Wang et al., 2015). Microscopic studies have similarly revealed intimate physical connections between LDs and other organelles. In particular, LDs show extensive interactions with the ER. Often, mature LDs remain completely connected to the ER membrane through membrane bridges (reviewed in Gao and Goodman, 2015). In fact, in yeast cells, LDs never fully dissociate from the ER membrane (Szymanski et al., 2007). These bridges allow for the continuous transfer of lipids from the ER to LDs, and some enzymes involved in neutral lipid biosynthesis, such as the yeast diacylglycerol acyltransferase, Lro1p, have been found concentrated at these sites (Wang and Lee, 2012).

Peroxisomes have also been found to interact with a number of other organelles, including lysosomes and mitochondria (reviewed in Lodhi and Semenkovich, 2014). It has been shown that cholesterol is trafficked via peroxisome-lysosome contact sites facilitated by the lysosomal Syt7 binding to peroxisomal $PI(4,5)P_2$, which bridges the two organelles (Chu et al., 2015). Peroxisomes have direct contact sites with mitochondria (Fan et al., 2016), and mitochondrially derived vesicles (MDVs) have been shown to fuse with PPVs during *de novo* biogenesis (Sugiura et al., 2017).

Peroxisomes also show intimate physical connections to LDs. These two organelles were first found to be in close proximity in rabbit ovarian tissue (Blanchette, 1966). This was also later observed in rat fat pads, although complete contact between the two organelles was never observed (Blanchette-Mackie et al., 1995). In yeast cells supplemented with oleate, an 18-carbon fatty acid, peroxisomes were found to stably adhere to the surface of LDs (Binns et al., 2006). Using TEM, membrane protrusions from the peroxisome were found to extend into the interior of LDs in cells cultured with oleate (Binns et al., 2006). In these same cells, the LD fraction was found to be enriched in peroxisomal β-oxidation enzymes (Binns et al., 2006). Peroxisome-LD interactions were similarly observed in COS7 cells (Schrader, 2001). In addition, protein-protein interactions have been observed between resident LD proteins and peroxisomal markers in yeast (Pu et al., 2011). These connections between peroxisomes and LDs appear to be functional, as the transfer of neutral lipids and phospholipids between the two organelles has been observed. Chapman and Trelease used radiolabelled lipid to perform an *in vitro* pulse-chase assay to confirm the transfer of lipids from isolated fractions of LDs to glyoxysomes (Chapman and Trelease, 1991), which are specialized peroxisomes found in plant cells. More recently, the transfer of the TG lipase, SDP1, in *Arabidopsis* from

peroxisomes to LDs was observed during plant development (Thazar-Poulot et al., 2015). However, it is unclear which lipase facilitates the release of FFA at the peroxisomal-LD junction.

Despite the evidence that peroxisomes and LDs physically interact and both metabolize lipids, little is known about the function of these interactions or what regulates this mechanism. I investigated the functional relationship between peroxisomes and LDs in *Drosophila melanogaster.*

Peroxisome biology in *Drosophila* is becoming increasingly well characterized and *Drosophila* have been utilized for the discovery of novel peroxisomal functions in the immune response (Di Cara et al., 2017). *Drosophila* encodes homologues of the human PEX1, PEX2, PEX3, PEX5, PEX6, PEX7, PEX10, PEX11A/B, PEX11C, PEX12, PEX13, PEX14, PEX16, and PEX19 (see Chapter 2) and the initial steps of peroxisome biogenesis from the ER seem to be well conserved. Protein targeting via the PTS1 pathway also seems to be well conserved (see Chapter 2). LD biology is also well characterized in *Drosophila* (Beller et al., 2006; reviewed in Kühnlein, 2011; reviewed in Lee et al., 2013). *Drosophila* larvae have been used extensively to study LDs, as their development is strongly influenced by lipid metabolism, particularly in the fat body, which comprises a significant portion of the entire animal (reviewed in Kühnlein, 2011; reviewed in Lee et al., 2013; reviewed in Musselman and Kühnlein, 2018). *Drosophila* S2 cells have also been extensively used to study LD metabolism (Beller et al., 2006; Guo et al., 2008; Kory et al., 2015; Krahmer et al., 2011; Sui et al., 2018; Wang et al., 2016; Wilfling et al., 2013, 2014). While mammalian systems have five PLIN proteins, the *Drosophila* genome encodes two *PLIN* homologues: *Lsd1* and *Lsd2* (Beller et al., 2006; Bi et al., 2012; Guo et al., 2008). Lsd1 facilitates lipid mobilization by recruiting

Hsl, upon phosphorylation, to the LD surface during lipolysis (Bi et al., 2012). In contrast, Lsd2 serves to protect LDs from lipases, such as Bmm, the *Drosophila* homologue of ATGL (Bi et al., 2012).

This chapter outlines an analysis of the interactions observed between peroxisomal components, Pex13 and Pex14, with the LD surface in *Drosophila.* I will also describe observations investigating how Pex13 and Pex14 modulate LD-protein components, which serves to regulate lipid mobilization at the LD surface.

3.3. Results

3.3.1. Peroxisomes respond to oleate in S2 cells

In order to stimulate LD biogenesis, S2 cells were cultured in Schneider's medium with fetal bovine serum (FBS) and 1 mM oleate for 24 hours. Oleate, an 18-carbon fatty acid, is taken up by the cells and esterified to a glycerol backbone to form TG for storage within the LD (Darfler, 1990; Guo et al., 2008). Peroxisomes were visualized in S2 cells using an anti-SKL antibody, shown in Figure 3.1A. The presence of –SKL at the C-terminus of proteins targets them to the matrix of peroxisomes via the PTS1 pathway (Gould et al., 1989). The size and number of peroxisomes per cell were quantified in each state. In the oleate-supplemented state (+oleate), S2 cells possessed fewer peroxisomes per cell relative to the standard state (Schneider's medium with 10% FBS) (Figure 3.1 B). S2 cells in standard conditions possessed an average of 92 peroxisomes per cell, whereas S2 cells in oleate-supplemented conditions had an average of 51 peroxisomes per cell. In addition, the peroxisomes in these cells exhibited a larger

Figure 3.1.

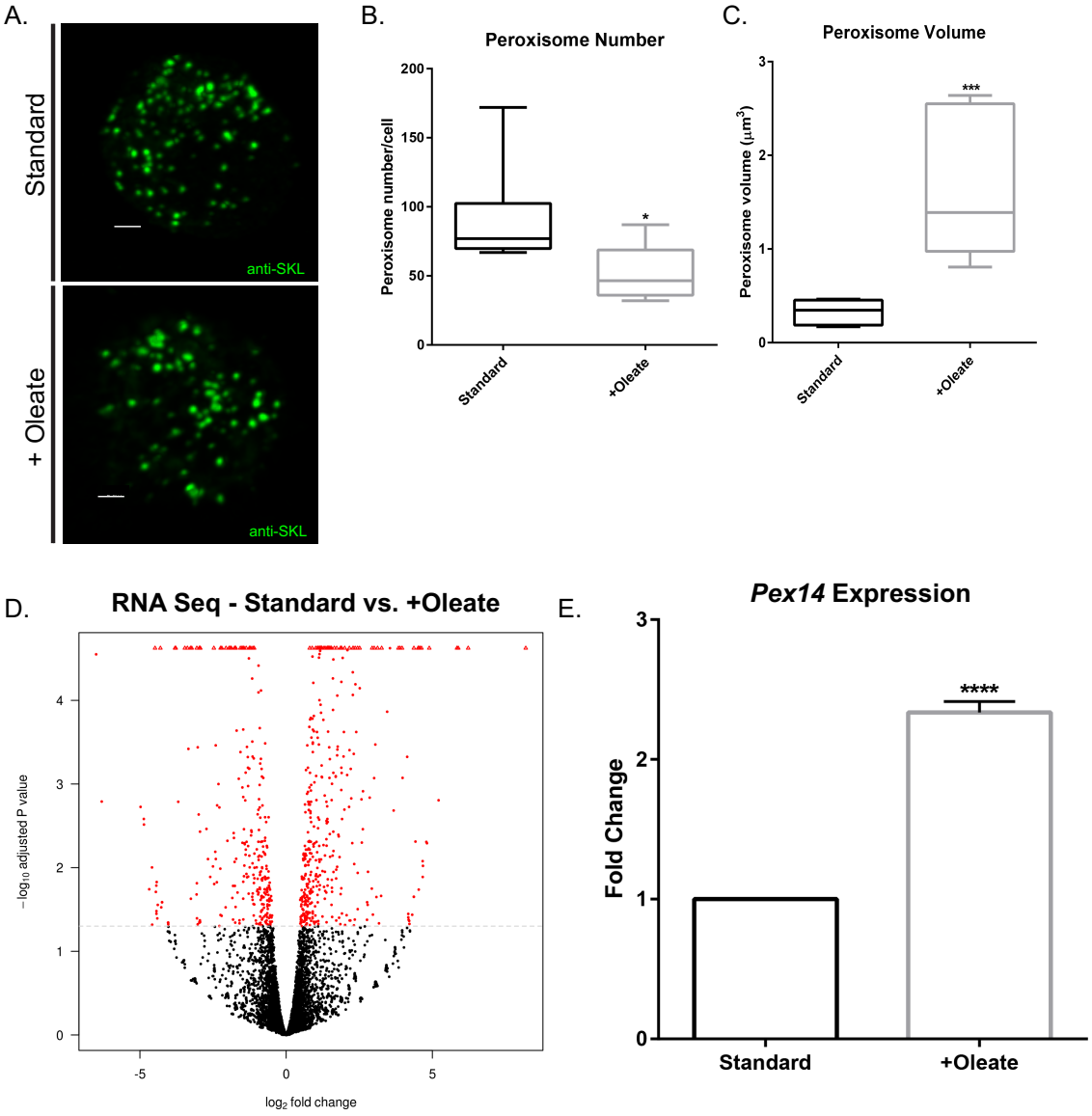
A.
Standard
+ Oleate
anti-SKL
anti-SKL
B.
Peroxisome Number
Peroxisome number/cell
200
150
100
50
0
*
Standard
+Oleate
C.
Peroxisome Volume
Peroxisome volume (μm3)
3
2
1
0
***
Standard
+Oleate
D.
RNA Seq - Standard vs. +Oleate
−log10 adjusted P value
4
3
2
1
0
-5
0
5
log2 fold change
E.
Pex14 Expression
Fold Change
3
2
1
0
****
Standard
+Oleate

Figure 3.1. Peroxisomes respond to excess oleate. A. Immunofluorescence images of fixed S2 cells in standard and oleate-supplemented conditions. Anti-SKL marks peroxisomes in green. Each image is a maximum projection of a three-dimensional volume encompassing the entire cell. Scale bar is 2 μm. B. A graph showing the average number of peroxisomes per cell in standard and oleate-supplemented conditions, calculated using Imaris software. *, $p < 0.05$ C. Graph showing the average volume of peroxisomes in each cell in standard and oleate-supplemented conditions, calculated using Imaris software ***, $p < 0.001$ For both peroxisome volume and number calculations, values represent an average of 10 cells measured from three independent biological replicates ($n = 3$) for a total of 30 cells measured. D. A volcano plot representing the expression profile of S2 cells in standard versus oleate-supplemented conditions, measured by RNA-Seq. Red dots represent genes that are differentially expressed to a statistically significant level between the two conditions. The p-value is on the y-axis, and the $\log_2$ fold change is on the x-axis. E. A graph showing the expression levels of *Pex14* in S2 cells in standard versus oleate-supplemented conditions, measured by qRT-PCR. The y- axis shows the fold change. **, $p < 0.01$. *Pex14* expression values shown are an average of three independent biological replicates ($n = 3$). All statistical analysis was performed using an unpaired Student's *t*-test.

average volume (Figure 3.1C). The average peroxisome volume increased from 0.329 μm^3 to 1.656 μm^3 when S2 cells were cultured with 1 mM oleate. This observation demonstrates that the peroxisome population responds phenotypically to the presence of excess oleate. It is unclear what mechanism is responsible for this phenotype as mature peroxisomes do not fuse. One possibility is that under oleate supplemented conditions peroxisomes begin to cluster, which causes the fluorescent signal from multiple peroxisomes to be detected as one.

In order to identify genes involved in the response to excess lipid, RNA-Seq was performed to compare S2 cells in standard conditions versus oleate-supplemented conditions. The red dots on the volcano plot (Figure 3.1D) represent genes that were significantly differentially expressed between the two conditions. Using EdgeR (Robinson et al., 2010) and DESeq2 (Love et al., 2014) software to determine differences in normalized transcript reads, 745 genes showed differential expression to a statistically significant level. This analysis was performed by Dr. Andrew Simmonds. A gene ontology analysis of the data showed enrichment in genes involved in protein glycosylation, fatty acid β-oxidation, MAP-kinase cascade, amino acid metabolism, carbohydrate metabolism, and proteolysis. Fatty acid β-oxidation showed a 6-fold enrichment, which included Mtpα, the homologue of LBP (*CG4389*). Epitope-tagged Mtpα was found to localize to peroxisomes shown in Chapter 2. *Pex14* was the only other peroxisome gene that showed significant differential expression. *Pex14* was found to be significantly ($p < 0.001$) upregulated in the oleate-supplemented state (Figure 3.1E). Pex14 is a peroxin that resides on the peroxisomal membrane and functions in the import of cargo into the peroxisome matrix (Albertini et al., 1997). Given that the relationship between LDs and peroxisomes was being explored, *Pex14* was chosen for further

investigation. The differential expression of *Pex14* between these two conditions was confirmed by qRT-PCR (Figure 3.1E), which showed a 2.5-fold increase in expression in the oleate-supplemented state ($p < 0.0001$).

3.3.2. Knockdown of Pex14 by dsRNA affects lipid droplet structure and metabolism in S2 cells

In order to determine if Pex14 affects LD activity, S2 cells were treated with dsRNA targeting *Pex14*. A scrambled dsRNA amplicon was used as a control for off-target effects. Knockdown of *Pex14* was confirmed by qRT-PCR, which showed an 80-90% reduction (Figure 3.2A). In order to measure lipolysis associated with LDs, the level of glycerol was measured in the media of S2 cells in a lipolytic state. This protocol was adopted from a previous study (Guo et al., 2008), whereby S2 cells were induced to form LDs, followed by a period of nutrient deprivation in order to upregulate lipolysis. S2 cells were supplemented with 1 mM oleate for 24 hours (+oleate), followed by the removal of FBS and oleate, and cultured in Schneider's medium alone for an additional 24 hours (lipolytic). These conditions were intended to induce lipolysis at the LD, during which the fatty acyl chains are cleaved from TG molecules and the glycerol backbone is released into the medium as a by-product (Ducharme and Bickel, 2008). S2 cells in standard and oleate supplemented conditions showed no significant change in glycerol production when treated with *Pex14* dsRNA (Figure 3.2B). In both standard and oleate-supplemented conditions, approximately 30-40 μg of glycerol per mg of protein was detected. These measurements were not affected when cells were pretreated with *Pex14*

Figure 3.2

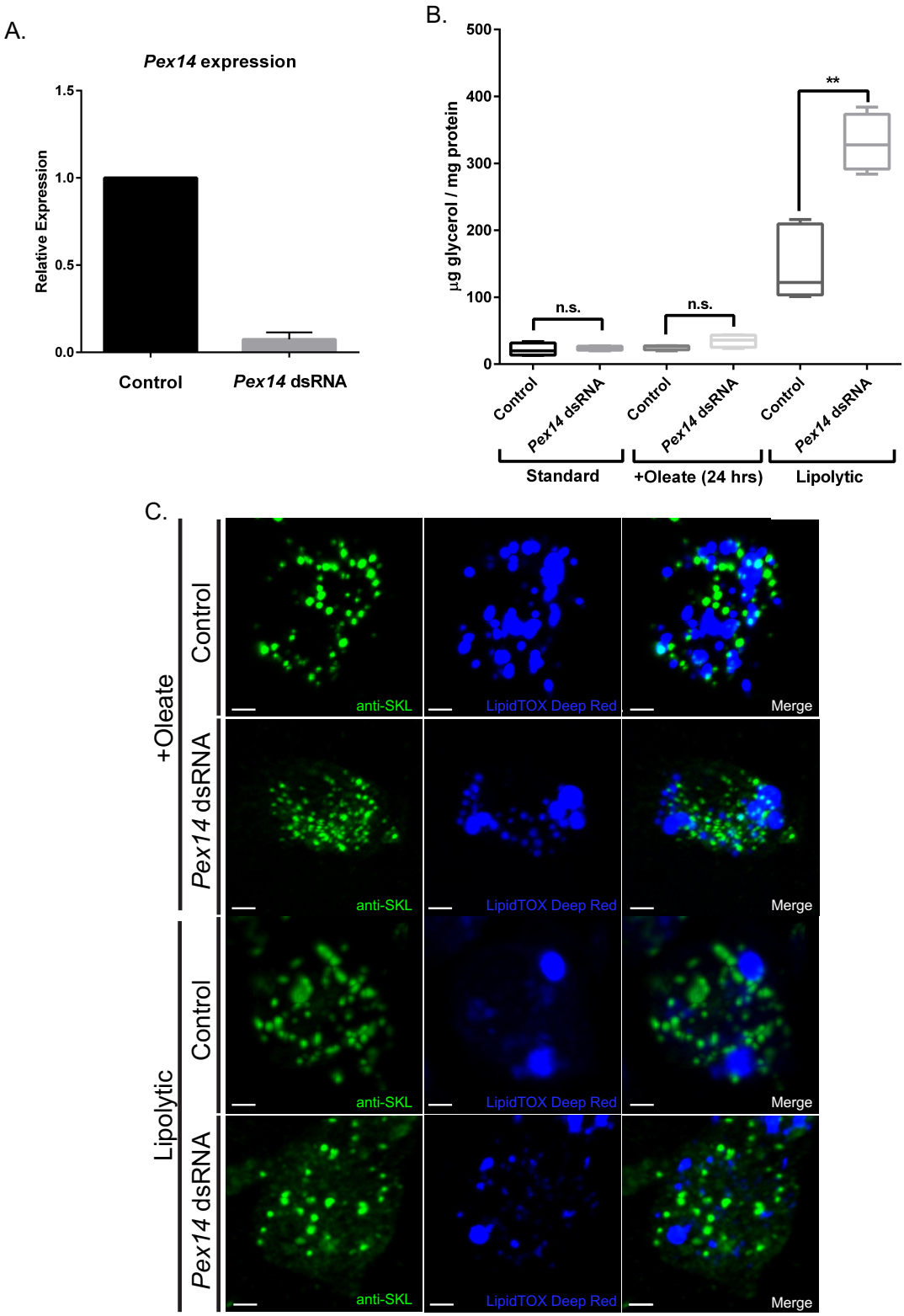
A.
Pex14 expression
Relative Expression
1.5
1.0
0.5
0.0
Control
Pex14 dsRNA
B.
µg glycerol / mg protein
500
400
300
200
100
0
n.s.
n.s.
**
Control
Pex14 dsRNA
Control
Pex14 dsRNA
Control
Pex14 dsRNA
Standard
+Oleate (24 hrs)
Lipolytic
C.
+Oleate
Control
Pex14 dsRNA
Lipolytic
Control
Pex14 dsRNA
anti-SKL
LipidTOX Deep Red
Merge

Figure 3.2

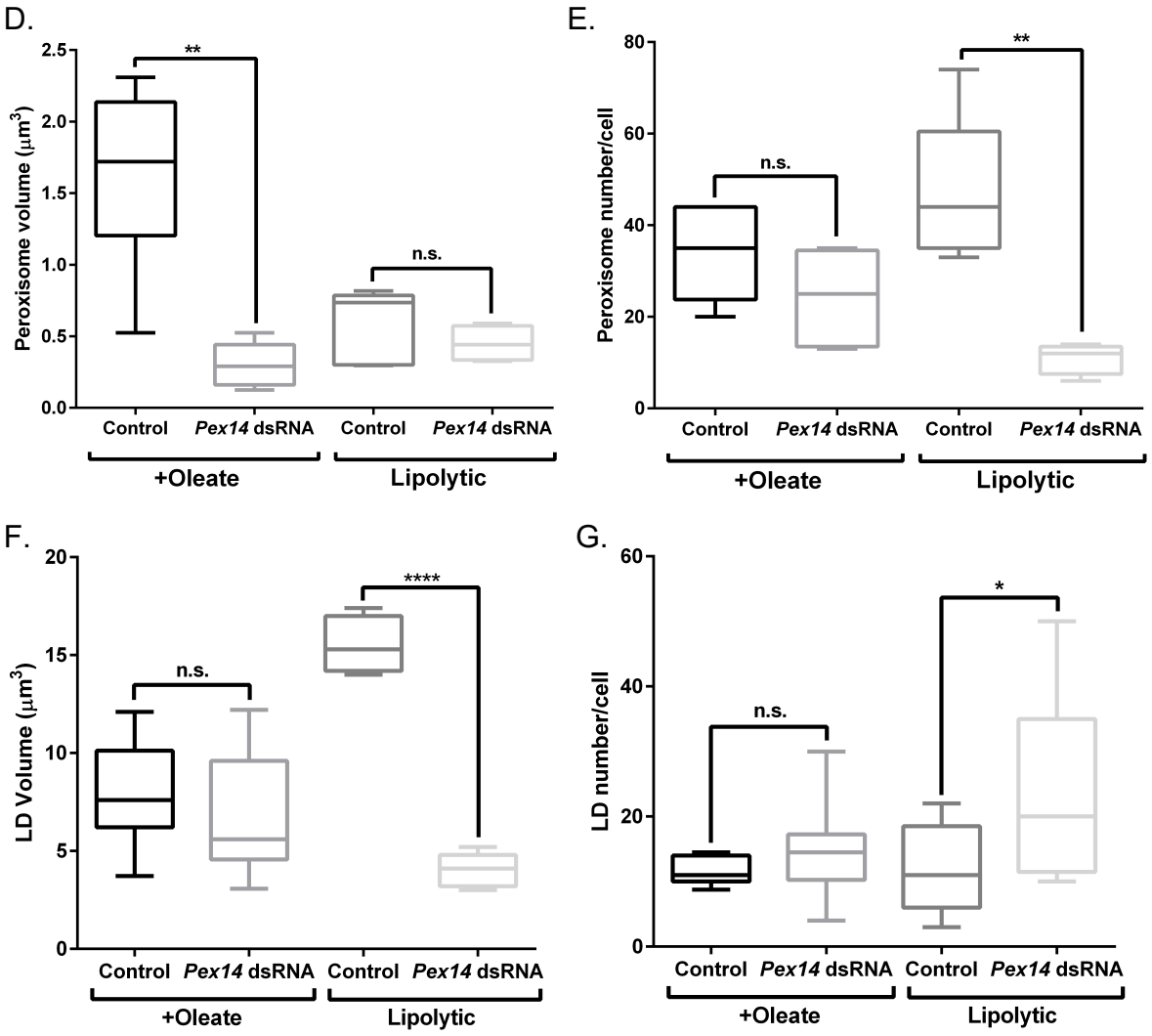
D.
Peroxisome volume (μm3)
2.5
2.0
1.5
1.0
0.5
0.0
**
n.s.
Control
Pex14 dsRNA
Control
Pex14 dsRNA
+Oleate
Lipolytic
E.
Peroxisome number/cell
80
60
40
20
0
**
n.s.
Control
Pex14 dsRNA
Control
Pex14 dsRNA
+Oleate
Lipolytic
F.
LD Volume (μm3)
20
15
10
5
0
****
n.s.
Control
Pex14 dsRNA
Control
Pex14 dsRNA
+Oleate
Lipolytic
G.
LD number/cell
60
40
20
0
*
n.s.
Control
Pex14 dsRNA
Control
Pex14 dsRNA
+Oleate
Lipolytic

Figure 3.2. Knockdown of *Pex14* increases lipolysis in S2 cells. A. The expression levels of *Pex14* transcript measured by qRT-PCR from S2 cells treated with scrambled dsRNA (control) or *Pex14* dsRNA. B. A graph showing the amount of glycerol in the medium of S2 cells in a lipolytic state treated with a scrambled dsRNA amplicon or dsRNA targeting *Pex14*. **, $p < 0.01$. The values shown are an average of six biological replicates ($n = 6$). C. S2 cells in oleate-supplemented or lipolytic state treated with scrambled dsRNA (control) or *Pex14* dsRNA. Anti-SKL marks the peroxisomes in green, and LipidTOX Deep Red marks the LDs in blue. The merge images are on the far right. Each image is a maximum projection of a three-dimensional volume encompassing the entire cell. Scale bar is 2 μm. Images shown are representative of six biological replicates. D,E. Graphs showing the average volume (F) and number (G) of peroxisomes per cell in an oleate-supplemented or lipolytic state treated with scrambled dsRNA (control) or *Pex14* dsRNA. **, $p < 0.01$. F,G. Graphs showing the average volume (F) and number (G) of LDs per cell in an oleate-supplemented or lipolytic state treated with scrambled dsRNA (control) or *Pex14* dsRNA. ****, $p < 0.0001$. *, $p < 0.05$. The values shown in D-G are an average of five individual measurements from six biological replicates, for a total of 30 cells measured. All statistical analysis was performed using an unpaired Student's *t*-test to measure the mean values between control and *Pex14* dsRNA treated cells under each metabolic condition, shown in each graph.

dsRNA. Conversely, lipolytic S2 cells treated with dsRNA targeting *Pex14* showed significantly elevated ($p < 0.01$) levels of glycerol in the medium, relative to control conditions (Figure 3.2B). Glycerol was measured relative to the protein content of the sample. In control conditions, an average of 150 μg of glycerol per mg of protein were detected. Conversely, when S2 cells were treated with *Pex14* dsRNA prior to lipolytic conditions, over 331 μg of glycerol per mg of protein were detected, demonstrating more than a two-fold increase in glycerol release (Figure 3.2B).

The morphology of LDs and peroxisomes were analyzed by staining the cells with LipidTOX Deep Red and probing with an anti-SKL antibody, respectively (Figure 3.2C). In control conditions, peroxisomes are abundant. In contrast, in cells treated with *Pex14* dsRNA, the anti-SKL signal appeared relatively diffuse throughout the cytoplasm, with some punctate structures remaining, suggesting *Pex14* expression was efficiently knocked down and PTS1 import into peroxisomes was disrupted. Both peroxisome volume and number were quantified (Figure 3.2D and 3.2E). Peroxisome volume was significantly reduced ($p < 0.01$) in oleate supplemented S2 cells pretreated with *Pex14* dsRNA (1.631 μm^3 to 0.299 μm^3); however, this effect was not observed in lipolytic conditions (Figure 3.2D). Conversely, peroxisome number was significantly reduced ($p < 0.01$) in lipolytic cells (Figure 3.2E). Lipolytic cells pretreated with a scrambled dsRNA amplicon showed an average of 47 peroxisomes per cell, whereas lipolytic cells pretreated with *Pex14* dsRNA showed an average of 11 peroxisomes per cell.

The LD volume and number per cell was quantified, shown in Figure 3.2F and 3.2G. LD volume and number were unaffected when oleate-supplemented S2 cells were pretreated with *Pex14* dsRNA (Figure 3.2F and 3.2G). S2 cells pretreated with dsRNA targeting *Pex14* prior to lipolytic conditions exhibited smaller, more numerous LDs

relative to the control cells (Figure 3.2F and 3.2G). LD volume was significantly reduced ($p < 0.0001$) from 15.57 μm^3 in control cells to 4.09 μm^3 in lipolytic cells treated with *Pex14* dsRNA (Figure 3.2F). In control conditions, each cell in lipolytic conditions contained an average of 12 LDs. Conversely, when lipolytic cells were treated with *Pex14* dsRNA, an average of 25 LDs per cell were detected (Figure 3.2G). Overall, these results suggest that perturbations to *Pex14* expression levels affect LD metabolism and morphology.

3.3.3. Tissue-specific knockdown of Pex14 in the Drosophila fat body affects the lipid content

In order to examine how Pex14 may affect lipid metabolism in the whole animal, *Pex14* was knocked down in the fat body of *Drosophila.* The fat body is the *Drosophila* equivalent of adipose tissue and comprises a significant proportion of the entire body at the larval stage (reviewed in Church and Robertson, 1966; reviewed in Musselman and Kühnlein, 2018). Tissue-specific knockdown of *Pex14* in *Drosophila* was performed using the GAL4-UAS system. UAS-*Pex14* dsRNA flies were crossed with R4-GAL4 flies, which drove the expression of dsRNA targeting the *Pex14* transcript in the fat body of the resulting progeny (Brand and Perrimon, 1993; Rodríguez et al., 2012). UAS-*Pex14* dsRNA flies were crossed to the *white*^{1118} (w^{1118}) line as a control. The w^{1118} fly line expresses a mutation that results in white eyes, whereas adult *Drosophila* have red eyes. The use of the w^{1118} line as a control allows alleles to be followed in a genetic cross. During *Drosophila* development, the 1st instar larvae hatch within 24 hours after egg-laying, which are deposited directly into the fly food. The first molt from 1st to 2nd instar

larvae occurs approximately 24 hours after egg-hatching, and the second molt from 2nd to 3rd instar larvae occurs another 24 hours after that. During this time, the larvae remain embedded in their food and continually consume nutrients. Approximately 24 hours after the transition from 2nd to 3rd instar occurs, the larvae crawl out of the food (Church and Robertson, 1966). Once wandering 3rd instar larvae emerged from the food, the animals were examined. A buoyancy assay was performed whereby 3rd instar larvae were suspended in a 12% sucrose solution (Reis et al., 2010). This examines the density of the animals, which is determined by their overall fat content and demonstrated by their propensity to float. Nearly all of the w^{1118} x UAS-*Pex14* dsRNA progeny floated in the sucrose solution (Figure 3.3A, vial labeled "C"), whereas less than 25% of the R4-GAL4 x UAS-*Pex14* dsRNA progeny floated (Figure 3.3A, vial labeled "14"). The results are quantified in Figure 3.3B. Progeny from the R4-GAL4 x UAS-*Pex14* dsRNA cross have a higher density, suggesting that they possess less overall fat. To confirm this biochemically, lysates were made from both crosses and the overall TG content of each was measured by a colorimetric assay. This analysis involved a biochemical reaction whereby larval lysates from each cross were treated with a lipase that hydrolyzed the TG found within each sample and the subsequent levels of glycerol were measured. The levels of glycerol detected would be an indirect measure of the TG per sample. R4-GAL4 x UAS-*Pex14* dsRNA progeny were found to possess significantly less ($p < 0.01$) TG than w^{1118} x UAS-*Pex14* larvae (Figure 3.3C). w^{1118} x UAS-*Pex14* dsRNA lysates contained an average of 761 μg of glycerol per mg of protein. In contrast, R4-GAL4 x UAS-*Pex14* dsRNA lysates contained an average of 189 μg of glycerol per mg of protein (Figure 3.3C). This suggests that the knockdown of *Pex14* in the fat body of *Drosophila* results in less overall fat storage or increased lipolysis in the fat body. This is consistent

Figure 3.3

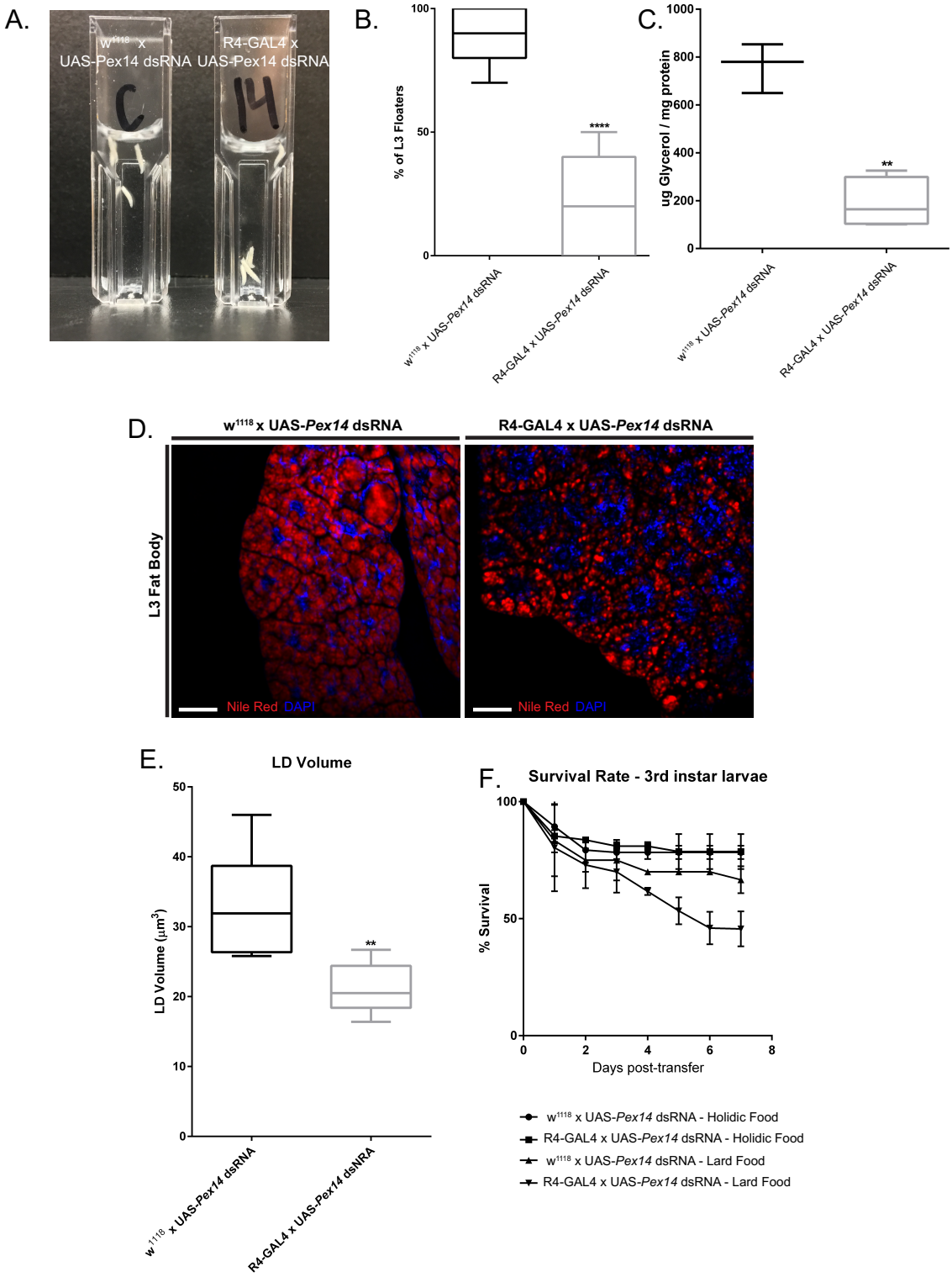
A.
w1118 x UAS-Pex14 dsRNA
R4-GAL4 x UAS-Pex14 dsRNA
B.
% of L3 Floaters
****
w1118 x UAS-Pex14 dsRNA
R4-GAL4 x UAS-Pex14 dsRNA
C.
ug Glycerol / mg protein
**
D.
w1118 x UAS-Pex14 dsRNA
R4-GAL4 x UAS-Pex14 dsRNA
L3 Fat Body
Nile Red DAPI
E.
LD Volume
LD Volume (μm3)
**
F.
Survival Rate - 3rd instar larvae
% Survival
Days post-transfer
w1118 x UAS-Pex14 dsRNA - Holidic Food
R4-GAL4 x UAS-Pex14 dsRNA - Holidic Food
w1118 x UAS-Pex14 dsRNA - Lard Food
R4-GAL4 x UAS-Pex14 dsRNA - Lard Food

Figure 3.3. Knockdown of *Pex14* in the fat body increase lipolysis in 3rd instar larvae. A. 3rd instar larvae were pulled from each cross and suspended in a 12% sucrose solution to test their overall fat content. B. A graph quantifying the number of 3rd instar larvae from each cross that floated in the sucrose solution. The values shown are an average of 10 larvae examined from three independent genetic crosses, for a total of 30 larvae examined. ****, $p < 0.0001$. C. A graph showing the quantification of overall TG from 3rd instar larvae. For each measurement, Lysates were made from 10 whole 3rd instar larvae, and total TG content was measured using a triglyceride quantification kit (Abcam). Measurements are shown as μg of glycerol per mg of protein. The values shown are an average of three biological replicates. **, $p < 0.01$. D. Fat body tissue was dissected from 3rd instar larvae from each cross and stained with Nile Red, which marks the LDs, shown in red. DAPI stains the nuclei in blue. Tissue was imaged using confocal microscopy. Images are individual slices and are representative of three biological replicates. Scale bar is 10 μm. E. A graph showing the average volume of LDs measured in the fat body of larvae from both genetic crosses. LD volume was measured using Imaris software and reported as μm^3. The values shown are an average of six independent measurements from three biological replicates for a total of 18 fat body images measured. F. Survival plot of 3rd instar larvae on holidic food versus lard food from each respective cross. Larvae were transferred from conventional food to holidic or lard food and the number of larvae remaining alive was measured after each day. Ten larvae from each cross were transferred to the different food types for each trial. The values reported are an average of five biological replicates for a total of 50 larvae examined. All statistical analysis was performed using an unpaired Student's *t*-test.

with the effects observed with the knockdown of *Pex14* in S2 cells (Figure 3.2). Fat body was dissected from 3rd instar larvae and stained with Nile Red, which marks neutral lipids (Figure 3.3D). In w^{1118} x UAS-*Pex14* dsRNA fat body, LDs appeared large and occupied the majority of each cell. In contrast, the R4-GAL4 x UAS-*Pex14* dsRNA fat body had smaller LDs (Figure 3.3D). The average LD volume in the R4-GAL4 x UAS-*Pex14* dsRNA fat body was 21.27 μm^3, which was significantly reduced ($p < 0.01$) compared to the average LD volume of 33.23 μm^3 found in control larval fat body (Figure 3.3E).

Larvae from both crosses were fed a high lipid food or minimal nutrition (holidic), and the effect on survival was measured. Four days after egg laying, 10 3rd instar larvae were transferred to new vials containing either holidic food or lard food (holidic food with the addition of lard at 22.2 g/L). Holidic food is defined by Piper et al. as "a synthetic medium for *Drosophila* made entirely from purified ingredients (holidic) that is adequate to support development, adult egg-laying and lifespan" (Piper et al., 2014). The animals were monitored and the number of larvae remaining alive was recorded each day. On either food, both crosses showed an initial loss in number, attributed to handling during the transfer process. However, after two days, both crosses on holidic food remained stable, with few changes in survival rate thereafter (Figure 3.3F). w^{1118} x UAS-*Pex14* dsRNA larvae on lard food showed reduced survival on lard food, with approximately 70% alive after seven days (Figure 3.3F). In contrast, larvae from the R4-GAL4 x UAS-*Pex14* dsRNA cross on lard food showed a steady decline in survival. Less than 40% of the initial sample remained alive after seven days (Figure 3.3F). This suggests that knockdown of *Pex14* in the fat body affects the ability of the larvae to metabolize excess dietary fat.

3.3.4. Pex3, Pex13, and Pex14 localize to the surface of lipid droplets when S2 cells are supplemented with oleate

Because the knockdown of *Pex14* had a significant effect on LD structure and metabolism, the subcellular localization of Pex14 relative to LDs was analyzed under different metabolic conditions. A 6xMyc-tagged Pex14 construct was utilized because at the time there were no antibodies available for endogenous *Drosophila* Pex14. Under standard conditions (Schneider's medium + 10% FBS), 6xMyc-Pex14 strongly localized to peroxisomes (Figure 3.4A). As previously observed (Chapter 2), epitope-tagged Pex14 strongly overlaps with the –SKL peroxisome marker. The degree of colocalization between 6xMyc-Pex14 and anti-SKL was measured using Pearson's coefficient. In addition, the degree of colocalization between the LDs and both epitope-tagged Pex14 and anti-SKL was likewise measured. When S2 cells were supplemented with 1 mM oleate for 48 hours, a portion of the 6xMyc-Pex14 signal was distinct from the peroxisome marker. Anti-SKL remained punctate, while the anti-Myc signal formed ring structures that decorated the periphery of LDs (Figure 3.4A). Some punctate structures comprised of 6xMyc-Pex14 remained overlapped with anti-SKL; however, a considerable portion of the anti-Myc signal appeared localized to the periphery of LDs. 6xMyc-Pex14 was no longer solely localized to peroxisomes, but rather displayed a dual-localization to both peroxisomes and LDs. The degree of colocalization between 6xMyc-Pex14 and anti-SKL was reduced from 80.8% in standard conditions to 37.9% in cells supplemented with oleate for 48 hours (Figure 3.4B). In addition, a concomitant increase in colocalization between 6xMyc-Pex14 and the LD marker from 17.5% in standard conditions to 47.1% in oleate-supplemented conditions was observed (Figure 3.4B). No

Figure 3.4

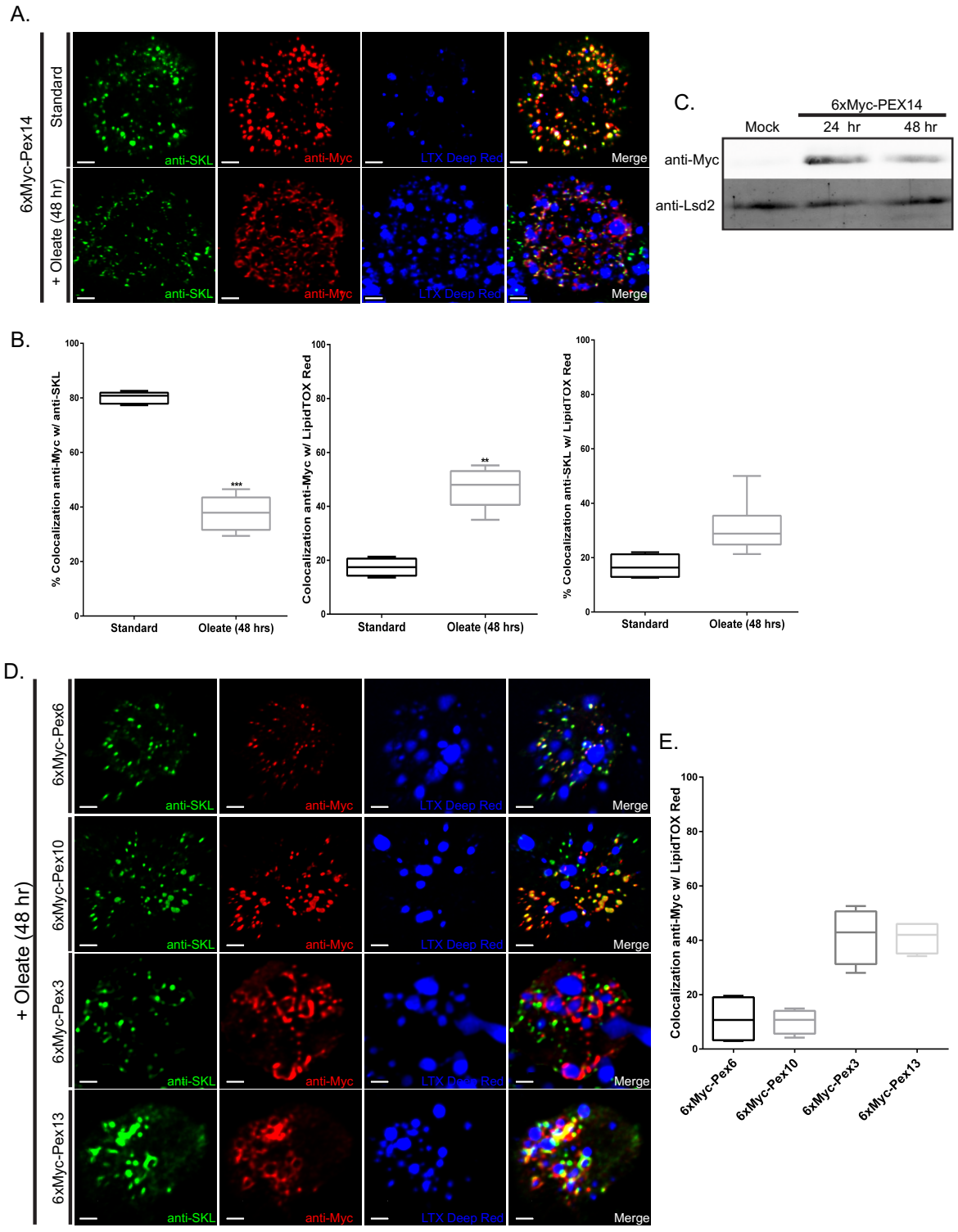
A.
6xMyc-Pex14
Standard
+ Oleate (48 hr)
anti-SKL
anti-Myc
LTX Deep Red
Merge
C.
6xMyc-PEX14
Mock
24 hr
48 hr
anti-Myc
anti-Lsd2
B.
% Colocalization anti-Myc w/ anti-SKL
Colocalization anti-Myc w/ LipidTOX Red
% Colocalization anti-SKL w/ LipidTOX Red
Standard
Oleate (48 hrs)
D.
+ Oleate (48 hr)
6xMyc-Pex6
6xMyc-Pex10
6xMyc-Pex3
6xMyc-Pex13
E.
Colocalization anti-Myc w/ LipidTOX Red

Figure 3.4. Epitope-tagged Pex3, Pex13, and Pex14 localize to LDs during periods of elevated LD metabolism. A. S2 cells transfected with 6xMyc-Pex14 in a standard or a 48-hour oleate-supplemented state. Anti-SKL marks peroxisomes in green, anti-Myc marks 6xMyc-Pex14 in red, LipidTOX Deep Red marks LDs in blue, and the merged images are in the far right panel. Each image is a maximum projection of a three-dimensional volume encompassing the entire cell. Images are representative cells from four biological replicates. The scale bar is 2 μm. B. The degree of colocalization between 6xMyc-Pex14 and anti-SKL (left graph), 6xMyc-Pex14 and LDs (middle graph), and anti-SKL and LDs (right graph) was calculated using Pearson's coefficient and expressed as a percentage. The values shown are an average of five individual measurements from four biological replicates, for a total of 20 cells measured. **, $p < 0.01$. ***, $p < 0.001$. C. A western blot probed with anti-Myc and anti-Lsd2 showing protein precipitated from LD fractions isolated from S2 cells transfected with 6xMyc-Pex14 in an oleate-supplemented state for 24 and 48 hours. D. S2 cells transfected with various 6xMyc tagged peroxin constructs in a 48-hour oleate-supplemented state. Anti-SKL marks peroxisomes in green, anti-Myc marks 6xMyc-tagged peroxins in red, LipidTOX Deep Red marks LDs in blue, and the merge is in the far right panel. Each image is a maximum projection of a three-dimensional volume encompassing the entire cell. Images are representative cells from three biological replicates. The scale bar is 2 μm. E. The degree of colocalization between the various 6xMyc-tagged peroxins and LDs was calculated using Pearson's coefficient and expressed as a percentage. The values shown are an average of five individual measurements from three biological replicates. All statistical analysis was performed using an unpaired Student's *t*-test.

significant change in the degree of colocalization between anti-SKL and the LD marker was observed between the two conditions (Figure 3.4B).

Subcellular fractionation was performed on S2 cells transfected with 6xMyc-Pex14 under the same conditions described above. As a control, the same procedure was performed on S2 cells that were mock transfected without plasmid. The western blot was probed with anti-Myc, which showed 6xMyc-Pex14 present in the LD fraction of oleate-supplemented samples after 24 and 48 hours (Figure 3.4C). No Myc was present in the mock-transfected sample. Lsd2 is a resident LD protein (Bi et al., 2012) that was used as a LD marker and loading control. These data further validate the presence of epitope-tagged Pex14 at the LD.

In order to determine whether this phenotype was specific to Pex14 or if other peroxins showed a similar localization, all 13 other peroxins in *Drosophila* were analyzed under the same conditions. Most peroxins in *Drosophila* localized solely to peroxisomes in S2 cells under standard conditions, as demonstrated in Chapter 2. The majority of the 6xMyc-tagged peroxins remained localized to peroxisomes in oleate-supplemented conditions except for two, Pex3 and Pex13. Figure 3.4D shows 6xMyc-Pex6 and 6xMyc-Pex10 as representative examples, both of which remain strongly localized to peroxisomes after 48 hours of oleate supplementation. In contrast, 6xMyc-Pex3 and 6xMyc-Pex13 showed a similar localization pattern to epitope-tagged Pex14. Both epitope-tagged Pex3 and Pex13 formed ring structures that coalesced around the periphery of LDs (Figure 3.4D). Of all the peroxins analyzed in *Drosophila,* only Pex3, Pex13, and Pex14 partially localized to LDs in S2 cells supplemented with oleate. Similar to Pex14, epitope-tagged Pex3 and Pex13 exhibited 41.6% and 41.0% colocalization with LDs, respectively, measured by Pearson's coefficient (Figure 3.4E). In contrast, epitope-

tagged Pex6 and Pex10 exhibited around 10% colocalization with LDs (Figure 3.4E). These data are consistent with previous literature that describes Pex13 and Pex14 functioning together to make up the peroxisome import complex and residing in one distinct subclass of PPV originating at the ER (Albertini et al., 1997; van der Zand et al., 2012).

3.3.5. Endogenous PEX14 localizes to the lipid droplet surface when NRK cells are supplemented with oleate

The plasmid used to drive the expression of 6xMyc-Pex14 in S2 cells contains an actin promoter. This drives the expression of the epitope-tagged Pex14 at higher than endogenous levels, which could lead to artifacts. In order to examine the conservation of the LD association of Pex14 and resolve potential artifacts of overexpression, the localization of endogenous PEX14 was analyzed in NRK cells using commercial antibodies (Invitrogen). The subcellular localization of PEX14 was analyzed in NRK cells under conditions previously described. In standard conditions (DMEM + 10% FBS), PEX14 strongly localized to peroxisomes, marked with anti-PMP70 (Figure 3.5A). In contrast, when NRK cells were cultured in oleate-supplemented conditions (DMEM + 10% FBS + 1 mM oleate) for 48 hours, PEX14 formed punctate structures that both overlapped with and were distinct from the peroxisome marker, anti-PMP70. The puncta that were distinct from anti-PMP70 localized to LDs (Figure 3.4A). The degree of colocalization between PEX14, PMP70, and LDs was calculated using Pearson's coefficient. The degree of colocalization between PEX14 and the LDs significantly increased ($p < 0.01$) from 3.5% in standard conditions to 42.8% in oleate-supplemented

conditions (Figure 3.5B). In contrast, the degree of colocalization between PMP70 and LDs did not appear to change from standard to oleate-supplemented conditions (Figure 3.5B). These results are consistent with the phenotype observed for epitope-tagged *Drosophila* Pex14 in S2 cells under the same conditions. Peroxisome volume and number was calculated in NRK cells under standard and oleate-supplemented conditions. No change in peroxisome volume was observed in NRK cells supplemented with oleate for 48 hours (Figure 3.5D); however, peroxisome number significantly increased ($p < 0.01$) from 110 per cell in standard conditions to 165 per cell in oleate-supplemented conditions (Figure 3.5E).

In order to analyze the expression levels of PEX14 in NRK cells, the protein levels were probed by western blot. Lysates were made from NRK cells under the same conditions described above (standard and oleate-supplemented for 24 and 48 hours) and probed with anti-PEX14. Similar to the expression pattern observed in S2 cells by qRT-PCR (Figure 3.1E), PEX14 expression was elevated in cells cultured with oleate after 24 and 48 hours. PEX14 protein levels were quantified, relative to the β-tubulin loading control, shown in the graph in Figure 3.5F.

Due to the limited resolution of immunofluorescence, it is not possible from the data to conclude whether PEX14 was physically at the LD surface or merely in close proximity. For increased resolution, immuno-TEM (iTEM) was performed on oleate-supplemented NRK cells. NRK cells were supplemented with oleate for 48 hours, fixed with glutaraldehyde (GA), probed with anti-PEX14, and embedded for sectioning. Figure 3.5G.i shows PEX14 localized to the LD surface. LDs appeared as large ovals that are lightly shaded due to their low electron density. This localization was not exclusive as PEX14 appeared to be also localized elsewhere (presumably to peroxisomes). Figure

Figure 3.5

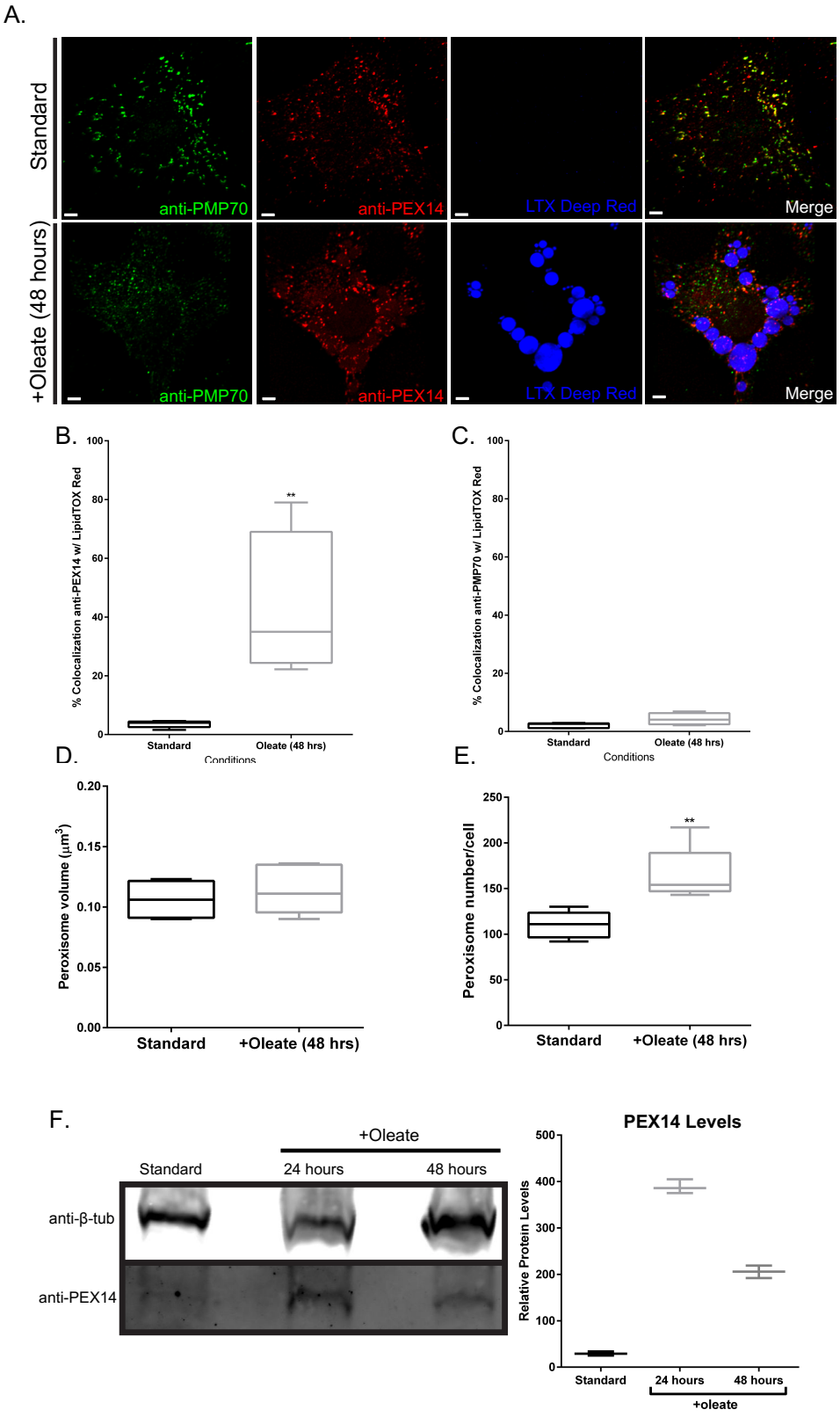
A.
Standard
+Oleate (48 hours)
anti-PMP70
anti-PEX14
LTX Deep Red
Merge
B.
% Colocalization anti-PEX14 w/ LipidTOX Red
Standard
Oleate (48 hrs)
Conditions
C.
% Colocalization anti-PMP70 w/ LipidTOX Red
Standard
Oleate (48 hrs)
Conditions
D.
Peroxisome volume (μm3)
Standard
+Oleate (48 hrs)
E.
Peroxisome number/cell
Standard
+Oleate (48 hrs)
F.
+Oleate
Standard
24 hours
48 hours
anti-β-tub
anti-PEX14
PEX14 Levels
Relative Protein Levels
Standard
24 hours
48 hours
+oleate

Figure 3.5

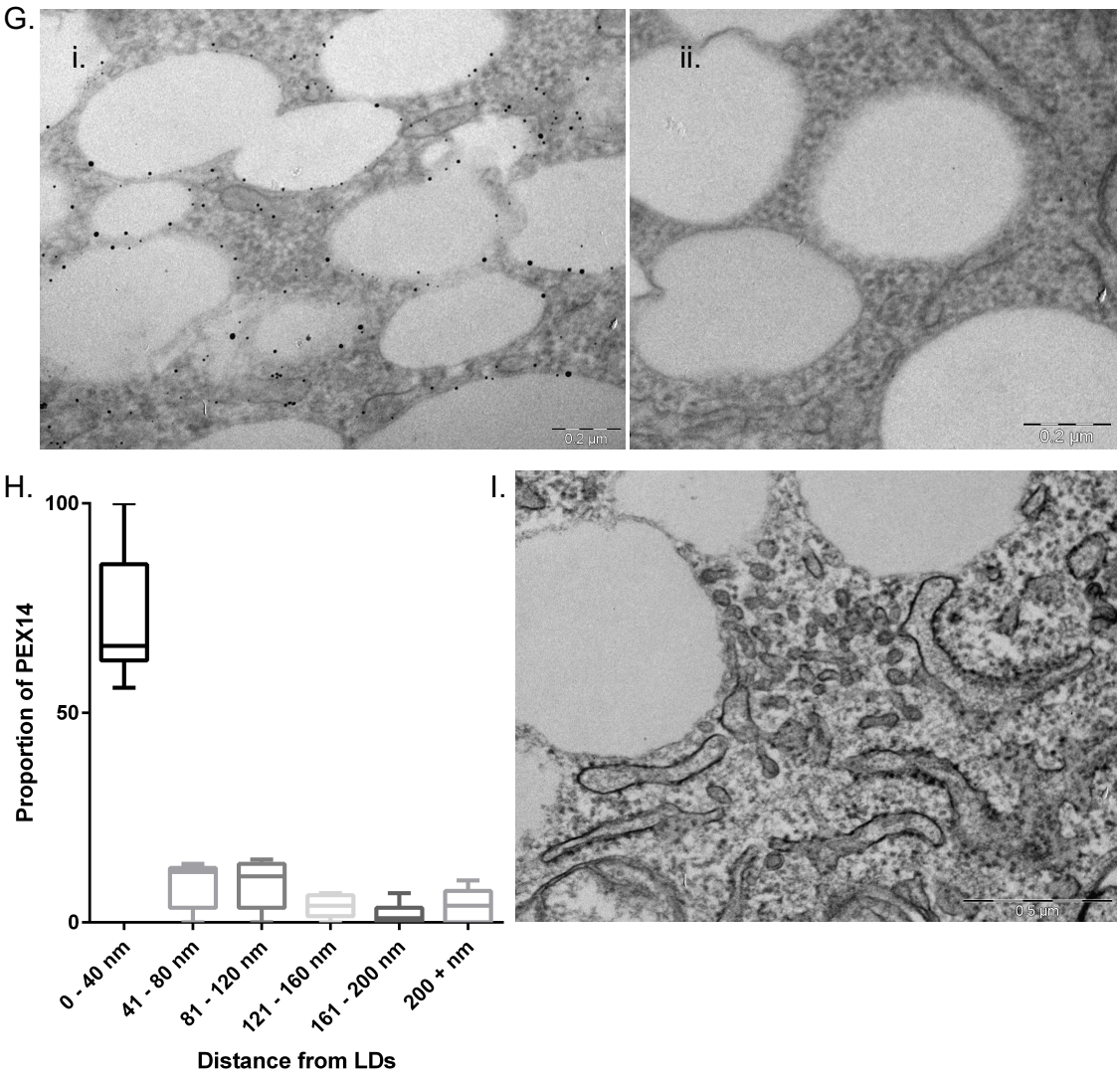
G.
i.
0.2 µm
ii.
0.2 µm
H.
100
50
0
Proportion of PEX14
0 - 40 nm
41 - 80 nm
81 - 120 nm
121 - 160 nm
161 - 200 nm
200 + nm
Distance from LDs
I.
0.5 µm

Figure 3.5. Endogenous PEX14 localizes to the LD surface in NRK cells cultured in oleate. A. Immunofluorescence images of NRK cells in a standard or a 48-hour oleate-supplemented state. Anti-PMP70 marks peroxisomes in green, anti-PEX14 is shown in red, LipidTOX Deep Red marks LDs in blue, and the merge is in the far right panel. Each image is a maximum projection of a three-dimensional volume encompassing the entire cell. Images are representative cells from three biological replicates. Scale bar is 2 μm. B,C. The degree of colocalization between LDs and PEX14 (B) and PMP70 (C) was measured under standard and oleate-supplemented conditions using Pearson's coefficient and displayed as a percentage. The values shown are an average of five individual measurements from three biological replicates, for a total of 15 cells measured. **, $p < 0.01$. D,E. The average peroxisome volume (D) and number per cell (E) was measured in standard and oleate-supplemented conditions using Imaris software. The y-axis shows peroxisome volume in μm^3 (D) and peroxisome number per cell (E). The values shown are an average of five individual measurements from three biological replicates, for a total of 15 cells measured. **, $p < 0.01$. F. A western blot probed with anti-PEX14 showing relative levels of PEX14 in NRK cell lysates in a standard and oleate-supplemented state for 24 and 48 hours. β-tubulin was used as a loading control. The graph on the right is a quantification of the intensities of the PEX14 protein bands relative to the β-tubulin loading control. The values shown in the graph are averages from three biological replicates. Western blots were processed using Odyssey Imaging software. G.i. Representative iTEM images of NRK cells probed with anti-PEX14 and visualized with NanoGold anti-rabbit secondary antibodies. Black electron-dense spots represent PEX14. ii. Representative iTEM image of NRK cells probed with NanoGold anti-rabbit secondary antibody only (Negative control). H. The distance of PEX14 from the LD surface was measured and grouped into six ranges. The values shown are the proportion of the total PEX14 signal that was found in each range. The values shown are the averages from 10 individual iTEM images. I. Representative TEM images of NRK cells supplemented with 1 mM oleate for 24 hours. The scale bar is 0.5 μm. All statistical analysis was performed using an unpaired Student's *t*-test.

3.5G.ii shows the negative control whereby cells were incubated with secondary antibody only (no anti-PEX14). The distance between PEX14-positive spots and LDs was measured and reported based on the proportion of the total PEX14 signal within a given image (Figure 3.5H). These distances were grouped into six ranges: 0 – 40 nm, 41 – 80 nm, 81 – 120 nm, 121 – 160 nm, 161 – 200 nm, and 200+ nm. The majority of PEX14 localized within 40 nm of the LD surface (Figre 3.5H).

Preparing samples for iTEM required a gentler fixation than regular TEM, 0.05% GA versus 2% GA, respectively in order to retain the protein antigenicity. As a result, morphology and membrane structures detail was lost. Thus, regular TEM was also performed on oleate-supplemented NRK cells. After culturing NRK cells in oleate-supplemented conditions for 48 hours, the cells were fixed in 2% GA and membranes were stained with uranyl acetate (UA). Figure 3.5D shows a representative image from this sample. The ER was clearly visible as tubular structures decorated with electron-dense ribosomes. Clusters of electron-dense vesicles were often observed adjacent to the ER and LDs. A portion of these vesicles appeared in close proximity to the LD surface (Figure 3.5I).

3.3.6. The perilipins affect the lipid droplet localization of Pex14 in S2 cells

In order to determine what functional role peroxins may be playing at the LD surface, the localization of 6xMyc-Pex14 was analyzed when various LD proteins were concomitantly overexpressed. Lipid mobilization at the LD is controlled by the family of PLIN proteins (reviewed in Ducharme and Bickel, 2008; reviewed in Itabe et al., 2017).

Figure 3.6

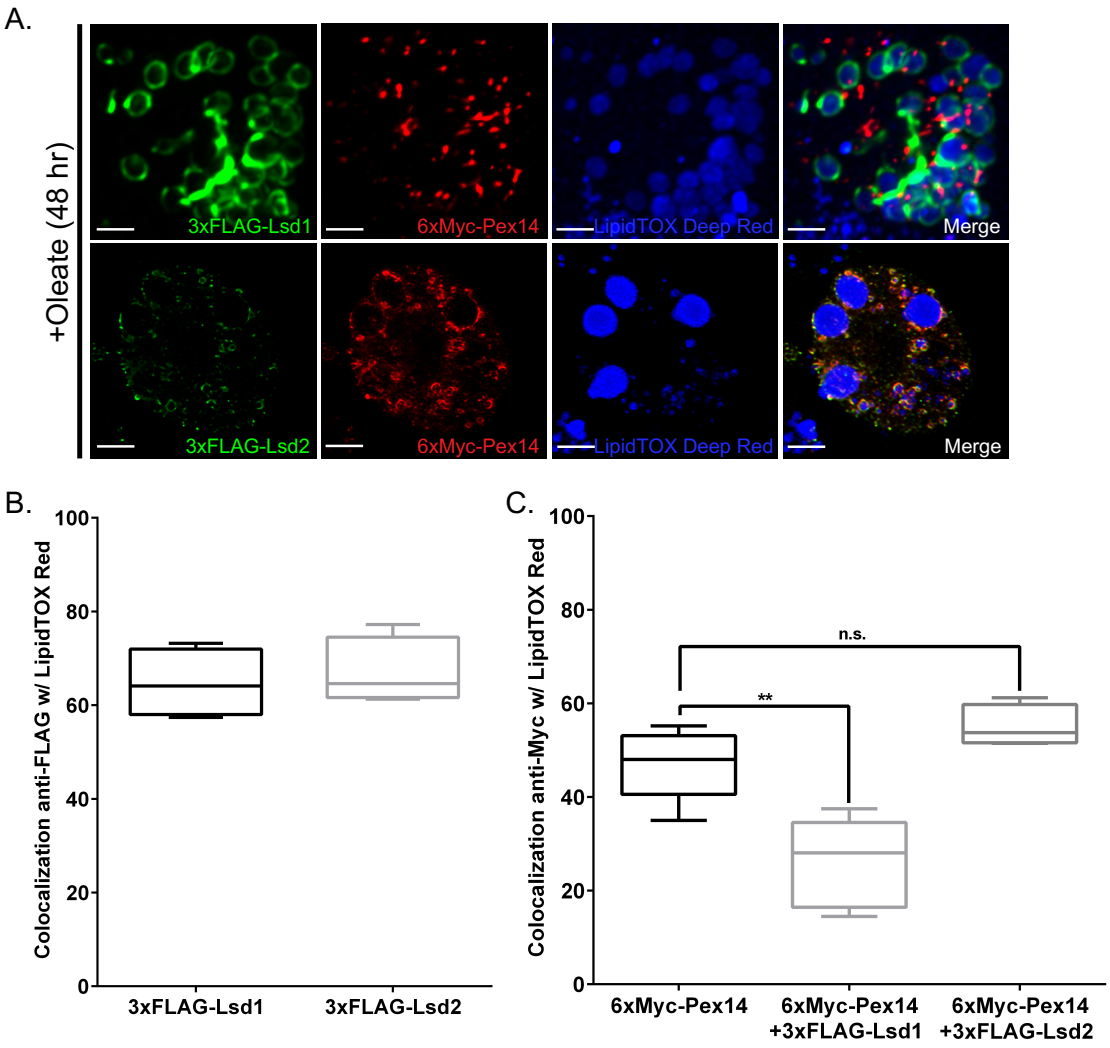
A.
+Oleate (48 hr)
3xFLAG-Lsd1
6xMyc-Pex14
LipidTOX Deep Red
Merge
3xFLAG-Lsd2
6xMyc-Pex14
LipidTOX Deep Red
Merge
B.
Colocalization anti-FLAG w/ LipidTOX Red
100
80
60
40
20
0
3xFLAG-Lsd1
3xFLAG-Lsd2
C.
Colocalization anti-Myc w/ LipidTOX Red
n.s.
**
6xMyc-Pex14
6xMyc-Pex14 +3xFLAG-Lsd1
6xMyc-Pex14 +3xFLAG-Lsd2

Figure 3.6. Overexpression of *Lsd1* affects the localization of Pex14 at the LD. A. Immunofluorescence images of S2 cells overexpressing 6xMyc-Pex14 concomitantly with either 3xFLAG-Lsd1 or 3xFLAG-Lsd2. Transfected cells supplemented with oleate for 48 hours, fixed, and probed with anti-FLAG, shown in green, and anti-Myc, shown in red. LipidTOX Deep Red marks the LDs in blue. The merged images are on the far right. Each image is a maximum projection of a three-dimensional volume encompassing the entire cell. Images are representative cells from three biological replicates. The scale bar is 2 μm. B. The degree of colocalization between LDs and FLAG-tagged Lsd1 and Lsd2 was measured in oleate-supplemented conditions using Pearson's coefficient and displayed as a percentage. The values shown are an average of five independent measurements from three biological replicates, for a total of 15 cells measured. C. The degree of colocalization between LDs and 6xMyc-Pex14 was measured in oleate-supplemented conditions with simultaneous overexpression of FLAG-tagged Lsd1 or Lsd2. Measurements were made using Pearson's coefficient and displayed as a percentage. The values shown are an average of five independent measurements from three biological replicates, for a total of 15 cells measured. **, $p < 0.01$. Statistical analysis was performed using an unpaired Student's *t*-test to compare the mean values between each condition, indicated in C.

PLINs are LD-associated proteins that function to regulate the access of TG stores in the LD to the various lipase enzymes found in the cytosol. PLINs are regulated by phosphorylation, which, during the stimulation of lipolysis, allows for the recruitment of cytoplasmic lipases to the LD surface (reviewed in Ducharme and Bickel, 2008; reviewed in Itabe et al., 2017). There are two perilipins in *Drosophila*, Lsd1 and Lsd2, which play important roles in regulating lipolysis (Bi et al., 2012). Lsd2 prevents lipolysis and resides on the LD surface to block the lipases from accessing TG stores within the LD core. In contrast, phosphorylated Lsd1 recruits Hsl to the LD surface in order to mobilize FFA (Bi et al., 2012). Both Lsd1 and Lsd2 were tagged at their N-terminus with a 3xFLAG epitope and co-transfected into S2 cells along with 6xMyc-Pex14. Transfected cells were treated with oleate as previously described. After 48 hours, the cells were fixed, probed with anti-FLAG and anti-Myc antibodies, and imaged by confocal microscopy. 3xFLAG-Lsd2 and 6xMyc-Pex14 strongly colocalized at the LD surface (Figure 3.6A). 6xMyc-Pex14 showed few punctate structures, with the majority of its signal localized to LDs. In contrast, in cells simultaneously overexpressing epitope-tagged Pex14 and Lsd1, 6xMyc-Pex14 primarily formed punctate structures that did not localize to LDs (Figure 3.6A). In these cells, 3xFLAG-Lsd1 appeared to localize completely to the LD surface. The degree of colocalization between both PLINs and LDs was calculated using Pearson's coefficient. Both epitope-tagged Lsd1 and Lsd2 exhibited nearly 70% colocalization with LDs (Figure 3.6B). The degree of colocalization between 6xMyc-Pex14 and LDs was measured in the presence of Lsd1 and Lsd2 overexpression. When 6xMyc-Pex14 was overexpressed alone, it showed approximately 47.1% colocalization with LDs. This measurement was not significantly affected when epitope-tagged Pex14 was simultaneously overexpressed with 3xFLAG-Lsd2 (Figure 3.6C). In

contrast, the degree of colocalization between 6xMyc-Pex14 was significantly reduced ($p < 0.01$) to 26.5% when overexpressed with 3xFLAG-Lsd1 (Figure 3.5C).

3.3.7. Overexpression of Pex14 blocks the recruitment of Hsl to the lipid droplet surface in S2 cells

During lipolysis, each fatty acyl chain is cleaved from TG molecules, a reaction that is catalyzed by various cytoplasmic lipases (reviewed in Ducharme and Bickel, 2008; reviewed in Lass et al., 2011). The first step is catalyzed by ATGL, or Bmm in *Drosophila* (Grönke et al., 2005), which cleaves the first fatty acyl chain to produce DG. Hsl then catalyzes the cleavage of the next fatty acyl chain from DG, to produce MG (reviewed in Lass et al., 2011). Bmm was tagged with a 3xFLAG epitope at its N-terminus and transfected into S2 cells. Transfected cells were supplemented with oleate for 24 hours, at which point the cells were washed and incubated for an additional 24 hours in the absence of oleate and FBS in order to induce lipolysis, as previously described (Guo et al., 2008). Transfected cells were fixed, and immunofluorescence was performed using an anti-FLAG antibody. LipidTOX Deep Red was used to mark the LDs. Fixed cells were imaged by confocal microscopy. Under lipolytic conditions, 3xFLAG-Bmm formed small ring-shaped structures that completely surrounded the periphery of LDs (Figure 3.7A). Similarly, when cells were co-transfected with 3xFLAG-Bmm and 6xMyc-Pex14 under these same conditions, the localization of 3xFLAG-Bmm was not perturbed and remained at the surface of LDs. In addition, 6xMyc-Pex14 also localized to the periphery of LDs when 3xFLAG-Bmm was simultaneously

Figure 3.7

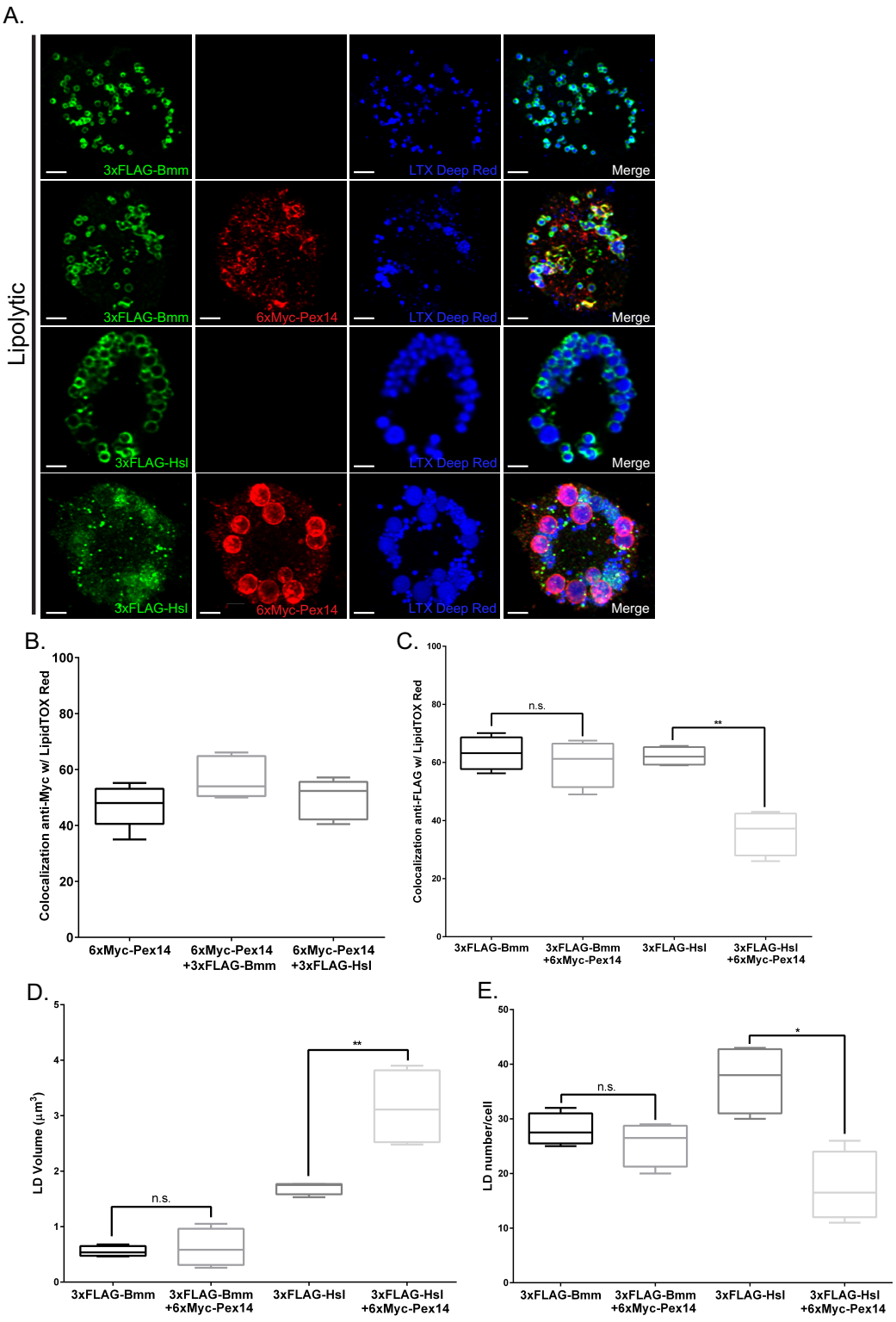
A.
Lipolytic
3xFLAG-Bmm
LTX Deep Red
Merge
3xFLAG-Bmm
6xMyc-Pex14
LTX Deep Red
Merge
3xFLAG-Hsl
LTX Deep Red
Merge
3xFLAG-Hsl
6xMyc-Pex14
LTX Deep Red
Merge
B.
Colocalization anti-Myc w/ LipidTOX Red
6xMyc-Pex14
6xMyc-Pex14 +3xFLAG-Bmm
6xMyc-Pex14 +3xFLAG-Hsl
C.
Colocalization anti-FLAG w/ LipidTOX Red
n.s.
**
3xFLAG-Bmm
3xFLAG-Bmm +6xMyc-Pex14
3xFLAG-Hsl
3xFLAG-Hsl +6xMyc-Pex14
D.
LD Volume (µm3)
n.s.
**
3xFLAG-Bmm
3xFLAG-Bmm +6xMyc-Pex14
3xFLAG-Hsl
3xFLAG-Hsl +6xMyc-Pex14
E.
LD number/cell
n.s.
*
3xFLAG-Bmm
3xFLAG-Bmm +6xMyc-Pex14
3xFLAG-Hsl
3xFLAG-Hsl +6xMyc-Pex14

Figure 3.7 Overexpression of *Pex14* affects the localization of Hsl at the LD. A. Immunofluorescence images of lipolytic S2 cells overexpressing 6xMyc-Pex14 simultaneously with either 3xFLAG-Bmm or 3xFLAG-Hsl. FLAG-tagged Bmm and Hsl were also transfected and examined alone. Transfected cells were fixed, and probed with anti-FLAG, shown in green, and anti-Myc, shown in red. LipidTOX Deep Red marks the LDs in blue. Merge is on the far right. Images were taken in lipolytic conditions. Each image is a maximum projection of a three-dimensional volume encompassing the entire cell. Images are representative cells from three biological replicates. The scale bar is 2 μm. B. The degree of colocalization between LDs and 6xMyc-Pex14 was measured in cells simultaneously overexpressing either 3xFLAG-Bmm or 3xFLAG-Hsl. The values shown are the average of five individual measurements from three biological replicates, for a total of 15 cells measured. C. The degree of colocalization between LDs and 3xFLAG-Bmm or 3xFLAG-Hsl was measured in cells overexpressing the construct alone or with 6xMyc-Pex14. The values shown are the average of five individual measurements from three biological replicates, for a total of 15 cells measured. **, $p < 0.01$. D,E. Graphs showing the average volume (D) and number (E) of LDs per cell in a lipolytic state overexpressing FLAG-tagged Bmm or Hsl with or without 6xMyc-Pex14. The y-axis shows the average volume of LDs in μm^3 (D) or the average number of LDs per cell (E). The values shown in D and E are an average of five individual measurements from three biological replicates, for a total of 15 cells measured. *, $p < 0.05$. **, $p < 0.01$. Statistical analysis was performed using an unpaired Student's *t*-test to compare the mean values between each condition, indicated in C, D, and E.

overexpressed (Figure 3.7A). The degree of colocalization between LDs and both epitope-tagged Pex14 and Bmm was calculated using Pearson's coefficient. Both Pex14 and Bmm localization to LDs was unaffected when overexpressed together (Figures 3.7B and 3.7C, respectively).

The localization of Hsl was similarly investigated. Hsl was tagged with a 3xFLAG epitope at its N-terminus and imaged under the same conditions. 3xFLAG-Hsl strongly localized to LDs under lipolytic conditions (Figure 3.7A). When 3xFLAG-Hsl was co-transfected with 6xMyc-Pex14, the localization of 3xFLAG-Hsl was disrupted. When 6xMyc-Pex14 was simultaneously overexpressed, 3xFLAG-Hsl appeared mainly cytosolic with small puncta formations that were not localized to the LDs (Figure 3.7A). In addition, 6xMyc-Pex14 appeared to be almost entirely localized to the surface of LDs. The degree of colocalization between LDs and both epitope-tagged Pex14 and Hsl was calculated using Pearson's coefficient. The degree of colocalization between 3xFLAG-Hsl and LDs was significantly reduced ($p < 0.01$) from 62.2% when overexpressed alone to 35.9% in the presence of Pex14 overexpression (Figure 3.7C). The localization of 6xMyc-Pex14 was unaffected by 3xFLAG-Hsl overexpression (Figure 3.7B). Both LD volume and LD number per cell were relatively unaffected when Bmm overexpressing cells simultaneously overexpressed 6xMyc-Pex14 (Figures 3.7D and 3.7E). In contrast, Hsl overexpressing cells showed a significant increase ($p < 0.01$) in LD volume when simultaneously overexpressing 6xMyc-Pex14 (Figure 3.7D). Average LD volume increased from 1.70 μm^3 in Hsl overexpressing cells to 3.15 μm^3 when Pex14 was simultaneously overexpressed. In addition, a concomitant significant decrease ($p < 0.05$) in LD number per cell was observed in Hsl overexpressing cells simultaneously overexpressing 6xMyc-Pex14 (Figure 3.7E). The number of LDs decreased from 37 per

cell to 18 per cell when 3xFLAG-Hsl was simultaneously overexpressed with 6xMyc-Pex14.

3.3.8. Pex14 affects the expression of CGI-58

CGI-58 is a major regulator of lipolysis and activates the rate-limiting lipase, Bmm, in *Drosophila* (Gruber et al., 2010; Yamaguchi et al., 2007). In basal conditions, CGI-58 is bound to Lsd1 at the LD surface. When lipolysis is stimulated, a signaling cascade causes the phosphorylation of Lsd1, which releases CGI-58 allowing interaction with Bmm and activating it (Gruber et al., 2010; Yamaguchi et al., 2007; reviewed in Lass et al., 2006). The localization of CGI-58 was analyzed in the presence of *Pex14* overexpression. CGI-58 was tagged with a 3xFLAG epitope at its N-terminus and transfected into S2 cells. Transfected cells were supplemented with oleate for 24 hours, followed by lipolytic induction by removal of FBS and oleate, as previously described (see 3.3.7). Under conditions that promote lipolysis, 3xFLAG-CGI-58 was localized to the LD surface. 3xFLAG-CGI-58 formed ring structures that surrounded the periphery of LDs (Figure 3.8A). S2 cells were also concomitantly transfected with 3xFLAG-CGI-58 and 6xMyc-Pex14 expressing plasmids. Transfected cells were analyzed under lipolytic conditions, as previously described. When 6xMyc-Pex14 was simultaneously overexpressed, the localization of CGI-58 appeared unaffected. 3xFLAG-CGI-58 formed large ring structures that surrounded the LDs (Figure 3.8A). In addition, 6xMyc-Pex14 was found primarily at the LD surface, with some small punctate formations that were distinct from the LD (Figure 3.8A). The colocalization between each epitope-tagged protein and the LD was measured using Pearson's coefficient (Figure 3.8E and 3.8F). No

Figure 3.8

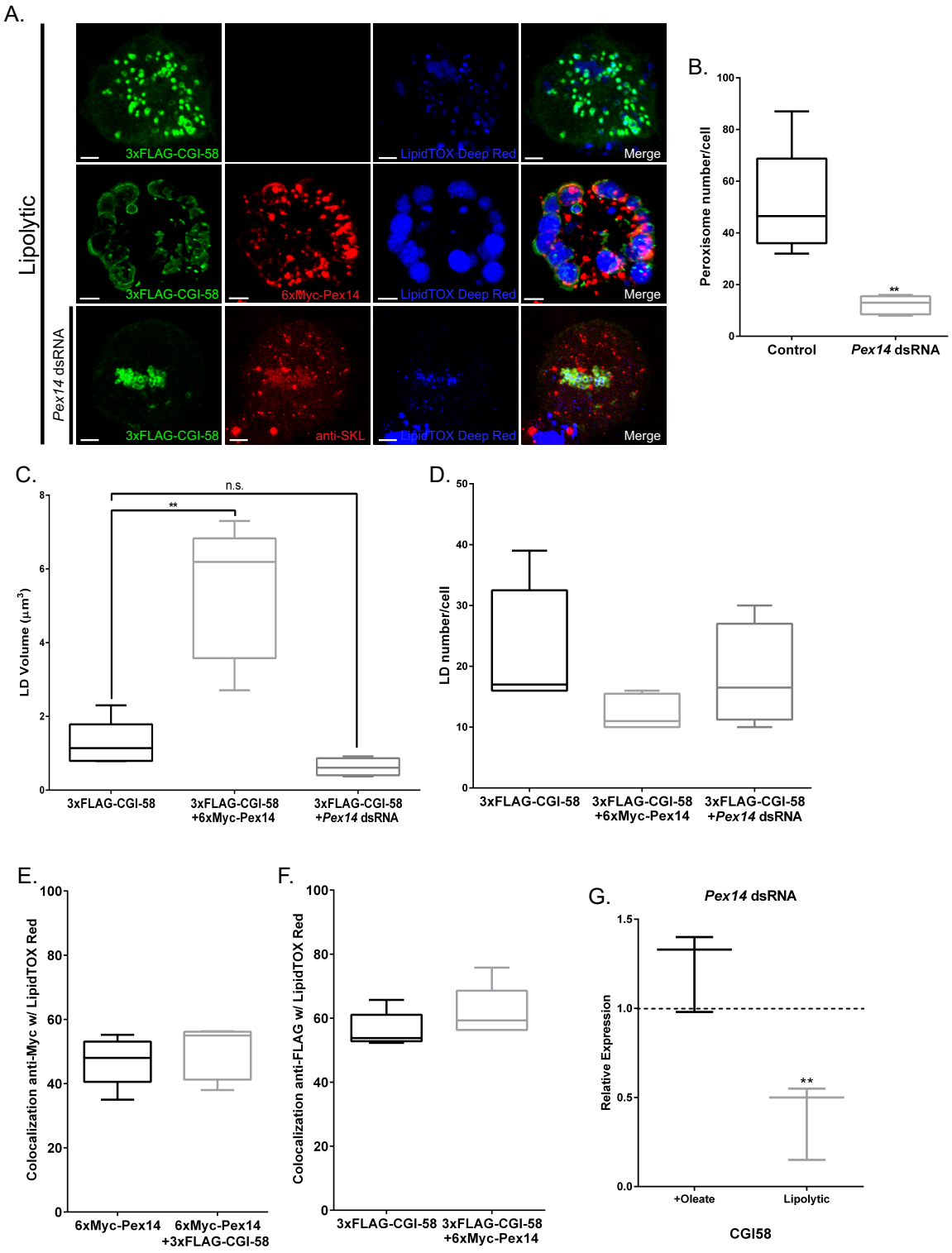
A.
Lipolytic
Pex14 dsRNA
3xFLAG-CGI-58
LipidTOX Deep Red
Merge
6xMyc-Pex14
anti-SKL
B.
Peroxisome number/cell
Control
Pex14 dsRNA
C.
LD Volume (μm3)
n.s.
3xFLAG-CGI-58
3xFLAG-CGI-58 +6xMyc-Pex14
3xFLAG-CGI-58 +Pex14 dsRNA
D.
LD number/cell
E.
Colocalization anti-Myc w/ LipidTOX Red
6xMyc-Pex14
6xMyc-Pex14 +3xFLAG-CGI-58
F.
Colocalization anti-FLAG w/ LipidTOX Red
G.
Pex14 dsRNA
Relative Expression
+Oleate
Lipolytic
CGI58

Figure 3.8. Pex14 affects the expression levels of *CGI-58*. A. Immunofluorescence images of lipolytic S2 cells overexpressing 3xFLAG-CGI-58 alone (top panels) or simultaneously with 6xMyc-Pex14 (middle panels). FLAG-tagged CGI-58 was also examined in lipolytic cells treated with *Pex14* dsRNA for three days (bottom panels). Transfected cells were fixed, and probed with anti-FLAG, shown in green, and anti-Myc, shown in red. LipidTOX Deep Red marks the LDs in blue. Merge is on the far right. In *Pex14* dsRNA treated cells, anti-SKL marks the peroxisomes in red. Images were taken in lipolytic conditions. Each image is a maximum projection of a three-dimensional volume encompassing the entire cell. Images are representative cells from three biological replicates. The scale bar is 2 μm. B. The number of peroxisomes per cell was measured using the Surfaces function of Imaris software from images taken of S2 cells treated with scrambled dsRNA (control) or *Pex14* dsRNA. The values shown are an average of five individual measurements from three biological replicates, for a total of 15 cells measured. **, $p < 0.01$. C, D. Graphs showing the average volume (C) and number (D) of LDs per cell in a lipolytic state overexpressing FLAG-tagged CGI-58 alone or with 6xMyc-Pex14 or *Pex14* dsRNA treatment. Measurements were taken using the Surfaces function of Imaris software. The values shown in C and D are an average of five individual measurements from three biological replicates, for a total of 15 cells measured. **, $p < 0.01$. E,F. The degree of colocalization between LDs and 6xMyc-Pex14 (E) or 3xFLAG-CGI-58 (F) was measured in cells overexpressing both constructs alone or together. Measurements were made using Pearson's coefficient and displayed as a percentage. The values shown are the average of five individual measurements from three biological replicates, for a total of 15 cells measured. G. The relative expression levels of *CGI-58* were measured in oleate-supplemented or lipolytic conditions in S2 cells treated with *Pex14* dsRNA. Measurements were taken by qPCR and displayed relative to control conditions (scrambled dsRNA). The values shown are an average of three biological replicates. **, $p < 0.01$. Statistical analysis was performed using an unpaired Student's *t*-test to compare the mean values between each condition, indicated in C.

effect on localization was observed when the epitope-tagged proteins were overexpressed simultaneously. Both epitope-tagged CGI-58 and Pex14 exhibited between 50 and 60% colocalization with LDs when overexpressed alone. These measurements were unaffected when the proteins were overexpressed simultaneously (Figures 3.8E and 3.8F).

LDs found in cells overexpressing both fusion proteins were significantly larger ($p < 0.01$) than those found in cells overexpressing 3xFLAG-CGI-58 alone (Figure 3.8C); however, no effect on LD number per cell was observed (Figure 3.8D). The average LD volume in cells overexpressing 3xFLAG-CGI58 alone was 1.26 μm^3, whereas the average LD volume in cells overexpressing both 3xFLAG-CGI-58 and 6xMyc-Pex14 was 5.40 μm^3 (Figure 3.8C).

S2 cells were also pretreated with dsRNA targeting the *Pex14* transcript prior to transfection with 3xFLAG-CGI-58 plasmid. Transfected cells were analyzed under lipolytic conditions, as previously described. Knockdown of *Pex14* was confirmed by qPCR. On average, knockdown was achieved at roughly 80-90% (see Figure 3.2A). In addition, the number of peroxisomes was significantly reduced ($p < 0.01$) from 52 to 12 per cell when 3xFLAG-CGI-58 overexpressing cells were pretreated with *Pex14* dsRNA (Figure 3.8B). In transfected cells pretreated with *Pex14* dsRNA, 3xFLAG-CGI-58 remained at the LD surface, although few LDs were found (Figure 3.8A). The average LD volume in *Pex14* knockdown cells was reduced to 0.63 μm^3 (Figure 3.8C), which is likely caused by a depletion of TG stores in these cells.

The relative expression levels of *CGI-58* were also analyzed when *Pex14* levels were reduced under different conditions. S2 cells were treated with dsRNA targeting *Pex14* or a scrambled dsRNA amplicon. The knockdown of *Pex14* expression was verified by qRT-PCR. In cells treated with *Pex14* dsRNA and oleate supplemented for 24

hours, *CGI-58* expression appeared relatively unchanged, compared to the oleate-supplemented control samples. In contrast, in lipolytic cells treated *Pex14* dsRNA *CGI-58* expression levels were significantly reduced ($p < 0.01$) to roughly 50% of the lipolytic control sample (Figure 3.8G). Overall, this suggests that a reduction of *Pex14* expression causes differential expression of *CGI-58* under lipolytic conditions. *CGI-58* expression levels are downregulated in lipolytic conditions when *Pex14* levels are reduced.

3.4. Summary and conclusions

In this chapter, I sought more details regarding the interactions between peroxisomes and LDs using *Drosophila melanogaster*. Expression data showed that *Pex14* was upregulated during periods of elevated lipid metabolism in S2 cells. In addition, the knockdown of *Pex14* increased lipolysis in both S2 cells and *Drosophila* 3rd instar larvae. This suggested that Pex14 might play a role in regulating lipolysis. Furthermore, when the localization of epitope-tagged Pex14 was analyzed under different metabolic conditions, it was found at the LD surface in oleate-supplemented cells. When all *Drosophila* peroxins were analyzed, only Pex3, Pex13, and Pex14 localized to the LD under these conditions, which suggested that this localization is specific to a subset of peroxins. The LD localization of endogenous Pex14 was also conserved in NRK cells. The localization of Pex14 to the LD surface was affected by the perilipins. Overexpression of *Lsd1* appeared to block Pex14 from the LD surface. Conversely, overexpression of *Lsd2* did not affect the localization of Pex14 to the LD surface. In addition, the expression levels of Pex14 seemed to have an effect on different proteins

that regulate lipolysis. While the overexpression of Pex14 seemed to block Hsl from the LD surface, the localization of Bmm was unaffected. Lastly, lipolytic cells treated with *Pex14* dsRNA show significantly decreased expression levels of *CGI-58.*

Collectively, these data suggest that Pex13 and Pex14 are diverted to the LD surface during periods of elevated LD metabolism, which serve to regulate lipolysis along with the perilipins, Lsd1 and Lsd2 and the lipase activator, CGI-58. In addition, Pex13 and Pex14 seem to regulate the access of certain lipases, specifically Hsl, to the LD surface.

Further investigation into the mechanism and function of Pex13 and Pex14 at the LD surface is needed. Moving forward, specific questions to be asked are: 1) How are Pex13 and Pex14 targeted to the LD surface? 2) How are they being held at the LD surface, i.e. with what are they interacting? 3) What is the specific function of these proteins at the LD surface? While the data generated so far address some of these questions, the answers remain partial and further work is required to provide a more comprehensive description of the relationship between these peroxins and LDs. Specific details regarding how these questions may be addressed will be discussed in Chapter 4.

Chapter 4: Discussion and conclusions

4.1. Drosophila melanogaster as a model to study peroxisome-lipid droplet interactions

Drosophila melanogaster is one of the oldest model systems used in biological research. Its utility stems from a combination of simple genetics and fully formed tissues that are orthologous to those found in higher eukaryotes. The field of LD research is fairly extensive in *Drosophila*. In contrast, until recently, there has been a dearth of research on peroxisome biology in *Drosophila.* Therefore, it was necessary to first establish conservation of peroxisome protein trafficking in *Drosophila* in to facilitate my investigation of peroxisome-LD interactions.

4.1.1. The predicted peroxins localize to peroxisomes Drosophila S2 cells

Based on an *in silico* analysis performed by Faust et al*.,* 14 potential peroxins were identified in *Drosophila* (Faust et al., 2012). It was found that the majority of these peroxins, when fused to a 3xFLAG-epitope, localized to peroxisomes in S2 cells. This included the RING complex composed of Pex2, Pex10, and Pex12 (Platta et al., 2009; Reguenga et al., 2001), the fission machinery composed of two isoforms of Pex11 (Marshall et al., 1995), the exportomer complex composed of Pex1 and Pex6 (Miyata and Fujiki, 2005), the import complex composed of Pex13 and Pex14 (Albertini et al., 1997; Elgersma et al., 1996b), and Pex16, which facilitates the docking of membrane proteins destined for the peroxisome (Honsho et al., 1998; Matsuzaki and Fujiki, 2008) (Figure 2.2A). Of note, the degree of colocalization between Pex6 and the peroxisome marker was below 60%, measured using Pearson's coefficient (Figure 2.2A). Pex6 is tethered to

the peroxisomal membrane via protein-protein interactions with Pex15p in yeast (Birschmann et al., 2003) or PEX26 in mammals (Matsumoto et al., 2003). A homologue to Pex15p or PEX26 in *Drosophila* was not identified in the original *in silico* screen (Faust et al., 2012), nor in the bioinformatic analysis performed by Chris Klinger (Table 2.3). It is possible that the overexpression of Pex6 resulted in some mistargeting due to a stoichiometric imbalance between Pex6 and its membrane anchor. If the membrane anchor becomes saturated, the excess Pex6 may be consequently mislocalized to the cytosol. Identification of the *Drosophila* homologue to Pex15p/PEX26 would be needed to confirm this experimentally.

In addition, it is important to consider the conditions in which these peroxins were analyzed. In the analysis in Chapter 2, S2 cells were cultured in Schneider's medium supplemented with 10% FBS. In regard to the metabolic state of the cells, this represents standard conditions. My work has shown alternative trafficking of some Pex proteins depending on the culture conditions. In Chapter 3, it was observed that Pex13 and Pex14 partially localize to the surface of LDs when cells are supplemented with oleate, which will be discussed later.

Pex5, the soluble cargo receptor for the PTS1 pathway (Van der Leij et al., 1993), formed punctate structures that strongly colocalized with the peroxisome marker, but also showed an appreciable cytosolic signal (Figure 2.3). Previous reports had shown Pex5 in the cytosol, which is consistent with its proposed function. In fact, it has been suggested that membrane-associated Pex5 is actually artifactual (Brocard and Hartig, 2006). In *S. cerevisiae* and *H. sapiens*, it has been shown that the majority of Pex5p/PEX5 is found in the cytosolic fraction (Dodt and Gould, 1996; Elgersma et al., 1996a), although, in *H. polymorpha* and *Y. lipolytica*, Pex5p was found within the peroxisome matrix (Klei et al.,

1995; Szilard et al., 1995). Despite the high conservation of the PTS1 pathway across species, it is possible that some small variations exist in the transport processes of Pex5, which result in the slight discrepancies observed in Pex5 localization. In addition, the slight differences observed in Pex5 localization could be a result of the recycling kinetics into and out of the peroxisome. In any case, it appears that the localization of *Drosophila* Pex5 in S2 cells is consistent with previous reports in other species.

Pex19, the receptor for the membrane protein import pathway (Sacksteder et al., 2000), showed a similar localization pattern to Pex5, although the degree of colocalization with the peroxisome marker was markedly less (Figure 2.2A). Pex19 formed punctate structures that overlapped to a degree with the peroxisome marker, although the majority of the signal was found in the cytosol. These results are consistent with previous reports, in which PEX19 was found to be primarily cytosolic in human fibroblasts (Jones et al., 2004), although, Pex19 has shown differences in its localization, depending on the tissue or cell being analyzed. In cells within tissues such as the heart or skeletal muscle, PEX19 was found primarily localized to the peroxisomal membrane, with varying amounts in the cytosolic fraction in mouse cells (Colasante et al., 2017). The distribution of Pex19 observed in S2 cells may reflect a cell-specific phenotype, in which Pex19 localizes to both the cytosol and the peroxisome membrane. In addition, an increase in the cytosolic portion may be a result of *Pex19* overexpression.

Pex7, the cargo receptor for the PTS2 pathway (Marzioch et al., 1994; Zhang and Lazarow, 1995), formed punctate structures that overlapped with the peroxisome marker, albeit to small degree (Figures 2.2A and 2.5A). The majority of the Pex7 signal was found in the cytosol, which is consistent with its proposed function as a soluble cargo receptor. A putative PTS2 signal has not yet been identified in *Drosophila*, nor did the

results from Chapter 2 suggest otherwise. Despite the lack of an apparent PTS2 pathway, it is likely that the homologue of Pex7 performs a function at the peroxisome. This is evidenced by its partial peroxisomal localization (Figure 2.2A) and its effect on the peroxisome population when overexpressed (Figure 2.6). It is possible that, similar to what is found in *C. elegans*, PTS2-containing proteins in *Drosophila* have evolved to utilize the PTS1 pathway and the putative Pex7 is involved in other aspects of peroxisome biogenesis and function. This is supported by a recently discovered role for peroxisomes in immune function in *Drosophila.* This immune function was perturbed when *Pex7* expression was knocked down by dsRNA (Di Cara et al., 2017). This suggests that Pex7 serves a function in mediating the role of peroxisomes in *Drosophila* immunity. Moreover, it has been shown that *Drosophila* Pex7 can rescue the targeting of human thiolase to peroxisomes in *PEX7* mutant human fibroblasts (Di Cara et al., 2018).

Of all the peroxins analyzed, Pex3 showed the lowest degree of colocalization with peroxisomes (Figure 2.2A). 3xFLAG-Pex3 appeared to form reticular-like structures (Figure 2.4), which suggested that it might be retained in the ER as a consequence of overexpression. Pex3p is known to localize to the ER as it functions in PPV formation in yeast (Ghaedi et al., 2000). However, PEX3 has also been shown to assist in the docking of PEX19 at the peroxisomal membrane in human fibroblasts (Fang et al., 2004), which suggests that complete ER-localization in S2 cells is likely an aberrant phenotype. It is possible that overexpression of Pex3 in S2 cells causes the protein to be retained in the ER and therefore, does not localize to peroxisomes. In addition, it has been shown that mammalian PEX3 is targeted to mitochondria in peroxisome-deficient cells (Aranovich et al., 2014; Fang et al., 2004; Kim et al., 2006). Moreover, Sugiura et al. showed that mitochondrially-derived PPVs contain PEX3 in human fibroblasts lacking functional

peroxisomes (Sugiura et al., 2017) This poses the possibility that the observations made in Chapter 2 show mitochondria-targeted Pex3. It is possible that Pex3 overexpression in S2 cells causes mitochondrial targeting. Pex3 may have to be analyzed at endogenous levels in *Drosophila* in order to determine its subcellular localization.

4.1.2. The majority of non-peroxin proteins analyzed localized to peroxisomes in S2 cells

Of the 68 non-peroxin proteins analyzed, 34 localized exclusively to peroxisomes and eight at least partially localized to peroxisomes (Figure 2.2B). The majority of these proteins possessed a canonical PTS1 signal, or some variation. In addition, when *Pex5* was knocked down by dsRNA treatment, targeting of RFP-DBP (a PTS1-containing protein) to the peroxisome was disrupted (Figure 2.7). Moreover, a reanalysis of the original *in silico* data by Faust et al., performed by Chris Klinger, found that 10 of the proteins did not retrieve peroxisomal proteins in a reciprocal BLASTp. This suggests that they may not be homologues of peroxisomal proteins. Of those 10, seven were found to localize to structures other than the peroxisome. Altogether, this suggests that the PTS1 pathway is well conserved in *Drosophila.* In addition, several predicted peroxisomal membrane proteins localized to peroxisomes, and knockdown of *Pex19* resulted in their mistargeting to the cytosol. This suggests that the membrane protein import pathway is likewise conserved. Altogether with the localization of the peroxins analyzed, the data support a strong conservation of the peroxisome pathway in *Drosophila melanogaster*, with the exception of the PTS2 import pathway.

One aspect to consider is the use of GFP-SKL and/or anti-SKL as a peroxisome marker. One caveat of this method is that a portion of the cellular pool of SKL-containing

peptides would be found in the cytosol at any given time. It should be noted that because of the nature of the PTS1 import pathway, PTS1-containing peptides would exist, at least transiently, in the cytosol, as peroxisome proteins are post-translationally targeted in the cytosol to peroxisomes. One method to analyze the proportion of total SKL found in the cytosol would be to fractionate the cells into cytosolic and membrane fractions and analyze the amount of protein in each fraction by western blot marked with an anti-SKL antibody. The membrane fraction would contain all the peroxisomes and by extension, all the SKL-containing proteins that have been imported into peroxisomes. By comparing the amount of protein marked with anti-SKL in the cytosolic fraction versus the membrane fraction, the relative proportion of SKL-containing peptides residing in the cytosol under basal conditions could be extrapolated. While this caveat is important to consider, the fluorescent signal detected in the cytosol is minimal in GFP-SKL expressing cells or cells marked with anti-SKL and should not have a significant effect on colocalization calculations.

4.2. Pex14 is upregulated in response to oleate supplementation

When S2 cells were cultured in 1 mM oleate for 24 hours, the expression of *Pex14* was significantly upregulated (Figure 3.1E). This was also observed with endogenous PEX14 in NRK cells (Figure 3.5B) Together, these data suggested Pex14 plays a role in lipid metabolism. To date, there are no post-translational modifications known to regulate Pex14 activity (reviewed in Azevedo and Schliebs, 2006). It is likely that Pex14 is regulated at the level of transcription, and its activity is intrinsically linked

to its expression level. The expression levels of *Pex14* have been previously linked to lipid metabolism. Yin *et al.* performed a microarray analysis in the human liposarcoma SW782 cell line to determine genes that are upregulated during the late stages of adipogenesis (Yin et al., 2014). From this analysis, 11 genes showed a greater than 10-fold increase in expression. One of those genes was *PEX14*, which showed a 12.65-fold increase in expression (Yin et al., 2014). Another group performed an analysis of SW872 apidopcytes and similarly found that *PEX14* was significantly upregulated during adipocyte differentiation (Zhu et al., 2014). Adipogenesis is the process by which pre-adipocytes differentiate into mature adipocytes (Cornelius et al., 1994). These results are consistent with the observations made in Figure 3.1 whereby *Pex14* expression is elevated in response to increased lipid metabolism.

One caveat to consider is the effect of the various lipid species found in serum on the cellular lipid metabolism. Because the S2 cells were being cultured in Schneider's media with 10% FBS, the lipids found in the serum may have affected the cell's metabolism. Many of the protein components of FBS have been extensively studied (Gstraunthaler, 2003); however, the lipid component remains less defined. Therefore, it is possible that serum contains trace amounts of lipid species, such as oleate. In some cases, it may be important to delipidate serum, which has been shown to have an effect on cell metabolism (Giles et al., 1981) However, few LDs are observed in S2 cells cultured in standard conditions, and in contrast, the LD population is greatly increased when cells are supplemented with oleate. Therefore it is unlikely that FBS contains sufficient amounts of lipid to have a significant effect. In addition, all localization studies in Chapter 3 were repeated in serum free HyClone SFX-Insect cell culture media (VWR)

and found to replicate the observations made in Schneider's media, which suggests that the presence of serum did not influence the results.

4.3. Knockdown of Pex14 induces lipolysis in S2 cells

When *Pex14* was knocked down by dsRNA in S2 cells, a significant reduction in LD volume was observed (Figure 3.2F). There was also a concomitant increase in LD number (Figure 3.2G). In S2 cells, the change in LD volume and number was not observed in 24-hour oleate-supplemented conditions, but only in lipolytic conditions (Figure 3.2). During lipolysis, MG and DG molecules that are produced by TG hydrolysis can be reesterified by the MGATs and DGAT1 to form TG at the ER producing new iLDs (Coleman and Haynes, 1985). It is possible that the small LDs observed when *Pex14* was knocked down represent iLDs that are formed from the reesterification of MG and DG molecules produced by elevated lipolysis. In addition, Guo et al. found that mutations in genes that resulted in smaller dispersed LDs also showed increased lipolytic activity in S2 cells (Guo et al., 2008). The LD phenotype observed in these cells, in combination with increased glycerol production (Figure 3.2B), a hallmark of lipolysis, support the conclusion that knockdown of *Pex14* expression leads to increased lipolysis in *Drosophila*.

4.4. Knockdown of Pex14 in the fat body affects the lipid content

When *Pex14* was knocked down in the fat body of 3rd instar larvae, a significant reduction in LD volume was observed (Figure 3.3E). Besides a reduction in LD size observed in the fat body, an overall reduction in TG content was observed in 3rd instar larvae when *Pex14* expression was knocked down using the GAL4-UAS system (Figure 3.3C). This was measured by the enzymatic cleavage of TG molecules in each sample, followed by fluorescence detection of the resulting glycerol molecule. There is a direct correlation between the amount of glycerol and the amount of TG in a given sample. It is assumed that the R4-GAL4 x UAS-*Pex14* dsRNA 3rd instar larvae consume the same amount of food, and therefore the reduction in overall fat content is a result of increased lipid mobilization.

R4-GAL4 x UAS-*Pex14* dsRNA 3rd instar larvae also showed decreased survival when placed on lard food, relative to the control (w^{1118} x UAS-*Pex14* dsRNA) (Figure 3.3F). On average, less than 50% of the population remained alive after one week on lard food. This suggested that the animals died as a result of lipotoxicity. The animals would continually absorb excess lipid from consuming the lard food. In addition, FFAs are constantly being released as a consequence of increased lipolytic activity in the fat body. In combination this would lead to elevated circulating FFA, which causes lipotoxicity. Increased lipolysis in *Pex14* knockdown larvae is consistent with the results of another study by Bülow et al. *Pex19 Drosophila* mutants showed elevated levels of lipolysis, which lead to mitochondrial defects as a result of the increased metabolic load on the mitochondria (Bülow et al., 2018). A significant upregulation in *lipase3* was observed in *Pex19* mutants, which could be responsible for the increased lipolytic activity (Bülow et

al., 2018). The expression levels of *Hsl and Bmm* were examined in *Pex14* dsRNA treated S2 cells and were found unperturbed. Given the findings of Bülow et al., *lipase3* expression should also be examined in *Pex14* knockdown cells.

4.6. The localization of specific peroxins to the lipid droplet

Under specific metabolic conditions, Pex3, Pex13, and Pex14 were observed at the surface of the LD (Figure 3.4). This was evident from an observed increase in the measured degree of colocalization between epitope-tagged Pex3, Pex13, and Pex14 with the LDs. In addition, a concomitant decrease in the degree of colocalization between 6xMyc-Pex14 and anti-SKL was observed (Figure 3.2B). In addition, the degree of colocalization between anti-SKL and LDs did not increase (Figure 3.2B), which suggests that the localization of these peroxins to LDs is independent of mature peroxisomes.

The oleate-supplemented conditions used were specifically chosen to increase LD metabolism in the cell. Previous studies have used 1 mM oleate supplementation in S2 cells in order to induce LD biogenesis and formation (Guo et al., 2008; Krahmer et al., 2011). The localization of these peroxins to the LD surface seems to occur sometime between 24 and 48 hours after the addition of oleate. Peroxins visualized 24 hours after oleate supplementation were found primarily localized to peroxisomes. In addition, these peroxins localized to the LD surface in lipolytic conditions. In lipolytic conditions, S2 cells were supplemented with oleate for 24 hours, followed by removal of oleate and FBS for 24 hours, as described in Chapter 3. In lipolytic conditions, the localization of the peroxins appeared identical to their localization after 48 hours of oleate supplementation.

This suggests that the trafficking of peroxins to the LD occurs in a time-dependent manner following the induction of LD metabolism.

The localization of endogenous PEX14 was analyzed in NRK cells and found to similarly localize to LDs under the same conditions (Figure 3.5). NRK cells have been previously used to study LD biology (Bartz et al., 2007; Tan et al., 2013; Wilfling et al., 2014). Similar to S2 cells, NRK cells cultured in the presence of oleate rapidly form large LDs. In addition, peroxisomes have a significant role in kidney function, which is highlighted by the disease phenotype of kidneys in PBD patients (Braverman and Moser, 2012; Steinberg et al., 2006). Moreover, this disease phenotype of PBDs has been recapitulated in the Malpighian tubules of *Pex1* mutant *Drosophila,* which is the functional equivalent of the mammalian kidney (Mast et al., 2011). Altogether, this supports the use of NRK cells for this study.

Similar to the observations made in S2 cells, the degree of colocalization between Pex14 and LDs increased in 48-hour oleate-supplemented conditions (Figure 3.5B). In addition, the degree of colocalization between PMP70 and LDs did not increase (Figure 3.5C), which again suggests that PEX14 targets to the LD independently of mature peroxisomes. PEX14 expression levels in NRK cells (Figure 3.5F) also recapitulated the observed increase in *Pex14* expression in S2 cells (Figure 3.1). Peroxisome volume did not change in NRK cells when supplemented with oleate (Figure 3.5D), whereas peroxisome volume significantly increased in oleate-supplemented S2 cells (Figure 3.1C). In addition, peroxisome number increased in oleate-supplemented NRK cells (Figure 3.5D), whereas peroxisome number decreased in oleate-supplemented S2 cells (Figure 3.1B). The observed differences could be a species-specific response to oleate or a result of the peroxisome marker used (SKL versus PMP70).

4.7. PEX14 is found on the lipid droplet surface in NRK cells

Using iTEM, endogenous PEX14 was found at the LD surface in NRK cells (Figure 3.5G). iTEM allows for higher resolution imaging than immunofluorescence. This provided greater detail at the cellular level, which allowed for the determination of the precise subcellular localization of PEX14. The majority of PEX14 was found within 40 nm of the LD surface (Figure 3.5H) and in many cases, in direct contact with the LD surface (Figure 3.5G).

It is unclear whether this localization is due to interactions directly with the LD surface or if it is facilitated via interactions with resident LD proteins. The LD surface consists of a phospholipid monolayer (reviewed in Fujimoto and Parton, 2011). Because Pex14 is a known bilayer transmembrane protein, it is unlikely that it could be inserted into the LD membrane, as the hydrophobic forces on the interior surface would be too great to overcome. Soluble proteins have been found within the interior of the LD core (Bozza et al., 1997; Dvorak et al., 1992). It is likely that these soluble proteins would be complexed with phospholipids in order to reduce hydrophobic forces. The most likely situation is one in which Pex14 remains embedded in the vesicle that facilitates its delivery to the LD surface and is tethered to the LD via interactions with a LD-resident protein. This is supported by TEM images in Figure 3.5I which show an abundance of vesicles between the ER and the LD population. It is possible that these vesicles represent Pex13/Pex14 containing vesicles that are targeted to the LD surface under these conditions. In addition, the vesicles observed in Figure 3.5I are approximately 40 – 50

nm in diameter, which is consistent with the observation that the majority of Pex14 is found within 40 nm of the LD surface.

Potential interaction partners have been identified. I have also performed a co-immunoprecipitation assay using anti-Myc cross-linked beads on S2 cell lysates transfected with 6xMyc-Pex14 under oleate-supplemented conditions. The proteins found within the samples immunoprecipitated from the lysates were identified by mass spectroscopy. In 48-hour oleate supplemented conditions, 6xMyc-Pex14 was found to interact with Reticulon-like 1 (Rtnl1). Rtnl1 is a member of the Reticulon family of proteins and functions in ER network organization (O'Sullivan et al., 2012; Yang and Strittmatter, 2007). Given that LD biogenesis occurs at the ER and reticulons control ER organization, it is possible that they are localized to the LD surface. In fact, Rtnl1 has been detected in LD fractions prepared from *Drosophila* fat body of various genotypes (Beller et al., 2006). Furthermore, in mice, Reticulon-3 plays a critical role in regulating LD expansion (Xiang et al., 2018). This poses the possibility that Rtnl1 is localized to the LD surface and plays a role in facilitating Pex14 localization at the LD surface; however, further studies are required to confirm this.

4.8. Overexpression of the Lsd1 affects Pex14 localization to the lipid droplet surface

Overexpression of the gene encoding *Drosophila* PLIN1, *Lsd1*, blocked the localization of 6xMyc-Pex14 to the LD surface in S2 cells (Figure 3.6A). This is evident from the observed decrease in the degree of colocalization observed between 6xMyc-

Pex14 and LDs when S2 cells are simultaneously transfected with 3xFLAG-Lsd1 (Figure 3.6C). Under these conditions, 6xMyc-Pex14 formed punctate structures that are presumably localized to peroxisomes, as is observed by its localization under standard conditions (Schneider's medium + 10% FBS). 3xFLAG-Lsd1 appears to exclusively localize to the LD surface (Figure 3.6A). In addition, the localization of both 3xFLAG-Lsd1 and 3xFLAG-Lsd2 to the LD was not affected by Pex14 overexpression (Figure 3.6B).

It has been shown that proteins on the LD surface are subject to molecular crowding and compete for limited space. In particular, during lipolysis, as the LD surface area shrinks, certain proteins are preferentially removed from the LD surface in order to create space for others (Kory et al., 2016). This poses a possible mechanism for the removal of 6xMyc-Pex14 from the LD surface when 3xFLAG-Lsd1 is overexpressed. Excess Lsd1 may block Pex14 from accessing the LD surface or preferentially forces its removal from the LD surface. Although, the data suggests that this is not the case, as overexpression of 3xFLAG-Lsd2 does not affect 6xMyc-Pex14 localization to the LD (Figure 3.6A and 3.6C). This suggests that the effect observed of *Lsd1* overexpression on Pex14-LD localization is specific. Phosphorylated Lsd1 functions to recruit Hsl to the LD surface during lipolysis in *Drosophila* (Bi et al., 2012). In contrast, Pex14 appears to block the recruitment of Hsl to the LD surface during lipolysis (Figure 3.7). Therefore, it is possible that Lsd1 modulates the LD-localization of Pex14, whereby Lsd1 functions antagonistically to Pex14 and, by extension, specifically prevents Pex14 from localizing to the LD surface.

4.9. Overexpression of Pex14 affects Hsl localization, but not Bmm

The overexpression of 6xMyc-Pex14 did not affect the localization of 3xFLAG-Bmm in lipolytic S2 cells. Similarly, the overexpression of 3xFLAG-Bmm did not affect the localization of 6xMyc-Pex14 to the LD surface (Figure 3.7A). The degree of colocalization between both 3xFLAG-Bmm and 6xMyc-Pex14 with the LD was not affected when the fusion proteins were simultaneously overexpressed (Figures 3.7B and 3.7C). In addition, LD volume and number per cell in Bmm overexpressing cells were not affected by the simultaneous overexpression of 6xMyc-Pex14 (Figures 3.7D and 3.7E).

In contrast, the simultaneous overexpression of 6xMyc-Pex14 and 3xFLAG-Hsl resulted in the mislocalization of 3xFLAG-Hsl to the cytosol (Figure 3.7A). In these cells, 3xFLAG-Hsl was primarily diffuse throughout the cytosol, with small punctate structures that likely represent protein aggregates. A small amount of protein appeared to be localized to the LD; however, the majority appears to be cytosolic. The degree of colocalization between 3xFLAG-Hsl and LDs was significantly reduced from approximately 65% to less than 40% when lipolytic S2 cells simultaneously overexpressed 6xMyc-Pex14 (Figure 3.7C). It is unclear how 6xMyc-Pex14 overexpression causes 3xFLAG-Hsl to mislocalize to the cytosol. As previously mentioned, it is possible that this is caused by molecular crowding, whereby excess 6xMyc-Pex14 at the LD surface blocks 3xFLAG-Hsl from the LD due to lack of physical space. However, this is unlikely given that the effect is specific to Hsl, whereas Bmm is unaffected. It is possible that this is a result of the anti-lipolytic effects of Pex14 functioning antagonistically to Hsl. It is possible that Pex14 functions at the LD surface to perturb the interaction between Hsl and Lsd1 during lipolysis. This is consistent with

the antagonistic effects of 3xFLAG-Lsd1 on 6xMyc-Pex14 localization. Further studies will be required to elucidate the mechanism by which Pex14 perturbs Hsl localization.

The LDs found in cells overexpressing both 6xMyc-Pex14 and 3xFLAG-Hsl were significantly larger than those found in cells overexpressing 3xFLAG-Hsl alone (Figure 3.6D). In addition, fewer LDs were found in cells overexpressing both fusion proteins, relative to cells overexpressing 3xFLAG-Hsl alone (Figure 3.6E). It has been shown in mammalian cells that HSL may have some affinity for TG molecules in catalyzing hydrolysis; however, they have a much higher affinity for DG (Haemmerle et al., 2002; reviewed in Lass et al., 2011). In lipolytic S2 cells overexpressing both 6xMyc-Pex14 and 3xFLAG-Hsl, levels of DG should be elevated as endogenous Bmm continues to hydrolyze TG. It is possible that DG is reesterified to TG at the LD surface by the LD-localized isoform, DGAT2 (Stone et al., 2009). If conserved in S2 cells, this would cause TG stores to be maintained, which would explain the increase in LD volume.

4.10. Overexpression of Pex14 affects CGI-58 expression

The simultaneous overexpression of 6xMyc-Pex14 and 3xFLAG-CGI-58 did not affect the localization of either protein, as both appeared to localize to the LD surface under lipolytic conditions. (Figure 3.8A, E, F). CGI-58 functions at the LD surface during lipolysis to activate ATGL in the lipolytic pathway (Yamaguchi et al., 2004, 2007). When *Pex14* expression is attenuated by the dsRNA treatment, the proportion of 3xFLAG-CGI-58 found in the cytosol was increased (Figure 3.8A). This is likely caused by the observed depletion of LDs under these conditions. Very few LDs are visible in

lipolytic cells overexpressing 3xFLAG-CGI-58 treated with *Pex14* dsRNA. Therefore, if the LD surface is unavailable, excess CGI-58 will be mislocalized in the cytosol.

CGI-58 has been shown to interact with the peroxisomal ABC-transporter PXA1 in co-regulating lipid homeostasis and signalling in *Arapadopsis* (Park et al., 2013). PXA1 is the homologue of ABCD1 in *Drosophila* and functions to take up FFA into the peroxisome (Morita and Imanaka, 2012). Moreover, CGI-58 was shown to regulate the function of PXA1 in lipid signalling (Park et al., 2013). This further supports the relationship between CGI-58 and components of the peroxisome, particularly in regulating lipid metabolism.

Cells overexpressing 3xFLAG-CGI-58 alone possessed smaller dispersed LDs. This is likely a result of *CGI-58* overexpression, which would increase the activation of Bmm. Moreover, TG stores were further depleted in cells treated with *Pex14* dsRNA and overexpressing 3xFLAG-CGI-58. This is likely a synergistic effect of CGI-58 overexpression and the loss of the proposed anti-lipolytic effects of Pex14. In contrast, in cells simultaneously overexpressing 6xMyc-Pex14 and 3xFLAG-CGI-58, LD volume significantly increased (Figure 3.8C). This suggests that the effects of Pex14 at the LD may suppress the lipolytic activation function of CGI-58, thereby maintaining TG stores within the LD.

When S2 cells were treated with *Pex14* dsRNA, a significant decrease in *CGI-58* expression was observed in lipolytic conditions (Figure 3.8G). Given that CGI-58 activates Bmm, this result was counterintuitive to the increased lipolysis observed in S2 cells treated with *Pex14* dsRNA (Figure 3.2). *CGI-58* expression levels would be expected to increase during active lipolysis. However, it is possible that the function of Pex14 in lipolytic regulation is within a network of *CGI-58* transcriptional regulation. In

cells with attenuated *Pex14* expression, lipolysis would be aberrantly active due to the loss of Pex14 anti-lipolytic function. This signals a transcriptional response to down-regulate *CGI-58* expression. This would serve as a functional feedback loop to regulate lipolysis in the cell.

4.11. Model and mechanism

Based on my observations, I have proposed a model to guide future experiments that will help elucidate more details of this mechanism. In this model, I propose that a subclass of PPVs containing Pex13 and Pex14 are diverted from the *de novo* biogenesis pathway to the LD surface during periods of elevated lipid metabolism. Because of the topology of Pex13 and Pex14, it would be energetically unfavourable for these proteins to insert into the LD monolayer. Therefore, it is most likely that Pex13 and Pex14 reside within the membrane of small vesicles that are directed to the LD surface. These vesicles interact with components on the LD surface, which serve to regulate lipolysis. Pex13/Pex14-containing vesicles act as physical barriers that specifically block the recruitment of Hsl to the LD surface during lipolysis. This speculative model is outlined in Figure 4.1.

4.12. Future directions

The model described above provides the foundation for future experiments to further investigate the role of Pex13 and Pex14 at the LD. It is likely that Pex13 and Pex14 are trafficked to the LD surface on vesicles originating at the ER. It is possible that these vesicles are PPVs; however, based on the data, it is not clear that these are in fact PPVs. In addition, it is not clear whether peroxins found at the LD surface are newly synthesized via the ER, or if it is an existing pool of protein that is delivered to LDs via mature peroxisomes. Future work will be required to determine the nature of the peroxins found at the LD. However, some of the data acquired so far support the model that LD-localized peroxins are delivered via newly synthesized PPVs. First, TEM images in Figure 3.5I show an abundance of electron-dense vesicles found between the ER and the LD pool. A number of these vesicles are found in close proximity to the LD surface. It is possible that these vesicles are PPVs containing Pex13 and Pex14. In addition, immunofluorescence images of 6xMyc-Pex14-transfected S2 cells show a clear distinction between the epitope-tagged Pex14 signal and the anti-SKL signal. If Pex14 were trafficked to the LD via mature peroxisomes, SKL and Pex14 would remain colocalized. This is also evident in the discrepancy between the degree of colocalization between anti-SKL and 6xMyc-Pex14 with LDs (Figure 3.4). Lastly, this is consistent with the upregulation of *Pex14* expression in oleate-supplemented conditions (Figure 3.1E). Upregulation of *Pex14* expression may represent the newly synthesized Pex14 that is destined for the LD surface.

Assuming that LD-localized peroxins are newly synthesized proteins, another avenue of investigation will be determining the sorting mechanism by which Pex13/Pex14-containing vesicles become destined for the LD. During periods of

Figure 4.1

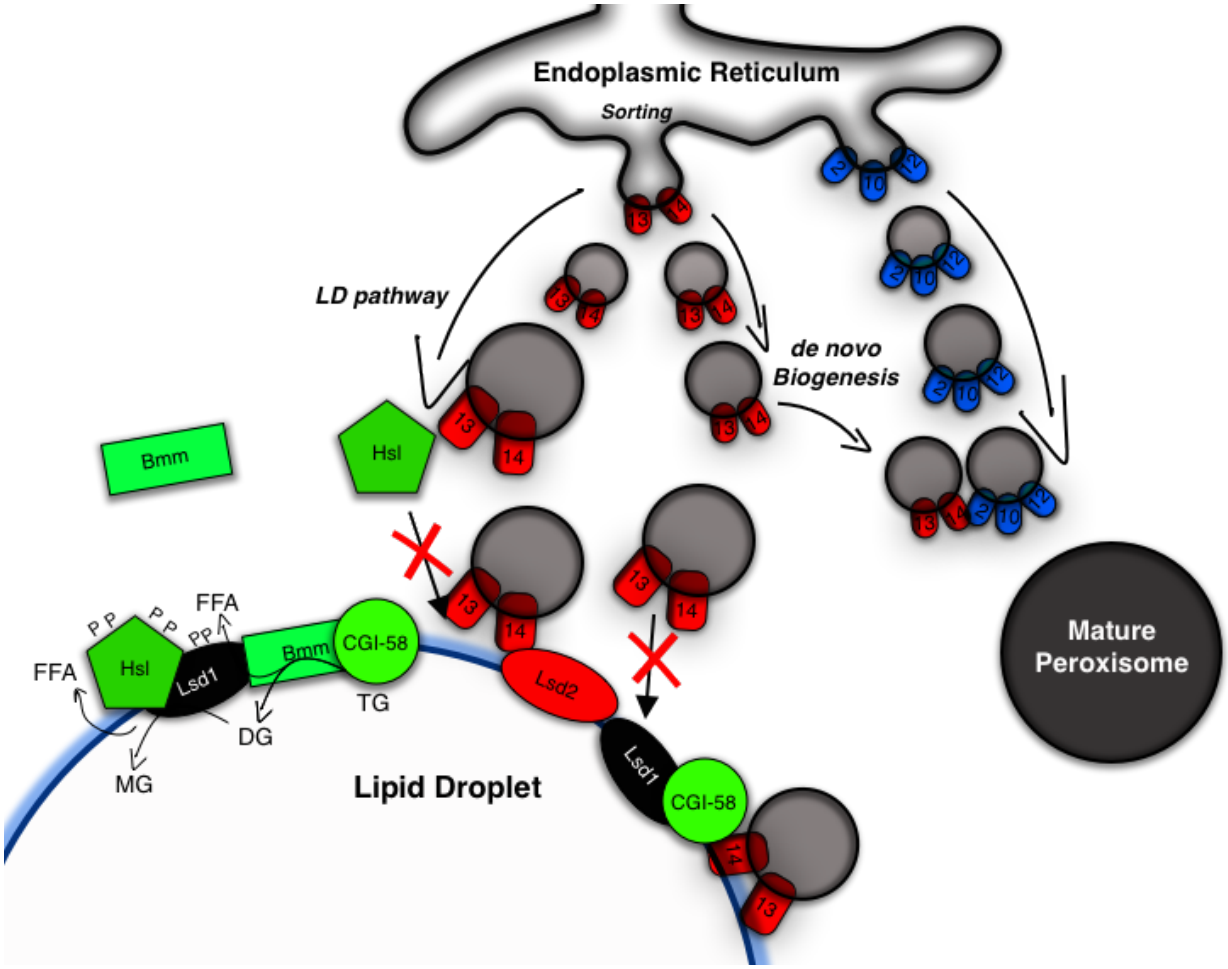
Endoplasmic Reticulum
Sorting
LD pathway
de novo
Biogenesis
Bmm
Hsl
Mature
Peroxisome
FFA
FFA
Hsl
Lsd1
Bmm
CGI-58
TG
DG
MG
Lipid Droplet
Lsd2
Lsd1
CGI-58

Figure 4.1. Model. PPVs containing Pex13 and Pex14 are sorted into two separate pathways at the ER during periods of elevated LD metabolism, the *de novo* biogenesis pathway and the LD pathway. Pex13/Pex14-containing vesicles are diverted to the LD surface where they are anchored through protein-protein interactions with resident LD proteins. Lsd1 blocks Pex13/Pex14-containing vesicles from the LD surface. Pex13/Pex14-containing vesicles function at the LD surface by preventing Hsl from accessing the LD surface. This serves to gate lipolytic activity and maintain TG stores within the LD.

increased lipid metabolism, what signalling mechanism causes Pex13 and Pex14 to be sorted at the ER into vesicles that become targeted to the LD surface? This process likely occurs via intra-ER chaperone proteins that sort newly synthesized Pex13 and Pex14. In addition, given the role of Pex3 in peroxisome biogenesis at the ER (Ghaedi et al., 2000), Pex3 may be involved in this sorting process. This may also explain why epitope-tagged Pex3 also seems to localize to the LD in S2 cells during the same conditions (Figure 3.4D).

Once Pex13/Pex14-containing vesicles have budded from the ER, how are they trafficked to the LD surface? What mechanism diverts them directly to LDs and prevents them from following the *de novo* biogenesis pathway to form mature peroxisomes? It is likely that these vesicles are trafficked via actin to the LD surface. PEX14 is known to interact with microtubules and PEX14 is required for peroxisome motility in human cells (Bharti et al., 2011). In fact, "TubStain" is a peptide-tool to label microtubules and is composed of the N-terminus of human PEX14 labeled with GFP (Theiss et al., 2012). It is possible that Pex14 serves as the vesicle anchor to microtubules, allowing their transport from the ER to the LD surface. This could be analyzed by using a microtubule stain (available from Thermo Fisher) and monitoring the colocalization of Pex14 relative to microtubules. Although, it is likely that super-resolution microscopy would be required to perform this analysis. For example, Galiani et al. used stimulated emission depletion (STED) microscopy to visualize the compartmentalization of various peroxisome proteins in human fibroblasts (Galiani et al., 2016). Using STED microscopy, Pex14 could be visualized relative to the microtubule network and its role in trafficking Pex14 to LDs could be monitored.

After Pex13/Pex14-containing vesicles have been delivered to the LD surface, by what mechanism is their localization maintained? It is likely that these vesicles are maintained at the LD via interactions between Pex14 and resident LD proteins. Rtnl1 is a LD-localized protein that was found to interact with 6xMyc-Pex14 under oleate supplemented conditions. Because of the reported function of the family of reticulon proteins, it is also possible that Rtnl1 may be involved in retaining Pex13/Pex14-containing vesicles at the LD surface, although, no evidence exists to confidently conclude that either of these proteins facilitates this localization.

What happens to Pex13/Pex14-containing vesicles after they have localized to the LD surface and performed their function? It is possible that after these vesicles have received lipids from the LD core, they dissociate from the LD surface and fuse with the corresponding partner PPV to form mature peroxisomes. It is likely that the dissociation of these vesicles from the LD surface correlates with lipolytic activity. As LDs shrink and TG stores are depleted, it is possible that Pex13/Pex14-containing vesicles dissociate from the LD as surface area is reduced. In order to monitor the activity of these vesicles, a visual marker is needed to discern LD-localized Pex13 and Pex14 from the cellular pool of peroxins existing at peroxisomes. This could be accomplished by appending a photo-convertible GFP epitope to Pex14. This may even be possible for existing GFP fusion proteins. It has been demonstrated that GFP can be photoconverted from a 505-525 nm emission to a 580-670 nm emission by bleaching with the 405 nm laser (Sattarzadeh et al., 2015). This shifts the fluorescence from green to red. In fact, the photoconverted GFP is no longer excitable by 488 nm light, as conventional GFP is. This technique has been demonstrated in *Drosophila* cells (Sattarzadeh et al., 2015). Alternatively, specially evolved photoconvertible fluorescent proteins, such as DENDRA (Guruharsha et al.,

2011) could be used. LD-localized GFP-tagged Pex14 could be photoconverted, which would make it discernable from the rest of the cellular pool. This population of Pex14 could then be followed over time to monitor Pex14-LD dynamics. This could also be performed in live cells, as LipidTOX Red will mark LDs in live cells as well. One concern with this method is that it was found from the experiments outlined in Chapter 2, larger epitope tags, such as RFP, disrupted the localization of Pex14. In this case, it is possible an internal GFP tag may have to be used in order to retain the functional localization of Pex14.

4.13. Conclusions

The results of the experiments outlined in this thesis have demonstrated that Pex13 and Pex14 are localized to the LD surface during periods of increased cellular lipid metabolism. Decreased levels of Pex14 resulted in depletion of TG stores and the formation of smaller LDs in S2 cells and *Drosophila* fat body, suggesting that Pex14 may function to regulate lipolysis. In addition, Pex14 appears to block the recruitment of Hsl to the LD surface during lipolysis. Further investigation is required to thoroughly characterize this relationship.

Chapter 5: Materials and methods

Portions of this chapter are published in: **Baron, M.N., Klinger, C.M, Rachubinski, R.A., and Simmonds, A.J.** (2016). A Systematic Cell-Based Analysis of Localization of Predicted *Drosophila* Peroxisomal Proteins. Traffic *17*: 536 – 553.

5.1. Cell culture

S2 cells were grown in Schneider's medium (Sigma Aldrich) containing 10% FBS (Thermo Fisher) at 25°C. NRK cells were grown in DMEM (Sigma Aldrich) containing 10% FBS at 37 °C and 5% CO_2. Both were supplemented with 100 U penicillin per mL and 100 µg streptomycin per mL streptomycin (Thermo Fisher). Both S2 cells and NRK cells were passaged in a log phase before they reached confluency. Cultures were not used for experiments beyond passage 25.

S2 cells and NRK were supplemented with 1 mM oleate to induce LD biogenesis. Cells were cultured in 1 mM oleate-supplemented conditions for 24 or 48 hours, where specified. For lipolytic conditions, following 24 hours oleate supplementation, S2 cells and NRK cells were washed in fresh medium and incubated in Schneider's medium or DMEM, respectively, for 24 hours to induce lipolysis. This protocol was adapted from Guo, et al. in order to induce LD biogenesis and subsequent lipolysis (Guo et al., 2008)

5.2. Drosophila strains

The w^{1118} strain was obtained from the Bloomington *Drosophila* Stock Center. The R4-GAL4 strain was a gift from the Foley Lab, University of Alberta. The UAS-*Pex14* dsRNA strain was obtained from the Vienna *Drosophila* Research Center. All crosses were performed at 25°C. Flies were kept on Bloomington *Drosophila* Stock Center standard cornmeal food agar, unless specified. Fly strains were passaged once per week to prevent overcrowding in vials.

5.3. Cloning

cDNA libraries were made from mRNA harvested from *Drosophila* embryos at 2 – 4, 4 – 6, and 10 – 14 hours after egg laying and reverse transcribed using oligo-dT primers with a One-Step RT kit (Bio-Rad). The coding sequence for each gene encoding a gene of interest was amplified from a cDNA template using Phusion High Fidelity DNA polymerase (Thermo Fisher). Full-length coding sequences were amplified with or without a stop codon for N-terminal and C-terminal tagging of proteins, respectively. Blunt-end purified PCR products with a CACC motif at the 5' end were directionally cloned into the pENTR/D entry vector by TOPO cloning for the Gateway System (Thermo Fisher). Plasmids were verified by sequencing. Gene inserts were then recombined into pARW/pAWR, pAFW/pAWF, or pAMW/pAWM destination vectors (*Drosophila* Gateway Vector Collection, originally developed by Terence Murphy, Cornell University) for fusion with sequence encoding RFP, FLAG, or Myc, respectively, using LR Clonase II (Thermo Fisher).

5.4. Transfections

Plasmids containing a tagged gene of interest were transfected into *Drosophila* S2 cells using Effectene transfection reagent (Qiagen). Manufacturer's protocol was

followed. S2 cells were passaged 24 hours prior to transfection. Approximately 5.0 x 10^5 cells were transfected with 150 ng of plasmid DNA. Transfected S2 cells were incubated at 25°C for 3 days before imaging or further processing.

5.5. Microscopy

Live S2 cells were observed by live-cell imaging using a Zeiss 63× water immersion objective (NA = 1.4) on a Zeiss AxioObserver M1 microscope coupled to an ERS spinning disk confocal imager using Volocity imaging software (PerkinElmer). Images were captured using a C9100 EMCCD camera (Hamamatsu) at 130 μm vertical (*z*) spacing. S2 cells were fixed in 4% paraformaldehyde in PBS and blocked with 3% bovine serum albumin (BSA). Cells were incubated for one hour with anti-FLAG M2 monoclonal mouse primary antibody (Sigma-Aldrich) or anti-Myc rabbit primary antibody (Sigma Aldrich). Both primary antibodies were used at a 1:200 dilution. Anti-SKL rabbit primary antibody was used at 1:250 dilution to mark peroxisomes. In cases where 6xMyc-tagged proteins were analyzed relative to peroxisomes, 9E10 anti-Myc mouse primary antibody (produced from an ATCC hybridoma, obtained from Dr. Paul Lapointe, University of Alberta) was used at a 1:250 dilution. Primary antibody incubation was followed by incubation with Alexa Fluor 568 anti-mouse goat secondary antibody and Alexa Fluor 488 anti-rabbit secondary antibody (Abcam), both at 1:2000 dilution. Cells were imaged as above, except that for fixed cells, a Zeiss 63× oil immersion objective (NA = 1.4) was used. For mitochondrial colocalization, S2 cells were stained with MitoTracker Green FM (Thermo Fisher) three days post-transfection.

To detect LDs, cells were stained with HCS LipidTOX Deep Red (Thermo Fisher) at 1:500 dilution for one hour after secondary antibody incubation. For larval fat body staining, the fat body from 3rd instar larvae were dissected and fixed in 4% paraformaldehyde for 15 minutes. The tissue was rinsed three times in PBS. The tissue was then stained with Nile Red (Thermo Fisher) and 4,6′ -diamidino-2-phenylindole (DAPI) at a 1:1000 and 1:500 dilutions, respectively. Tissues were mounted on slides with Prolong Gold (Thermo Fisher) mounting medium and imaged. NRK cells were fixed in 4% paraformaldehyde and blocked in 3% BSA for one hour. Cells were incubated in rabbit anti-PEX14 primary antibody (Thermo Fisher) and mouse anti-PMP70 primary antibody (produced by the Rachubinski lab, University of Alberta) at 1:200 dilutions, for one hour. Primary antibody incubation was followed by incubation with Alexa Fluor 568 anti-mouse goat secondary antibody and Alexa Fluor 488 anti-rabbit secondary antibody (Abcam), both at 1:2000 dilutions. LipidTOX Deep Red (Thermo Fisher) was used at 1:500 dilution to mark the LDs. Cells were imaged with a 63x objective lens, as above.

The images shown best represented the quantitative data that accompanies them. In Chapter 2, images are representative of three biological replicates. In Figure 3.2, images are representative of six biological replicates. In Figure 3.4A, images are representative of four biological replicates. In Figures 3.1, 3.3, 3.4D, 3.5, 3.6, 3.7, and 3.8, images are representative of three biological replicates.

5.6. Bioinformatics

Assistance in bioinformatic analysis was provided by Chris Klinger, University of Alberta. Putative *Drosophila melanogaster* peroxisomal proteins identified in the original

screen (Faust et al., 2012) were subjected to reciprocal BLASTp analysis (Altschul et al., 1997) against the 'refseq' *Homo sapiens* proteome at NCBI (taxid:9606). BLAST settings were left at their default values. In cases where no *H. sapiens* protein could be identified, additional queries of the entirety of the NR database were made. This analysis allowed for reciprocal confirmation of the putative gene identities that were made in the original screen.

5.7. Image processing

Confocal image stacks were processed to remove noise and reassign blur using a classical maximum likelihood estimation confocal algorithm provided by Huygens Professional Software (Scientific Volume Imaging) and an experimentally determined point spread function constructed from multiple images of 0.1 μm Tetraspeck beads (Thermo Fisher). Three-dimensional-based colocalization analysis using Pearson's coefficient was performed with Huygens Professional Software. Individual peroxisome or LD volume and average number of peroxisomes or LDs per cell were calculated using IMARIS 8 software (Bitplane). Organelle volume and number were measured using the Surfaces function as follows: the specific channel for the appropriate organelle marker was selected. A Gaussian filter was applied by selecting "Smooth" and the surfaces detail was set to 0.1 μm. Thresholding was set to "Background Subtraction (Local Contrast)". The diameter of the smallest organelle signal to be included in the measurement was measured in the "Slice" mode and the value was inputted into the Surfaces creator below "Background Subtraction". A surface is now created and background signal was removed

by adjusting the slider in the Surfaces creator. Finally, the surfaces were created by selecting the green arrow to perform the appropriate calculations. Values were found under the "Statistics" tab, which gives the total number of surfaces (organelle number). Organelle volume was given by selecting "Average values".

For chapter 2 colocalization, peroxisome volume and number measurements, each value shown represents a mean of a minimum of three independent cells from each biological sample. Each calculation represents three biological replicates.

In Figures 3.1B and 3.1C, peroxisome volume and number values represent averages based on 10 cells measured from three biological replicates, for a total of 30 cells measured. In Figures 3.2D-G, peroxisome and LD volume and number values represent averages based on five cells measured from six biological replicates, for a total of 30 cells measured. In Figure 3.3E, LD volume values represent averages based on six images measured from three biological replicates, for a total of 18 cells measured. In Figures 3.4B, colocalization values represent averages based on five cells measured from four biological replicates, for a total of 20 cells measured. In Figure 3.4E, colocalization values represent averages based on five cells measured from three biological replicates, for a total of 15 cells measured. In Figures 3.5 – 3.8, all colocalization, peroxisome volume and number, and LD volume and number values represent averages based on five cells measured from three biological replicates for a total of 15 cells measured. For statistical analysis of all colocalization and organelle volume/number data, an unpaired Student's *t*-test was performed. Statistical analysis was performed using Prism 7 software (Graphpad).

5.8. dsRNA treatments

dsRNA amplicons were made from a template library courtesy of the Foley Lab, University of Alberta (Foley and O'Farrell, 2004). RNA was amplified using a T7 RNA Polymerase Kit (Thermo Fisher). S2 cells were passaged 24 hours prior to dsRNA treatments. Cells were treated with dsRNA using Effectene Transfection Reagent (Qiagen) to enhance uptake. S2 cells were incubated for 72 hours at 25°C before further processing. A scrambled dsRNA amplicon was used as a control.

5.9. qPCR Analysis

RNA was isolated from S2 cells using the RNeasy Plus Mini Kit (Qiagen). RNA was reverse transcribed using the iScript Select cDNA synthesis kit with oligo(dT) primers (BioRad). Quantification of each transcript was performed using iQ SYBR Green (BioRad) and an Eppendorf MasterCycler RealPlex2. All samples were measured in triplicate and calculations were made relative to *Ribosomal Protein L30* (*RpL30*) expression. Primers for target genes were experimentally validated primer pairs from the FlyPrimerBank (Hu et al., 2013). For all qPCR experiments, values reported are averages based on three biological replicates. Statistical significance was determined by unpaired Student's *t*-test using Prism 7 software (Graphpad).

5.10. RNA-Seq

RNA was isolated from S2 cells using an RNeasy Plus Mini Kit (Qiagen) and RNA integrity was analyzed using an Agilent RNA Nano assay (Agilent Genomics). Ribosomal RNA was removed from samples using a Ribo-Zero Gold rRNA Removal Kit (Illumina). Libraries were prepared using a NEBNext Ultra RNA Library Prep Kit and NEBNext Multiplex Oligos (New England BioLabs). The library quality and size distribution were assessed by running an Agilent High Sensitivity DNA assay (Agilent Genomics), and the average size of library inserts was found to be 290 - 300 base pairs. 2 nM of pooled multiplexed libraries were submitted to the TAGC core facility, and 10 pM pooled libraries was loaded onto an Illumina MiSeq v2 300 cycle kit (2 x 150 cycles, paired-end reads).

Each condition was analyzed in triplicate. Paired-end reads were aligned to the *Drosophila menalagaster* genome (6.79 genome release) using both the Tuxedo suite (Kim et al., 2013; Langmead and Salzberg, 2012) and HiSat2 (Kim et al., 2015). Read counts were performed by HTSeq (Anders et al., 2015) and weakly expressed reads were filtered out as noise. Reads with less than one count per million in at least three samples were filtered out (Pertea et al., 2016). Analysis of differential expression was performed using both EdgeR (Robinson et al., 2010) and DESeq2 (Love et al., 2014). Both models assume a negative binomial distribution of the data. In both models, normalization relies on the hypothesis that most reads are not differential expressed across conditions. In each case, individual reads were normalized to genes with high expression and little variation amongst the conditions and a normalization factor was applied to each gene. Both EdgeR and DESeq2 were used to calculate the differential expression between the samples and generate a *p*-value, *q*-value, and a False Discovery Rate (FDR) for each gene. Genes that

were found to be differentially expressed by both models were used for subsequent analysis.

5.11. Glycerol quantification

The glycerol content of cell culture media was quantified using a Glycerol Assay Kit (Sigma Aldrich) according to the manufacturer's protocol. S2 cells were pelleted by centrifugation and the resulting Schneider's medium was removed. Each sample was diluted 1:1000 in water. The assay was performed per the manufacturer's instructions, and end-point fluorescence was measured at 587 nm in a BioTek Synergy 4 plate-reader with Gen 5 software. Glycerol measurements were made relative to the protein content in each sample, measured using a Pierce BCA Protein Assay Kit (Thermo Fisher). For protein measurements, cells were lysed in Mild Lysis Buffer, and protein measurements were taken, as per manufacturer's instructions. Colorimetric absorption was measured at 562 nm using a BioTek Synergy 4 plate-reader with Gen 5 software. The values reported are based on averages from six biological replicates. Statistical significance was measured by unpaired Student's *t*-test using Prism 7 software (Graphpad).

5.12. Larval flotation assay

Four days after egg-laying, 3rd instar larvae were removed from their vials, rinsed in sterile PBS and suspended in a 12% sucrose solution, as per Reis et al. (Reis et al., 2010). Larvae were scored by their propensity to float in the sucrose solution. In each

trial, 10 larvae were analyzed. Three biological replicates were performed for each sample, for a total of 30 larvae analyzed. Statistical significance was measured by unpaired Student's *t*-test using Prism 7 software (Graphpad).

5.13. Triglyceride quantification

Approximately 4 days after egg-laying, 3rd instar larvae were removed from their vials and rinsed in sterile PBS. Lysates were made by homogenizing tissue in 5% NP-40 in distilled, deionized water. Samples were heated at 80°C for 5 minutes, cooled to room temperature, and centrifuged to remove any insoluble material. TG measurements from each sample were made using a Triglyceride Assay Kit (Abcam), as per the manufacturer's instructions. Fluorometric detection was made at 587 nm using a BioTek Synergy 4 plate-reader with Gen 5 software. TG measurements were made relative to the protein concentration of each sample, measured using the Pierce BCA Protein Assay Kit. Lysates were made from 10 larvae for each trial. The values reported are averages from three biological replicates. Statistical significance was measured by unpaired Student's *t*-test using Prism 7 software (Graphpad).

5.14. Larval survival analysis

For the lipotoxicity experiments shown in Figure 3.3F, 3rd instar larvae were transferred to holidic food or lard food. Holidic food was prepared according to Piper et al. (Piper et al., 2014). Lard food was prepared as holidic food with the addition of lard at

22.2 g/L. For each trial, 10 3rd instar larvae from each genetic cross were transferred to holidic food or lard food. The values shown are averages from five individual genetic crosses, for a total of 50 larvae examined from each genetic cross.

5.15. Subcellular fractionation

LDs were isolated from transfected S2 cells, as described (Krahmer et al., 2011). In brief, cells from a T25 flask were pelleted, washed in cold PBS, and resuspended in 2 mL of buffer (200 mM Tris/HCl pH 7.5, 2 mM magnesium acetate) with protease inhibitors (Roche). The cells were lysed using a cell homogenizer and a 10-µm ball bearing (Isobiotec). The lysates were then cleared by centrifugation at 1,000x g for 10 minutes. The cleared lysates were adjusted to 1.08 M sucrose, and a step-wise gradient of sucrose was layered on top with 2 mL of 0.27 M sucrose, followed by 2 mL of 0.135 M sucrose. Finally, one mL of 0 M buffer was layered at the top. Samples were spun at 100,000x g for 90 minutes at 4°C in an ultracentrifuge. The floating LD fraction was isolated, and the proteins within the fraction were precipitated by methanol: chloroform extraction, as per Wessel and Flügge (Wessel and Flügge, 1984). In brief, 2 mL of methanol and 500 µl of chloroform was added to 500 µl of LD fraction isolate. The mixture was vortexed, and centrifuged at 9,000 g for 10 seconds. 1.5 mL of ddH_2O was added and the mixture was again vortexed and centrifuged at 14,000 g for one minute. The top aqueous layer was removed and an additional 2 mL of methanol was added and vortexed. The sample was centrifuged at 20,000 g for 5 minutes to pellet the protein. The methanol was carefully removed and the protein pellet was dried. The dried protein pellet was resuspended in 30 µl of gel sample buffer, boiled, and size separated by SDS-PAGE.

5.16. Western blot

Samples were boiled in gel sample buffer for 5 minutes, size separated by SDS-PAGE, and transferred to a nitrocellulose membrane (Bio-Rad). Membranes were blocked in Odyssey Blocking Buffer (LI-COR). For subcellular fractionation experiments, membranes were incubated with rabbit anti-Lsd2 primary antibody (obtained from Dr. Michael Welte, University of Rochester) and mouse 9E10 anti-MYC primary antibody (ATCC). For NRK cell lysates, membranes were probed with rabbit anti-PEX14 primary antibody (Thermo Fisher) and mouse anti-β-tubulin primary antibody [Devlopmental Studies Hybridoma Bank (DHSB)]. Membranes were then probed with Alexa Fluor anti-rabbit A680 secondary antibody and Alexa Fluor anti-mouse A790 secondary antibody (Abcam). Membranes were visualized using an Odyssey Infrared Imaging System (LI-COR) and band were quantified using Odyssey software (LI-COR). The western blots shown are representative of three independent biological replicates.

5.17. Transmission electron microscopy

NRK cells were grown in 6-well dishes to 80% confluency prior to processing. Cells were rinsed in PBS and fixed in Karnovsky's fixative (2% paraformaldehyde/2% glutaraldehyde (GA) in 0.1M sodium cacodylate buffer). The cells were then rinsed three

times in buffer and a cell scraper was used to remove the cells from the surface of the dish. Cells were pelleted at increasing speeds of 1,000, 3,000, 6,000, and 12,000x g for five minutes each. Cell pellets were then incubated for one hour in 1% osmium tetroxide, protected from light. Pellets were rinsed several times in water and 1% uranyl acetate was added overnight at room temperature, protected from light. The next day, the pellets were dehydrated in a series of steps: 70% ethanol (two times, five minutes each), 90% ethanol (two times, five minutes each), and 100% ethanol (three times, five minutes each). Pellets were left in acetonitrile overnight at room temperature under vacuum. The next day, resin was added to the pellets and left at 60°C for 48 hours. Finally, the pellets were sectioned and imaged. TEM imaging was performed by Nasser Tahbaz, Department of Cell Biology, University of Alberta.

5.18. Immuno-transmission electron microscopy

NRK cells were grown in 6-well dishes to 80% confluency prior to processing. Cells were rinsed in PBS and fixed in 3% paraformaldehyde/2% sucrose + 0.05% GA in PBS. Cells were rinsed three times in PBS followed by two rinses in 50 mM ammonium chloride. Cells were permeabilized in 0.1% saponin for 10 minutes, followed by two rinses in PBS. Cells were blocked in blocking buffer (PBS + 1 % BSA + 0.05% Fish Skin Gelatin (FSG) + Saponin 0.05%) for one hour. Cells were incubated with anti-PEX14 primary antibody (Thermo Fisher) at 1:100 dilution in blocking buffer for two hours at room temperature. Cells were washed three times in wash buffer (0.2% BSA + 0.05% FSG + 0.05% saponin) and incubated in anti-rabbit Nanogold antibody (Nanoprobes) at a

1:1000 dilution in blocking buffer overnight at room temperature. The next day, cells were washed three times in PBS and fixed again in 2% GA in PBS + 2% Sucrose for one hour. Cells were rinsed three times in water, and GoldEnhance EM (Nanoprobes) was used as per the manufacturer's instructions. Cells were washed several times in water followed by two rinses in 0.1 M sodium cacodylate buffer. Cells were scraped off the dish with a cell scraper and pelleted in a microfuge tube at increasing speeds: 1,000, 3,000, 6,000, and 12,000x g, for 10 minutes each at 4°C. The resulting pellets were incubated with 1% osmium tetroxide on ice for one hour. The pellets were rinsed several times in water. The pellets were then incubated in uranyl acetate overnight at 4°C, protected from light. The next day, pellets were rinsed several times in 30% ethanol, followed by progressive dehydration steps at 50%, 60%, 70%, 80%, and 90% ethanol for 10 minutes each. Lastly, three 10-minute washes with 100% ethanol were performed to remove any residual water. Pellets were left in acetonitrile overnight at room temperature under vacuum. The next day, resin was added to the pellets and left at 60°C for 48 hours. Finally, the pellets were sectioned and imaged. iTEM imaging was performed by Nasser Tahbaz, Department of Cell Biology, University of Alberta.

In Figure 3.5I, the distance of PEX14 spots from the LD surface was measured by hand, and grouped into six ranges: 0 – 40 nm, 41 – 80 nm, 81 – 120 nm, 121 – 160 nm, 161 – 200 nm, and 200+ nm. The values shown are the proportion of PEX14 in each range for a given image. A total of 10 images were quantified from three biological replicates.

Table 5.1. Kits and reagents

Item	Catalogue #	Source
Agilent High Sensitivity DNA Kit	5067-4626	Agilent Genomics
Agilent RNA 6000 Nano Kit	5067-1511	Agilent Genomics
Complete, mini Protease Inhibitors	11836153001	Roche
4,6'-diamidino-2-phenylindole (DAPI)	D9542	Sigma Aldrich
Dulbecco's modified eagle's medium	11965092	Thermo Fisher
Effectene Transfection Reagent	301425	Qiagen
Fetal Bovine Serum	10438026	Thermo Fisher
Gateway LR Clonase II Enzyme Mix	11791100	Thermo Fisher
Glucose (GO) Assay Kit	GAGO20	Sigma Aldrich
Glycerol Assay Kit	MAK117	Sigma Aldrich
GoldEnhance EM	2113	Nanoprobes
HCS LipidTOX Deep Red Lipid Stain	H34477	Thermo Fisher
iQ SYBR Green Supermix	170-8880	Bio-Rad
iScript Select cDNA Synthesis Kit	170-8897	Bio-Rad
Mitotracker Green FM	M7514	Thermo Fisher
NEBNext Multiplex Oligos	E7335	New England BioLabs
NEBNext Ultra RNA Library Prep Kit	E7530	New England BioLabs
Nile Red	N3013	Sigma Aldrich
Odyssey Blocking Buffer	927-4000	LI-COR
Paraformaldehyde	158127	Sigma Aldrich
pENTR/D-TOPO Cloning Kit	K240020	Thermo Fisher
Phusion High Fidelity DNA polymerase	F530L	Thermo Fisher

Pierce BCA Protein Assay Kit	23225	Thermo Fisher
Prolong Gold Antifade Mountant	P36930	Thermo Fisher
Ribo-Zero Gold rRNA Removal Kit	MRZG12324	Illumina
RNeasy Plus Mini Kit	74136	Qiagen
Schneider's media	S0146	Sigma Aldrich
T7 RNA Polymerase	18033-019	Thermo Fisher
TetraSpeck Microspheres, 0.1 um	T7279	Thermo Fisher
Trehalase from porcine kidney	T8778	Sigma Aldrich
Triglyceride Assay Kit - Quantitation	ab65336	Abcam

Table 5.2. Primary antibodies

Antibody	**Species**	**Catalogue #**	**Source**
anti-FLAG M2	Mouse	F3165	Sigma-Aldrich
anti-Lsd2	Rabbit	N/A	Michael Welte
anti-Myc	Rabbit	SAB4503660	Sigma-Aldrich
anti-Myc 9E10	Mouse	CRL-1729	ATCC hybridoma
anti-PEX14	Rabbit	PA5-61151	Thermo Fisher
anti-PMP70	Mouse	N/A	Richard Rachubinski
anti-SKL	Rabbit	N/A	Richard Rachubinski
anti-β-tubulin E57	Mouse	AB_2315513	DHSB

Table 5.3. Secondary antibodies

Antibody	Species	Catalogue #	Source
Alexa Fluor 488 anti-rabbit	Donkey	ab150077	Abcam
Alexa Fluor 568 anti-mouse	Donkey	ab175473	Abcam
Alexa Fluor A680 anti-rabbit	Donkey	ab186696	Abcam
Alexa Fluor A790 anti-mouse	Donkey	ab175783	Abcam
Nanogold anti-rabbit	Goat	2004	Nanoprobes

.

Bibliography

Abell, B.M., High, S., and Moloney, M.M. (2002). Membrane Protein Topology of Oleosin Is Constrained by Its Long Hydrophobic Domain. J. Biol. Chem. *277*, 8602–8610.

Adams, M.D., Celniker, S.E., Holt, R.A., Evans, C.A., Gocayne, J.D., Amanatides, P.G., Scherer, S.E., Li, P.W., Hoskins, R.A., Galle, R.F., et al. (2000). The Genome Sequence of *Drosophila melanogaster*. Science *287*, 2185–2195.

Adler, J., and Parmryd, I. (2010). Quantifying colocalization by correlation: The Pearson correlation coefficient is superior to the Mander's overlap coefficient. Cytometry A *77A*, 733–742.

Agrawal, G., Fassas, S.N., Xia, Z.-J., and Subramani, S. (2016). Distinct requirements for intra-ER sorting and budding of peroxisomal membrane proteins from the ER. J Cell Biol *212*, 335–348.

Aitchison, A.J., Arsenault, D.J., Ridgway, N.D., and Riezman, H. (2015). Nuclear-localized CTP:phosphocholine cytidylyltransferase α regulates phosphatidylcholine synthesis required for lipid droplet biogenesis. Mol. Biol. Cell *26*, 2927–2938.

Albertini, M., Rehling, P., Erdmann, R., Girzalsky, W., Kiel, J.A.K.W., Veenhuis, M., and Kunau, W.H. (1997). Pex14p, a Peroxisomal Membrane Protein Binding Both Receptors of the Two PTS-Dependent Import Pathways. Cell *89*, 83–92.

Altschul, S.F., Madden, T.L., Schäffer, A.A., Zhang, J., Zhang, Z., Miller, W., and Lipman, D.J. (1997). Gapped BLAST and PSI-BLAST: a new generation of protein database search programs. Nucleic Acids Res. *25*, 3389–3402.

Anders, S., Pyl, P.T., and Huber, W. (2015). HTSeq—a Python framework to work with high-throughput sequencing data. Bioinformatics *31*, 166–169.

Arrese, E.L., Rivera, L., Hamada, M., Mirza, S., Hartson, S.D., Weintraub, S., and Soulages, J.L. (2008). Function and structure of lipid storage droplet protein 1 studied in lipoprotein complexes. Arch. Biochem. Biophys. *473*, 42–47.

Ashmarina, L.I., Rusnak, N., Miziorko, H.M., and Mitchell, G.A. (1994). 3-Hydroxy-3-methylglutaryl-CoA lyase is present in mouse and human liver peroxisomes. J. Biol. Chem. *269*, 31929–31932.

Aubourg, P., and Wanders, R. (2013). Chapter 163 - Peroxisomal disorders. In Handbook of Clinical Neurology, O. Dulac, M. Lassonde, and H.B. Sarnat, eds. (Elsevier), pp. 1593–1609.

Azevedo, J.E., and Schliebs, W. (2006). Pex14p, more than just a docking protein. Biochim. Biophys. Acta BBA - Mol. Cell Res. *1763*, 1574–1584.

Bartz, R., Li, W.H., Venables, B., Zehmer, J.K., Roth, M.R., Welti, R., Anderson, R.G.W., Liu, P., and Chapman, K.D. (2007). Lipidomics reveals that adiposomes store ether lipids and mediate phospholipid traffic. J. Lipid Res. *48*, 837–847.

Beard, M.E., and Holtzman, E. (1987). Peroxisomes in wild-type and *rosy* mutant *Drosophila melanogaster.* Proc. Natl. Acad. Sci. *84*, 7433–7437.

Beller, M., Riedel, D., Jänsch, L., Dieterich, G., Wehland, J., Jäckle, H., and Kühnlein, R.P. (2006). Characterization of the *Drosophila* Lipid Droplet Subproteome. Mol. Cell. Proteomics *5*, 1082–1094.

Beller, M., Bulankina, A.V., Hsiao, H.-H., Urlaub, H., Jäckle, H., and Kühnlein, R.P. (2010). PERILIPIN-Dependent Control of Lipid Droplet Structure and Fat Storage in *Drosophila*. Cell Metab. *12*, 521–532.

Bharti, P., Schliebs, W., Schievelbusch, T., Neuhaus, A., David, C., Kock, K., Herrmann, C., Meyer, H.E., Wiese, S., Warscheid, B., et al. (2011). PEX14 is required for microtubule-based peroxisome motility in human cells. J Cell Sci *124*, 1759–1768.

Bi, J., Xiang, Y., Chen, H., Liu, Z., Grönke, S., Kühnlein, R.P., and Huang, X. (2012). Opposite and redundant roles of the two *Drosophila* perilipins in lipid mobilization. J Cell Sci *125*, 3568–3577.

Bilder, D., and Irvine, K.D. (2017). Taking Stock of the *Drosophila* Research Ecosystem. Genetics *206*, 1227–1236.

Binns, D., Januszewski, T., Chen, Y., Hill, J., Markin, V.S., Zhao, Y., Gilpin, C., Chapman, K.D., Anderson, R.G.W., and Goodman, J.M. (2006). An intimate collaboration between peroxisomes and lipid bodies. J. Cell Biol. *173*, 719–731.

Birschmann, I., Stroobants, A.K., van den Berg, M., Schäfer, A., Rosenkranz, K., Kunau, W.H., and Tabak, H.F. (2003). Pex15p of Saccharomyces cerevisiae Provides a Molecular Basis for Recruitment of the AAA Peroxin Pex6p to Peroxisomal Membranes. Mol. Biol. Cell *14*, 2226–2236.

Birse, R.T., Choi, J., Reardon, K., Rodriguez, J., Graham, S., Diop, S., Ocorr, K., Bodmer, R., and Oldham, S. (2010). High-Fat-Diet-Induced Obesity and Heart Dysfunction Are Regulated by the TOR Pathway in *Drosophila.* Cell Metab. *12*, 533–544.

Bjørkøy, G., Lamark, T., Brech, A., Outzen, H., Perander, M., Øvervatn, A., Stenmark, H., and Johansen, T. (2005). p62/SQSTM1 forms protein aggregates degraded by autophagy and has a protective effect on huntingtin-induced cell death. J. Cell Biol. *171*, 603–614.

Blanchette, E.J. (1966). OVARIAN STEROID CELLS: II. The Lutein Cell. J. Cell Biol. *31*, 517–542.

Blanchette-Mackie, E.J., Dwyer, K., Barber, L.T., Coxey, R.A., Takeda, T., and Greenberg, A.S. (1995). Perilipin is located on the surface layer of intracellular lipid droplets in adipocytes. 16.

Bozza, P.T., Yu, W., Penrose, J.F., Morgan, E.S., Dvorak, A.M., and Weller, P.F. (1997). Eosinophil Lipid Bodies: Specific, Inducible Intracellular Sites for Enhanced Eicosanoid Formation. J. Exp. Med. *186*, 909–920.

Brand, A.H., and Perrimon, N. (1993). Targeted gene expression as a means of altering cell fates and generating dominant phenotypes. Development *118*, 401–415.

Braverman, N.E., and Moser, A.B. (2012). Functions of plasmalogen lipids in health and disease. Biochim. Biophys. Acta BBA - Mol. Basis Dis. *1822*, 1442–1452.

Brocard, C., and Hartig, A. (2006). Peroxisome targeting signal 1: Is it really a simple tripeptide? Biochim. Biophys. Acta BBA - Mol. Cell Res. *1763*, 1565–1573.

Bülow, M.H., Wingen, C., Senyilmaz, D., Gosejacob, D., Sociale, M., Bauer, R., Schulze, H., Sandhoff, K., Teleman, A.A., Hoch, M., et al. (2018). Unbalanced lipolysis results in lipotoxicity and mitochondrial damage in peroxisome-deficient *Pex19* mutants. Mol. Biol. Cell *29*, 396–407.

Buszczak, M., Lu, X., Segraves, W.A., Chang, T.Y., and Cooley, L. (2002). Mutations in the *midway* Gene Disrupt a *Drosophila* Acyl Coenzyme A: Diacylglycerol Acyltransferase. Genetics *160*, 1511–1518.

Campbell, R.E., Tour, O., Palmer, A.E., Steinbach, P.A., Baird, G.S., Zacharias, D.A., and Tsien, R.Y. (2002). A monomeric red fluorescent protein. Proc. Natl. Acad. Sci. *99*, 7877–7882.

Cases, S., Smith, S.J., Zheng, Y.-W., Myers, H.M., Lear, S.R., Sande, E., Novak, S., Collins, C., Welch, C.B., Lusis, A.J., et al. (1998). Identification of a gene encoding an acyl CoA:diacylglycerol acyltransferase, a key enzyme in triacylglycerol synthesis. Proc. Natl. Acad. Sci. U. S. A. *95*, 13018–13023.

Casso, D., Ramírez-Weber, F.-A., and Kornberg, T.B. (1999). GFP-tagged balancer chromosomes for *Drosophila melanogaster*. Mech. Dev. *88*, 229–232.

Cermelli, S., Guo, Y., Gross, S.P., and Welte, M.A. (2006). The Lipid-Droplet Proteome Reveals that Droplets Are a Protein-Storage Depot. Curr. Biol. *16*, 1783–1795.

Chang, C.R., and Blackstone, C. (2007). Drp1 phosphorylation and mitochondrial regulation. EMBO Rep. *8*, 1088–1089.

Chang, C.C., South, S., Warren, D., Jones, J., Moser, A.B., Moser, H.W., and Gould, S.J. (1999). Metabolic control of peroxisome abundance. J. Cell Sci. *112*, 1579–1590.

Chao, Y.H., Robak, L.A., Xia, F., Koenig, M.K., Adesina, A., Bacino, C.A., Scaglia, F., Bellen, H.J., and Wangler, M.F. (2016). Missense variants in the middle domain of

DNM1L in cases of infantile encephalopathy alter peroxisomes and mitochondria when assayed in *Drosophila*. Hum. Mol. Genet. *25*, 1846–1856.

Chapman, K.D., and Trelease, R.N. (1991). Acquisition of membrane lipids by differentiating glyoxysomes: role of lipid bodies. J. Cell Biol. *115*, 995–1007.

Chen, H., Liu, Z., and Huang, X. (2010). *Drosophila* models of peroxisomal biogenesis disorder: peroxins are required for spermatogenesis and very-long-chain fatty acid metabolism. Hum. Mol. Genet. *19*, 494–505.

Chintapalli, V.R., Wang, J., and Dow, J.A.T. (2007). Using FlyAtlas to identify better *Drosophila melanogaster* models of human disease. Nat. Genet. *39*, 715–720.

Cho, D.-H., Kim, Y.S., Jo, D.S., Choe, S.-K., and Jo, E.-K. (2018). Pexophagy: Molecular Mechanisms and Implications for Health and Diseases. Mol. Cells *41*, 55–64.

Chorlay, A., and Thiam, A.R. (2018). An Asymmetry in Monolayer Tension Regulates Lipid Droplet Budding Direction. Biophys. J. *114*, 631–640.

Chu, B.-B., Liao, Y.C., Qi, W., Xie, C., Du, X., Wang, J., Yang, H., Miao, H.-H., Li, B.L., and Song, B.-L. (2015). Cholesterol Transport through Lysosome-Peroxisome Membrane Contacts. Cell *161*, 291–306.

Church, R.B., and Robertson, F.W. (1966). A biochemical study of the growth of *Drosophila melanogaster*. J. Exp. Zool. *162*, 337–351.

Colasante, C., Chen, J., Ahlemeyer, B., Bonilla-Martinez, R., Karnati, S., and Baumgart-Vogt, E. (2017). New insights into the distribution, protein abundance and subcellular localisation of the endogenous peroxisomal biogenesis proteins PEX3 and PEX19 in different organs and cell types of the adult mouse. PLOS ONE *12*, e0183150.

Coleman, R.A., and Haynes, E.B. (1985). Subcellular location and topography of rat hepatic monoacylglycerol acyltransferase activity. Biochim. Biophys. Acta BBA - Lipids Lipid Metab. *834*, 180–187.

Cornelius, P., MacDougald, O.A., and Lane, M.D. (1994). Regulation of Adipocyte Development. Annu. Rev. Nutr. *14*, 99–129.

Corpas, F.J., de la Colina, C., Sánchez-Rasero, F., and del Rio, L.A. (1997). A role for leaf peroxisomes in the catabolism of purines. J. Plant Physiol. *151*, 246–250.

Dalen, K.T., Ulven, S.M., Arntsen, B.M., Solaas, K., and Nebb, H.I. (2006). PPARα activators and fasting induce the expression of adipose differentiation-related protein in liver. J. Lipid Res. *47*, 931–943.

Darfler, P.J. (1990). Preparation and use of lipid microemulsions as nutritional supplements for culturing mammalian cells. In Vitro Cell. Dev. Biol. *26*, 779–783.

De Duve, C., and Baudhuin, P. (1966). Peroxisomes (microbodies and related particles). Physiol. Rev. *46*, 323–357.

Delille, H.K., Agricola, B., Guimaraes, S.C., Borta, H., Lüers, G.H., Fransen, M., and Schrader, M. (2010). Pex11pβ-mediated growth and division of mammalian peroxisomes follows a maturation pathway. J Cell Sci *123*, 2750–2762.

Deosaran, E., Larsen, K.B., Hua, R., Sargent, G., Wang, Y., Kim, S., Lamark, T., Jauregui, M., Law, K., Lippincott-Schwartz, J., et al. (2013). NBR1 acts as an autophagy receptor for peroxisomes. J Cell Sci *126*, 939–952.

Di Cara, F., Sheshachalam, A., Braverman, N.E., Rachubinski, R.A., and Simmonds, A.J. (2017). Peroxisome-Mediated Metabolism Is Required for Immune Response to Microbial Infection. Immunity *47*, 93-106.e7.

Di Cara, F., Rachubinski, R.A., and Simmonds, A.J. (2018). Distinct Roles for Peroxisomal Targeting Signal Receptors Pex5 and Pex7 in *Drosophila*. Genetics genetics.301628.2018.

DiAngelo, J.R., and Birnbaum, M.J. (2009). Regulation of Fat Cell Mass by Insulin in *Drosophila melanogaster*. Mol. Cell. Biol. *29*, 6341–6352.

Dietzl, G., Chen, D., Schnorrer, F., Su, K.-C., Barinova, Y., Fellner, M., Gasser, B., Kinsey, K., Oppel, S., Scheiblauer, S., et al. (2007). A genome-wide transgenic RNAi library for conditional gene inactivation in *Drosophila*. Nature *448*, 151–156.

Dodt, G., and Gould, S.J. (1996). Multiple PEX genes are required for proper subcellular distribution and stability of Pex5p, the PTS1 receptor: evidence that PTS1 protein import is mediated by a cycling receptor. J. Cell Biol. *135*, 1763–1774.

Ducharme, N.A., and Bickel, P.E. (2008). Minireview: Lipid Droplets in Lipogenesis and Lipolysis. Endocrinology *149*, 942–949.

Duncan, R.E., Wang, Y., Ahmadian, M., Lu, J., Sarkadi-Nagy, E., and Sul, H.S. (2010). Characterization of desnutrin functional domains: critical residues for triacylglycerol hydrolysis in cultured cells. J. Lipid Res. *51*, 309–317.

Dunn, K.W., Kamocka, M.M., and McDonald, J.H. (2011). A practical guide to evaluating colocalization in biological microscopy. Am. J. Physiol.-Cell Physiol. *300*, C723–C742.

Dvorak, A.M., Morgan, E., Schleimer, R.P., Ryeom, S.W., Lichtenstein, L.M., and Weller, P.F. (1992). Ultrastructural immunogold localization of prostaglandin endoperoxide synthase (cyclooxygenase) to non-membrane-bound cytoplasmic lipid bodies in human lung mast cells, alveolar macrophages, type II pneumocytes, and neutrophils. J. Histochem. Cytochem. *40*, 759–769.

Elgersma, Y., Vos, A., Berg, M. van den, Roermund, C.W.T. van, Sluijs, P. van der, Distel, B., and Tabak, H.F. (1996a). Analysis of the Carboxyl-terminal Peroxisomal Targeting Signal 1 in a Homologous Context in *Saccharomyces cerevisiae*. J. Biol. Chem. *271*, 26375–26382.

Elgersma, Y., Kwast, L., Klein, A., Voorn-Brouwer, T., Berg, M. van den, Metzig, B., America, T., Tabak, H.F., and Distel, B. (1996b). The SH3 domain of the *Saccharomyces cerevisiae* peroxisomal membrane protein Pex13p functions as a docking site for Pex5p, a mobile receptor for the import PTS1-containing proteins. J. Cell Biol. *135*, 97–109.

Emanuelsson, O., Elofsson, A., von Heijne, G., and Cristóbal, S. (2003). In Silico Prediction of the Peroxisomal Proteome in Fungi, Plants and Animals. J. Mol. Biol. *330*, 443–456.

Fakieh, M.H., Drake, P.J.M., Lacey, J., Munck, J.M., Motley, A.M., and Hettema, E.H. (2013). Intra-ER sorting of the peroxisomal membrane protein Pex3 relies on its luminal domain. Biol. Open *2*, 829–837.

Fan, J., Li, X., Issop, L., Culty, M., and Papadopoulos, V. (2016). ACBD2/ECI2-Mediated Peroxisome-Mitochondria Interactions in Leydig Cell Steroid Biosynthesis. Mol. Endocrinol. *30*, 763–782.

Fang, Y., Morrell, J.C., Jones, J.M., and Gould, S.J. (2004). PEX3 functions as a PEX19 docking factor in the import of class I peroxisomal membrane proteins. J Cell Biol *164*, 863–875.

Faust, J.E., Verma, A., Peng, C., and McNew, J.A. (2012). An Inventory of Peroxisomal Proteins and Pathways in *Drosophila melanogaster*. Traffic *13*, 1378–1392.

Faust, J.E., Manisundaram, A., Ivanova, P.T., Milne, S.B., Summerville, J.B., Brown, H.A., Wangler, M., Stern, M., and McNew, J.A. (2014). Peroxisomes Are Required for Lipid Metabolism and Muscle Function in *Drosophila melanogaster*. PLOS ONE *9*, e100213.

Foley, E., and O'Farrell, P.H. (2004). Functional Dissection of an Innate Immune Response by a Genome-Wide RNAi Screen. PLOS Biol. *2*, e203.

Fujiki, Y., Rachubinski, R.A., and Lazarow, P.B. (1984). Synthesis of a major integral membrane polypeptide of rat liver peroxisomes on free polysomes. Proc. Natl. Acad. Sci. U. S. A. *81*, 7127–7131.

Fujimoto, T., and Parton, R.G. (2011). Not Just Fat: The Structure and Function of the Lipid Droplet. Cold Spring Harb. Perspect. Biol. *3*.

Galagovsky, D., Katz, M.J., Acevedo, J.M., Sorianello, E., Glavic, A., and Wappner, P. (2014). The *Drosophila* insulin-degrading enzyme restricts growth by modulating the PI3K pathway in a cell-autonomous manner. Mol. Biol. Cell *25*, 916–924.

Galiani, S., Waithe, D., Reglinski, K., Cruz-Zaragoza, L.D., Garcia, E., Clausen, M.P., Schliebs, W., Erdmann, R., and Eggeling, C. (2016). Super-resolution Microscopy Reveals Compartmentalization of Peroxisomal Membrane Proteins. J. Biol. Chem. *291*, 16948–16962.

Gao, J., and Serrero, G. (1999). Adipose Differentiation Related Protein (ADRP) Expressed in Transfected COS-7 Cells Selectively Stimulates Long Chain Fatty Acid Uptake. J. Biol. Chem. *274*, 16825–16830.

Gao, Q., and Goodman, J.M. (2015). The lipid droplet—a well-connected organelle. Front. Cell Dev. Biol. *3*.

Gaudet, P., Fey, P., Basu, S., Bushmanova, Y.A., Dodson, R., Sheppard, K.A., Just, E.M., Kibbe, W.A., and Chisholm, R.L. (2011). dictyBase update 2011: web 2.0 functionality and the initial steps towards a genome portal for the Amoebozoa. Nucleic Acids Res. *39*, D620–D624.

Gautam, N.K., Verma, P., and Tapadia, M.G. (2017). *Drosophila* Malpighian Tubules: A Model for Understanding Kidney Development, Function, and Disease. In Kidney Development and Disease, (Springer, Cham), pp. 3–25.

Gautier, E.L., Shay, T., Miller, J., Greter, M., Jakubzick, C., Ivanov, S., Helft, J., Chow, A., Elpek, K.G., Gordonov, S., et al. (2012). Gene-expression profiles and transcriptional regulatory pathways that underlie the identity and diversity of mouse tissue macrophages. Nat. Immunol. *13*, 1118–1128.

Gelbart, W.M., and Emmert, D.B. (2011). FlyBase Reference Report: Gelbart and Emmert, 2011.8.23, Calculation of RPKM to generate quantitative expression data: read-length values for modENCODE developmental timecourse RNA-Seq data.

Gelbart, W.M., McCarron, M., Pandey, J., and Chovnick, A. (1974). Genetic Limits of the Xanthine Dehydrogenase Structural Element Within the Rosy Locus in *Drosophila Melanogaster*. Genetics *78*, 869–886.

Ghaedi, K., Tamura, S., Okumoto, K., Matsuzono, Y., Fujiki, Y., and Guidotti, G. (2000). The Peroxin Pex3p Initiates Membrane Assembly in Peroxisome Biogenesis. Mol. Biol. Cell *11*, 2085–2102.

GOA Curators, HGNC Curators, AgBase Curators, and UniProtKB Curators (2007). Manual transfer of experimentally-verified manual GO annotation data to orthologs by curator judgment of sequence similarity.

Gong, L., Puri, M., Ünlü, M., Young, M., Robertson, K., Viswanathan, S., Krishnaswamy, A., Dowd, S.R., and Minden, J.S. (2004). *Drosophila* ventral furrow morphogenesis: a proteomic analysis. Development *131*, 643–656.

Götte, K., Girzalsky, W., Linkert, M., Baumgart, E., Kammerer, S., Kunau, W.-H., and Erdmann, R. (1998). Pex19p, a Farnesylated Protein Essential for Peroxisome Biogenesis. Mol. Cell. Biol. *18*, 616–628.

Gould, S.J., Keller, G.-A., and Subramani, S. (1988). Identification of peroxisomal targeting signals located at the carboxy terminus of four peroxisomal proteins. J. Cell Biol. *107*, 897–905.

Gould, S.J., Keller, G.A., Hosken, N., Wilkinson, J., and Subramani, S. (1989). A conserved tripeptide sorts proteins to peroxisomes. J. Cell Biol. *108*, 1657–1664.

Granneman, J.G., Moore, H.-P.H., Granneman, R.L., Greenberg, A.S., Obin, M.S., and Zhu, Z. (2007). Analysis of Lipolytic Protein Trafficking and Interactions in Adipocytes. J. Biol. Chem. *282*, 5726–5735.

Grönke, S., Mildner, A., Fellert, S., Tennagels, N., Petry, S., Müller, G., Jäckle, H., and Kühnlein, R.P. (2005). Brummer lipase is an evolutionary conserved fat storage regulator in *Drosophila*. Cell Metab. *1*, 323–330.

Grönke, S., Müller, G., Hirsch, J., Fellert, S., Andreou, A., Haase, T., Jäckle, H., and Kühnlein, R.P. (2007). Dual Lipolytic Control of Body Fat Storage and Mobilization in *Drosophila*. PLOS Biol. *5*, e137.

Gross, D.A., Zhan, C., and Silver, D.L. (2011). Direct binding of triglyceride to fat storage-inducing transmembrane proteins 1 and 2 is important for lipid droplet formation. Proc. Natl. Acad. Sci. U. S. A. *108*, 19581–19586.

Gruber, A., Cornaciu, I., Lass, A., Schweiger, M., Poeschl, M., Eder, C., Kumari, M., Schoiswohl, G., Wolinski, H., Kohlwein, S.D., et al. (2010). The N-terminal Region of Comparative Gene Identification-58 (CGI-58) Is Important for Lipid Droplet Binding and Activation of Adipose Triglyceride Lipase. J. Biol. Chem. *285*, 12289–12298.

Grygiel-Górniak, B. (2014). Peroxisome proliferator-activated receptors and their ligands: nutritional and clinical implications - a review. Nutr. J. *13*, 17.

Guimarães, C.P., Sá-Miranda, C., and Azevedo, J.E. (2005). Probing substrate-induced conformational alterations in adrenoleukodystrophy protein by proteolysis. J. Hum. Genet. *50*, 99–105.

Guo, Y., Walther, T.C., Rao, M., Stuurman, N., Goshima, G., Terayama, K., Wong, J.S., Vale, R.D., Walter, P., and Farese, R.V. (2008). Functional genomic screen reveals genes involved in lipid-droplet formation and utilization. Nature *453*, 657–661.

Guruharsha, K.G., Rual, J.-F., Zhai, B., Mintseris, J., Vaidya, P., Vaidya, N., Beekman, C., Wong, C., Rhee, D.Y., Cenaj, O., et al. (2011). A Protein Complex Network of *Drosophila melanogaster*. Cell *147*, 690–703.

Haemmerle, G., Zimmermann, R., Hayn, M., Theussl, C., Waeg, G., Wagner, E., Sattler, W., Magin, T.M., Wagner, E.F., and Zechner, R. (2002). Hormone-sensitive Lipase Deficiency in Mice Causes Diglyceride Accumulation in Adipose Tissue, Muscle, and Testis. J. Biol. Chem. *277*, 4806–4815.

Hagstrom, D., Ma, C., Guha-Polley, S., and Subramani, S. (2014). The unique degradation pathway of the PTS2 receptor, Pex7, is dependent on the PTS receptor/coreceptor, Pex5 and Pex20. Mol. Biol. Cell *25*, 2634–2643.

Hawkins, J., Mahony, D., Maetschke, S., Wakabayashi, M., Teasdale, R.D., and Bodén, M. (2007). Identifying novel peroxisomal proteins. Proteins Struct. Funct. Bioinforma. *69*, 606–616.

Hazkani-Covo, E., Levanon, E.Y., Rotman, G., Graur, D., and Novik, A. (2004). Evolution of multicellularity in Metazoa: comparative analysis of the subcellular localization of proteins in *Saccharomyces, Drosophila* and *Caenorhabditis*. Cell Biol. Int. *28*, 171–178.

Heckmann, B.L., Zhang, X., Xie, X., and Liu, J. (2013). The G0/G1 Switch Gene 2 (G0S2): Regulating metabolism and beyond. Biochim. Biophys. Acta *1831*, 276–281.

Hoepfner, D., Berg, M. van den, Philippsen, P., Tabak, H.F., and Hettema, E.H. (2001). A role for Vps1p, actin, and the Myo2p motor in peroxisome abundance and inheritance in *Saccharomyces cerevisiae*. J Cell Biol *155*, 979–990.

Höhfeld, J., Veenhuis, M., and Kunau, W.H. (1991). PAS3, a *Saccharomyces cerevisiae* gene encoding a peroxisomal integral membrane protein essential for peroxisome biogenesis. J. Cell Biol. *114*, 1167–1178.

Holmes, H.C., Burns, S.P., Chalmers, R.A., Bain, M.S., and Iles, R.A. (1995). Ketogenic flux from lipids and leucine, assessment in 3-hydroxy-3-methylglutaryl CoA lyase deficiency. Biochem. Soc. Trans. *23*, 489S-489S.

Honsho, M., Tamura, S., Shimozawa, N., Suzuki, Y., Kondo, N., and Fujiki, Y. (1998). Mutation in PEX16 is causal in the peroxisome-deficient Zellweger syndrome of complementation group D. Am. J. Hum. Genet. *63*, 1622–1630.

Hryb, D.J., and Hogg, J.F. (1979). Chain length specificities of peroxisomal and mitochondrial β-oxidation in rat liver. Biochem. Biophys. Res. Commun. *87*, 1200–1206.

Hu, J., Shibata, Y., Zhu, P.-P., Voss, C., Rismanchi, N., Prinz, W.A., Rapoport, T.A., and Blackstone, C. (2009). A Class of Dynamin-like GTPases Involved in the Generation of the Tubular ER Network. Cell *138*, 549–561.

Hu, Y., Sopko, R., Foos, M., Kelley, C., Flockhart, I., Ammeux, N., Wang, X., Perkins, L., Perrimon, N., and Mohr, S.E. (2013). FlyPrimerBank: An Online Database for *Drosophila melanogaster* Gene Expression Analysis and Knockdown Evaluation of RNAi Reagents. G3 GenesGenomesGenetics *3*, 1607–1616.

Huang, L., Pike, D., Sleat, D.E., Nanda, V., and Lobel, P. (2014). Potential Pitfalls and Solutions for Use of Fluorescent Fusion Proteins to Study the Lysosome. PLOS ONE *9*, e88893.

Huang, Y., Huang, S., Lam, S.M., Liu, Z., Shui, G., and Zhang, Y.Q. (2016). Acsl, the *Drosophila* ortholog of intellectual-disability-related ACSL4, inhibits synaptic growth by altered lipids. J Cell Sci *129*, 4034–4045.

Hughes, J.R., Meireles, A.M., Fisher, K.H., Garcia, A., Antrobus, P.R., Wainman, A., Zitzmann, N., Deane, C., Ohkura, H., and Wakefield, J.G. (2008). A Microtubule Interactome: Complexes with Roles in Cell Cycle and Mitosis. PLOS Biol. *6*, e98.

Hui, D.Y., and Howles, P.N. (2002). Carboxyl ester lipase structure-function relationship and physiological role in lipoprotein metabolism and atherosclerosis. J. Lipid Res. *43*, 2017–2030.

Imamura, M., Inoguchi, T., Ikuyama, S., Taniguchi, S., Kobayashi, K., Nakashima, N., and Nawata, H. (2002). ADRP stimulates lipid accumulation and lipid droplet formation in murine fibroblasts. Am. J. Physiol.-Endocrinol. Metab. *283*, E775–E783.

Inlow, J.K., and Restifo, L.L. (2004). Molecular and Comparative Genetics of Mental Retardation. Genetics *166*, 835–881.

Islinger, M., Li, K.W., Seitz, J., Völkl, A., and Lüers, G.H. (2009). Hitchhiking of Cu/Zn Superoxide Dismutase to Peroxisomes – Evidence for a Natural Piggyback Import Mechanism in Mammals. Traffic *10*, 1711–1721.

Itabe, H., Yamaguchi, T., Nimura, S., and Sasabe, N. (2017). Perilipins: a diversity of intracellular lipid droplet proteins. Lipids Health Dis. *16*.

Jacquier, N., Choudhary, V., Mari, M., Toulmay, A., Reggiori, F., and Schneiter, R. (2011). Lipid droplets are functionally connected to the endoplasmic reticulum in *Saccharomyces cerevisiae*. J Cell Sci *124*, 2424–2437.

Jakobs, S., Martini, N., Schauss, A.C., Egner, A., Westermann, B., and Hell, S.W. (2003). Spatial and temporal dynamics of budding yeast mitochondria lacking the division component Fis1p. J. Cell Sci. *116*, 2005–2014.

Jansen, G.A., Oftnan, R., Ferdinandusse, S., Ijlst, L., Muijsers, A.O., Skjeldal, O.H., Stokke, O., Jakobs, C., Besley, G.T.N., Wraith, J.E., et al. (1997). Refsum disease is caused by mutations in the phytanoyl–CoA hydroxylase gene. Nat. Genet. *17*, 190–193.

Jensen, F.C., Girardi, A.J., Gilden, R.V., and Koprowski, H. (1964). INFECTION OF HUMAN AND SIMIAN TISSUE CULTURES WITH ROUS SARCOMA VIRUS. Proc. Natl. Acad. Sci. U.S.A. *52*, 53–59.

Jiang, H.P., and Serrero, G. (1992). Isolation and characterization of a full-length cDNA coding for an adipose differentiation-related protein. Proc. Natl. Acad. Sci. U. S. A. *89*, 7856–7860.

Jones, J.M., Morrell, J.C., and Gould, S.J. (2004). PEX19 is a predominantly cytosolic chaperone and import receptor for class 1 peroxisomal membrane proteins. J. Cell Biol. *164*, 57–67.

Jones, N.L., Reagan, J.W., and Willingham, M.C. (2000). The pathogenesis of foam cell formation: modified LDL stimulates uptake of co-incubated LDL via macropinocytosis. Arterioscler. Thromb. Vasc. Biol. *20*, 773–781.

Joshi, A.S., Huang, X., Choudhary, V., Levine, T.P., Hu, J., and Prinz, W.A. (2016). A family of membrane-shaping proteins at ER subdomains regulates pre-peroxisomal vesicle biogenesis. J. Cell Biol. *215*, 515–529.

Kao, L.-R., and Megraw, T.L. (2004). RNAi in Cultured *Drosophila* Cells. Methods Mol. Biol. Clifton NJ *247*, 443–457.

Karlsson, M., Contreras, J.A., Hellman, U., Tornqvist, H., and Holm, C. (1997). cDNA Cloning, Tissue Distribution, and Identification of the Catalytic Triad of Monoglyceride Lipase. J. Biol. Chem. *272*, 27218–27223.

Kaufman, T.C. (2017). A Short History and Description of *Drosophila melanogaster* Classical Genetics: Chromosome Aberrations, Forward Genetic Screens, and the Nature of Mutations. Genetics *206*, 665–689.

Kaushik, S., and Cuervo, A.M. (2015). Degradation of lipid droplet-associated proteins by chaperone-mediated autophagy facilitates lipolysis. Nat. Cell Biol. *17*, 759–770.

Kiel, J.A.K.W., Veenhuis, M., and Klei, I.J. van der (2006). PEX Genes in Fungal Genomes: Common, Rare or Redundant. Traffic *7*, 1291–1303.

Kim, D., Pertea, G., Trapnell, C., Pimentel, H., Kelley, R., and Salzberg, S.L. (2013). TopHat2: accurate alignment of transcriptomes in the presence of insertions, deletions and gene fusions. Genome Biol. *14*, R36.

Kim, D., Langmead, B., and Salzberg, S.L. (2015). HISAT: a fast spliced aligner with low memory requirements. Nat. Methods *12*, 357–360.

Kim, H., Ling, S.-C., Rogers, G.C., Kural, C., Selvin, P.R., Rogers, S.L., and Gelfand, V.I. (2007). Microtubule binding by dynactin is required for microtubule organization but not cargo transport. J. Cell Biol. *176*, 641–651.

Kim, P.K., Hailey, D.W., Mullen, R.T., and Lippincott-Schwartz, J. (2008). Ubiquitin signals autophagic degradation of cytosolic proteins and peroxisomes. Proc. Natl. Acad. Sci. *105*, 20567–20574.

Kim, Y.S., Nam, H.J., Chung, H.Y., Kim, N.D., Ryu, J.H., Lee, W.J., Arking, R., and Yoo, M.A. (2001). Role of xanthine dehydrogenase and aging on the innate immune response of *Drosophila*. J. Am. Aging Assoc. *24*, 187–193.

Kimmel, A.R., Brasaemle, D.L., McAndrews-Hill, M., Sztalryd, C., and Londos, C. (2010). Adoption of PERILIPIN as a unifying nomenclature for the mammalian PAT-family of intracellular lipid storage droplet proteins. J. Lipid Res. *51*, 468–471.

Kitamura, T., Tanaka, N., Watanabe, J., Uchida, null, Kanegasaki, S., Yamada, Y., and Nakata, K. (1999). Idiopathic pulmonary alveolar proteinosis as an autoimmune disease with neutralizing antibody against granulocyte/macrophage colony-stimulating factor. J. Exp. Med. *190*, 875–880.

Klei, I.J. van der, Hilbrands, R.E., Swaving, G.J., Waterham, H.R., Vrieling, E.G., Titorenko, V.I., Cregg, J.M., Harder, W., and Veenhuis, M. (1995). The Hansenula polymorpha PER3 Gene Is Essential for the Import of PTS1 Proteins into the Peroxisomal Matrix. J. Biol. Chem. *270*, 17229–17236.

Klemm, R.W., Norton, J.P., Cole, R.A., Li, C.S., Park, S.H., Crane, M.M., Li, L., Jin, D., Boye-Doe, A., Liu, T.Y., et al. (2013). A Conserved Role for Atlastin GTPases in Regulating Lipid Droplet Size. Cell Rep. *3*, 1465–1475.

Knoops, K., Manivannan, S., Cepińska, M.N., Krikken, A.M., Kram, A.M., Veenhuis, M., and Klei, I.J. van der (2014). Preperoxisomal vesicles can form in the absence of Pex3. J Cell Biol *204*, 659–668.

Koch, A., Yoon, Y., Bonekamp, N.A., McNiven, M.A., and Schrader, M. (2005). A Role for Fis1 in Both Mitochondrial and Peroxisomal Fission in Mammalian Cells. Mol. Biol. Cell *16*, 5077–5086.

Komatsu, M., Waguri, S., Koike, M., Sou, Y., Ueno, T., Hara, T., Mizushima, N., Iwata, J., Ezaki, J., Murata, S., et al. (2007). Homeostatic Levels of p62 Control Cytoplasmic Inclusion Body Formation in Autophagy-Deficient Mice. Cell *131*, 1149–1163.

Kory, N., Thiam, A.-R., Farese, R.V., and Walther, T.C. (2015). Protein Crowding Is a Determinant of Lipid Droplet Protein Composition. Dev. Cell *34*, 351–363.

Kory, N., Farese, R.V., and Walther, T.C. (2016). Targeting Fat: Mechanisms of Protein Localization to Lipid Droplets. Trends Cell Biol. *26*, 535–546.

Krahmer, N., Guo, Y., Wilfling, F., Hilger, M., Lingrell, S., Heger, K., Newman, H.W., Schmidt-Supprian, M., Vance, D.E., Mann, M., et al. (2011). Phosphatidylcholine Synthesis for Lipid Droplet Expansion Is Mediated by Localized Activation of CTP:Phosphocholine Cytidylyltransferase. Cell Metab. *14*, 504–515.

Kramar, R., Hüttinger, M., Gmeiner, B., and Goldenberg, H. (1978). β-oxidation in peroxisomes of brown adipose tissue. Biochim. Biophys. Acta BBA - Lipids Lipid Metab. *531*, 353–356.

Kuerschner, L., Moessinger, C., and Thiele, C. (2008). Imaging of Lipid Biosynthesis: How a Neutral Lipid Enters Lipid Droplets. Traffic *9*, 338–352.

Kühnlein, R.P. (2011). The contribution of the *Drosophila* model to lipid droplet research. Prog. Lipid Res. *50*, 348–356.

Kühnlein, R.P. (2012). Lipid droplet-based storage fat metabolism in *Drosophila* Thematic Review Series: Lipid Droplet Synthesis and Metabolism: from Yeast to Man. J. Lipid Res. *53*, 1430–1436.

Kulić, I.M., Brown, A.E.X., Kim, H., Kural, C., Blehm, B., Selvin, P.R., Nelson, P.C., and Gelfand, V.I. (2008). The role of microtubule movement in bidirectional organelle transport. Proc. Natl. Acad. Sci. *105*, 10011–10016.

Kural, C., Kim, H., Syed, S., Goshima, G., Gelfand, V.I., and Selvin, P.R. (2005). Kinesin and Dynein Move a Peroxisome in Vivo: A Tug-of-War or Coordinated Movement? Science *308*, 1469–1472.

Langin, D. (2006). Control of fatty acid and glycerol release in adipose tissue lipolysis. C. R. Biol. *329*, 598–607.

Langmead, B., and Salzberg, S.L. (2012). Fast gapped-read alignment with Bowtie 2. Nat. Methods *9*, 357–359.

Lanyon-Hogg, T., Warriner, S.L., and Baker, A. (2010). Getting a camel through the eye of a needle: the import of folded proteins by peroxisomes. Biol. Cell *102*, 245–263.

Lardizabal, K.D., Mai, J.T., Wagner, N.W., Wyrick, A., Voelker, T., and Hawkins, D.J. (2001). DGAT2 Is a New Diacylglycerol Acyltransferase Gene Family. J. Biol. Chem. *276*, 38862–38869.

Lass, A., Zimmermann, R., Haemmerle, G., Riederer, M., Schoiswohl, G., Schweiger, M., Kienesberger, P., Strauss, J.G., Gorkiewicz, G., and Zechner, R. (2006). Adipose triglyceride lipase-mediated lipolysis of cellular fat stores is activated by CGI-58 and defective in Chanarin-Dorfman Syndrome. Cell Metab. *3*, 309–319.

Lass, A., Zimmermann, R., Oberer, M., and Zechner, R. (2011). Lipolysis – A highly regulated multi-enzyme complex mediates the catabolism of cellular fat stores. Prog. Lipid Res. *50*, 14–27.

Lavin, Y., Winter, D., Blecher-Gonen, R., David, E., Keren-Shaul, H., Merad, M., Jung, S., and Amit, I. (2014). Tissue-Resident Macrophage Enhancer Landscapes Are Shaped by the Local Microenvironment. Cell *159*, 1312–1326.

Law, K.B., Bronte-Tinkew, D., Di Pietro, E., Snowden, A., Jones, R.O., Moser, A., Brumell, J.H., Braverman, N., and Kim, P.K. (2017). The peroxisomal AAA ATPase complex prevents pexophagy and development of peroxisome biogenesis disorders. Autophagy *13*, 868–884.

Lazarow, P.B. (1978). Rat liver peroxisomes catalyze the beta oxidation of fatty acids. J. Biol. Chem. *253*, 1522–1528.

Lazarow, P.B. (2006). Chapter 3.1.7. The import receptor Pex7p and the PTS2 targeting sequence. Biochim. Biophys. Acta BBA - Mol. Cell Res. *1763*, 1599–1604.

Lazarow, P.B., and Fujiki, Y. (1985). Biogenesis of Peroxisomes. Annu. Rev. Cell Biol. *1*, 489–530.

Lee, H., Peng, Y., and Guo, Y. (2013). Chapter 4 - Analysis of Lipid Droplet Dynamics and Functions in *Drosophila melanogaster*. In Methods in Cell Biology, H. Yang, and P. Li, eds. (Academic Press), pp. 53–69.

Lin, T.-Y., Pringle, M.J., and Fuller, M.T. (2000). Regulation of Meiosis and Spermatid Differentiation in *Drosophila* Primary Spermatocytes. In The Testis, (Springer, New York, NY), pp. 120–132.

Lodhi, I.J., and Semenkovich, C.F. (2014). Peroxisomes: A Nexus for Lipid Metabolism and Cellular Signaling. Cell Metab. *19*, 380–392.

Longo, I., Frints, S.G.M., Fryns, J.-P., Meloni, I., Pescucci, C., Ariani, F., Borghgraef, M., Raynaud, M., Marynen, P., Schwartz, C., et al. (2003). A third MRX family (MRX68) is the result of mutation in the long chain fatty acid-CoA ligase 4 (FACL4) gene: proposal of a rapid enzymatic assay for screening mentally retarded patients. J. Med. Genet. *40*, 11–17.

Love, M.I., Huber, W., and Anders, S. (2014). Moderated estimation of fold change and dispersion for RNA-seq data with DESeq2. Genome Biol. *15*, 550.

Luong, N., Davies, C.R., Wessells, R.J., Graham, S.M., King, M.T., Veech, R., Bodmer, R., and Oldham, S.M. (2006). Activated FOXO-mediated insulin resistance is blocked by reduction of TOR activity. Cell Metab. *4*, 133–142.

Ma, C., Hagstrom, D., Polley, S.G., and Subramani, S. (2013). Redox-regulated Cargo Binding and Release by the Peroxisomal Targeting Signal Receptor, Pex5. J. Biol. Chem. *288*, 27220–27231.

Magraoui, F.E., Bäumer, B.E., Platta, H.W., S. Baumann, J., Girzalsky, W., and Erdmann, R. (2012). The RING-type ubiquitin ligases Pex2p, Pex10p and Pex12p form a heteromeric complex that displays enhanced activity in an ubiquitin conjugating enzyme-selective manner. FEBS J. *279*, 2060–2070.

Malheiro, A.R., Silva, T.F. da, and Brites, P. (2015). Plasmalogens and fatty alcohols in rhizomelic chondrodysplasia punctata and Sjögren-Larsson syndrome. J. Inherit. Metab. Dis. *38*, 111–121.

Manders, E.M.M., Verbeek, F.J., and Aten, J.A. (1993). Measurement of co-localization of objects in dual-colour confocal images. J. Microsc. *169*, 375–382.

Marshall, P.A., Krimkevich, Y.I., Lark, R.H., Dyer, J.M., Veenhuis, M., and Goodman, J.M. (1995). Pmp27 promotes peroxisomal proliferation. J. Cell Biol. *129*, 345–355.

Martens, K., Bottelbergs, A., Peeters, A., Jacobs, F., Espeel, M., Carmeliet, P., Van Veldhoven, P.P., and Baes, M. (2012). Peroxisome deficient aP2-Pex5 knockout mice display impaired white adipocyte and muscle function concomitant with reduced adrenergic tone. Mol. Genet. Metab. *107*, 735–747.

Marzioch, M., Erdmann, R., Veenhuis, M., and Kunau, W.H. (1994). PAS7 encodes a novel yeast member of the WD-40 protein family essential for import of 3-oxoacyl-CoA thiolase, a PTS2-containing protein, into peroxisomes. EMBO J. *13*, 4908–4918.

Mast, F.D., Li, J., Virk, M.K., Hughes, S.C., Simmonds, A.J., and Rachubinski, R.A. (2011). A *Drosophila* model for the Zellweger spectrum of peroxisome biogenesis disorders. Dis. Model. Mech. *4*, 659–672.

Mast, F.D., Jamakhandi, A., Saleem, R.A., Dilworth, D.J., Rogers, R.S., Rachubinski, R.A., and Aitchison, J.D. (2016). Peroxins Pex30 and Pex29 Dynamically Associate with Reticulons to Regulate Peroxisome Biogenesis from the Endoplasmic Reticulum. J. Biol. Chem. *291*, 15408–15427.

Matsumoto, N., Tamura, S., and Fujiki, Y. (2003). The pathogenic peroxin Pex26p recruits the Pex1p–Pex6p AAA ATPase complexes to peroxisomes. Nat. Cell Biol. *5*, 454–460.

Matsuzaki, T., and Fujiki, Y. (2008). The peroxisomal membrane protein import receptor Pex3p is directly transported to peroxisomes by a novel Pex19p- and Pex16p-dependent pathway. J Cell Biol *183*, 1275–1286.

Maxfield, F.R., and Tabas, I. (2005). Role of cholesterol and lipid organization in disease. Nature *438*, 612–621.

Mayerhofer, P.U. (2016). Targeting and insertion of peroxisomal membrane proteins: ER trafficking versus direct delivery to peroxisomes. Biochim. Biophys. Acta BBA - Mol. Cell Res. *1863*, 870–880.

McGettigan, B.M., McMahan, R.H., and Rosen, H.R. (2017). The transcriptional response of Kupffer Cells to fat and cholesterol is non-canonical and distinct from bone-marrow derived macrophages. J. Immunol. *198*, 197.15-197.15.

McNew, J.A., and Goodman, J.M. (1994). An oligomeric protein is imported into peroxisomes in vivo. J. Cell Biol. *127*, 1245–1257.

Mehtälä, M.L., Haataja, T.J.K., Blanchet, C.E., Hiltunen, J.K., Svergun, D.I., and Glumoff, T. (2013). Quaternary structure of human, *Drosophila melanogaster* and *Caenorhabditis elegans* MFE-2 in solution from synchrotron small-angle X-ray scattering. FEBS Lett. *587*, 305–310.

Mercade, A., Sanchez, A., and Folch, J.M. (2005). Assignment of the acyl-CoA synthetase long-chain family member 4 (ACSL4) gene to porcine chromosome X. Anim. Genet. *36*, 76–76.

Miceli, R.M., DeGraaf, M.E., and Fischer, H.D. (1994). Two-stage selection of sequences from a random phage display library delineates both core residues and permitted structural range within an epitope. J. Immunol. Methods *167*, 279–287.

Miyata, N., and Fujiki, Y. (2005). Shuttling Mechanism of Peroxisome Targeting Signal Type 1 Receptor Pex5: ATP-Independent Import and ATP-Dependent Export. Mol. Cell. Biol. *25*, 10822–10832.

Morita, M., and Imanaka, T. (2012). Peroxisomal ABC transporters: Structure, function and role in disease. Biochim. Biophys. Acta BBA - Mol. Basis Dis. *1822*, 1387–1396.

Motley, A.M., and Hettema, E.H. (2007). Yeast peroxisomes multiply by growth and division. J. Cell Biol. *178*, 399–410.

Motley, A.M., Hettema, E.H., Ketting, R., Plasterk, R., and Tabak, H.F. (2000). *Caenorhabditis elegans* has a single pathway to target matrix proteins to peroxisomes. EMBO Rep. *1*, 40–46.

Musselman, L.P., and Kühnlein, R.P. (2018). *Drosophila* as a model to study obesity and metabolic disease. J. Exp. Biol. *221*, jeb163881.

Myllymäki, H., Valanne, S., and Rämet, M. (2014). The *Drosophila* Imd Signaling Pathway. J. Immunol. *192*, 3455–3462.

Nakayama, M., Sato, H., Okuda, T., Fujisawa, N., Kono, N., Arai, H., Suzuki, E., Umeda, M., Ishikawa, H.O., and Matsuno, K. (2011). *Drosophila* Carrying Pex3 or Pex16 Mutations Are Models of Zellweger Syndrome That Reflect Its Symptoms Associated with the Absence of Peroxisomes. PLOS ONE *6*, e22984.

Namgaladze, D., and Brüne, B. (2016). Macrophage fatty acid oxidation and its roles in macrophage polarization and fatty acid-induced inflammation. Biochim. Biophys. Acta BBA - Mol. Cell Biol. Lipids *1861*, 1796–1807.

Neuhaus, A., Kooshapur, H., Wolf, J., Meyer, N.H., Madl, T., Saidowsky, J., Hambruch, E., Lazam, A., Jung, M., Sattler, M., et al. (2014). A Novel Pex14 Protein-interacting Site of Human Pex5 Is Critical for Matrix Protein Import into Peroxisomes. J. Biol. Chem. *289*, 437–448.

Notari, L., Baladron, V., Aroca-Aguilar, J.D., Balko, N., Heredia, R., Meyer, C., Notario, P.M., Saravanamuthu, S., Nueda, M.-L., Sanchez-Sanchez, F., et al. (2006). Identification of a Lipase-linked Cell Membrane Receptor for Pigment Epithelium-derived Factor. J. Biol. Chem. *281*, 38022–38037.

Oba, Y., Ojika, M., and Inouye, S. (2004). Characterization of CG6178 gene product with high sequence similarity to firefly luciferase in *Drosophila melanogaster*. Gene *329*, 137–145.

Oelkers, P., Behari, A., Cromley, D., Billheimer, J.T., and Sturley, S.L. (1998). Characterization of Two Human Genes Encoding Acyl Coenzyme A:Cholesterol Acyltransferase-related Enzymes. J. Biol. Chem. *273*, 26765–26771.

Opaliński, Ł., Kiel, J.A.K.W., Williams, C., Veenhuis, M., and van der Klei, I.J. (2011). Membrane curvature during peroxisome fission requires Pex11. EMBO J. *30*, 5–16.

O'Sullivan, N.C., Jahn, T.R., Reid, E., and O'Kane, C.J. (2012). Reticulon-like-1, the *Drosophila* orthologue of the Hereditary Spastic Paraplegia gene reticulon 2, is required

for organization of endoplasmic reticulum and of distal motor axons. Hum. Mol. Genet. *21*, 3356–3365.

Osumi, T., Tsukamoto, T., Hata, S., Yokota, S., Miura, S., Fujiki, Y., Hijikata, M., Miyazawa, S., and Hashimoto, T. (1991). Amino-terminal presequence of the precursor of peroxisomal 3-ketoacyl-CoA thiolase is a cleavable signal peptide for peroxisomal targeting. Biochem. Biophys. Res. Commun. *181*, 947–954.

Otera, H., Harano, T., Honsho, M., Ghaedi, K., Mukai, S., Tanaka, A., Kawai, A., Shimizu, N., and Fujiki, Y. (2000). The Mammalian Peroxin Pex5pL, the Longer Isoform of the Mobile Peroxisome Targeting Signal (PTS) Type 1 Transporter, Translocates the Pex7p·PTS2 Protein Complex into Peroxisomes via Its Initial Docking Site, Pex14p. J. Biol. Chem. *275*, 21703–21714.

Pandey, U.B., and Nichols, C.D. (2011). Human Disease Models in *Drosophila melanogaster* and the Role of the Fly in Therapeutic Drug Discovery. Pharmacol. Rev. *63*, 411–436.

Park, S., Gidda, S.K., James, C.N., Horn, P.J., Khuu, N., Seay, D.C., Keereetaweep, J., Chapman, K.D., Mullen, R.T., and Dyer, J.M. (2013). The α/β Hydrolase CGI-58 and Peroxisomal Transport Protein PXA1 Coregulate Lipid Homeostasis and Signaling in Arabidopsis. Plant Cell *25*, 1726–1739.

Pertea, M., Kim, D., Pertea, G.M., Leek, J.T., and Salzberg, S.L. (2016). Transcript-level expression analysis of RNA-seq experiments with HISAT, StringTie and Ballgown. Nat. Protoc. *11*, 1650–1667.

Pinto, M.P., Grou, C.P., Alencastre, I.S., Oliveira, M.E., Sá-Miranda, C., Fransen, M., and Azevedo, J.E. (2006). The Import Competence of a Peroxisomal Membrane Protein Is Determined by Pex19p before the Docking Step. J. Biol. Chem. *281*, 34492–34502.

Pinto, M.P., Grou, C.P., Fransen, M., Sá-Miranda, C., and Azevedo, J.E. (2009). The cytosolic domain of PEX3, a protein involved in the biogenesis of peroxisomes, binds membrane lipids. Biochim. Biophys. Acta BBA - Mol. Cell Res. *1793*, 1669–1675.

Piper, M.D.W., Blanc, E., Leitão-Gonçalves, R., Yang, M., He, X., Linford, N.J., Hoddinott, M.P., Hopfen, C., Soultoukis, G.A., Niemeyer, C., et al. (2014). A holidic medium for *Drosophila melanogaster*. Nat. Methods *11*, 100–105.

Platta, H.W., Magraoui, F.E., Bäumer, B.E., Schlee, D., Girzalsky, W., and Erdmann, R. (2009). Pex2 and Pex12 Function as Protein-Ubiquitin Ligases in Peroxisomal Protein Import. Mol. Cell. Biol. *29*, 5505–5516.

Pu, J., Ha, C.W., Zhang, S., Jung, J.P., Huh, W.-K., and Liu, P. (2011). Interactomic study on interaction between lipid droplets and mitochondria. Protein Cell *2*, 487–496.

Purdue, P., and Lazarow, P.B. (1996). Targeting of human catalase to peroxisomes is dependent upon a novel COOH-terminal peroxisomal targeting sequence. J. Cell Biol. *134*, 849–862.

Purdue, P.E., Yang, X., and Lazarow, P.B. (1998). Pex18p and Pex21p, a Novel Pair of Related Peroxins Essential for Peroxisomal Targeting by the PTS2 Pathway. J Cell Biol *143*, 1859–1869.

Quiroga, A.D., and Lehner, R. (2018). Pharmacological intervention of liver triacylglycerol lipolysis: The good, the bad and the ugly. Biochem. Pharmacol. *155*, 233–241.

Radyuk, S.N., Klichko, V.I., Spinola, B., Sohal, R.S., and Orr, W.C. (2001). The peroxiredoxin gene family in *Drosophila melanogaster.* Free Radic. Biol. Med. *31*, 1090–1100.

Reaume, A.G., Knecht, D.A., and Chovnick, A. (1991). The rosy locus in *Drosophila melanogaster*: xanthine dehydrogenase and eye pigments. Genetics *129*, 1099–1109.

Reguenga, C., Oliveira, M.E.M., Gouveia, A.M.M., Sá-Miranda, C., and Azevedo, J.E. (2001). Characterization of the Mammalian Peroxisomal Import Machinery. J. Biol. Chem. *276*, 29935–29942.

Reis, T., Gilst, M.R.V., and Hariharan, I.K. (2010). A Buoyancy-Based Screen of *Drosophila* Larvae for Fat-Storage Mutants Reveals a Role for Sir2 in Coupling Fat Storage to Nutrient Availability. PLOS Genet. *6*, e1001206.

Remmerie, A., and Scott, C.L. (2018). Macrophages and lipid metabolism. Cell. Immunol. *330*, 27–42.

Rhodin, J. (1954). Correlation of ultrastructural organization and function in normal and experimentally changed proximal convoluted tubule cells of the mouse kidney: and electron microscopic study. Karolinska Institutet.

del Río, L.A. (2011). Peroxisomes as a cellular source of reactive nitrogen species signal molecules. Arch. Biochem. Biophys. *506*, 1–11.

del Río, L.A., Sandalio, L.M., Corpas, F.J., Palma, J.M., and Barroso, J.B. (2006). Reactive Oxygen Species and Reactive Nitrogen Species in Peroxisomes. Production, Scavenging, and Role in Cell Signaling. Plant Physiol. *141*, 330–335.

Robinson, M.D., McCarthy, D.J., and Smyth, G.K. (2010). edgeR: a Bioconductor package for differential expression analysis of digital gene expression data. Bioinformatics *26*, 139–140.

Rodríguez, A. del V., Didiano, D., and Desplan, C. (2012). Power tools for gene expression and clonal analysis in *Drosophila*. Nat. Methods *9*, 47–55.

Rohrer, J., Schweizer, A., Russell, D., and Kornfeld, S. (1996). The targeting of Lamp1 to lysosomes is dependent on the spacing of its cytoplasmic tail tyrosine sorting motif relative to the membrane. J. Cell Biol. *132*, 565–576.

Rottensteiner, H., Kramer, A., Lorenzen, S., Stein, K., Landgraf, C., Volkmer-Engert, R., and Erdmann, R. (2004). Peroxisomal Membrane Proteins Contain Common Pex19p-

binding Sites that Are an Integral Part of Their Targeting Signals. Mol. Biol. Cell *15*, 3406–3417.

Rowe, E.R., Mimmack, M.L., Barbosa, A.D., Haider, A., Isaac, I., Ouberai, M.M., Thiam, A.R., Patel, S., Saudek, V., Siniossoglou, S., et al. (2016). Conserved Amphipathic Helices Mediate Lipid Droplet Targeting of Perilipins 1–3. J. Biol. Chem. *291*, 6664–6678.

Roy, S., Kharchenko, P.V., Kheradpour, P., Negre, N., Eaton, M.L., Landolin, J.M., Bristow, C.A., Ma, L., Lin, M.F., Washietl, S., et al. (2010). Identification of Functional Elements and Regulatory Circuits by *Drosophila* modENCODE. Science *330*, 1787–1797.

Rudd, E.A., and Brockman, H.L. (1984). Pancreatic carboxyl ester lipase (cholesterol esterase). Lipases.

Sacksteder, K.A., Jones, J.M., South, S.T., Li, X., Liu, Y., and Gould, S.J. (2000). Pex19 Binds Multiple Peroxisomal Membrane Proteins, Is Predominantly Cytoplasmic, and Is Required for Peroxisome Membrane Synthesis. J. Cell Biol. *148*, 931–944.

Santel, A., Winhauer, T., Blümer, N., and Renkawitz-Pohl, R. (1997). The *Drosophila* don juan (dj) gene encodes a novel sperm specific protein component characterized by an unusual domain of a repetitive amino acid motif. Mech. Dev. *64*, 19–30.

Sargent, G., van Zutphen, T., Shatseva, T., Zhang, L., Di Giovanni, V., Bandsma, R., and Kim, P.K. (2016). PEX2 is the E3 ubiquitin ligase required for pexophagy during starvation. J. Cell Biol. *214*, 677–690.

Sattarzadeh, A., Saberianfar, R., Zipfel, W.R., Menassa, R., and Hanson, M.R. (2015). Green to red photoconversion of GFP for protein tracking *in vivo*. Sci. Rep. *5*, 11771.

Sauro, V.S., Klamut, H.J., Lin, C.H., and Strickland, K.P. (1985). Lysosomal triacylglycerol lipase activity in L6 myoblasts and its changes on differentiation. Biochem. J. *227*, 583–589.

Schneider, I. (1972). Cell lines derived from late embryonic stages of *Drosophila melanogaster*. Development *27*, 353–365.

Schneider, M.D., Najand, N., Chaker, S., Pare, J.M., Haskins, J., Hughes, S.C., Hobman, T.C., Locke, J., and Simmonds, A.J. (2006). Gawky is a component of cytoplasmic mRNA processing bodies required for early *Drosophila* development. J. Cell Biol. *174*, 349–358.

Schrader, M. (2001). Tubulo-Reticular Clusters of Peroxisomes in Living COS-7 Cells: Dynamic Behavior and Association with Lipid Droplets1. J. Histochem. Cytochem. *49*, 1421–1429.

Scott, C.L., Zheng, F., De Baetselier, P., Martens, L., Saeys, Y., De Prijck, S., Lippens, S., Abels, C., Schoonooghe, S., Raes, G., et al. (2016). Bone marrow-derived monocytes give rise to self-renewing and fully differentiated Kupffer cells. Nat. Commun. *7*, 10321.

Seelig, J. (2004). Thermodynamics of lipid–peptide interactions. Biochim. Biophys. Acta BBA - Biomembr. *1666*, 40–50.

Shah, P.L., Hansell, D., Lawson, P.R., Reid, K.B.M., and Morgan, C. (2000). Pulmonary alveolar proteinosis: clinical aspects and current concepts on pathogenesis. Thorax *55*, 67–77.

Smith, J.J., and Aitchison, J.D. (2013). Peroxisomes take shape. Nat. Rev. Mol. Cell Biol. *14*, 803–817.

Smith, J.J., Brown, T.W., Eitzen, G.A., and Rachubinski, R.A. (2000). Regulation of Peroxisome Size and Number by Fatty Acid β-Oxidation in the Yeast *Yarrowia lipolytica*. J. Biol. Chem. *275*, 20168–20178.

Smith, J.J., Marelli, M., Christmas, R.H., Vizeacoumar, F.J., Dilworth, D.J., Ideker, T., Galitski, T., Dimitrov, K., Rachubinski, R.A., and Aitchison, J.D. (2002). Transcriptome profiling to identify genes involved in peroxisome assembly and function. J Cell Biol *158*, 259–271.

Soni, K.G., Mardones, G.A., Sougrat, R., Smirnova, E., Jackson, C.L., and Bonifacino, J.S. (2009). Coatomer-dependent protein delivery to lipid droplets. J. Cell Sci. *122*, 1834–1841.

Southall, T.D., Terhzaz, S., Cabrero, P., Chintapalli, V.R., Evans, J.M., Dow, J.A.T., and Davies, S.-A. (2006). Novel subcellular locations and functions for secretory pathway Ca2+/Mn2+-ATPases. Physiol. Genomics *26*, 35–45.

St Jules, R., Beard, M., and Holtzman, E. (1989). Cytochemical localization of a D-amino acid oxidizing enzyme in peroxisomes of *Drosophila melanogaster*. Tissue Cell *21*, 661–671.

St Jules, R., Setlik, W., Kennard, J., and Holtzman, E. (1990). Peroxisomes in the head of *Drosophila melanogaster*. Exp. Eye Res. *51*, 607–617.

St Jules, R., Kennard, J., Setlik, W., and Holtzman, E. (1991). Peroxisomal oxidation of thiazolidine carboxylates in firefly fat body, frog retina, and rat liver and kidney.

Steinberg, S.J., Dodt, G., Raymond, G.V., Braverman, N.E., Moser, A.B., and Moser, H.W. (2006). Peroxisome biogenesis disorders. Biochim. Biophys. Acta BBA - Mol. Cell Res. *1763*, 1733–1748.

Stojanovski, D., Koutsopoulos, O.S., Okamoto, K., and Ryan, M.T. (2004). Levels of human Fis1 at the mitochondrial outer membrane regulate mitochondrial morphology. J Cell Sci *117*, 1201–1210.

Stone, S.J., Levin, M.C., Zhou, P., Han, J., Walther, T.C., and Farese, R.V. (2009). The Endoplasmic Reticulum Enzyme DGAT2 Is Found in Mitochondria-associated Membranes and Has a Mitochondrial Targeting Signal That Promotes Its Association with Mitochondria. J. Biol. Chem. *284*, 5352–5361.

Su, X., and Abumrad, N.A. (2009). Cellular Fatty Acid Uptake: A Pathway Under Construction. Trends Endocrinol. Metab. TEM *20*, 72–77.

Subramani, S. (1998). Components Involved in Peroxisome Import, Biogenesis, Proliferation, Turnover, and Movement. Physiol. Rev. *78*, 171–188.

Sugiura, A., Mattie, S., Prudent, J., and McBride, H.M. (2017). Newly born peroxisomes are a hybrid of mitochondrial and ER-derived pre-peroxisomes. Nature *542*, 251–254.

Sui, X., Arlt, H., Brock, K.P., Lai, Z.W., DiMaio, F., Marks, D.S., Liao, M., Farese, R.V., and Walther, T.C. (2018). Cryo–electron microscopy structure of the lipid droplet–formation protein seipin. J Cell Biol jcb.201809067.

Suzuki, T., Sakagami, T., Rubin, B.K., Nogee, L.M., Wood, R.E., Zimmerman, S.L., Smolarek, T., Dishop, M.K., Wert, S.E., Whitsett, J.A., et al. (2008). Familial pulmonary alveolar proteinosis caused by mutations in CSF2RA. J. Exp. Med. *205*, 2703–2710.

Swinkels, B.W., Gould, S.J., Bodnar, A.G., Rachubinski, R.A., and Subramani, S. (1991). A novel, cleavable peroxisomal targeting signal at the amino-terminus of the rat 3-ketoacyl-CoA thiolase. EMBO J. *10*, 3255–3262.

Szilard, R.K., Titorenko, V.I., Veenhuis, M., and Rachubinski, R.A. (1995). Pay32p of the yeast *Yarrowia lipolytica* is an intraperoxisomal component of the matrix protein translocation machinery. J. Cell Biol. *131*, 1453–1469.

Szymanski, K.M., Binns, D., Bartz, R., Grishin, N.V., Li, W.-P., Agarwal, A.K., Garg, A., Anderson, R.G.W., and Goodman, J.M. (2007). The lipodystrophy protein seipin is found at endoplasmic reticulum lipid droplet junctions and is important for droplet morphology. Proc. Natl. Acad. Sci. *104*, 20890–20895.

Tan, D.J.L., Dvinge, H., Christoforou, A., Bertone, P., Martinez Arias, A., and Lilley, K.S. (2009). Mapping Organelle Proteins and Protein Complexes in *Drosophila melanogaster*. J. Proteome Res. *8*, 2667–2678.

Tan, R., Wang, W., Wang, S., Wang, Z., Sun, L., He, W., Fan, R., Zhou, Y., Xu, X., Hong, W., et al. (2013). Small GTPase Rab40c Associates with Lipid Droplets and Modulates the Biogenesis of Lipid Droplets. PLoS ONE *8*.

Teixeira, L., Rabouille, C., Rørth, P., Ephrussi, A., and Vanzo, N.F. (2003). *Drosophila* Perilipin/ADRP homologue Lsd2 regulates lipid metabolism. Mech. Dev. *120*, 1071–1081.

Thazar-Poulot, N., Miquel, M., Fobis-Loisy, I., and Gaude, T. (2015). Peroxisome extensions deliver the Arabidopsis SDP1 lipase to oil bodies. Proc. Natl. Acad. Sci. *112*, 4158–4163.

Theiss, C., Neuhaus, A., Schliebs, W., and Erdmann, R. (2012). TubStain: a universal peptide-tool to label microtubules. Histochem. Cell Biol. *138*, 531–540.

Thiam, A.R., and Beller, M. (2017). The why, when and how of lipid droplet diversity. J Cell Sci *130*, 315–324.

Thiam, A.R., and Forêt, L. (2016). The physics of lipid droplet nucleation, growth and budding. Biochim. Biophys. Acta BBA - Mol. Cell Biol. Lipids *1861*, 715–722.

Thoms, S. (2015). Import of proteins into peroxisomes: piggybacking to a new home away from home. Open Biol. *5*.

Tian, Y., Bi, J., Shui, G., Liu, Z., Xiang, Y., Liu, Y., Wenk, M.R., Yang, H., and Huang, X. (2011). Tissue-Autonomous Function of Drosophila Seipin in Preventing Ectopic Lipid Droplet Formation. PLOS Genet. *7*, e1001364.

Titorenko, V.I., Chan, H., and Rachubinski, R.A. (2000). Fusion of Small Peroxisomal Vesicles in Vitro Reconstructs an Early Step in the in Vivo Multistep Peroxisome Assembly Pathway of Yarrowia lipolytica. J Cell Biol *148*, 29–44.

Ugrankar, R., Liu, Y., Provaznik, J., Schmitt, S., and Lehmann, M. (2011). Lipin Is a Central Regulator of Adipose Tissue Development and Function in *Drosophila melanogaster*. Mol. Cell. Biol. *31*, 1646–1656.

Ulvila, J., Parikka, M., Kleino, A., Sormunen, R., Ezekowitz, R.A., Kocks, C., and Rämet, M. (2006). Double-stranded RNA Is Internalized by Scavenger Receptor-mediated Endocytosis in *Drosophila* S2 Cells. J. Biol. Chem. *281*, 14370–14375.

Underhill, D.M., and Ozinsky, A. (2002). Phagocytosis of Microbes: Complexity in Action. Annu. Rev. Immunol. *20*, 825–852.

Uziel, G., Ghezzi, D., and Zeviani, M. (2011). Infantile mitochondrial encephalopathy. Semin. Fetal. Neonatal Med. *16*, 205–215.

Valente, V., Maia, R.M., Vianna, M.C.B., and Paçó-Larson, M.L. (2010). *Drosophila melanogaster* lipins are tissue-regulated and developmentally regulated and present specific subcellular distributions. FEBS J. *277*, 4775–4788.

Van der Leij, I., Franse, M.M., Elgersma, Y., Distel, B., and Tabak, H.F. (1993). PAS10 is a tetratricopeptide-repeat protein that is essential for the import of most matrix proteins into peroxisomes of *Saccharomyces cerevisiae*. Proc. Natl. Acad. Sci. *90*, 11782–11786.

Van Veldhoven, P.P., and Baes, M. (2013). Peroxisome deficient invertebrate and vertebrate animal models. Front. Physiol. *4*.

van der Zand, A., Gent, J., Braakman, I., and Tabak, H.F. (2012). Biochemically Distinct Vesicles from the Endoplasmic Reticulum Fuse to Form Peroxisomes. Cell *149*, 397–409.

de Vet, E.C.J.M., IJlst, L., Oostheim, W., Wanders, R.J.A., and van den Bosch, H. (1998). Alkyl-Dihydroxyacetonephosphate Synthase. J. Biol. Chem. *273*, 10296–10301.

Villanueva, C.J., Monetti, M., Shih, M., Zhou, P., Watkins, S.M., Bhanot, S., and Farese, R.V. (2009). Specific role for acyl CoA:Diacylglycerol acyltransferase 1 (Dgat1) in hepatic steatosis due to exogenous fatty acids. Hepatology *50*, 434–442.

Voeltz, G.K., Prinz, W.A., Shibata, Y., Rist, J.M., and Rapoport, T.A. (2006). A Class of Membrane Proteins Shaping the Tubular Endoplasmic Reticulum. Cell *124*, 573–586.

Walther, T.C., Chung, J., and Farese, R.V. (2017). Lipid Droplet Biogenesis. Annu. Rev. Cell Dev. Biol. *33*, 491–510.

Walton, P.A., Hill, P.E., and Subramani, S. (1995). Import of stably folded proteins into peroxisomes. Mol. Biol. Cell *6*, 675–683.

Wanders, R.J.A., and Romeijn, G.J. (1998). Cholesterol biosynthesis, peroxisomes and peroxisomal disorders: Mevalonate kinase is not only deficient in Zellweger syndrome but also in rhizomelic chondrodysplasia punctata. J. Inher. Metab. Dis. *21*, 309–312.

Wang, C.-W., and Lee, S.-C. (2012). The ubiquitin-like (UBX)-domain-containing protein Ubx2/Ubxd8 regulates lipid droplet homeostasis. J Cell Sci *125*, 2930–2939.

Wang, H., Becuwe, M., Housden, B.E., Chitraju, C., Porras, A.J., Graham, M.M., Liu, X.N., Thiam, A.R., Savage, D.B., Agarwal, A.K., et al. (2016). Seipin is required for converting nascent to mature lipid droplets. ELife *5*.

Wang, J., Lin, Y., and Wang, P.C. and H. (2010). Effects of Vector Fusion Peptides on the Conformation and Immune Reactivity of Epitope-Shuffled, Recombinant Multi-Epitope Antigens.

Wang, W., Wei, S., Li, L., Su, X., Du, C., Li, F., Geng, B., Liu, P., and Xu, G. (2015). Proteomic analysis of murine testes lipid droplets. Sci. Rep. *5*, 12070.

Wangler, M.F., Yamamoto, S., and Bellen, H.J. (2015). Fruit Flies in Biomedical Research. Genetics *199*, 639–653.

Wangler, M.F., Chao, Y.-H., Bayat, V., Giagtzoglou, N., Shinde, A.B., Putluri, N., Coarfa, C., Donti, T., Graham, B.H., Faust, J.E., et al. (2017). Peroxisomal biogenesis is genetically and biochemically linked to carbohydrate metabolism in *Drosophila* and mouse. PLOS Genet. *13*, e1006825.

Watkins, P.A., Maiguel, D., Jia, Z., and Pevsner, J. (2007). Evidence for 26 distinct acyl-coenzyme A synthetase genes in the human genome. J. Lipid Res. *48*, 2736–2750.

Weinhofer, I., Kunze, M., Forss-Petter, S., and Berger, J. (2013). Involvement of Human Peroxisomes in Biosynthesis and Signaling of Steroid and Peptide Hormones. In Peroxisomes and Their Key Role in Cellular Signaling and Metabolism, (Springer, Dordrecht), pp. 101–110.

Weiss, S.B., and Kennedy, E.P. (1956). The Enzymatic Synthesis of Triglycerides. J. Am. Chem. Soc. *78*, 3550–3550.

Wessel, D., and Flügge, U.I. (1984). A method for the quantitative recovery of protein in dilute solution in the presence of detergents and lipids. Anal. Biochem. *138*, 141–143.

Wiemer, E.A.C., Wenzel, T., Deerinck, T.J., Ellisman, M.H., and Subramani, S. (1997). Visualization of the Peroxisomal Compartment in Living Mammalian Cells: Dynamic Behavior and Association with Microtubules. J. Cell Biol. *136*, 71–80.

Wilfling, F., Wang, H., Haas, J.T., Krahmer, N., Gould, T.J., Uchida, A., Cheng, J.-X., Graham, M., Christiano, R., Fröhlich, F., et al. (2013). Triacylglycerol Synthesis Enzymes Mediate Lipid Droplet Growth by Relocalizing from the ER to Lipid Droplets. Dev. Cell *24*, 384–399.

Wilfling, F., Thiam, A.R., Olarte, M.-J., Wang, J., Beck, R., Gould, T.J., Allgeyer, E.S., Pincet, F., Bewersdorf, J., Jr, R.V.F., et al. (2014). Arf1/COPI machinery acts directly on lipid droplets and enables their connection to the ER for protein targeting.

Williams, C., Opalinski, L., Landgraf, C., Costello, J., Schrader, M., Krikken, A.M., Knoops, K., Kram, A.M., Volkmer, R., and Klei, I.J. van der (2015). The membrane remodeling protein Pex11p activates the GTPase Dnm1p during peroxisomal fission. Proc. Natl. Acad. Sci. *112*, 6377–6382.

Winberg, M.E., Khalaj Motlagh, M., Stenkula, K.G., Holm, C., and Jones, H.A. (2014). Adiponutrin: A multimeric plasma protein. Biochem. Biophys. Res. Commun. *446*, 1114–1119.

Wolins, N.E., Brasaemle, D.L., and Bickel, P.E. (2006). A proposed model of fat packaging by exchangeable lipid droplet proteins. FEBS Lett. *580*, 5484–5491.

Wu, J.S., and Luo, L. (2006). A protocol for mosaic analysis with a repressible cell marker (MARCM) in *Drosophila*. Nat. Protoc. *1*, 2583–2589.

Wu, L.-F., Chanal, A., and Rodrigue, A. (2000). Membrane targeting and translocation of bacterial hydrogenases. Arch. Microbiol. *173*, 319–324.

Wynant, N., Santos, D., and Vanden Broeck, J. (2014). Chapter Five - Biological Mechanisms Determining the Success of RNA Interference in Insects. In International Review of Cell and Molecular Biology, K.W. Jeon, ed. (Academic Press), pp. 139–167.

Xia, J., and Wishart, D.S. (2011). Metabolomic Data Processing, Analysis, and Interpretation Using MetaboAnalyst. Curr. Protoc. Bioinforma. *34*, 14.10.1-14.10.48.

Xiang, R., Fan, L.-L., Huang, H., Chen, Y., He, W., Guo, S., Li, J.-J., Jin, J., Du, R., Yan, R., et al. (2018). Increased RTN3 Leads to Obesity and Hypertriglyceridemia by Interacting with HSPA5. Circulation.117.030718.

Yamaguchi, T., Omatsu, N., Matsushita, S., and Osumi, T. (2004). CGI-58 Interacts with Perilipin and Is Localized to Lipid Droplets. J. Biol. Chem. *279*, 30490–30497.

Yamaguchi, T., Omatsu, N., Morimoto, E., Nakashima, H., Ueno, K., Tanaka, T., Satouchi, K., Hirose, F., and Osumi, T. (2007). CGI-58 facilitates lipolysis on lipid droplets but is not involved in the vesiculation of lipid droplets caused by hormonal stimulation. J. Lipid Res. *48*, 1078–1089.

Yanagawa, S., Lee, J.-S., and Ishimoto, A. (1998). Identification and Characterization of a Novel Line of *Drosophila* Schneider S2 Cells That Respond to Wingless Signaling. J. Biol. Chem. *273*, 32353–32359.

Yang, Y.S., and Strittmatter, S.M. (2007). The reticulons: a family of proteins with diverse functions. Genome Biol. *8*, 234.

Yang, X., Edward Purdue, P., and Lazarow, P.B. (2001). Eci1p uses a PTS1 to enter peroxisomes: either its own or that of a partner, Dci1p. Eur. J. Cell Biol. *80*, 126–138.

Yang, X., Lu, X., Lombès, M., Rha, G.B., Chi, Y.-I., Guerin, T.M., Smart, E.J., and Liu, J. (2010). The G0/G1 Switch Gene 2 Regulates Adipose Lipolysis through Association with Adipose Triglyceride Lipase. Cell Metab. *11*, 194–205.

Yen, C.-L.E., and Farese, R.V. (2003). MGAT2, a Monoacylglycerol Acyltransferase Expressed in the Small Intestine.

Yen, C.-L.E., Monetti, M., Burri, B.J., and Farese, R.V. (2005). The triacylglycerol synthesis enzyme DGAT1 also catalyzes the synthesis of diacylglycerols, waxes, and retinyl esters. J. Lipid Res. *46*, 1502–1511.

Yin, C., Xiao, Y., Zhang, W., Xu, E., Liu, W., Yi, X., and Chang, M. (2014). DNA microarray analysis of genes differentially expressed in adipocyte differentiation. J. Biosci. *39*, 415–423.

Yu, X.-H., Fu, Y.-C., Zhang, D.-W., Yin, K., and Tang, C.-K. (2013). Foam cells in atherosclerosis. Clin. Chim. Acta Int. J. Clin. Chem. *424*, 245–252.

Yun, J., Puri, R., Yang, H., Lizzio, M.A., Wu, C., Sheng, Z.-H., and Guo, M. (2014). MUL1 acts in parallel to the PINK1/parkin pathway in regulating mitofusin and compensates for loss of PINK1/parkin. ELife *3*.

Zhang, J.W., and Lazarow, P.B. (1995). PEB1 (PAS7) in *Saccharomyces cerevisiae* encodes a hydrophilic, intra-peroxisomal protein that is a member of the WD repeat family and is essential for the import of thiolase into peroxisomes. J. Cell Biol. *129*, 65–80.

Zhu, S., Cheng, G., Zhu, H., and Guan, G. (2014). A study of genes involved in adipocyte differentiation. J. Pediatr. Endocrinol. Metab. *28*, 93–99.

Zimmermann, R., Strauss, J.G., Haemmerle, G., Schoiswohl, G., Birner-Gruenberger, R., Riederer, M., Lass, A., Neuberger, G., Eisenhaber, F., Hermetter, A., et al. (2004). Fat Mobilization in Adipose Tissue Is Promoted by Adipose Triglyceride Lipase. Science *306*, 1383–1386.